Interventional Systems Neuroscience Group
Imperial College of Science, Technology and Medicine
Department of Brain Sciences

Development of Non-Invasive Deep Brain Stimulation Intervention for Cognitive Decline in Alzheimer's Disease

Ketevan Alania

Submitted in part fulfilment of the requirements for the degree of Doctor of Philosophy in Clinical Medicine Research
and the Diploma of Imperial College,
March 2025

Abstract

Alzheimer's disease (AD) is a progressive neurodegenerative disorder characterised by cognitive decline, for which current treatment options remain limited. Non-invasive brain stimulation (NIBS) has emerged as a promising strategy to modulate aberrant neural activity and associated cognitive symptoms. Temporal Interference (TI) stimulation is a novel technique that addresses key limitations of existing NIBS methods by enabling non-invasive targeting of deep brain structures, with the added potential for concurrent real-time neural monitoring.

This thesis investigates the therapeutic potential of hippocampal TI stimulation for improving episodic memory function in AD. As a first step, the feasibility of single-session hippocampal TI to modulate episodic memory performance was demonstrated in 21 healthy young adults, providing early evidence of both neuromodulatory and behavioural effects. Building on these findings, a 10-day hippocampal TI stimulation protocol was tested in 21 patients with AD to evaluate the safety, tolerability, and feasibility of repeated stimulation. The intervention was well tolerated and resulted in selective improvements in episodic memory. Individual differences in baseline hippocampal volume and task performance during stimulation predicted the degree of memory benefit, suggesting that disease stage may influence responsiveness to TI.

Finally, to address the key methodological challenge of concurrent neural recording during TI stimulation, novel hardware and signal processing strategies were implemented to enable real-time EEG monitoring. These methods allowed reliable detection of steady-state visually evoked potentials during stimulation and revealed frequency- and state-dependent effects of TI on cortical activity.

Collectively, this work demonstrates the feasibility of hippocampal TI stimulation in both healthy individuals and AD patients. It also introduces new methodological tools for real-time neurophysiological monitoring, laying the groundwork for future closed-loop and personalised stimulation paradigms in neurodegenerative disease.

Acknowledgements

I would like to thank my supervisor, Dr Nir Grossman, for his guidance and support. Working under his supervision has shaped the way I think about science, and I am grateful for the opportunity to be part of such exciting and meaningful research.

I would also like to thank Dr Ines Violante, who provided much-valued mentorship and support.

To everyone in the Interventional Systems Neuroscience Lab, thank you for your curiosity, camaraderie, and for making the lab such an enjoyable place to work. I would especially like to thank Dr Edward Rhodes for his help, insights, and numerous debugging sessions.

I also want to acknowledge our collaborators and the clinical teams at Imperial, Invicro, MIT and IT'IS Foundation – your technical expertise and commitment made this work possible.

To the volunteers who took part in our studies, thank you for your trust, time, and generosity. You are at the heart of this research.

Finally, to my family, thank you for everything. Your love and encouragement have carried me through.

Statement of Publications

The data presented in Chapter 2 have been published in Nature Neuroscience:

Violante, I. R., Acerbo, E., Alania, K., Cassarà, A. M., Neufeld, E., Carron, R., Williamson, A., Kurtin, D. L., Rhodes, E., Hampshire, A., Kuster, N., Boyden, E. S., Pascual-Leone, A., & Grossman, N. (2023). Non-invasive temporal interference electrical stimulation of the human hippocampus. Nature Neuroscience, 26(11), 1994–2004. https://doi.org/10.1038/s41593-023-01456-8

Statement of Originality

Chapter 2: I contributed to the conceptualisation and development of the TI validation study in healthy human volunteers described in the Introduction and in Chapter 2. I managed the study and collected the data. The data analysis pipeline and experimental tasks used in this study were developed by Dr. Ines Violante.

Chapter 3: The conceptualisation of the study design was carried out in collaboration with Dr. Ines Violante, Dr. Nir Grossman, and Dr. Chris Butler. I set up the study pipeline and developed the experimental protocols and study materials. I led the study management, data collection and performed all data analysis, as well as developing the computational pipelines presented in this chapter (unless otherwise specified). Patient recruitment and testing support were provided by Evelyn Martin, Julia Borella, and Kaarin Sabad. Clinical interviews were conducted by Dr. Chris Butler and Dr. Lucia Li. I designed and sourced the stimuli for the custom associative memory tasks used during TI stimulation across the 10-day intervention period; these tasks were programmed by William Turner. The recognition memory task (ROC) was adapted from Argyropoulos et al. (2022).

Chapter 4: All custom-made devices used in this project were developed by our collaborating engineers. I conducted troubleshooting, validation, and implementation of the hardware in human experiments, and documented the optimisation strategies and outcomes. I performed all experiments described in this chapter, with support from Dr. Edward Rhodes in setting up both the pilot and Study 1 protocols. Hardware validation was carried out with assistance from Thomas Deegan and Dr. Rhodes. Preprocessing of EEG data was performed using scripts developed by Dr. Edward Rhodes. I conducted all subsequent analyses.

All other work contained in this thesis is my own, unless otherwise stated, and conforms to the rules and guidelines set out for PhD theses by Imperial College London.

Copyright declaration

The copyright of this thesis rests with the author. Unless otherwise indicated, its contents are licensed under a Creative Commons Attribution-NonCommercial 4.0 International Licence (CC BY-NC).

Under this licence, you may copy and redistribute the material in any medium or format. You may also create and distribute modified versions of the work. This is on the condition that: you credit the author and do not use it, or any derivative works, for a commercial purpose.

When reusing or sharing this work, ensure you make the licence terms clear to others by naming the licence and linking to the licence text. Where a work has been adapted, you should indicate that the work has been changed and describe those changes.

Please seek permission from the copyright holder for uses of this work that are not included in this licence or permitted under UK Copyright Law.

Table of Contents

Abstract *2*

Acknowledgements *3*

Statement of Publications *4*

Statement of Originality *5*

Copyright declaration *6*

List of Figures *10*

List of Tables *12*

List of Abbreviations *14*

Chapter 1: General Introduction *17*

1.1 Alzheimer's Disease: clinical symptoms, pathophysiology and current treatments 17

1.2 Network dysfunction in AD 19

1.3 Electrical brain stimulation for targeting aberrant network activity 20

1.4 Non-invasive deep brain stimulation via Temporal Interference (TI) of electric fields 24

1.5 Thesis overview and aims 28

Chapter 2: Enhancing episodic memory performance via non-invasive temporal interference electrical stimulation of the hippocampus *29*

2.1 Introduction 29

2.2 Methods 31

2.2.1 Participants 31

2.2.2 Experimental Design 31

2.2.3 Face-Name Task 31

2.2.4 TI stimulation setup and protocol 32

2.2.5 Stimulation sensation thresholding protocol 35

2.2.6 Data Analysis 35

2.2.7 Assessment of sham blinding and TI safety 35

2.3 Results 35

2.3.1 TI Stimulation of the hippocampus enhanced episodic memory performance 35

2.3.2 Effect of stimulation on reaction time 38
2.3.3 Blinding and Safety 39
2.4 Discussion 39
Chapter 3: Repeated TI Stimulation of The Hippocampus in Alzheimer's Disease *42*
3.1 Introduction 42
3.2 Materials and methods 46
3.2.1 Study participants 46
3.2.2 Study design 48
3.2.3 Data analysis 62
3.3 Results 68
3.3.1 Demographic and clinical characteristics 68
3.3.2 Repeated 10-day TI stimulation of the hippocampus in early-stage AD patients is safe and well-tolerated 69
3.3.3 AD patients showed selective improvement in episodic memory function following 10 days of TI stimulation 75
3.3.4 Associative memory task performance during TI stimulation predicts the degree of improvement in episodic memory function 81
3.3.5 Changes in Grey Matter volume following TI stimulation 83
3.3.6 Baseline hippocampal volume predicts the degree of improvement in episodic memory 86
3.3.7 No changes in ^{18}F-BCPP-EF SUVR in the hippocampus following 10 days of TI stimulation 88
3.3.8 Relationship between hippocampal and global changes in ^{18}F-BCPP-EF SUVR 88
3.3.9 No changes in hippocampal perfusion following 10 days of TI stimulation 91
3.4 Discussion 95
Chapter 4: Combined TI stimulation and EEG monitoring in humans: hardware approaches for recording artefact-free EEG during TI stimulation. *102*
4.1 Project Overview 102
4.2 Introduction 102
4.3 Methods 104
4.3.1 Pilot study 104

4.3.2 Technical validation tests 105
4.3.3 Data analysis 105
4.3.4 Study 1 107
4.4 Results 111
4.4.1 Mitigation of low frequency non-linear artefacts originating in the recording hardware with low-pass filtering 111
4.4.2 Experimental protocol and signal processing methods influence the detection of subtle IMD artefact 115
4.4.3 Mitigation strategies for non-linear low frequency artefacts originating in the stimulation hardware 120
4.4.4 Non-linear artefacts persist after the implementation of both low-pass (LP) and high-pass filters (HP) 122
4.4.5 Alpha and Beta TI stimulation of the occipital cortex differentially modulate SSVEP 124
4.4.6 The effects of alpha and beta TI stimulation on SSVEP are spatially distinct 126
4.4.7 TI stimulation of the occipital cortex modulates event-related potentials (ERPs) 128
4.5 Discussion 129
4.5.1 Mitigation of low frequency non-linear artefact in a combined TI-EEG setup 129
4.5.2 State and frequency-dependent effects of TI stimulation on SSVEPs 130
4.5.3 Limitations and future directions 133
Chapter 5: General Discussion *134*
5.1 Overview of experimental chapters 134
5.2 Key advances and contributions 135
5.3 Future directions 138
Bibliography *139*
Appendix *166*

List of Figures

Figure 1.1 Temporal Interference (TI) electrical stimulation targeting the anterior hippocampus in humans.....25
Figure 1.2 Validation of TI for hippocampal neuromodulation in humans 27
Figure 2.1 Experimental paradigm for TI stimulation of the hippocampus in healthy adults. 34
Figure 2.2 Effects of hippocampal TI stimulation on episodic memory recall.....37
Figure 2.3 Effect of hippocampal TI stimulation on episodic memory reaction time 38
Figure 3.1 The study timeline. 49
Figure 3.2 Patient recruitment flow chart. 48
Figure 3.3 Memory tasks performed during TI stimulation. 49
Figure 3.4 Hippocampal TI stimulation protocol in AD patients. 50
Figure 3.5 The episodic memory task designs. 56
Figure 3.6 The general cognition task designs. 59
Figure 3.7 Safety and tolerability of repeated TI hippocampal stimulation in AD patients. 73
Figure 3.8 Neurocognitive task performance at baseline and post-TI stimulation. 76
Figure 3.9 Performance on individual episodic memory tasks at baseline and post-TI. 78
Figure 3.10 Performance on individual general cognition tasks at baseline and post-TI. 79
Figure 3.11 Performance on associative memory tasks performed during TI stimulation. 82
Figure 3.12 Relationship between memory training scores during TI stimulation and improvement in episodic memory score. 83
Figure 3.13 Changes in brain volume following TI stimulation. 84
Figure 3.14 Correlation between changes in cluster volumes and performance from baseline to post-TI. 85
Figure 3.15 Relationship between baseline hippocampal volumes and improvement in episodic memory performance. 87
Figure 3.16 Changes in ^{18}F-BCPP-EF SUVR from baseline to post-TI. 89
Figure 3.17 Relationship between hippocampal and brain wide SUVR changes. 90
Figure 3.18 Perfusion image of an example patient. 91
Figure 3.19 Changes in hippocampal perfusion from baseline to post-TI. 92
Figure 3.20 Relationship between hippocampal CBF and AD biomarkers. 93
Figure 4.1 Study 1 experimental paradigm. 109
Figure 4.2 The low-pass filter (LPF) solution for low frequency non-linear artefact. 112
Figure 4.3 Demonstration of LPF solution for low frequency non-linear artefact. 113
Figure 4.4 Pilot study testing the effectiveness of LPF in suppressing IMD artefacts. 115

Figure 4.5 Signal processing pipeline for detecting IMD in the EEG recording. 116
Figure 4.6 Effect of recording duration on IMD detection. 117
Figure 4.7 Effect of background biological signal power on low frequency IMD peak detection. 119
Figure 4.8 High-pass filter solution for the low frequency IMD artefacts originating in the stimulation hardware. 121
Figure 4.9 Low frequency non-linear artefacts following implementation of high-pass and low-pass hardware filters. 123
Figure 4.10 The effects of TI stimulation of the right visual cortex on SSVEP at the O2 channel. 125
Figure 4.11 Effect of f TI on SSVEP and pre-LED baseline amplitude at the unstimulated O1 channel. 127
Figure 4.12 Tests for the confounding effects of low frequency artefacts on the observed effects of TI-27Hz on SSVEP. 128

Figure A1 Custom-made post-stimulation questionnaire. 172
Figure A2 Performance on associative memory tasks performed during TI stimulation. 173
Figure A3 Relationship between change in general cognition tasks and baseline hippocampal volumes. 174
Figure A4 Raw and imputed data at basleine and post-TI. 175
Figure A5 Synthetic EEG data simulation with and without low frequency IMD component. 179
Figure A6 Relationship between baseline alpha frequency and the effect of TI-10 Hz on pre-LED baseline. 181
Figure A7 The effect of TI on ERP. 181

List of Tables

Table 3.1 Individual patients' demographic data, clinical diagnosis, and testing status. 47
Table 3.2 Neurocognitive tasks administered at baseline and post-TI stimulation. 54
Table 3.3 Combined PET/MRI image acquisition protocol. 57
Table 3.4 Patient demographic and clinical characteristics summary. 68
Table 3.5 Results of patients' blood biomarkers of AD. 69
Table 3.6 Average stimulation sensation thresholds per patient across 10 days 70
Table 3.7 TI stimulation intensities delivered to each patient throughout 10 sessions. 71
Table 3.8 Statistical results for Figure 3.7. 74
Table 3.9 Statistical results for Figure 3.8. 77
Table 3.11 Statistical results for Figure 3.10. 80
Table 3.10 Statistical results for Figure 3.9. 80
Table 3.12 Statistical results for Figure 3.11. 83
Table 3.14 Statistical results for Figure 3.13. 85
Table 3.15 Statistical results for Figure 3.15. 87
Table 3.16 Statistical results for Figure 3.16. 90
Table 3.17 Statistical results for Figure 3.17. 90
Table 3.18 Statistical results Figure 3.19. 94
Table 3.19 Statistical results for Figure 3.20. 94
Table 4.1 Sensation thresholds during TI stimulation at 10 Hz. 108

Table A1 Perceptual sensations and threshold across participants (ID) for conventional transcranial alternating current stimulation (tACS) and TI stimulation – Session 1 behavioural experiment 166
Table A2 Perceptual sensations and threshold across participants (ID) for conventional transcranial alternating current stimulation (tACS) and TI stimulation – Session 2 behavioural experiment 167
Table A3 Blinding effectiveness 168
Table A4 Summary of post-stimulation side effects questionnaire for TI and Sham sessions. 169
Table A5 The patient inclusion and exclusion criteria 170
Table A6 Post-stimulation side effects questionnaire. 171
Table A7 Percentage of imputed data across neurocognitive tasks. 176
Table A8 Raw and imputed data at baseline and post-TI. 177
Table A9 Stimulation current amplitudes delivered in study 1. 178
Table A10 Statistical results for Figure 4.10. 180

Table A11 Statistics for Figure A 6 Relationship between baseline alpha frequency and the effect of TI-10 Hz on pre-LED baseline. 181

List of Abbreviations

Abbreviation	Full Term
AA	Alzheimer's Association
ACE-III	Addenbrooke’s Cognitive Examination Form
AD	Alzheimer's Disease
AE	Adverse Event
AIC	Akaike Information Criterion
ASL	Arterial Spin Labelling
AUC	Area Under the Curve
Aβ	Amyloid-Beta
BOLD fMRI	Blood-Oxygen-Level-Dependent Functional Magnetic Resonance Imaging
CBF	Cerebral Blood Flow
CIF	Clinical Imaging Facility
CRT	Choice Response Task
CS	Centrum Semiovale
CSF	Cerebrospinal Fluid
DBS	Deep Brain Stimulation
DLPFC	Dorsolateral Prefrontal Cortex
DRI	UK Dementia Research Institute
DWI	Diffusion-Weighted Imaging
ECG	Electrocardiogram
EEG	Electroencephalogram
EEG-TI	Combined EEG-TI Stimulation
EMM	Estimated Marginal Means
ERP	Event-Related Potential
FA	Flip Angle
FDR	False Discovery Rate
FLIRT	FSL's Linear Image Registration Tool
fMRI	Functional Magnetic Resonance Imaging
FOV	Field of View
FRFSE	Fast Recovery Fast Spin Echo
FSL	FMRIB Software Library
FSPGR	Fast Spoiled Gradient Echo

GFAP	Glial Fibrillary Acidic Protein
GLME	General Linear Mixed Effects Model
GLMM	Generalized Linear Mixed Model
GM	Grey Matter
HCRW	Health and Care Research Wales
HPF	High-Pass Filter
HRA	Health Research Authority
IAF	Individual Alpha Frequency
ICRF	Imperial Clinical Research Facility
IMD	Intermodulation Distortion
IQR	Interquartile Range
IR-FSPGR	Inversion Recovery Fast Spoiled Gradient Echo
ISI	Inter-Stimulus Interval
LME	Linear Mixed Effects Model
LPF	Low-Pass Filter
LRT	Likelihood Ratio Test
LTP	Long-Term Potentiation
LTD	Long-Term Depression
MCI	Mild Cognitive Impairment
MEG	Magnetoencephalography
MICE	Multivariate Imputation by Chained Equations
ML	Maximum Likelihood
MMSE	Mini-Mental State Examination
MNI	Montreal Neurological Institute
mPCA	Multi-Level Principal Component Analysis
MRI	Magnetic Resonance Imaging
NART	National Adult Reading Test
NfL	Neurofilament Light
NIBS	Non-Invasive Brain Stimulation
OSA	Object-Scene Association
OSEM	Ordered Subset Expectation Maximization
PAL	Object-Location Association
PC1	First Principal Component
PCA	Principal Component Analysis

pCASL	Pseudo-Continuous Arterial Spin Labelling
PET	Positron Emission Tomography
PET/MRI	Positron Emission Tomography–Magnetic Resonance Imaging
PIC	Patient Identification Centre
QC	Quality Control
REC	Research Ethics Committee
ROC	Receiver Operating Characteristic
ROC AUC	Area Under Receiver Operating Characteristic Curve
ROI	Region of Interest
rs-fMRI	Resting-state Functional Magnetic Resonance Imaging
rTMS	Repetitive Transcranial Magnetic Stimulation
SD	Standard Deviation
SEM	Standard Error of the Mean
SNR	Signal-to-Noise Ratio
SPM12	Statistical Parametric Mapping Software
SSVEP	Steady-State Visually Evoked Potential
STDP	Spike-Time-Dependent Plasticity
SUV	Standardised Uptake Value
SUVR	Standardized Uptake Value Ratio
tACS	Transcranial Alternating Current Stimulation
tDCS	Transcranial Direct Current Stimulation
TE	Echo Time
TENS	Transcutaneous Electrical Nerve Stimulation
tES	Transcranial Electrical Stimulation
TI	Temporal Interference
TMS	Transcranial Magnetic Stimulation
TR	Repetition Time
VBM	Voxel-Based morphometry
VOSP	Visual Object and Space Perception
WM	White Matter
WMS-IV	Wechsler Memory Scale - Fourth Edition
WPA	Word-Pair Association
WSA	Word-Scene Association

Chapter 1: General Introduction

1.1 Alzheimer's Disease: clinical symptoms, pathophysiology and current treatments

Alzheimer's disease (AD) is a complex neurodegenerative disorder and the leading cause of age-related dementia, accounting for 60–80% of all cases (Zheng & Wang, 2025). Dementia due to AD poses significant global health and economic challenges, affecting over 57 million people worldwide, a number projected to triple by 2050 (Chen et al., 2024). Women are at greater risk of developing AD compared to men, with menopause-related estrogen decline proposed as one potential factor (Lopez-Lee et al., 2024). Additionally, women disproportionately bear the caregiving responsibilities and associated psychological burdens related to dementia (de Graaff et al., 2025).

Clinical Symptoms

Clinically, dementia due to AD is characterised by slow and progressive cognitive decline, with an amnestic phenotype accounting for approximately 85% of cases (Dubois et al., 2023). This amnestic syndrome is typically defined by deficits in learning and episodic memory, initially presenting as mild cognitive impairment (MCI). As the disease progresses, additional cognitive domains become impaired, including language, visuospatial function, executive function, and changes in personality and behaviour (McKhann et al., 2011). Dementia is fatal, and most individuals with cognitive impairment die within 10 years of diagnosis (Rajendran & Krishnan, 2024). However, clinical phenotypes and disease trajectories are highly variable, influenced by several factors including sociodemographic characteristics, lifestyle variables, and disease comorbidities (Yu et al., 2020; Lanctôt et al., 2024; Ding et al., 2025), complicating both diagnosis and intervention.

Pathophysiology

At the cellular level, AD is defined primarily by two types of protein aggregates accumulating in distinct brain regions: (i) extracellular amyloid-β (Aβ) plaques, and (ii) intracellular neurofibrillary tangles (NFTs) composed of hyperphosphorylated tau (Hampel et al., 2021; Knopman et al., 2021). The initial formation of Aβ plaques typically begins in neocortical regions, often decades before cognitive symptoms appear, subsequently spreading to subcortical structures (Therriault et al., 2024; Taddei & Duff, 2025). Aβ deposition is commonly measured in vivo via positron emission tomography (PET) using amyloid tracers (e.g., ^{18}F-florbetapir, ^{11}C-PiB) or quantified through reductions in cerebrospinal fluid (CSF) Aβ42 and the Aβ42/40 ratio, reflecting shifts in soluble peptide levels (Hampel et al., 2021).

In contrast, NFTs initially develop in the entorhinal cortex and hippocampus (according to Braak staging) and later spread to wider limbic and cortical regions as the disease progresses (Zheng & Wang, 2025; Jia et al., 2025). Tau pathology can be assessed using PET (e.g., ^{18}F-flortaucipir) or by measuring elevated tau levels in CSF and plasma (Therriault et al., 2024). More recently, minimally invasive biomarker methods measuring Aβ, tau, and neurodegeneration (ATN markers) in blood plasma have been developed; however, they are not yet standard in clinical practice and remain primarily research tools (Hansson et al., 2023). Tau distribution aligns more closely with clinically affected brain regions and accumulates selectively in areas of significant neurodegeneration, while Aβ deposition is more diffused (Taddei & Duff, 2025). Although these protein aggregates remain hallmarks of AD, there is a growing consensus that recognises AD as a multifactorial disorder. Other contributing mechanisms under investigation include neuroinflammation, oxidative stress, lipid and metabolic dysregulation, and neurovascular dysfunction (Korczyn & Grinberg, 2024).

Current Pharmacological Treatments

Several pharmacological treatments are currently available for AD, broadly categorised into medications that temporarily alleviate symptoms and those targeting underlying pathology to slow disease progression. FDA-approved medications addressing cognitive symptoms (memory, attention, learning) include cholinesterase inhibitors: donepezil, galantamine, rivastigmine, the glutamate regulator memantine, and a combination of donepezil and memantine (Guo et al., 2020; Marucci et al., 2021). Additional treatments manage neuropsychiatric symptoms such as sleep disturbances, agitation, and psychological symptoms (Alzheimer's Association, 2024). However, these medications provide only temporary symptom relief, have significant side effects and risks, especially in elderly populations, and are effective in only a subset of patients (Marucci et al., 2021; Zeng et al., 2023; Rajendran & Krishnan, 2024).

Recent advances in disease-modifying therapies have resulted in FDA approval of three anti-amyloid monoclonal antibodies (mAbs) since 2021: Aducanumab, Donanemab, and Lecanemab. These intravenous treatments target Aβ plaques in early to mild AD patients (van Dyck et al., 2023). While these therapies represent significant progress, concerns regarding efficacy, safety, and usability persist. Clinical benefits, though evident in slowing cognitive and functional decline in certain patients, have been modest, and clinically meaningful improvement remains debated (Daly, 2024; Dantas et al., 2024). Additionally, these mAbs pose risks of amyloid-related imaging abnormalities (ARIA), including cerebral microhaemorrhages, necessitating careful patient selection and monitoring. Prior trials have indicated that substantial amyloid reduction does not always correlate with proportional cognitive improvements (Avgerinos et al., 2024), challenging their therapeutic potential. Furthermore, anti-

amyloid therapies carry substantial medical costs. For example, the estimated annual cost of Lecanemab, including drug administration, safety monitoring, and biomarker testing, is approximately $109,000 USD per patient in the United States. Contextually, administering Lecanemab to all eligible patients would represent roughly 11.3% of the entire EU health budget (Bradshaw & Georges, 2024).

Thus, despite extensive research into amyloid-targeted therapies, many pharmacological trials have failed to achieve significant clinical efficacy and remain inaccessible to many due to high costs. This has prompted a shift toward alternative pharmacological targets. As of 2023, 141 disease-modifying drugs were in ongoing clinical trials, primarily targeting neuroinflammation (25%), amyloid (23%), and synaptic plasticity (18%; Rajendran & Krishnan, 2024).

Non-Pharmacological Treatments

Currently, no non-pharmacological treatments have received clinical approval for AD. However, given the limited success of pharmacological therapies and growing recognition of the need for a multi-targeted approach, research into alternative treatments is expanding. Brain stimulation and exercise therapies, in particular, are gaining significant interest (Wang et al., 2025).

1.2 Network dysfunction in AD

One of the most clinically meaningful indicators of cognitive decline in AD is synaptic loss, which displays a strong correlation with both the onset and severity of cognitive impairment (Taddei & Duff, 2025). While cellular pathology and clinical symptoms do not always align, synaptic loss is a key determinant of clinical manifestation. Interestingly, individuals who display resilience to AD pathology also show preserved synaptic integrity, where synapses are less susceptible to Aβ and tau toxicity and thus maintain neural connectivity despite significant pathological burden (Taddei & Duff, 2025; de Vries et al., 2024). Additionally, this preservation has been associated with strong synaptic plasticity, effective neurotransmission, and stable neural circuits (Jia et al., 2025). At the network level, resilient individuals often show greater connectivity and compensatory activity within critical cognitive areas (de Vries et al., 2024; Jia et al., 2025). Hence, synapses may represent a key target of the processes driving AD-related dementia. Considering this, interventions that focus on synaptic preservation could offer greater clinical benefits than those solely targeting pathophysiology.

Increasing evidence shows that alterations in brain network function and the breakdown of synaptic integrity are interrelated processes in AD. Synapses serve as the fundamental sites of information transfer in neuronal circuits, and their degeneration is strongly correlated with cognitive decline in AD (Hong et al., 2016; Tzioras et al., 2023). New neuroimaging and electrophysiological studies show significant disturbances in brain network activity and connectivity, ranging from hyperexcitability in

early disease stages to disrupted synchrony, general slowing of oscillations, and reduced functional connectivity later on (Vossel et al., 2016; Zott et al., 2019).

New models now regard AD not merely as a protein-aggregation disorder but as a vicious cycle in which synaptic damage disrupts network stability, and network dysfunction in turn accelerates synaptic loss (Busche & Hyman, 2020). Hyperactive networks are therefore not simply an epiphenomenal symptom of the disease but appear to drive downstream processes that compromise the synaptic integrity. For example, overactive neuronal networks increase the release of soluble Aβ species, which interfere with synaptic transmission and plasticity (Zott et al., 2019). Elevated Aβ levels then promote further neuronal hyperexcitability, perpetuating a cycle of network destabilisation and synaptic breakdown. Clinical imaging studies also report a close association between increased epileptiform activity in individuals with MCI and early AD and cognitive decline, linking abnormal network hypersynchrony to disease progression (Vossel et al., 2013; 2016).

1.3 Electrical brain stimulation for targeting aberrant network activity

Electrical brain stimulation refers to a class of techniques that modulate neural activity by delivering controlled electric fields to target brain regions, providing a direct means of perturbing circuit dynamics in both research and therapeutic settings. In humans, these approaches include invasive methods like deep brain stimulation (DBS), where electrodes are surgically implanted to precisely target deep-seated structures, and non-invasive modalities such as transcranial alternating current stimulation (tACS) and transcranial direct current stimulation (tDCS), which apply weak currents through the scalp. Each technique differs in its mechanism of action, mode of delivery, application, and limitations.

Invasive DBS

DBS is an established neurosurgical therapy that delivers chronic, programmable electrical pulses to specific subcortical targets via an implanted system. Stimulation is typically delivered as continuous biphasic rectangular pulses, using either constant-voltage or constant-current sources, with parameters such as pulse width (60–450 μs), frequency (commonly 130–185 Hz), and amplitude tailored to individual clinical response (Perlmutter & Mink, 2006; Davidson et al., 2024). The resulting electric field magnitudes typically range from 0.13 to 0.46 V/mm, which are sufficient to directly depolarise axonal membranes and reliably elicit action potentials (Johansson & Zsigmond, 2021).

DBS has been transformative in the management of several neurological disorders and is a clinically approved treatment for movement disorders such as Parkinson’s disease and essential tremor

(Cernera et al., 2021; Hariz & Blomstedt, 2022). In these conditions, stimulation significantly reduces motor symptoms including tremor, rigidity, and bradykinesia, and can also improve gait dysfunction (Lozano et al., 2019). More recently, DBS has been approved for the treatment of medically refractory epilepsy (Bahadori et al., 2024) and severe refractory obsessive-compulsive disorder (OCD; Mar-Barrutia et al., 2021). In epilepsy, significant progress has been made in closed-loop neurostimulation approaches (Nair et al., 2020), facilitating the shift towards biomarker-driven closed-loop brain stimulation.

More recently, the application of DBS has been extended to cognitive domains, with preliminary studies suggesting that stimulation of memory-related structures such as the entorhinal cortex and fornix may enhance episodic memory performance in patients with AD (Mankin, 2020). However, despite growing interest in DBS as a potential therapeutic strategy for AD, several critical limitations continue to impede its clinical translation. First, outcomes across clinical trials have been highly variable (Picton et al., 2023), with group-level cognitive improvements failing to reach statistical significance in phase 2 studies (Davidson et al., 2024). Moreover, stimulation parameters for DBS in AD have largely been adapted from movement disorder protocols, despite the absence of clear evidence regarding the optimal frequency, amplitude, or duty cycle for cognitive enhancement (Davidson et al., 2024). This limitation in part reflects the restricted capacity for exploratory parameter space mapping and target selection due to the inherently invasive nature of DBS.

Non-invasive electrical stimulation

Transcranial electrical stimulation (tES) methods modulate neural activity through the application of weak electric fields via scalp electrodes. Among the most widely studied are tDCS and tACS, both of which apply low-intensity currents (typically 1-2 mA) but differ fundamentally in their mode of action. TDCS applies a constant, unidirectional current between anodal and cathodal electrodes, producing a tonic shift in resting membrane potential in the underlying cortex. Anodal stimulation generally leads to subthreshold depolarisation, increasing the likelihood of neuronal firing, while cathodal stimulation produces hyperpolarisation and tends to reduce excitability (Nitsche & Paulus, 2000; Yamada & Sumiyoshi, 2021). Hence, although the electric fields generated by tDCS are too weak to directly elicit action potentials, they can modulate spontaneous and task-evoked brain activity by altering the excitability landscape of the stimulated region. These effects are highly dependent on neuronal orientation, local cytoarchitecture, and the underlying functional state. Repeated sessions of tDCS may further lead to long-term potentiation (LTP) or depression-like (LTD) effects via plastic changes at the synaptic level (Yamada & Sumiyoshi, 2021). For tDCS, meta-analyses have reported modest but

consistent improvements in verbal and visuospatial working memory following prefrontal stimulation, especially when stimulation is paired with task performance (Hill et al., 2016). TDCS has also been reported to offer benefits in age-related cognitive decline, particularly in visual attention, verbal episodic memory, and working memory (Indahlastari et al., 2021). In AD, a recent meta-analysis reported positive effects of tDCS protocols targeting dorsolateral prefrontal cortex (DLPFC) and temporoparietal cortices on learning, memory and global cognitive function (Majdi et al., 2022). Several mechanisms have been proposed to explain how tDCS exert positive effects in AD. Anodal tDCS may enhance cortical excitability in hypoactive networks, whereas cathodal tDCS could reduce the hyperactivity often observed in the early stages of AD (Hansen, 2012). Repeated tDCS applications may also induce synaptic and structural plasticity, supporting learning and memory processes (Jog et al., 2023; Podda et al., 2016; Stagg & Nitsche, 2011; Hansen, 2012) and modulate network activity and connectivity (Polanía et al., 2011).

In contrast to tDCS, tACS delivers a zero-mean sinusoidal current (typically 0.5-2 mA peak-to-peak) across scalp electrodes, generating oscillating electric fields in cortical tissue (Vöröslakos et al., 2018; Wischnewski et al., 2023). Although a significant proportion of the applied current (~75%) is shunted by the skin and skull, the resulting intracranial fields (~0.1-1 V/m) are sufficient to induce subtle but physiologically relevant effects on neural activity (Vöröslakos et al., 2018; Krause et al., 2019). At these field strengths, tACS does not directly drive action potentials but rhythmically depolarises and hyperpolarises neuronal membranes, biasing spike timing and modulating activity within targeted networks (Wischnewski et al., 2023; Vöröslakos et al., 2018; Krause et al., 2019). This temporal biasing enables weak electric fields to influence ongoing oscillatory activity through mechanisms such as entrainment and spike-timing dependent plasticity (STDP). Entrainment synchronises endogenous oscillations to the applied “driving” frequency. This process is particularly effective when the stimulation frequency closely matches the natural resonance of the targeted network (Vogeti et al., 2022; Dowsett et al., 2020). In parallel, repeated tACS can induce longer-lasting offline effects, including changes in synaptic efficacy via STDP and resonance-driven alterations in connectivity (Vogeti et al., 2022; Wischnewski et al., 2023).

The effects of tACS on ongoing brain activity are shaped by multiple interacting factors, including stimulation frequency, phase, current intensity, and the dynamic state of the targeted network. Evidence from human and animal studies demonstrates that electric field strengths of $\geq$0.3-0.4 V/m are sufficient to modulate spike timing, with higher intensities recruiting more neurons and potentially reorganising network-level oscillations (Vöröslakos et al., 2018; Krause et al., 2019). Critically, tACS

can either amplify or disrupt oscillatory synchrony, depending on the interplay between the strength of ongoing brain rhythms and the tACS-induced electric fields at the target site (Krause et al., 2022). These frequency and state-dependent effects have been demonstrated in both primate (Krause et al., 2022) and human studies (Luo et al., 2025; Bradley et al., 2022; Neuling et al., 2013).

The cognitive effects of tACS have been explored across a wide range of domains, with studies reporting improvements in working memory (Nissim et al., 2023), episodic memory (Lang et al., 2019; Shtoots et al., 2024) and attention (Rostami et al., 2021). However, a substantial body of research has also reported null findings (Hu et al., 2022; Zhang et al., 2025), and, in some cases, negative effects on cognitive performance have also been observed (Murray et al., 2023). In AD, applications of tACS remain limited. While some studies suggest modest benefits in specific cognitive domains, effect sizes are generally small, and findings remain inconsistent (Kehler et al., 2020; Benussi et al., 2021, 2022; Tang et al., 2024).

Although both invasive and non-invasive electrical brain stimulation techniques have shown potential for modulating aberrant neural activity across a range of neuropsychiatric and neurodegenerative disorders, critical limitations continue to impede their broader clinical translation. Invasive DBS, despite its established efficacy in movement disorders, carries surgical risks, high costs, and limited flexibility for parameter optimisation – challenges that are particularly salient in complex conditions such as AD. Non-invasive approaches such as tDCS and tACS offer safer and more accessible alternatives but are constrained by their limited capacity to target deep brain structures with precision. Moreover, the low spatial precision of tES reduces its network specificity and raises concerns about unintended (Murray et al., 2023) or indirect effects on cognition, for example, via peripheral nerve activation (Vanneste et al., 2020; Vöröslakos et al., 2018).

A further challenge lies in the inability to monitor brain activity during stimulation, as the strong electric fields generated by tES contaminate electrophysiological recordings. This limitation has impeded the mechanistic understanding of tES effects on brain oscillations and may contribute to the variability observed in stimulation outcomes (Vöröslakos et al., 2018). These challenges are particularly critical for tACS, where the large parameter space and the state-dependency of the targeted networks shape the outcome (Vogeti et al., 2022). Finally, current tES methods lack the capacity for focal targeting of deep brain structures, which is a critical limitation in conditions such as AD, where key pathological structures lie in subcortical regions.

Together, these challenges underscore the need for innovative neuromodulation strategies capable of delivering spatially targeted, frequency-specific modulation of deep brain networks without the need for invasive procedures.

1.4 Non-invasive deep brain stimulation via Temporal Interference (TI) of electric fields

Temporal Interference (TI) is a novel, non-invasive electrical brain stimulation technique developed by Grossman et al. (2017) that can achieve DBS without surgery. In TI, two high-frequency (kHz-range) oscillating electrical fields with slightly different frequencies (e.g., f_1 and $f_2 = f_1 + \Delta f$) are delivered simultaneously via two electrode pairs on the scalp (**Figure 1.1A**). The spatial overlap of these fields in the brain tissue produces an amplitude-modulated envelope oscillating at the frequency Δf. When the difference frequency is set within the dynamic range of neural activity, neurons respond to Δf, while the carrier frequencies are assumed not to affect neuronal activity due to the low-pass filtering properties of neuronal membranes. The locus of the interference can be manipulated by adjusting electrode locations on the head and thus can be localised in deeper brain structures. Additionally, the peak envelope can be steered by shifting the current ratio between two electrode pairs.

TI effects were first validated in anesthetised mice, where TI stimulation at the difference frequency reliably induced spiking in the hippocampus while pure kHz stimulation did not. Moreover, immunohistochemistry analysis confirmed selective activation of these deep regions, with minimal effects observed in the overlying cortex (Grossman et al., 2017). Since then, TI has been found to suppress epileptic biomarkers in rodents (Acerbo et al., 2022), while more recently, Vieira et al. (2024) showed that in awake non-human primates, TI-stimulation induced spike-time biasing in the target area without significantly changing overall firing rates.

Validation of TI hippocampal stimulation in humans

We recently validated TI stimulation as a non-invasive method to selectively modulate activity in the human hippocampus (see Violante et al., 2023). Specifically, we set out to address four key objectives: (1) to demonstrate that the locus of stimulation could be directed to the hippocampus using a transcranial TI setup; (2) to test whether the stimulation focus could be steered within the hippocampus along its anterior-posterior axis; (3) to evaluate whether TI stimulation could modulate hippocampal activity at a physiological level; and (4) to assess whether this modulation could lead to measurable effects on memory performance.

We addressed the first two aims through computational modelling, followed by experimental validation in a human cadaver. Using high-resolution head models incorporating both anatomical and diffusion MRI data, we simulated the distribution of TI-induced electric fields and demonstrated that the resulting envelope modulation could be targeted to the hippocampus while minimising exposure in the overlying cortex. These simulations used the electrode placement shown in **Figure 1.1B**, where electrodes e1-e2 (anterior pair) delivered a 2 kHz sinusoidal current at 2 mA, and electrodes e3-e4 (posterior pair) delivered a 2.005 kHz current at 2 mA. By adjusting the relative current amplitudes to a 1:3 ratio (i.e., delivering 1 mA and 3 mA) between anterior and posterior pairs, we were able to steer

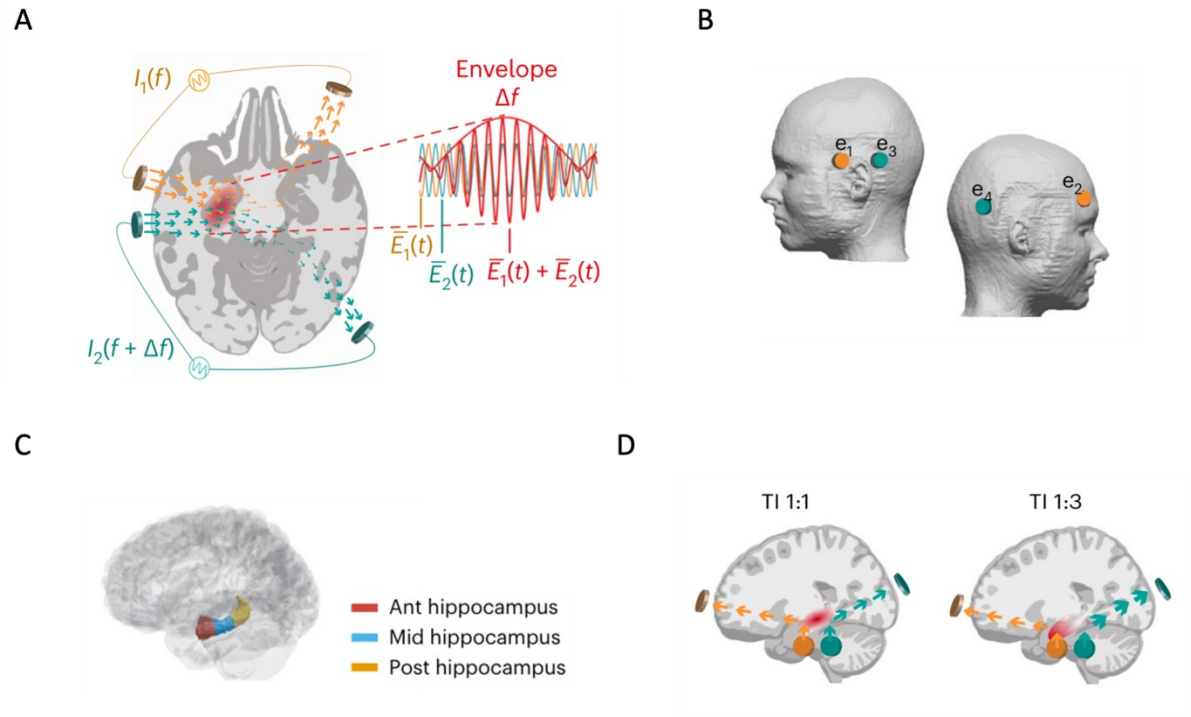


Figure 1.1 Temporal Interference (TI) electrical stimulation targeting the anterior hippocampus in humans

A. The concept of TI. Two high-frequency alternating currents in the kilohertz range (I1 at frequency f, and I2 at frequency f + Δf) are simultaneously applied via electrically isolated pairs of scalp electrodes. The frequencies differ slightly, with Δf set within the range of natural neural rhythms. These currents generate oscillating electric fields in the brain tissue, E1(t) and E2(t), illustrated by the orange and green arrows, respectively. The spatial overlap of these fields produces an amplitude-modulated envelope oscillating at the frequency Δf. By controlling this interference pattern, the maximal amplitude of the modulation envelope can be selectively targeted to deeper brain structures, such as the hippocampus (highlighted in red). Figure adapted with permission from Violante et al., 2023. **B.** Electrode placement optimised for targeting left hippocampus. e1-e2 anterior electrode pair delivered 2 kHz waveform while e3-e4 delivered 2.005 kHz, thus aiming maximum modulation envelope at 5 Hz to the left hippocampus. **C.** An illustration of hippocampal segmentation along its longitudinal axis into anterior, middle and posterior segments. **D.** TI steering implementation for targeting the anterior hippocampus without moving electrodes. By changing the current ratio between two pairs of electrodes – in this case setting e1-e2 channel to 1 mA and e3-e4 to 3 mA, the electric field is steered towards the anterior hippocampus. Figure adapted with permission from Violante et al., 2023.

the locus of the peak envelope modulation along the anterior-posterior axis of the hippocampus (**Figure 1.1C-D**). These modelling results were validated in cadaver recordings, where depth electrodes implanted along the hippocampal axis confirmed that the envelope modulation amplitude was stronger in the hippocampus than in surrounding cortical regions, and that varying the current ratio shifted the peak modulation to the anterior hippocampal segment.

To assess whether TI stimulation could modulate hippocampal activity in vivo, we conducted a functional MRI experiment in 20 healthy young adults while they performed a hippocampal-dependent episodic memory task with concurrent TI stimulation. The task consisted of an encoding phase in which participants were instructed to memorise 16 novel face-name pairs (each presented for 2 s), followed by a short delay and a recall phase where they selected the correct name for each face and rated their confidence (**Figure 1.2A**). Stimulation was delivered only during the encoding phase, using the same electrode configuration and stimulation frequencies as in the modelling and cadaver experiments. Three conditions were tested in a counterbalanced order: (1) Sham – no stimulation; (2) TI 1:1 – stimulation with a 1:1 current ratio, targeting the middle left hippocampus; and (3) TI 1:3 – stimulation with a 1:3 current ratio between anterior and posterior electrode pairs, steering the field toward the anterior hippocampus (**Figure 1.1C**). All stimulation used a 2 kHz carrier and a 5 Hz envelope frequency, consistent with prior work demonstrating the role of theta-band activity in episodic memory encoding (Herweg et al., 2020; Zheng et al., 2024).

Regions of interest (ROIs) were defined along the anterior–posterior axis of the left hippocampus, as well as in the right hippocampus and cortical areas underneath the stimulation electrodes. In the sham condition, the task reliably evoked a significant BOLD signal increase during encoding in both hippocampi, with the strongest response observed in the anterior portion of the left hippocampus **(Figure 1.2C-E**). This confirmed consistent task engagement and was in line with previous findings implicating the anterior hippocampus in associative memory encoding (Chua et al., 2007; Sperling et al., 2003; Zeineh et al., 2003). Under the TI 1:3 stimulation condition, which steered the electric fields toward the left anterior hippocampus, we observed a significant reduction in BOLD signal compared to both sham and TI 1:1 conditions (**Figure 1.2F-G**). This effect was specific to the encoding phase and was not observed during recall. Importantly, no changes were detected in the right hippocampus or in the overlying cortical ROIs, supporting the spatial specificity of the effect.

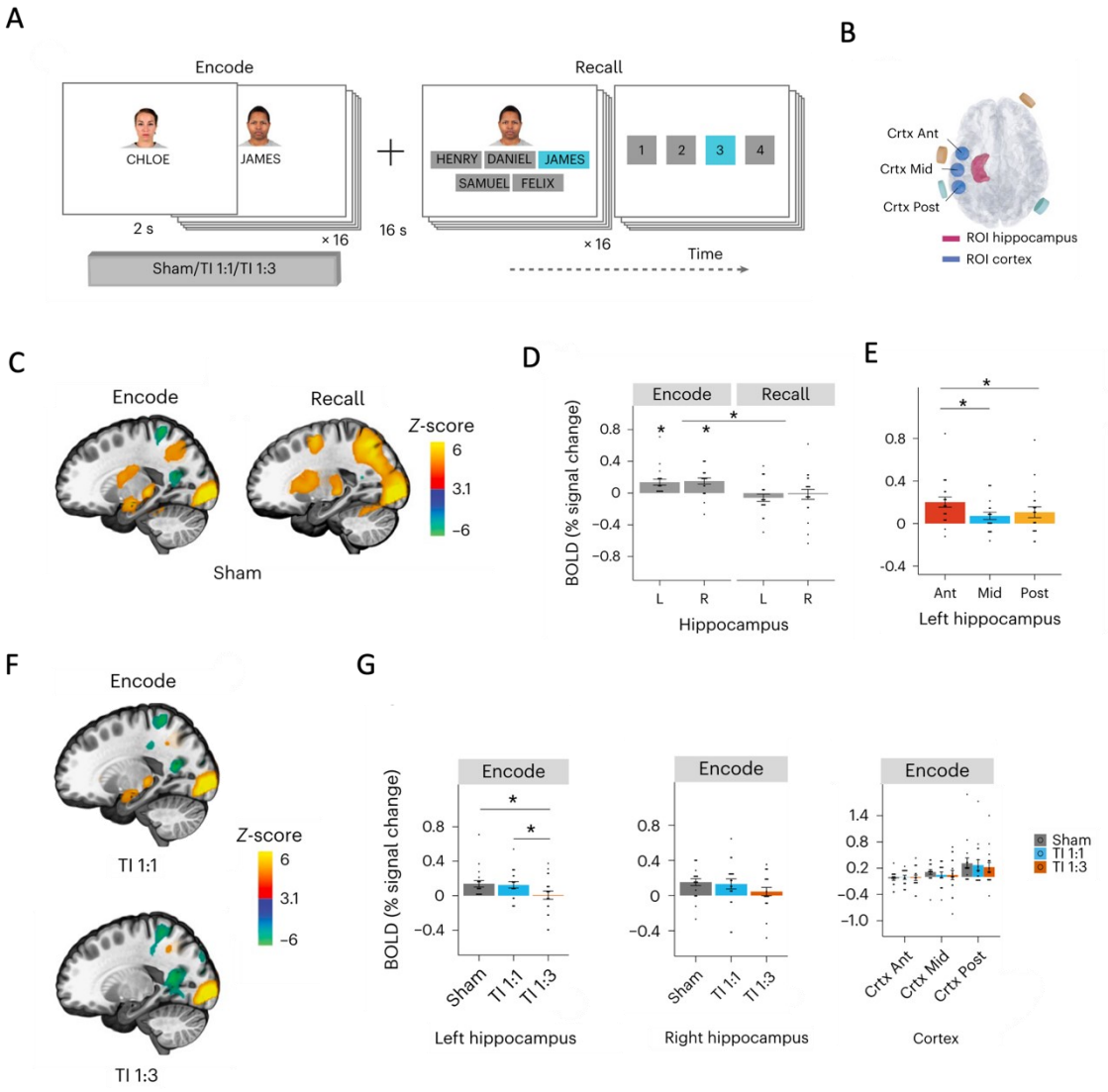


Figure 1.2 Validation of TI for hippocampal neuromodulation in humans

A. Episodic memory task paradigm. During encoding, participants were asked to memorise 16 pairs of novel faces and names presented on the screen sequentially for 2 s. After 16 s delay, they were asked to recall previously memorised faces and rate how confident they were in their responses. Task was performed inside an MRI scanner, TI stimulation during encoding phase in three conditions: (1) Sham – no stimulation, (2) TI 1:1 – theta stimulation targeted to the middle left hippocampus and (3) TI 1:3 – theta stimulation steered to left anterior hippocampus by changing the current ratio between anterior and posterior electrode pairs to 1:3 respectively. **B.** The regions of interest (ROIs) defined for the fMRI analysis including the hippocampus and cortical structures underneath the electrodes. **C.** Whole-brain group z-score change in BOLD signal during encode and recall in the sham condition. **D.** Group median change in BOLD signal in the left (L) and right (R) hippocampi in sham condition blocks. Showing significant BOLD signal increase during the encode but not recall. **E.** Group median change in BOLD signal in the anterior (Ant), middle (Mid) and posterior (Post) regions of the left hippocampus during the encoding stage in the sham condition. Showing a larger BOLD signal increase in the Ant hippocampal region compared to the Mid and Post regions. **F.** Whole-brain group z-score change in BOLD signal during encode stage of the task for TI 1:1 and TI 1:3 stimulation conditions. **G.** Comparison of group median change in BOLD signal between stimulation conditions, in the left (stimulated) hippocampus, right hippocampus and cortical ROIs under the electrodes during face-name encoding. Results show a main effect of stimulation with reduction in the evoked BOLD signal in the left hippocampus during encoding by TI 1:3 stimulation. No effects were observed in the right hippocampus or in cortical ROIs underneath the electrodes. Asterisks show significant differences, $p < 0.05$. Bar plots show mean and SE, black dots show individual participant data. Images in C and F were thresholded at $Z > 3.1$, with a cluster significance level of $p < 0.05$, and are displayed in $x = -21$ plane of the MNI template. $n = 20$. Figure adapted with permission from Violante et al., 2023.

While our neuroimaging experiment demonstrated that TI stimulation can selectively modulate task-evoked hippocampal activity, these physiological changes did not translate into observable behavioural effects. This is likely due to the experimental design, which was optimised to detect neural responses rather than behavioural effects. Specifically, stimulation was delivered only during the encoding phase, with a total duration of approximately 96 seconds per condition, which is considerably shorter than what is typically reported in other NIBS studies (Booth et al., 2022). Therefore, to assess whether hippocampal TI stimulation could impact episodic memory, we conducted a follow-up experiment with an experimental paradigm powered to observe behavioural effects, presented in Chapter 2 of this thesis.

1.5 Thesis overview and aims

This thesis explores the potential of temporal interference (TI) stimulation as a novel non-invasive intervention for cognitive decline in Alzheimer's disease. Specifically, the research aims to:

1. Validate the effects of TI stimulation on the hippocampal-dependent memory function (**Chapter 2**).
2. Evaluate the safety, tolerability, and efficacy of repeated multi-day TI stimulation of the hippocampus in AD patients (**Chapter 3**).
3. Develop and validate technical methods for artefact-free EEG recording during TI stimulation, enabling real-time neurophysiological monitoring of stimulation effects (**Chapter 4**).

Chapter 2: Enhancing episodic memory performance via non-invasive temporal interference electrical stimulation of the hippocampus

2.1 Introduction

Neurological disorders represent a major global health challenge, affecting approximately 43% of the global population and constituting one of the leading causes of disability worldwide (Steinmetz et al., 2024). Among these, brain-related conditions comprise a significant portion of the overall neurological disease burden (Feigin et al., 2020). Cognitive impairment has emerged as a prominent transdiagnostic feature, frequently present in psychiatric (Sha et al., 2019; Kinon et al., 2024; Xie et al., 2023) and neurological conditions (Jehi, 2025; Harpaz et al., 2017; Rajendran & Krishnan, 2024; Korczyn & Grinberg, 2024), significantly impacting global health and quality of life (Feigin et al., 2020; Korczyn & Grinberg, 2024). Despite substantial efforts, existing pharmacological interventions, which predominantly rely on targeting specific pathological hallmarks, have had limited success in effectively targeting cognitive deficits across these disorders (Kinon et al., 2024; Siskind et al., 2022; Saelens et al., 2024; Yildiz et al., 2023; Nierenberg et al., 2023; Jehi, 2025; Harpaz et al., 2017; Rajendran & Krishnan, 2024; Korczyn & Grinberg, 2024).

This limited therapeutic efficacy is often attributed to considerable clinical heterogeneity and poor alignment between targeted pathology and functional deficits. For instance, recent advances in disease-modifying therapies that reduce extracellular beta-amyloid plaques in Alzheimer's disease (AD) have yielded only marginal improvements in cognitive function, despite significant reductions in amyloid pathology (Rajendran & Krishnan, 2024; Korczyn & Grinberg, 2024).

Emerging evidence highlights aberrant neural network activity as a central pathological feature and a strong predictor of functional deficits across multiple psychiatric (Segal et al., 2023; Vanes & Dolan, 2021; Sha et al., 2019) and neurological conditions (Leng et al., 2023; Delbeuck et al., 2003; Zott et al., 2019). Brain stimulation techniques, which directly modulate neural activity, represent promising non-pharmacological therapeutic approaches (Camacho-Conde et al., 2022). Among these, surgical deep-brain stimulation (DBS) has achieved widespread clinical adoption for movement disorders such as Parkinson's disease and essential tremor (Cernera et al., 2021; Hariz & Blomstedt, 2022) and has been approved for severe refractory obsessive-compulsive disorder (OCD; Mar-Barrutia et al., 2021) and epilepsy (Bahadori et al., 2024). Additionally, DBS is being investigated for treatment-resistant depression (Mayberg et al., 2005; Reddy et al., 2024) and Alzheimer's disease (Majdi et al., 2023;

Davidson et al., 2024). However, DBS is associated with serious surgical risks and adverse effects, restricting its broader therapeutic and research potential (Majdi et al., 2023; Davidson et al., 2024).

Unlike DBS, Non-invasive brain stimulation (NIBS) techniques provide methods to modulate brain activity transcranially without surgical intervention. NIBS methods are associated with relatively low risk and minimal side effects, which has facilitated their widespread adoption in both clinical and healthy human research (Antal et al., 2022; Begemann et al., 2020; Grover et al., 2023). Among the NIBS methods, Transcranial magnetic stimulation (TMS) has been clinically approved for several psychiatric conditions, including treatment-resistant depression, migraine, and refractory OCD (Cotovio et al., 2023). Recently, it has also shown promising outcomes in targeting cognitive decline in AD (Huang et al., 2024). Similarly, Transcranial electrical stimulation (tES) techniques have been widely applied in research contexts to modulate cortical activity and associated cognitive functions (Grover et al., 2023; Majdi et al., 2022; Liu et al., 2018). Despite these advancements, the clinical utility of current NIBS methods remains limited due to their inability to effectively and selectively target deeper brain structures without engaging superficial cortical regions (Antal et al., 2017; Liu et al., 2018; Menardi et al., 2022; Vöröslakos et al., 2018).

Temporal interference (TI) electrical stimulation is a novel, non-invasive DBS method capable of selectively targeting deep brain regions without perturbing superficial cortical structures (Grossman et al., 2017). In the General Introduction, I outlined the principles and first-in-human validation of the physiological effects of TI in 20 healthy young adults (Violante, Alania et al., 2023). In this study, we demonstrated that TI stimulation delivered to the anterior hippocampus during the encoding of episodic memories selectively reduced task-evoked hippocampal BOLD signal without affecting overlying cortical regions or the contralateral hippocampus. Additionally, TI reduced functional connectivity between the hippocampus and associated cortical networks. However, these physiological changes did not translate into observable behavioural effects. This is likely due to experimental design, which prioritised the measurement of physiological responses over behavioural modulation. Specifically, stimulation was applied only during memory encoding, with ~96 s of total stimulation duration per condition per participant. Such short stimulation is unlikely to be sufficient to elicit measurable behavioural effects (Booth et al., 2022).

In light of these findings, we conducted a follow-up experiment to evaluate the effects of TI hippocampal stimulation on related memory function. This study aims to extend previous findings by increasing stimulation duration, applying TI stimulation throughout all task phases, and enhancing

statistical power by increasing the number of behavioural trials in a single-blind, sham-controlled cross-over study design.

2.2 Methods

2.2.1 Participants

Twenty-one healthy adults (10 females; age range: 19–30 years, mean age ±SD: 22.8 ± 3.2 years) participated in the experiment. All participants were right-handed and had university-level education. Following the study inclusion criteria, participants reported no history of neurological or psychiatric illness, were not taking any psychoactive medications, and were generally healthy. Ethical approval was granted by the Imperial College Research Ethics Committee (ICREC). Participants gave written informed consent and were compensated for their time. The study was conducted following the Declaration of Helsinki.

2.2.2 Experimental Design

A visual summary of the experimental design is displayed in **Figure 2.1**. The study employed a single-blind, within-subjects, sham-controlled crossover design, with participants undergoing both active TI and sham stimulation in two separate sessions. The stimulation sessions were separated by a minimum of 24 hours and a maximum of seven days, allowing sufficient time to prevent carryover effects while maintaining consistency in the study timeline. The order of stimulation conditions was counterbalanced across participants using a balanced Latin square to control for order effects.

2.2.3 Face-Name Task

The behavioural task was adapted from the face-name associative memory paradigm used in study 1, outlined in the General Introduction, with some modifications. Faces were selected from the Chicago Face Database (v.2.0.3; Ma et al., 2021; Ma et al., 2015) and represented diverse ethnic backgrounds, with an equal distribution of black and white individuals and a balance of male and female faces. The names were chosen from the Office for National Statistics (Baby names in England and Wales: 2021). Only names between five and seven letters were included, with gender-neutral or duplicate spellings excluded.

Each participant completed 12 blocks of face-name associations per session, with a total task/stimulation duration of ~34 minutes (range: 28.5 – 42.1 minutes). Each block was divided into three phases: encoding, maintenance, and recall. During encoding, 16 unique face-name pairs were presented on the screen for 2 s one at a time. The faces appeared centrally, with the corresponding names positioned directly beneath. Participants were instructed to study the pairs to the best of their

abilities for later recall. The encoding period was followed by a 40-second distractor task before the recall phase. This task required participants to make odd/even judgments on random numbers ranging between 1 and 99, presented on the screen in series. This segment was designed to prevent active maintenance of the face-name associations in working memory.

This was immediately followed by the recall phase, where each face was displayed again, this time accompanied by five name options. These included the “target” (correct name), two "foils" (names that had been presented within the same block but were associated with different faces), and two "distractors" (novel names that had not appeared in the block). Using a keyboard, participants were asked to select the name they thought belonged to the face as quickly but as accurately as they could. After making a selection, they were prompted to rate how confident they were in their response on a scale from 1 (not confident at all) to 4 (extremely confident). The recall phase was self-paced, but participants were given a maximum of 8 s for name selection and 3 s for the confidence rating. At the end of every 4 consecutive blocks, participants had a short break during which they were asked if they thought they had stimulation and how confident they were on a scale from 1 (not confident at all) to 10 (extremely confident). At the end of 12 blocks, participants were disconnected from the TI device and the electrodes were removed.

The experiment also included a delayed re-test session, conducted thirty minutes after the last recall block. During this phase, all face-name pairs from that session were presented on the screen in series with five optional names underneath, and participants were asked to select the correct names. The re-test maintained the same format as the initial recall phase but omitted the confidence rating. During the 30-minute delay, participants first completed a side-effects questionnaire adapted from Brunoni et al. (2017) and then watched a nature documentary to minimise potential rehearsal.

2.2.4 TI stimulation setup and protocol

The TI stimulation protocol was created to deliver 5 Hz stimulation to the left anterior hippocampus using a custom-made device previously described in Grossman et al. (2017).

Two high-frequency sinusoidal waveforms at 2 kHz and 2.005 kHz were applied via two pairs of self-adhesive transcutaneous electrical nerve stimulation (TENS) electrodes, cut into 1.5 cm by 1.5 cm square shapes with rounded corners. After cleaning the skin with an ethanol solution, the electrodes were attached to the participant’s scalp using Ten20 conductive paste and medical tape to ensure stable contact throughout the experiment. The electrodes were configured to optimise the maximum envelope modulation at the target region. Electrodes e1 and e3 were positioned on the left

hemisphere at the level of the nasion, with e1 placed anterior to e3. The exact positioning was determined by measuring 50% of the subject's half-head circumference from the nasion, e1 was then placed 2.5 cm anterior to this point, while e3 was placed 2.5 cm posterior, creating a 5 cm gap between their centres. Electrodes e2 and e4 were positioned on the right hemisphere at a plane just above the eyebrow, with e2 anterior to e4. Their placement was determined by measuring 20% of the subject's half-head circumference from the nasion for e2 (minus 1 cm) and 70% for e4 (plus 1 cm). Thus, e1-e2 formed the anterior electrode pair, while e3-e4 formed the posterior electrode pair (**Figure 2.1A**).

Each session comprised either a sham or active stimulation protocol administered in a counterbalanced order. In the active stimulation condition, a 2 kHz waveform at 1 mA was delivered via the e1-e2 electrode pair, while e3-e4 delivered 2.005 kHz at 3 mA. The 1:3 current ratio steered the electric field towards the e1-e2 electrode pair, shifting the peak of the interference modulation toward the anterior hippocampus.

Stimulation was delivered in four periods. The first period started 10 minutes before the face-name task (**Figure 2.1B**). During this period participants were at rest for 5 minutes and performed a choice response task (CRT) for the following 5 minutes while receiving TI. In the CRT an arrow appeared pointing left or right, and participants were instructed to press the corresponding arrow key on the keyboard as quickly as possible. After a short break, participants performed the face-name task divided into three stimulation periods of four blocks (12 in total), separated by short breaks. TI stimulation was delivered continuously throughout each set of four blocks with ramp up (5 s) and damp down (5 s) at the start and end of each set. Given the self-paced design of the recall phase, total stimulation duration varied between participants (stimulation during the face-name task: mean ± SD = 34.5 ± 3 min, range 29.37–40.35 min; total stimulation duration TI session: 44.53 ± 3 min, range 39.37–50.35 min, which included 10 min of stimulation before the face-name task, 5 min during rest and 5 min during the CRT).

The sham stimulation protocol was designed to mimic the sensory experience of active TI stimulation while ensuring that no meaningful neural modulation was delivered and participants remained blind to the stimulation condition. In the sham session, stimulation began 10 min before the face-name task, ramping up over 5 s similar to active TI, but was ramped down to 0 mA after 30 s. TI stimulation was then briefly ramped up (5 s) and immediately ramped down (5 s) again at the end of the 5-minute rest and the 5-minute CRT periods. This was then repeated at the start and end of each set of four continuous blocks of the face-name task.

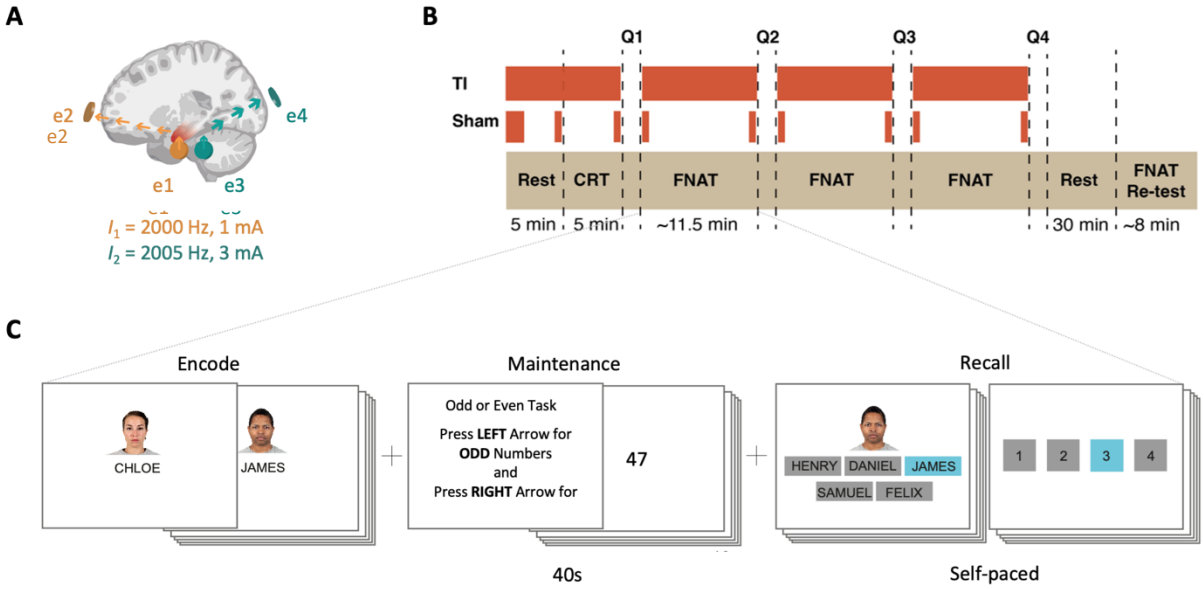


Figure 2.1 Experimental paradigm for TI stimulation of the hippocampus in healthy adults.

A. TI electrode setup and parameters optimised for targeting the anterior left hippocampus. The anterior electrode pair (e1–e2) delivered a 2 kHz sinusoidal waveform at 1 mA, while the posterior pair (e3–e4) delivered a 2.005 kHz waveform at 3 mA. This 1:3 current ratio ensured that TI was steered anteriorly, delivering a 5 Hz Δf to the anterior left hippocampus. **B.** Experimental timeline. The experiment comprised of two visits during which participants received either active or sham TI stimulation while performing a face-name task (FNAT). The condition order was counterbalanced across sessions using a balanced Latin square design. In the active stimulation condition, TI was delivered for 10 min before the face-name task; participants rested for the first 5 min and then performed a choice response task (CRT) for 5 min. In the CRT, an arrow appeared pointing left or right, and participants were instructed to press the corresponding arrow key on the keyboard as quickly as possible. Following CRT, participants performed 12 blocks of the face-name task presented in chunks of four blocks each, separated by short breaks. During each break, participants completed a questionnaire (Q1–Q4), reporting whether they thought they had received stimulation and rating their confidence on a scale from 1 (not confident at all) to 10 (extremely confident). After completing all 12 blocks, participants had a 30-min break during which they watched a nature documentary. After this break, participants were re-tested on the recall of face-name pairs. The sham condition mimicked the active stimulation protocol in every aspect except for stimulation delivery. During sham session, stimulation began 10 min before the face-name task, ramping up over 5 s similar to active TI, but was ramped down to 0 mA after 30 s. TI stimulation was then briefly ramped up (5 s) and immediately ramped down (5 s) again at the end of the 5-min rest and the 5-min CRT periods. This was then repeated at the start and end of each set of four continuous blocks of the face-name task. **C.** Face-name task paradigm. The memory task comprised of three phases: encoding, maintenance, and recall. During encoding, participants memorised 16 unfamiliar face-name pairs presented sequentially on-screen for 2 s each. Encoding was followed by a 40-s maintenance period, during which random numbers between 1 and 99 appeared on the screen one at a time. Participants responded whether each number was odd or even by pressing the left or right arrow key. Immediately after the maintenance phase, participants performed a self-paced recall task, during which they were tested on the previously memorised face-name pairs. After each recall response, participants rated how confident they were in their selection. Figure adapted with permission from Violante, Alania et al. (2023).

2.2.5 Stimulation sensation thresholding protocol

Before each experiment, participants' sensations and comfort during stimulation were assessed to determine their stimulation thresholds. This was done separately for low. frequency tACS and TI stimulation, and was carried out for each electrode pair separately (e1-e2 followed by e3-e4). During thresholding, stimulation started at 0.1 mA and was incrementally increased in steps of 0.1 mA until participants reported perceptual sensations, such as tingling, burning, or phosphenes, or until the predefined maximum stimulation intensity for that electrode was reached (2 mA for e1-e2 and 3 mA for e3-e4). The thresholding procedure results are summarised in **Table A1** and **Table A2.**

2.2.6 Data Analysis

Three primary behavioural outcomes were analysed: accuracy, measured as the proportion of correct names selected; reaction time, defined as the time taken to select a name during recall; and confidence ratings on a four-point scale. To assess the effect of the stimulation on performance, a generalised linear mixed model (GLMM) was used to compare accuracy between the TI and sham conditions. A separate binomial model was applied to assess correct versus incorrect responses, and reaction times were analysed using GLMM with an inverse Gaussian distribution.

2.2.7 Assessment of sham blinding and TI safety

The responses on the blinding questionnaire recorded at 4 points during the session were converted into weighted confidence scores by multiplying the confidence rating by -1 (participant did not think they received stimulation) or +1 (participant thought they received stimulation). For each time point and stimulation condition, the median score and associated 95% confidence intervals were estimated using a smooth bootstrap approach (Brown et al., 2001). This was performed with the *kernelboot* package in R, applying a Gaussian kernel and running 10,000 permutations for each probe point (Wolodzko, 2023). Safety was assessed using a post-stimulation side effects questionnaire (adapted from Brunoni et al., 2011). To statistically evaluate the strength and distribution of side effects, Wilcoxon signed-rank tests were performed using the coin package in R.

2.3 Results

2.3.1 TI Stimulation of the hippocampus enhanced episodic memory performance

All participants performed above chance on the face-name task (recall accuracy mean $\pm$ SD: 58.47 $\pm$ 14.73%, range 33.85–91.15%). The distribution of response types across the task followed the expected trend, with a higher proportion of responses for correct associations compared to foils and distractors, indicating that participants were engaged in the task (correct associations = 58.46%,

foils = 24.76%, distractors = 12.29%, omissions = 4.49%). Omission trials, i.e., where participants did not make a selection, were rare and thus excluded from the subsequent analyses.

TI stimulation had a significant effect on recall accuracy, with participants demonstrating a higher proportion of correctly recalled associations in the active TI condition compared to the sham condition ($\chi^2(2) = 6.35$, $p = 0.042$). Post hoc analyses confirmed that accuracy was significantly higher for target responses during TI ($M = 59.1$, $SD = 14.4$) than during sham ($M = 56.0$, $SD = 15.0$), $p = 0.007$. The number of foil ($p = 0.142$) and distractor ($p = 0.384$) responses did not differ between conditions (see **Figure 2.2A)**. The binomial model where the responses were collapsed in either correct or incorrect trials, confirmed that the odds of correctly recalling face-name pairs were high under the TI stimulation condition compared to sham ($\chi^2(2) = 5.85$, $p = 0.016$; **Figure 2.2B**). The confidence ratings did not differ between conditions ($\chi^2(1) = 0.35$, $p = 0.557$; **Figure 2.2C**). Stimulation duration, which varied slightly between subjects due to the self-paced recall phase, did not correlate with recall accuracy (r = -0.045, $p = 0.85$; Pearson correlation).

Overall, the main effect of the condition at re-test was not significant ($p = 0.175$; **Figure 2.2D**), however, when assessing the performance change from recall to re-test based on the response category (five categories were assessed: (1) Target -> Target refers to associations correctly identified in recall and re-test; 2,3) Target -> Foil/Distractor are associations correctly identified during recall but forgotten during re-test, with participant selecting foil or distractor, respectively; 4) Incorrect -> Target are associations incorrectly remembered at recall, but correctly matched at re-test; 5) Incorrect -> Incorrect are associations incorrectly remembered at both recall and re-test), a trend level main effect of stimulation was observed ($\chi^2(4) = 9.01$, $p = 0.061$), a greater number of associations correctly identified at both recall and re-test were present during TI 1:3 stimulation compared to sham (post-hoc test; $p = 0.027$; **Figure 2.2E**).

Analysis of the items that were correctly remembered at recall revealed a significant main effect of stimulation ($\chi^2(1) = 7.58$, $p = 0.006$) with significant effect of time of testing ($\chi^2(1) = 233.12$, $p < 0.01$) but no interaction effect ($\chi^2(1) = 0.063$, $p = 0.802$; **Figure 2.2F**). These results suggest that memories encoded under TI stimulation were better retained compared to sham. However, TI stimulation did not alter the rate of forgetting between recall and re-test.

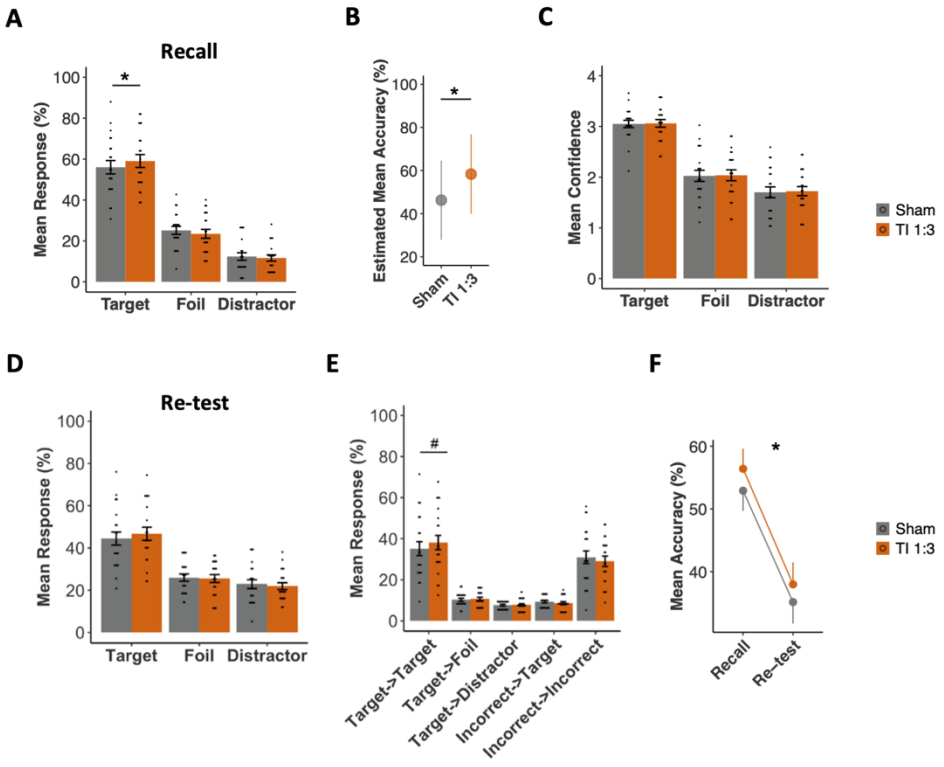


Figure 2.2 Effects of hippocampal TI stimulation on episodic memory recall

A. Participants showed higher accuracy in recalling face-name pairs during TI 1:3 stimulation compared to sham (GLMM: $\chi^2(2) = 6.353$, $p = 0.042$). Post-hoc paired t-tests revealed a significant increase in correctly remembered targets ($p = 0.007$) but no differences for foils ($p = 0.142$) or distractors ($p = 0.384$). **B.** A mixed-effects logistic regression model indicated higher odds of correct recall under TI stimulation ($p = 0.016$). **C.** Confidence ratings were unaffected. *$p < 0.05$; n = 21; Figure adapted with permission from Violante, Alania et al. (2023). **D.** Comparison of participants' memory performances during re-test between sham and TI 1:3 across response type (target, foil and distractor); there was no significant main effect of stimulation or interaction between stimulation and response type. **E.** Comparison between sham and TI 1:3 stimulation for the memory performance for each face-name pair. We assigned one of 5 categories to each face-name pair that summarise the outcome of each pair from recall to re-test: 1) Target -> Target are associations correctly identified in recall and re-test; 2,3) Target -> Foil/Distractor are associations correctly identified during recall, but forgotten during re-test, with participant selecting foil or distractor, respectively; 4) Incorrect -> Target are associations incorrectly remembered at recall, but correctly matched at re-test; 5) Incorrect -> Incorrect are associations incorrectly remembered at both recall and re-test. Cardinal (#) indicates significant exploratory post-hoc for Target ->Target condition, trend level main effect of stimulation**. F.** Comparison of correctly remembered items at recall. Improved recall observed in the TI 1:3 condition was maintained 30 min after initial recall (GLMM: $\chi^2(1) = 7.581$, $p = 0.006$.). Figure adapted with permission from Violante, Alania et al. (2023).

2.3.2 Effect of stimulation on reaction time

No significant differences were observed in response time (RT) between the TI and sham conditions during recall ($\chi^2(1) = 3.02$, $p = 0.082$) or re-test ($\chi^2(1) = 2.99$, p = 0.084; **Figure 2.3A-C**). Additionally, there was no interaction between stimulation condition and recall time ($p > 0.2$). These results indicate that TI selectively enhanced memory processing without altering overall processing speed.

In the CRT, no effect of stimulation was observed on accuracy (LMM: $\chi^2(1) = 0.18$, $p = 0.672$, accuracy mean ± SD, sham: 99.7±5.4%; TI: 99.6±6%) or median reaction times (LMM: $\chi^2(1) = 3.51$, $p = 0.061$, reaction time for correct trials, median ± SD, sham 0.39 ± 0.07 s; TI: 0.40± 0.08 s).

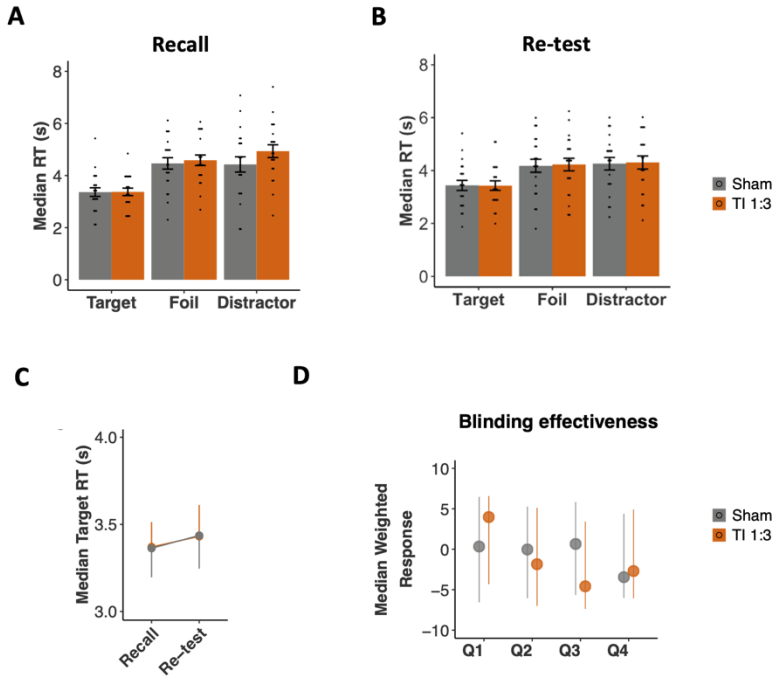


Figure 2.3 Effect of hippocampal TI stimulation on episodic memory reaction time

A. Comparison of participants' reaction time between sham and TI 1:3 across response type (target, foil and distractor) during recall; there was no significant main effect of stimulation or interaction between stimulation and response type. **B.** No differences were observed in reaction time at re-test. **C.** Reaction time for items successfully recalled. No stimulation effects were observed. **D.** Blinding effectiveness. There were no significant differences in perceived stimulation between sham and TI 1:3 conditions. n = 21; Figure adapted with permission from Violante, Alania et al. (2023).

2.3.3 Blinding and Safety

Analysis of the blinding effectiveness showed no significant difference between TI stimulation and sham in participants' ability to correctly identify the stimulation condition ($p > 0.2$), suggesting successful blinding (**Figure 2.3D; Table A3)**. TI stimulation was well tolerated, with no serious adverse effects reported. Mild side effects, such as itchiness at the electrode site, were slightly more common in the active TI condition compared to the sham ($Z = -2.35$, $p = 0.019$). However, other reported sensations, including tingling, fatigue, or discomfort, were comparable between conditions (**Table A4**).

2.4 Discussion

The present study provides evidence that TI stimulation targeting the hippocampus can enhance hippocampal-dependent episodic memory in healthy young adults. Combined with our initial findings from the neuroimaging experiment, these results provide the first-in-human validation of TI as a method for non-invasive DBS.

Our initial neuroimaging experiment was designed to probe the focal physiological effects of TI and showed that transient application of TI stimulation with theta-band difference frequency during the encoding of new memories reduced task-evoked BOLD signal. The strongest effects were observed when TI stimulation was steered towards the anterior segment of the hippocampus, which is consistent with previous research demonstrating the critical role of this region in the successful encoding of face-name associations (Chua et al., 2007; Sperling et al., 2003; Zeineh et al., 2003). No effects were observed in the contralateral hippocampus or the cortical regions underneath the electrodes. These results provided robust evidence for the focal neuromodulatory effect of TI on hippocampal activity.

The follow-up study presented here extended these findings by demonstrating that TI stimulation of the anterior hippocampus not only modulates memory-related neural activity but also enhances hippocampal-dependent episodic memory function. By applying ~20 times longer stimulation continuously during encoding, maintenance and recall, and increasing the number of face-name association trials, we increased the statistical power of the behavioural experiment and showed that TI improved episodic memory accuracy, and this benefit was maintained at re-test administered 30 minutes later.

While the magnitude of memory improvement during TI was small, it is consistent with studies investigating tACS effects on memory in healthy adults (Booth et al., 2022; Grover et al., 2023).

Moreover, a recent meta-analysis found that the largest cognitive benefits of tACS were observed in clinical and ageing populations compared to healthy adults (Grover et al., 2023), highlighting the translational potential of non-invasive stimulation strategies like TI.

What is the possible mechanism by which theta-band TI stimulation of the hippocampus improves episodic memory function?

Hippocampal theta oscillations (4–8 Hz) are known to organise spike timing during memory encoding and retrieval by modulating neuronal excitability across the theta cycle. This rhythmic modulation promotes spike synchrony, enhances signal propagation, and enables synaptic plasticity via spike-timing-dependent plasticity (STDP; Herweg et al., 2020; Wang et al., 2023). In this framework, the theta cycle functions as a temporal gate for learning, opening discrete windows for synaptic potentiation at specific phases. Crucially, this mechanism depends not on overall firing rates, but on the precise timing of spikes relative to the theta phase.

TI stimulation may enhance episodic memory by rhythmically modulating hippocampal excitability at theta frequency, increasing the probability that spikes occur during plasticity-favourable phases. In non-human primates, TI has been shown to bias the timing of neuronal spiking (Vieira et al., 2024). By applying rhythmic modulation at theta frequency during encoding, TI may increase the likelihood that hippocampal spiking occurs at plasticity-conducive phases, thereby facilitating stronger binding of face-name pairs and supporting memory formation that persisted over the 30-minute delay. This also suggests that repeated TI stimulation could progressively strengthen hippocampal memory networks by reinforcing theta-phase dependent long-term potentiation (LTP), providing a mechanistic rationale for evaluating multi-session TI as a strategy to improve memory.

Overall, TI stimulation was well tolerated, and no adverse effects were reported. The stimulation side effects were mild and primarily related to skin sensations, which are commonly reported with tACS protocols (Antal et al., 2017). The estimated current densities used in this study were within the established safety limits for human tES protocols (Bikson et al., 2016; Antal et al., 2017). Compared to low frequency tACS, sensory thresholds for TI stimulation were substantially higher, enabling us to deliver maximum pre-defined currents without compromising blinding effectiveness, which is a frequent challenge in tES protocols (Antal et al., 2017).

In summary, our findings demonstrate that TI stimulation targeting the anterior hippocampus can modulate task-evoked neural activity and improve hippocampal-dependent episodic memory with

minimal side effects, providing a solid foundation for further investigation of TI as a non-invasive DBS approach. These results also justify evaluating repeated TI in clinical populations such as Alzheimer's disease, particularly given that cognitive benefits are likely to be most pronounced in these groups (Grover et al., 2023), which I explore in the following chapter.

Finally, the present study highlights a broader challenge in NIBS research: although we observed both physiological and behavioural effects of TI, these were assessed in separate experiments. Thus, we cannot directly link focal neuromodulation effects to memory improvement. The most direct approach for establishing causal links between tES-induced neural perturbations and behavioural outcomes is to monitor brain activity in real time. However, this remains a technological challenge across all tES methods, including TI – a challenge I aim to address in Chapter 4.

Chapter 3: Repeated TI Stimulation of The Hippocampus in Alzheimer's Disease

3.1 Introduction

Alzheimer's disease (AD) is a neurodegenerative disorder and one of the leading causes of disability in the elderly worldwide (Scheltens et al., 2021). It has been identified as the most common cause of age-related dementias, for which the number of cases is expected to triple by 2050, exceeding 150 million (Chen et al., 2024). Clinically, AD is characterised by slow and progressive cognitive decline (Knopman et al., 2021), with an amnestic phenotype accounting for approximately 85% of cases (Dubois et al., 2023). At the cellular level, pathologies typically start decades before the onset of clinical symptoms and are characterised by extracellular deposits of amyloid-β (Aβ) plaques and intracellular neurofibrillary tangles (NFTs) composed of hyperphosphorylated tau (Hampel et al., 2021; Knopman et al., 2021; Palop and Mucke, 2016). The initial formation of Aβ plaques typically begins in neocortical regions and spreads to subcortical structures (Therriault et al., 2024; Taddei & Duff, 2025) while NFTs typically begin in subcortical structures such as the hippocampus and later progress to neocortical areas (Palop and Mucke, 2016; Zheng & Wang, 2025; Knopman et al., 2021). These aggregations are neurotoxic and can lead to neuroinflammation, neuroplasticity changes and, eventually, cell death (Duyckaerts et al., 2009).

Until recently, pharmacological treatments for AD offered only temporary mitigation of symptoms that eventually become ineffective as the disease progresses (Rajendran & Krishnan, 2024; Zhang et al., 2024). Advances in disease-modifying therapies for AD have been very recent, with three anti-amyloid monoclonal antibody (mAb) treatments having been approved by the FDA since 2021 (Kim et al., 2025). However, while these treatments have been effective in substantially reducing brain amyloid levels, the effects on cognitive decline or recovery have been minimal, and medication side effects are significant (Kim et al., 2025; Zhang et al., 2024).

The repeated failure of anti-amyloid therapies, despite decades of research and development, has led to a growing consensus that AD treatments should prioritise multi-target approaches aligned with disease complexity, highlighting the need for increased research into alternative therapeutic strategies (Rajendran & Krishnan, 2024; Korczyn & Grinberg, 2024).

System-level interventions targeting neural circuit activity are among the leading approaches to addressing cognitive decline in AD. The dynamics of neural circuits and network activity form the

fundamental basis of core cognitive processes, including perception, information processing, learning, memory, and higher-order cognitive functions (Medaglia et al., 2015; Buzsáki & Watson, 2012). Disturbances in these neuronal dynamics critically impair neural communication, leading to cognitive dysfunction observed across neurological and psychiatric conditions (Buzsáki et al., 2006; Buzsáki & Watson, 2012; Hanslmayr et al., 2019). A large number of electrophysiological and neuroimaging studies have revealed widespread network dysfunction in AD. For example, several studies show hippocampal hyperactivity during episodic memory encoding (Mondadori et al., 2006; Palop & Mucke, 2016; Stam et al., 2023), generalised slowing of neural oscillations, reduced inter-regional coherence and diminished oscillatory complexity (Jeong, 2004; Jafari et al., 2020; Lejko et al., 2020). Additionally, disruptions in excitation-inhibition balance and impairments in neural plasticity have also been documented (Chou et al., 2022; Targa Dias Anastacio et al., 2022; van Nifterick et al., 2023).

Dysregulation of intrinsic neuronal firing patterns is not only an early biomarker of AD but also actively contributes to its progression. For example, a recent study found that Aβ promotes tau spreading by inducing neuronal hyperactivity and hyperconnectivity, particularly between tau epicentres and functionally connected brain regions (Roemer-Cassiano et al., 2025). This aligns with previous neuroimaging evidence linking AD pathology to aberrant large-scale network dynamics (Vogel et al., 2023). Beyond facilitating the accumulation and propagation of pathological proteins, this hyperactivity places excessive metabolic demands on neurons and disrupts local bioenergetic homeostasis (Cunnane et al., 2020), ultimately destabilising the intrinsic mechanisms that maintain normal circuit function (Tzioras et al., 2023; Slutsky et al., 2018). The convergence of molecular pathology, metabolic stress, and network-level instability thus initiates a self-reinforcing cycle that ultimately results in synaptic dysfunction and loss, a key precursor to cognitive decline in AD (Taddei & Duff, 2025). Targeting aberrant neuronal activity may therefore offer a promising therapeutic strategy to interrupt this pathological cascade and preserve synaptic and cognitive function.

Electrical brain stimulation modalities in which weak electric currents are applied to the brain transcranially or via implanted electrodes can be used to directly modulate neural activity. Invasive DBS is clinically used to treat motor symptoms in patients with medication-refractory Parkinson's disease (PD) and essential tremor (Cernera et al., 2021; Hariz & Blomstedt, 2022). Additionally, recent evidence suggests that DBS can inhibit or reverse the reduction in mitochondrial volume in the substantia nigra of PD patients, which may enhance metabolic plasticity and support mitochondrial biogenesis or fusion, potentially delaying neuronal degeneration (Mallach et al., 2019). DBS has also been tested in AD; however, the results have been inconclusive as the effects are highly variable across patients, with some individuals even experiencing worsening symptoms (Aldehri et al., 2018; Majdi et

al., 2023). Despite a strong mechanistic rationale, the clinical use of DBS in AD remains limited by the risks associated with brain surgery, particularly in an elderly and cognitively vulnerable population. Consequently, exploratory research is limited, which, combined with the complexity of the disease, poses significant challenges for patient selection and the identification of optimal stimulation targets (Majdi et al., 2023).

Non-invasive, transcranial electrical stimulation (tES) is a low-risk method to modulate brain activity. Transcranial alternating current stimulation (tACS), in particular, has gained popularity as a tool to modulate neural activity and related functions in a frequency-dependent manner (Herrmann et al., 2013; Helfrich et al., 2014; Antal et al., 2017; Wischnewski et al., 2023). A growing number of studies have shown positive effects of tACS on cognition, especially memory, with larger benefits often observed in clinical populations (Grover, 2024; Diedrich et al., 2024; Lee et al., 2023; Shtoots et al., 2024; Wang et al., 2024). While tACS studies in AD are still limited, several have reported memory improvements (Kehler et al., 2020; Benussi et al., 2021, 2022; Tang et al., 2024). One study also reported trends toward a reduction in tau burden, suggesting potential disease-modifying effects of tES (Dhaynaut et al., 2020, 2022). However, tES approaches (including tACS) have several constraints that limit their clinical utility. Critically, tES can only effectively and selectively modulate neural activity in superficial cortical regions, as the electric fields are strongest just beneath the electrodes (Liu et al., 2018; Antal et al., 2017; Vöröslakos et al., 2018). This presents a major limitation for using tES in AD, where early dysfunction and pathology emerge in deep brain structures like the hippocampus.

Recently, our lab has developed a novel brain stimulation strategy that enables non-invasive DBS. The strategy, called temporal interference (TI) brain stimulation, uses two high-frequency electric fields, which are offset by a low frequency difference (Grossman et al., 2017). Due to their low-pass filtering properties, neurons do not respond to high frequencies, which allows the current to pass through the cortex without engaging the overlaying cortical regions. At the point of overlap, the two fields create an amplitude-modulated (AM) waveform where the envelope of the carrier frequencies varies periodically at the difference frequency (Δf). When the Δf is, set within the dynamic range of neural activity, neurons respond to this envelope frequency while, due to their low-pass filtering properties, the carrier frequencies are assumed to have no effect. The TI stimulation was first validated in mice using both electrophysiological and imaging c-fos as a biochemical marker of activation (Grossman et al., 2017).

We then conducted the first-in-human validation of TI stimulation for non-invasive DBS through a combination of field modelling, cadaver recordings, neuroimaging, and behavioural studies. Electric

field simulations and direct intracranial recordings in a human cadaver confirmed that the TI fields could be targeted to the hippocampus with minimal exposure to the overlying cortex. In a neuroimaging experiment, transient application of theta-band TI during memory encoding modulated task-evoked hippocampal BOLD activity, with the strongest effects observed when stimulation was directed towards the anterior segment. A follow-up behavioural study, which I presented in Chapter 2, showed that prolonged TI stimulation during face-name tasks enhanced memory performance, with effects persisting at re-test. Together, these findings provide compelling support for exploring TI as a non-invasive DBS strategy to target episodic memory dysfunction in AD, where stimulation effects may be greater relative to healthy populations (Grover et al., 2023).

Building on this work, the present chapter reports the first in-patient clinical study investigating the effects of repeated, multi-session TI stimulation of the hippocampus in 21 AD patients.

The primary aim of this study was to assess the feasibility, safety, and potential efficacy of repeated TI stimulation in AD patients. Specifically, the study aims to:

a. Evaluate the safety and tolerability of repeated hippocampal TI stimulation.

b. Examine the effects of TI stimulation on memory and cognitive function, using standardised and custom-designed neurocognitive test batteries.

c. Assess the impact of TI stimulation on hippocampal bioenergetics and vascular function, through:

1. Mitochondrial complex I density, measured via [^{18}F]-BCPP-EF PET imaging.
2. Regional cerebral blood flow (CBF), assessed via pseudo-continuous arterial spin labelling (pCASL).

Based on these aims, I hypothesised that, compared to baseline measures, repeated TI stimulation of the hippocampus in AD patients:

a. Would be well tolerated, with no adverse effects beyond those expected from conventional tACS.

b. Would enhance hippocampal-dependent memory function, as measured by episodic memory tasks.

c. Would (i) increase hippocampal mitochondrial complex I density, as measured by [^{18}F]-BCPP-EF SUVR, and (ii) increase regional blood perfusion, with greater effects expected in the left (stimulated) versus right (unstimulated) hippocampus.

These findings provide feasibility evidence supporting the safety, tolerability, and procedural viability of repeated TI stimulation in AD patients. Furthermore, observed selective improvements in episodic memory performance provide a rationale for future double-blind, sham-controlled trials to evaluate the efficacy and therapeutic potential of TI as a non-invasive neuromodulatory intervention targeting cognitive decline in AD.

3.2 Materials and methods

3.2.1 Study participants

The patient recruitment chart is shown in **Figure 3.2**. Patients with a diagnosis of AD or MCI due to probable AD were recruited from two patient identification centres (PIC) or were self-referred through advertisements. In total, 331 patients were referred; of these, 144 were pre-screened. Pre-screening was done remotely, and over the phone, patients were given information about the study, assessed on inclusion/exclusion criteria, and provided data on their AD diagnosis, general health, and social settings. The study's inclusion and exclusion criteria are shown in **Table A5**. Thirty-three patients came in for the screening procedure, which lasted approximately 4 hrs and involved the following:

- a detailed familiarisation of patients and their chaperones with the study design and procedures
- confirmation of inclusion/exclusion criteria by completing a screening questionnaire
- safety screening for PET, MRI, and TI
- signing of informed consent
- MMSE assessment
- a clinical interview and examination by a neurologist
- a familiarisation to TI stimulation
- a training run of memory tasks and
- blood sample collection and electrocardiogram (ECG)

Of the 33 patients screened, 24 were recruited for the study. Three patients dropped out at or following the baseline scan: 1 patient experienced a panic attack in the scanner due to the confined space and withdrew from the study. Another patient withdrew due to concerns about radiation exposure associated with the PET scan. The third patient was excluded following an incidental clinical finding in the brain scan. Thus, 21 patients completed the study. The individual patient information and demographics are shown in **Table 3.1.** The summary of demographics and clinical characteristics is presented in the results.

The study followed the ethical standards outlined in the Declaration of Helsinki. Ethical approval was granted by the Health Research Authority (HRA), the Health and Care Research Wales (HCRW), and the Research Ethics Committee (REC). The study was conducted at Imperial College (IC) Hammersmith Hospital Campus. The screening, neurocognitive assessments and TI stimulation sessions took place

Table 3.1 Individual patients' demographic data, clinical diagnosis, and testing status.

N	Age	MMSE	Diagnosis	Gender	Medication	Testing Status
1	76	28	MCI	M	Donepezil	Did not complete post PET due to radiation concerns
2	53	25	AD	F	Donepezil	Withdrew at baseline scan due to panic attack
3	74	20	AD	M	Memantine	
4	65	30	MCI (post-stroke MCI/ probable mixed dementia)	M	Donepezil	
5	79	26	AD	F	None	Missed day 10 and did not complete post neurocognitive assessment due to frustration with the length of the study protocol
6	82	26	AD	M	Donepezil	Missed day 9 due to ill health (unrelated to the stimulation)
7	70	24	AD	F	Donepezil	
8	79	20	AD	F	Donepezil	
9	76	29	MCI	F	None	Withdrew at baseline scan due to PET radiation concern
10	78	24	MCI	M	Donepezil	Excluded at baseline scan due to incidental finding
11	77	24	AD	F	Donepezil	
12	62	21	EOAD (LPA)	F	Donepezil	Missed day 9 due to fever
13	64	27	EOAD	M	Rivastigmine	
14	63	26	EOAD (LPA)	F	Donepezil	
15	75	27	AD	F	Donepezil	
16	65	25	EOAD	M	Donepezil	
17	79	28	MCI	F	None	Did not complete post PET due to failed tracer production
18	75	25	AD	M	Donepezil	
19	70	30	AD	M	Donepezil	
20	86	28	MCI	M	None	
21	74	24	AD	F	Memantine	
22	77	29	AD	F	Donepezil	
23	69	23	AD	F	Donepezil	
24	70	22	AD (LPA)	M	None	

LPA: Logopenic progressive aphasia, a rare form of Alzheimer's disease characterised by slow speech and word-finding difficulties. N.B. P03 and P04 are missing from the table because these patients were given subject numbers during screening, although they eventually failed screening and thus were never recruited to the study.

at the Clinical Imaging Facility (CIF), and the blood tests and health assessment were done at the Imperial College Research Facility (ICRF). Brain imaging took place at Invicro. The study was funded by the UK Dementia Research Institute (DRI) and the Alzheimer's Association (AA).

3.2.2 Study design

The study protocol consisted of 14 consecutive visits, excluding weekends. It was divided into three sections: a baseline neurocognitive and brain imaging assessment administered on two separate visits, 10 daily TI stimulation sessions during which patients performed associative memory tasks, followed by post-assessment sessions of imaging and cognition. See the study timeline in **Figure 3.1**.

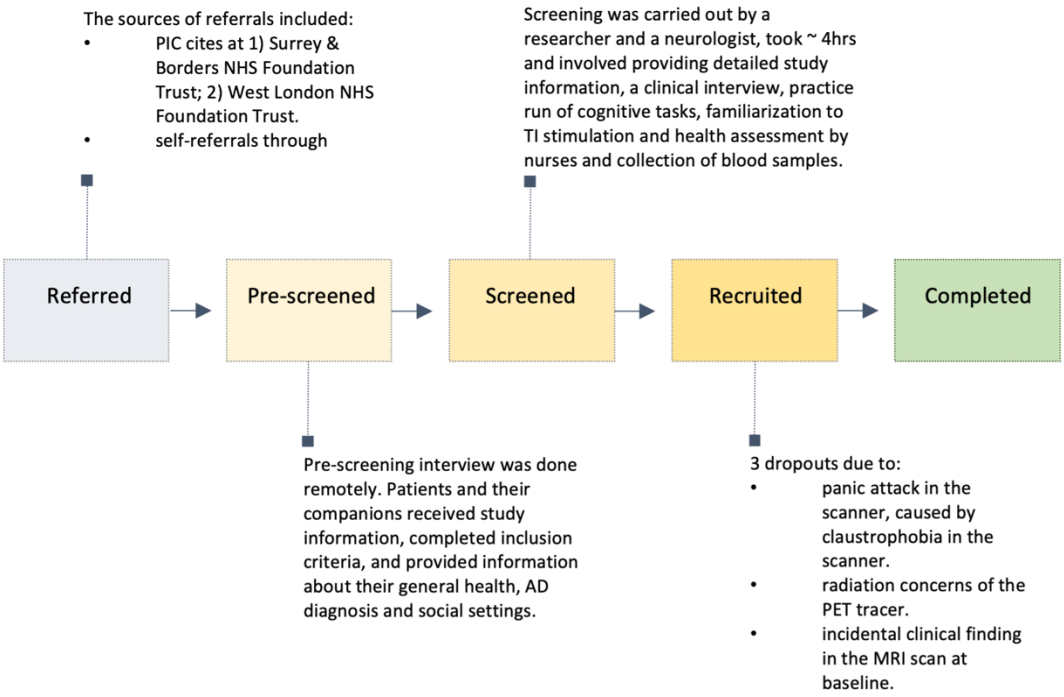


Figure 3.1 Patient recruitment flow chart.

3.2.2.1 TI stimulation protocol

Participants received a total of 50 minutes of daily TI stimulation in blocks of 5 minutes while they performed associative memory tasks, with 10 blocks in total per day. Each session started by completing a safety questionnaire to assess patients' general health, alcohol intake and hours of sleep from the previous day, and caffeine intake on the day (patients were advised to allow at least 2 hours between caffeine intake and TI stimulation). Finally, any side effects from the previous TI session were recorded. The TI electrode setup and stimulation parameters mirrored the study conducted in healthy young adults and are detailed in Chapter 2. In short, four 1 cm × 1 cm electrodes were attached to patients' scalps (**Figure 3.4**). The location of the electrodes was determined based on the patients' head circumference using the system described earlier. Each stimulation session started with a thresholding procedure and used the following parameters to target 5 Hz TI at the left hippocampus:

e1-e2 electrode pair delivered 2000 Hz current at 1 mA, and e3-e4 2005 Hz at 3 mA. To avoid charge accumulation and skin sensations, the current was ramped up for 5 s from 0 mA to the target amplitude and remained in stable delivery for 5 min before it was ramped down to 0 mA for 5 s. During TI stimulation, patients performed associative memory tasks (**Figure 3.3**). Five different tasks were custom-designed and piloted in healthy older adults to adjust parameters for AD patients. Each task

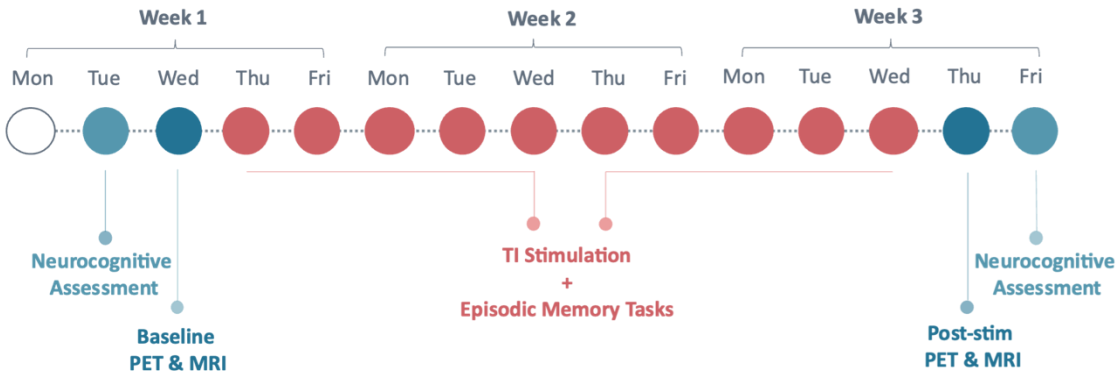


Figure 3.2 The study timeline.

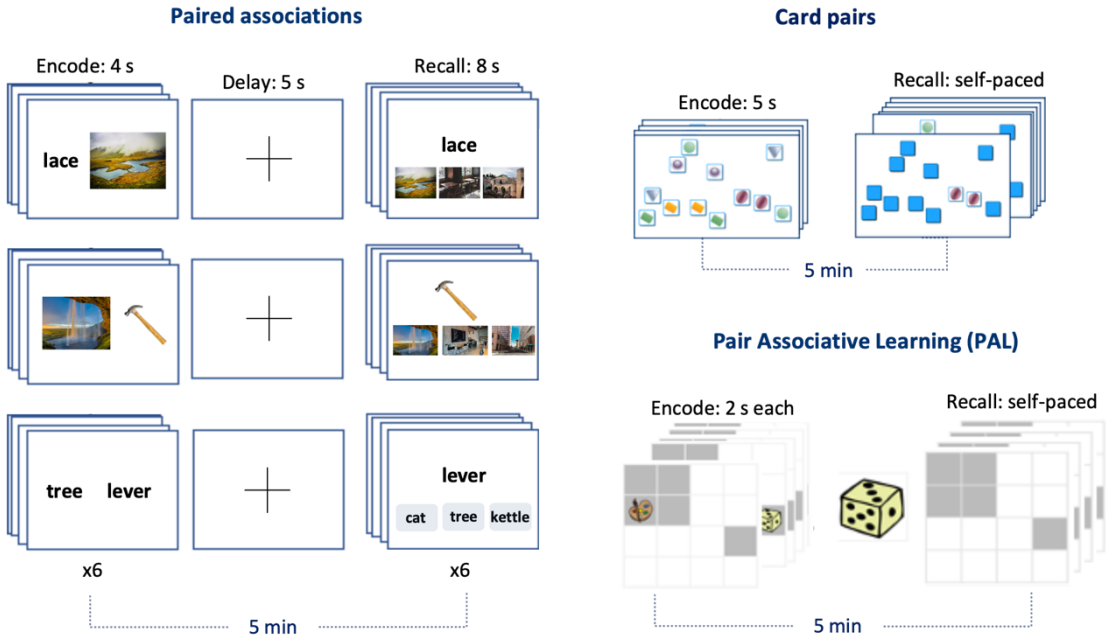


Figure 3.3 Memory tasks performed during TI stimulation.

took 5 minutes to complete and was repeated twice (thus 10 blocks of 5 tasks with two runs each). The task order was counterbalanced across 10 days using a Latin square and was kept the same across patients. For each 5-minute block, TI stimulation and the task started and finished at the same time, manually by the researcher. Patients took approximately 1-minute breaks between blocks, with a longer ~5-minute break after completing five blocks. During the practice run with the second patient at the screening visit, it became clear that patients who struggled with memory tasks and got anxious about performance. Thus, to ensure that they completed the tasks, patients were instructed as follows: “The goal of the task is memory engagement, try to memorise as many pairs as you can, but don’t worry too much about the performance”. At the end of the final block, patients completed a post-stimulation side effects questionnaire.

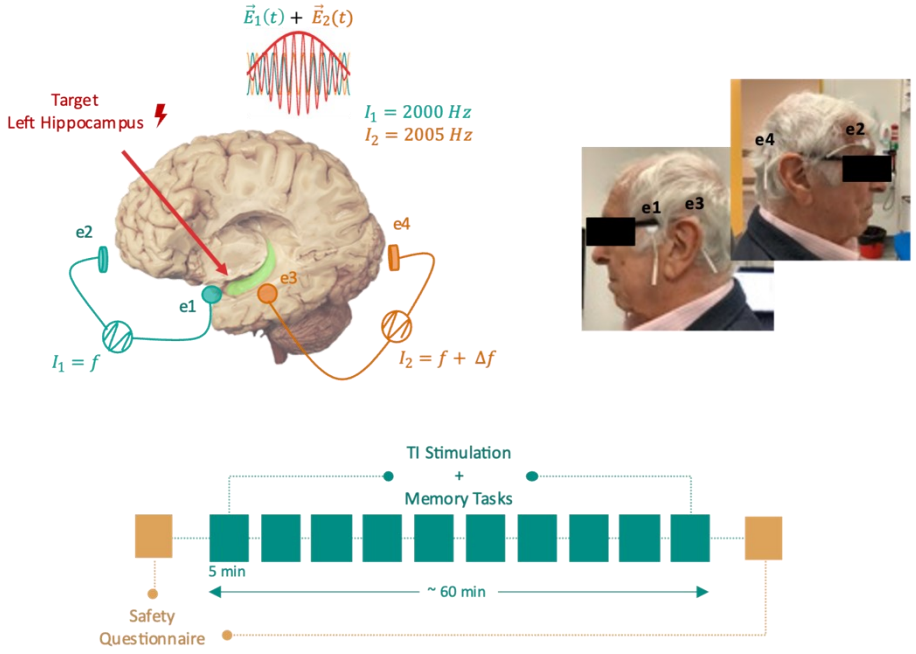


Figure 3.4 Hippocampal TI stimulation protocol in AD patients.

3.2.2.1.1 Memory tasks battery during TI stimulation

Three associative memory tasks were created to mirror the face-name association task used in the first study. These included word-scene, word pairs, and object-scene association tasks (**Figure 3.3**). Two other tasks, card pairs and paired associates learning with objects and locations, were adapted from the CogAssess application (Hampshire et al., 2022). All tasks were performed on an iPad.

Word-pair associations (WPA). The word stimuli for the task were selected from the SUBTLEX UK database, which includes words from the subtitles of daytime TV shows (van Heuven et al., 2014). The words were filtered based on type, frequency, length, and concreteness. The final dataset included a total of 1135 singular nouns with frequency > 100, concreteness > 4.0 and word length between 3 and 7 characters. The selection of stimuli was done based on previous research showing that the imaginability of the word in recognition memory tasks (i.e., concreteness) enhances hippocampal engagement (Caplan & Madan, 2016; Clark et al., 2018). The task comprised three stages: encoding, maintenance, and recall. During encoding a pair of words appeared in the centre of the screen for 4s followed by 750 ms $\pm$250 ms jittered inter-stimulus interval (ISI) and another novel pair. Six unrelated word pairs were presented in total. The encoding was followed by a 5-second delay with a fixation cross, and finally, a recall, during which one of the previously learned words appeared in the centre of the screen with three-word options below: the target, one foil (a word paired with a different stimulus in the same block) and one distractor (a previously unseen word). Patients were asked to select which word they thought was paired with the one above during the memorisation stage. They had 8 seconds to select, after which the task moved onto the next trial. Patients performed as many trials as they could in 5 minutes. The position in which the probe and the target stimuli appeared during encoding and recall, respectively, was randomised. Unique stimuli were used on each day across 10 days. The primary outcome measures of WPA were accuracy and response time (RT) for correct trials.

Word-scene associations (WSA). The WSA mirrored the task design of the WPA except for the stimuli. The words were selected from the same database as in WSA. I created a new scenes database for this task with 1333 unique images of scenes sourced from Unsplash (https://unsplash.com/). Scenes were divided roughly equally into three categories: outdoor nature, outdoor man-made (images of cities and man-made structures) and indoor scenes. During encoding, 6 images were selected equally from each category, and during recall, each of the three options was from one of each category. This was done to make the task easier for patients and to have enough unique stimuli for the 10 days. The primary outcome measures of WSA were accuracy and RT for correct trials.

Object-scene associations (OSA). This task also mirrored the design of WPA and WSA, except for the stimuli. The images of scenes were selected from the custom-made database used in WSA; The Bank of Standardised Stimuli (BOSS) was used for objects (Brodeur et al., 2014). During recall, patients selected which of the three scenes paired with the displayed object. As in WPA and WSA, unique stimuli were used across the 10 days, and none of the stimuli were reused from the other tasks with

the same stimulus type. The primary outcome measures of WSA were accuracy and RT for correct trials.

Paired associates learning (PAL). The PAL task is a well-established episodic memory assessment tool used in AD (Égerházi et al., 2007; Barnett et al., 2016) and has been shown to activate the hippocampus bilaterally in a load-dependent manner in patients with AD (de Rover et al., 2011). The PAL task in this study was adapted from the CogAssess application. During encoding, objects appeared in a random location on shaded squares of an 8 x 8 grid. Each object was displayed for 2 s and disappeared, and was immediately followed by another object in another location. The task started with a cognitive load of 5 items; patients were instructed to remember the object and location pairs. The Recall phase followed immediately after encoding, where the same icons appeared one at a time on the left side of the screen, the patient was asked to tap on the location in the grid they believe the icon was shown. In the case of error, the next round of encoding started with n – 1 items to memorise. If the patient completed the round successfully 3 times in a row, the encoding load increased to n + 1. The primary outcome measure of this task was the longest sequence successfully recalled.

3.2.2.1.2 TI safety and tolerability assessment

The primary outcome measures for the safety and tolerability of TI were side effects frequency, intensity and skin sensation threshold data recorded via standard and custom-made questionnaires. Post-stimulation side-effect data were acquired using a questionnaire adapted from Brunoni et al. (2011). At the end of each stimulation session, patients reported whether listed side effects were present, rated their severity and whether they thought they related to the TI stimulation (**Table A6**). A second questionnaire was custom-made and administered before the start of each stimulation session. It recorded information on patients' general health, sleep, alcohol, and caffeine intake and whether they experienced any side effects from the previous TI session (i.e., 24 hours later). Tolerability was recorded using a custom-made questionnaire administered during the TI parameter thresholding. Subjective sensations under each electrode pair were logged at varying intensities of TI current, starting from the minimum 0.2 mA and increasing in steps of 0.2 mA until the maximum intensity was reached (1 mA and 3 mA in the anterior and posterior electrode pairs, respectively) or patients experienced discomfort. Sensation thresholds were also logged for low frequency transcranial alternating current stimulation (tACS) stimulation administered at 5 Hz. For tACS, stimulation started at 0.1 mA and increased in steps of 0.1 mA until participants reached their comfort threshold.

3.2.2.2 Neurocognitive assessment at baseline and post-TI

Each session took approximately 3 hours to complete and included a battery of standard neurocognitive tests and custom-made tests developed in-house. One patient did not complete the post-neurocognitive assessment. These tests were divided into two groups: “Episodic Memory Tasks” and “General Cognition Tasks”. The former included the group of tasks that tend to be associated with episodic memory in the literature. The latter group comprised tasks from various cognitive domains, including executive function, visuospatial processing, processing speed, crystallised intelligence, and lexical processing. See **Table 3.2**, **Figure 3.5** and **Figure 3.6** for task summary and diagrams. Since the National Adult Reading Test (NART; Bright et al., 2018) is used to measure general intelligence, it was excluded from the analysis.

3.2.2.2.1 Episodic memory tasks

Word Memory (Immediate). 24 English words were presented sequentially on the screen for 1000 ms (encoding time). Words were randomly drawn from three categories: animals, vegetables, or clothes. Immediately after encoding, 24 words were presented on the screen sequentially. Patients were asked to assess whether the word appeared in the original list by responding “Yes” or “No”. 50% of the words in the recall stage were non-targets, of which half were foils (semantically similar words to the target). The main outcome measure was the percentage of accurately identified targets of the total presented trials. The secondary outcome measure was median RT.

Word Memory (Delayed). Patients were presented with the same task as above; however, the encoding period was removed. Thus, patients were asked to remember the stimuli presented approximately 15 minutes earlier. The main outcome measure was percentage accuracy as described above. The secondary outcome measure was median RT for correct trials.

Object Memory (Immediate). Participants were asked to memorise 20 black-and-white images of everyday objects presented sequentially on the screen for 2000 ms, with an ISI of 500 ms. Immediately after encoding, each stimulus was presented in turn within a grid of 7 distractors. The distractors are categorised by how similar they are to the stimulus along 3
dimensions. The dimensions are:

- Item - whether the image is of the same item as the target.
- Precision - whether the image is of the same pose or artistic style as the target.
- Mis-binding - whether the image is flipped left or right.

All 20 images were presented in a random order during recall. The main outcome measure was percentage accuracy, where all Item features were accurately recalled. Secondary measures included

Table 3.2 Neurocognitive tasks administered at baseline and post-TI stimulation.

Task Domain	Cognitive Domain	Task	Abbreviation	Delivery Mode
Episodic Memory	**Episodic Memory**	Word Memory (Immediate & Delayed)	WM-I WM-D	iPad
		Logical Memory (Immediate & Delayed)	LM-I LM-D	Verbal
		Object Memory (Immediate & Delayed)	OM-I OM-D	iPad
		Recognition Memory (Faces & Scenes)	RM-Faces RM-Scenes	PC
General Cognition	**Executive Function**	Digit Span	DS	iPad
	Visuospatial Processing	Dot-counting	DC	Pen & Paper
		Position Discrimination	PD	Pen & Paper
		Cube Analysis	CA	Pen & Paper
	Processing Speed	2D Manipulations	2D-Manip	iPad
		Choice Response Task	CRT	iPad
		Motor Control	MC	iPad
	Lexical Processing	Graded Naming Test	GNT	Pen & Paper
		Verbal Fluency (Semantic, Phonetic)	VF-S VF-P	Pen & Paper

the error types and median RT for correct trials.

Object Memory (Delayed). Patients were presented with the same task as in Object Memory: Immediate; however, the encoding period was removed. Thus, patients were asked to remember the stimuli presented approximately 15 minutes earlier. The main outcome measure was percentage accuracy, where all item features were accurately recalled. Secondary measures included the error types and median RT for correct trials. The error types were assessed as in immediate recall. The above tasks were performed on the CogAssess application on an iPad (Hampshire et al., 2020).

Logical Memory (Immediate). This task was a subtest of the Wechsler Memory Scale - Fourth Edition (WMS-IV) Older Adult standard neurocognitive battery. The patients were orally presented with two short stories: Story A, presented twice and Story B. They were then asked to retell the story from memory. A point was awarded for each correctly recalled detail (pre-defined). The main outcome measure was a total score, calculated by summing scores obtained for Story A first recall, Story A second recall and Story B (max: 53 points) and scaling the raw scores for each age group (65-69, 70-74, 75-79, 80-84, 85-90) using the table in the WMS-IV Administration and Scoring Manual.

Logical Memory (Delayed). After a delay of ~20–30 minutes, participants were asked to retell both stories again from memory. Just like the immediate recall, 1 point was awarded for each correctly recalled detail in Story A and Story B. The main outcome measure was a total score, calculated by summing the scores obtained for Story A and Story B (max: 39 points) and scaling them as described above. Patients performed other standard neurocognitive tests during the delay period. The Logical Memory I & II are subtests from the Wechsler Memory Scale IV (WMS-IV) Older Adult Battery (Drozdick et al., 2013)

Recognition Memory (faces and scenes). This was a custom-made task performed on a PC (adapted from Argyropoulos et al., 2022). The task consisted of three stages: encoding, washout period and recall. During encoding, 40 items were presented sequentially on the screen. Patients were asked to vote whether the item was *unpleasant, neutral, or pleasant* from the options displayed under the image; they had 4.5 s on each trial. The encoding period was followed by a filler task where patients responded which of the 2 numbers displayed on the screen was higher (or lower). Each item was presented for 3 s, with 20 items in total. This was immediately followed by a recall stage, adding up to 60 s of the total washout period between encoding and recall. During recall, 80 images were displayed sequentially, 40 new (distractors) and 40 old items presented during encoding, with 6 options underneath: *definitely old, probably old, maybe old, maybe new, probably new, definitely new*. Patients were asked to select which option they thought applied to the displayed image. This stage was self-paced and ended after patients responded to all 80 items. Patients completed 4 blocks, 2 with unfamiliar, neutral faces and 2 with scenes of nature. The main outcome measure from this task was the Area Under the Receiver Operating Characteristic (ROC) Curve (AUC). The ROC is a function that assesses a relationship between accuracy and response bias by modelling the relationship between hit rates (correctly identified old images) with false alarms (incorrectly identifying new images as old) across variations in the response confidence (Yonelinas & Parks, 2007; Koen et al., 2017). To create the ROC curve per subject and session, the frequency of each response confidence

(6-definitely old to 1-definitely new) is calculated for old and new items and divided by the sum of those frequencies. Then the cumulative sum is calculated for old items (hit rate) and new items (false

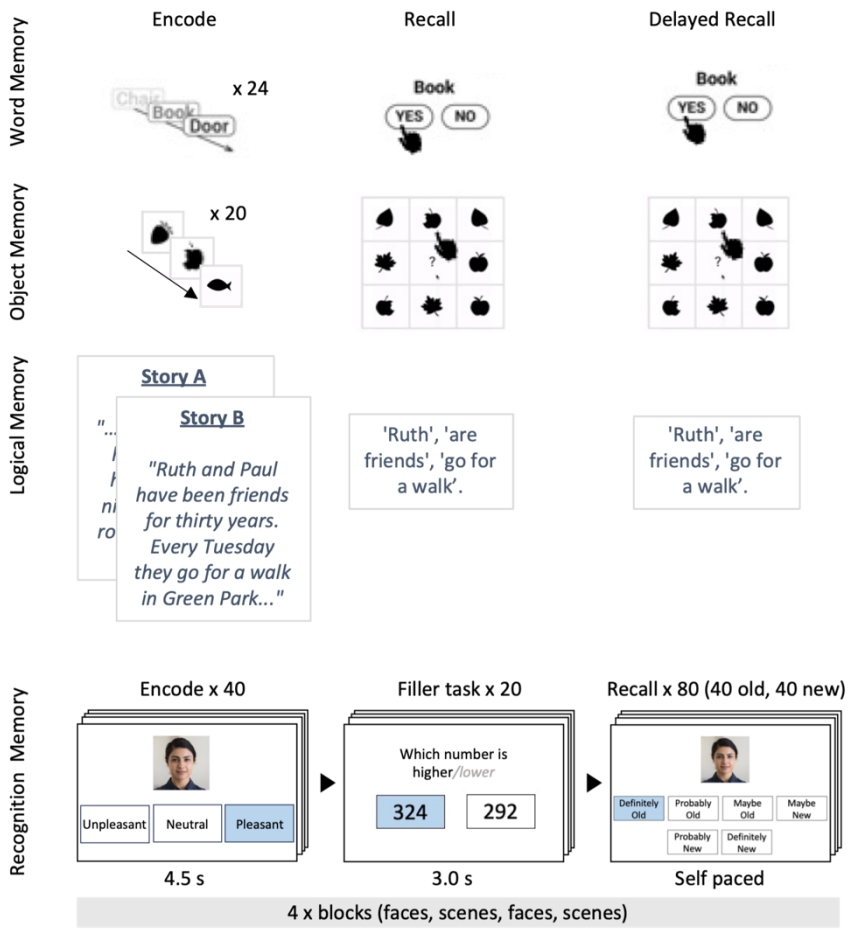


Figure 3.5 The episodic memory task designs.

alarms). The values for hit rate and false alarms are plotted against each other for each confidence bin except 1 (definitely new), as this, by design, equals 1. The area under the ROC curve is then computed for each stimulus type (faces and scenes). Thus, the AUC quantifies how well participants can distinguish between targets (old items) and lures (new items) across all possible decision thresholds. The AUC score ranges from 0 to 1, where 0.5 is a chance level, and higher scores indicate better discriminability.

3.2.2.2.2 General cognition tasks

Digit Span (Executive Function). Single digits between 0 and 9 were presented on a screen sequentially for 1000 ms. Participants were asked to memorise the digit sequence (as if they were

memorising a phone number). Immediately after encoding, participants were instructed to input the digits in the order they appeared on a keypad. The task started with a minimum difficulty at two digits, and the length of digits increased by one with each correct sequence recall. If participants made a mistake, a trial with the same length but a different sequence was repeated. The task ended after 3 consecutive mistakes on a particular sequence length. The outcome measure was the maximum sequence length correctly recalled.

Choice Response Task (Processing Speed). A black arrow pointing left or right appeared in the centre of the screen. Participants were asked to tap on the side of the screen, matching the direction of the arrow as quickly and accurately as possible, using only the index finger of their dominant hand. The task was composed of 60 trials, presented either until the participant responded or for 1 s, depending on which was faster. Arrows were presented in a random order, with a 50% chance of pointing left. The inter-stimulus interval (ISI) was jittered using a uniform random distribution between 0.5 and 2 s. The main outcome measure of this task was median response time for correct trials.

Table 3.3 Combined PET/MRI image acquisition protocol.

Scan	Time
Continuous blood sampling	10 min
MRAC 1	00:15
ZTE-MRAC 32ch NOVA	00:42
Asset Cal	00:06
Blood Sample 1	@10mins
Accelerated IR FSPGR	05:28
pCASL	06:48
Blood Sample 2	@25mins
rsfMRI	06:48
Faces fMRI	10:08
Blood Sample 3	@45min
pCASL	05:57
rsfMRI	06:48
Ax T2 FRFSE	05:02
Sag T2 FLAIR	05:18
Blood Sample 4	@70min
B0 Map	01:06
Ax DWI Tensor B-1000 64 Directions P/A HB	10:46
Ax DWI Tensor B-1000 10 Directions A/P HB	02:13
Blood Sample 5	@90min (End of Scan)

Motor Control (Processing Speed). A target appeared in a random location on a screen. Patients were instructed to tap the target (red circle) on the screen as quickly and accurately as possible. As soon as it was tapped, the target appeared in a random new location, with 30 trials in total. The main outcome measure of this task was median response time for correct trials.

2D Mental Manipulation (Visuospatial Processing). The task tested the ability to spatially manipulate objects in one's mind. A grid with coloured squares was presented at the top of the screen, with four probe grid options below. One of the probe grids matched the target grid exactly but was rotated by 90, 180 or 270 degrees. Participants were asked to identify the identical grid. The main outcome measure was the total number of correctly identified matches divided by the total number of trials completed. The secondary score was the median RT for correct trials. The above tasks were performed on the CogAssess application on an iPad (Hampshire et al., 2020).

Dot Counting, Position Discrimination, and Cube Analysis. Three subtests from the Visual Object and Spatial Perception (VOSP) Battery (Warrington & James, 1991). In the Dot Counting task, participants were asked to count how many dots were on a page without using their fingers. For the Position Discrimination task, participants were asked to indicate which box (left or right) had a dot exactly in the centre (the others will have a dot slightly off-centre). For the Cube Analysis task, participants were asked to count how many cubes were shown on the page, including those that were 'hidden', e.g., beneath another cube (Warrington & James, 1991). The main outcome measure for each task was the total score achieved.

Verbal Fluency (Lexical Processing): Verbal fluency is one of the 5 subdomains in the Addenbrooke's Cognitive Examination (ACE-III). Participants are asked to name as many words as possible in 1 minute that start with the letter 'S' (for phonetic fluency) and then name as many animals as possible (for semantic fluency). Both are scored from 0-7 using the scale on the ACE-III form (Hsieh et al. 2013).

Graded Naming Test (Lexical Processing): Patients were shown 30 images (graded in difficulty) and asked to name them. The maximum score was 30. (Warrington, 1997).

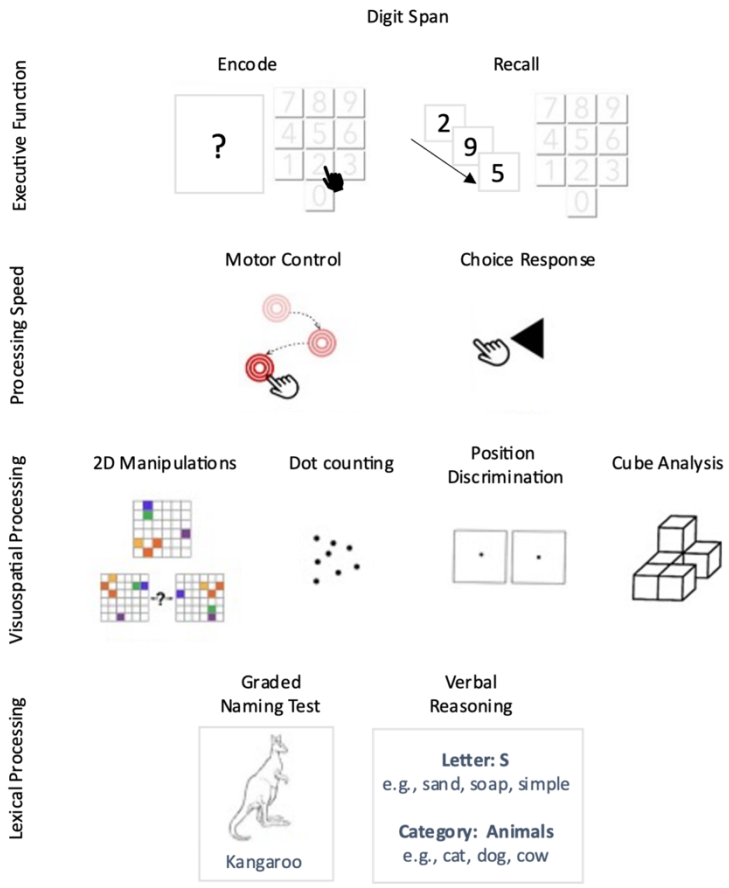


Figure 3.6 The general cognition task designs.

3.2.2.3 Brain Imaging at baseline and post-TI

The baseline and post-TI brain imaging sessions took approximately 4 hours and were carried out at Invicro, London's Hammersmith Hospital site, on an integrated 3T GE SIGNA PET/MR scanner (GE Healthcare, Milwaukee, WI, US) using a 32-channel head coil. The scanning protocol involved 90 min of PET image acquisition using [^{18}F]-BCPP-EF radiotracer with discrete arterial blood sampling. During the PET imaging, patients also underwent a series of MRI scans, which included structural T1, T2-weighted and T2 FLAIR images, pseudo-continuous arterial spin labelling (pCASL), resting state BOLD fMRI, task-based BOLD fMRI, and diffusion-weighted imaging (DWI). The resting state BOLD fMRI and pCASL were done in 2 runs. The scanning protocol is shown in **Table 3.3**. Over 50% of participants failed to perform the face-name association task. A subset of imaging, including resting-state Functional Magnetic Resonance Imaging (rsfMRI), DWI and task-based fMRI, are still being analysed and is not reported in this thesis.

3.2.2.3.1 Anatomical image acquisition and pre-processing

Acquisition: High-resolution T1-weighted structural images were acquired using a 3D inversion recovery fast spoiled gradient echo (IR-FSPGR) sequence. The imaging parameters included the following: 6.992 ms repetition time (TR), 2.996 ms echo time (TE), inversion time (TI) of 400 ms, 11^{o} flip angle (FA), and 240 x 240 x 200 mm field of view (FOV). Data was collected with 1 mm slice thickness and no spacing, resulting in 1 mm^3 isotropic voxels. The T1-weighted scans were used for the co-registration of PET, pCASL, fMRI and DWI images. Axial T2-weighted images were acquired using a 2D fast spin echo (FRFSE) sequence with the following parameters: TR = 4375 ms, TE = 82.7 ms, FA = 150°, FOV = 240 x 240 x 200 mm and 3 x 1 x 1 mm voxel size.

Pre-processing: T1-weighted anatomical images were first visually inspected for quality of contrast and motion artefacts and then processed using FreeSurfer's longitudinal pipeline, which reduces within-subject variability due to repeated measurements (Reuter et al., 2012). The longitudinal pipeline creates a subject-specific anatomical template (the *base template*) by averaging all time points using symmetric, robust registration. Segmentation in each time point is then initialised using the *base* template by registering all time points to the unbiased within-patient template image. This ensures that patients' average anatomy is constant across two time points and allows the detection of more subtle changes in volume. I first performed a standard cross-sectional segmentation pipeline using "*recon -all" (*FreeSurfer v7.4.1). The detailed pre-processing steps are described in prior publications (Dale et al., 1999; Dale and Sereno, 1993; Fischl and Dale, 2000; Fischl et al., 2001; Fischl et al., 2002; Fischl et al., 2004a; Fischl et al., 1999a; Fischl et al., 1999b; Fischl et al., 2004b; Han et al., 2006; Jovicich et al., 2006; Segonne et al., 2004, Reuter et al. 2010, Reuter et al. 2012). In short, the workflow included: motion correction (Reuter et al. 2010), skull stripping (Segonne et al., 2004), Talairach transformation and subcortical segmentation (Fischl et al., 2002; Fischl et al., 2004a), intensity normalisation (Sled et al., 1998), construction of both pial and white matter surfaces (Dale et al., 1999; Dale and Sereno, 1993; Fischl and Dale, 2000) and automated cortical parcellation using the Desikan-Killiany atlas (Desikan et al., 2006). To extract the volumes of hippocampal subfields, I also implemented the *hippocampal module* from FreeSurfer (Iglesias et al., 2015; Iglesias et al., 2016; Iglesias et al., 2017). To create patient-specific masks, the longitudinal FreeSurfer segmentation output was first resampled to patients' native anatomical space using nearest-neighbour interpolation to reduce partial volume effects (PVE) in the mask. To align anatomical masks with the functional imaging data, all region of interest (ROI) masks were resampled into the functional data space (e.g., CBF images) using FSL's Linear Image Registration Tool (FLIRT) (Jenkinson et al., 2002). For the primary analysis of regional volumes, CBF and SUVR, the ROIs included left and right hippocampi. Volumes

were also computed for the anterior, middle, and posterior hippocampus corresponding to head, body, and tail from the FreeSurfer segmentation of hippocampal subfields. In an exploratory analysis, additional ROIs included the left and right amygdala, parahippocampus, caudate, putamen, temporal cortex, occipital cortex, and prefrontal cortex.

3.2.2.3.2 PET image acquisition and pre-processing

Acquisition: Patients arrived 90 minutes before the scan and underwent safety procedures and health assessment. A cannula was then inserted into a cubital or forearm vein to administer the radioligand, and a second cannula was inserted into the radial artery for arterial blood collection during image acquisition. [^{18}F]-BCPP-EF was synthesised on-site as previously described by Harada et al., 2013. At the beginning of the scan, [^{18}F]-BCPP-EF tracer ≤100 MBq was administered intravenously over 20 s in a volume of 20mL. The dynamic images were reconstructed (post-injection frame durations: 8 x 15 s, 3 x 60 s, 5 x 120 s, 15 x 300 s) using Time of Flight Ordered Subset Expectation Maximization (OSEM) with resolution recovery (VPFX-S), with 6 iterations and 16 subsets and a 5 mm transaxial Gaussian filter on a 128 x 128 matrix giving 2 x 2x 2.7 mm voxels. Corrections were applied for attenuation, randoms and scatter. The whole-blood activity was measured using a continuous automatic blood sampling system (SwissTrace Twilite) at a rate of 5 mL/min for the first 10 min of the scan. Discrete blood samples were then collected at 10, 25, 45, 70 and 90 min after the start of the scan. High-performance liquid chromatography was used to determine the fraction of plasma radioactivity constituted by the unchanged parent radioligand (plasma parent fraction, or PPF). During the 90-minute PET image acquisition, patients also underwent a series of MRI scans. Two patients did not complete the post-PET scan. One was due to concerns with radiation, and another was due to failed tracer production. Thus, the final PET sample included 19 patients.

Pre-processing: PET data quantification was performed using Invicro's in-house MIAKAT^{TM} software package (MIAKAT_release_4.4.3.3). MIAKAT^{TM} is implemented using MATLAB (version R2022a; The Mathworks Inc., Natick, MA, USA) and makes use of SPM12 (Wellcome Trust Centre for Neuroimaging) for image segmentation and registration. MIAKAT^{TM} implements a robust analysis pipeline with a built-in audit trail and pre-specified quality control (QC) points. Each patient's structural MRI image underwent a grey matter segmentation, followed by registration to a standard reference space (Grabner et al., 2006). The MNI152 template brain image and associated atlases (CIC atlas; Tziortzi et al., 2011 and centrum semiovale atlas) were nonlinearly warped to the patient's MRI image to enable automated definition of ROIs. Dynamic PET images were registered to each patient's MRI scan and corrected for motion using a frame-to-frame registration process with a normalised mutual information cost function. Here, I used a simplified static model of standardised update value ratio

(SUVR) as the primary outcome measure of the PET imaging. SUVR does not rely on kinetic modelling of blood tracer activity and is calculated by computing normalising SUV in the ROI determined over 70-90 minutes after ^{18}F-BCPP-EF administration to the SUV in the Centrum Semiovale (CS). This produced regional SUVR values. CS has been shown previously to provide a good pseudo-reference region due to the minimal specific binding of the ^{18}F-BCPP-EF tracer.

3.2.2.3.3 CBF image acquisition and pre-processing

Acquisition: The CBF maps were acquired using GE Product 3D fast spin echo (FSE) pseudo-continuous arterial spin labelling (pCASL) sequence with a 3D spiral readout on the same 3T GE SIGNA PET/MRI scanner. Key parameters included TR = 4.854 s, TE = 10.7 ms, inversion time of 2025 ms, FA = 111°, and four signal averages. Data were collected with a 128 × 128 in-plane matrix over a 240 × 240 mm field of view, resulting in a voxel size of 1.875 × 1.875 × 4 mm.

Pre-processing: First, calibration images (M0 maps) were rigidly aligned across repetitions and averaged to create a single calibration map. The same rigid transformations were applied to the average CBF maps. Next, the averaged calibration map was co-registered to the corrected T1-weighted structural image using a rigid-body transformation. The resulting transformation matrix was then applied to the averaged CBF map to align it with the T1-weighted image. The patient-specific masks for the ROIs, derived from FreeSurfer segmentation, were transformed to the Arterial Spin Labelling (ASL) space using FSL's FLIRT tool and visually inspected for QC. The average CBF values in each region were then extracted using FSL's *"fslstats"* function and compiled for statistical analysis.

3.2.3 Data analysis

The data acquired in this study is multimodal, multidomain and large in volume. My approach to data analysis was to answer each of the hypotheses outlined in the introduction by first exploring each domain (task and brain imaging) separately, testing the effects of TI stimulation on cognition and brain function by comparing the primary task and brain imaging outcome measures acquired at baseline and post-TI intervention. Next, I explored the relationships and dependencies between brain function and neuroimaging in an exploratory analysis. A subset of outcome measures was not included in this thesis; these are outlined below.

3.2.3.1 Safety and tolerability

First, the percentage of total side-effect occurrence and severity were computed across all side effects, followed by the percentage occurrence of each side-effect category across 10 days for all subjects. Next, I tested whether there was a cumulative effect of TI stimulation on the probability of

reporting side effects. To do this, the side effect data was collapsed across the day, such that the presence of any side effects on the day was logged as “present” or “not present”. I then fit a GLME with a binomial distribution with “Subject” as a random intercept. First, a null model was fit with just an intercept. Next, I added “Day” as a fixed effect and used a likelihood ratio test (LRT) to determine whether the added predictor significantly improved the model fit. I also tested whether introducing patient demographics, specifically age, gender, and head size, significantly improved the model fit. This allowed me to test the effect while controlling for these variables and determine whether they had an independent contribution to the side-effect occurrence.

Next, I tested whether the average stimulation intensities increased with cumulative TI stimulation. The stimulation intensities (range: 1-none to 4-severe) were averaged across different side effect categories per day and modelled using GLME with Gamma distribution and log-link function (glmTMB R package). Finally, I tested whether the likelihood of reporting side effects decreased 24 hrs after TI stimulation. The data was once again collapsed across different side-effect categories to match the post-24-hr questionnaire that only recorded the presence or absence of side effects. I then used LRT to compare the null (Subject as a random intercept) and full model (adding “Time” as fixed effects with immediate or post-24 hours as categories, GLME with binomial distribution). The results are discussed in section **3.3.2**.

3.2.3.2 Neurocognitive data analysis at baseline and post-TI

3.2.3.2.1 Data cleaning and imputation

The neurocognitive tasks were divided into cognitive domains based on existing literature and separated into 2 groups of tasks: episodic and general cognition (**Table 3.2**). For each task, the most informative outcome measures were extracted, including accuracy, response time and scores or other composite accuracy measures computed using test manuals (see section **3.2.2.2** for task designs). One patient was removed before starting pre-processing as they missed the post-neurocognitive assessment. Thus, the final dataset included 20 patients. The data was then cleaned. Since the study has a repeated measures design, all performance levels were retained (e.g., accuracy at or below chance at baseline). The reasons for discarded data varied from task to task and were usually because of technical challenges on the testing day, patients abandoning the task after having completed less than 50% of the trials. This resulted in different participant numbers across different tasks. Given the small sample size and the desire to retain maximal information, I used Multivariate Imputation by Chained Equations (MICE; Azur et al., 2011) to impute the missing values. This approach has been successfully used in previous studies for imputing multivariate neurocognitive data in ageing and Alzheimer’s disease research (e.g., Hatahet & Seghier, 2024; Ding et al., 2023).

The MICE procedure has been described in detail by Azur et al. (2011). In short, MICE iteratively imputes missing values for each variable based on regression models conditioned on other variables in the dataset. Iterations continue until convergence is reached, defined as stability in imputed values and model parameters across iterations. I used the Python package *miceforest* (Wilson et al., 2022) for imputation. To improve imputation accuracy, all primary and secondary outcome measures of the tasks were included in the imputation model. Gradient boosting (*LightGBM*) was employed as the regression framework. *LightGBM* can handle non-linear relationships, outliers, and multicollinearity, which is particularly important when handling multivariate neurocognitive data. Predictive Mean Matching (PMM) was applied to ensure the imputed values retained the distribution of the observed data. PMM selects imputed values from observed values with similar predicted scores, maintaining the distribution of the raw dataset. Before imputation, *LightGBM* hyperparameters were optimised for each variable using the *tune_parameters* function. Five random parameter configurations were tested per variable, with a maximum of 500 boosting iterations. Hyperparameter tuning was performed via cross-validation on the observed portion of the data, and the best-performing configuration for each variable was selected. The MICE procedure was run for 10 iterations and generated 5 imputed datasets, as recommended by Azur et al. (2011). Convergence was assessed by monitoring changes in the mean and variance of imputed values across iterations.

The performance of data imputation was evaluated by comparing the mean and variance of raw and imputed data for each task at baseline and post-TI. Visual and numerical assessment confirmed that imputed data closely matched the observed data (Error! Reference source not found.). Given the consistency of results across the 5 imputed datasets, further analyses were conducted using the best-performing imputed dataset for simplicity. The percentage of missing data across tasks ranged from 2.5 to 20 % (**Table A7**).

3.2.3.2.2 Statistical analysis

For the neurocognitive data, I implemented two analysis steps to test whether patients improved in episodic memory and whether the improvement was greater than changes observed in other tasks from the mixed cognitive domains, termed “General Cognition” here. In the first step, I used factor analysis to reduce the dimensionality of the task space and extracted a single score for episodic memory and general cognition tasks. To do this, I employed Multilevel Principal Component (mPCA) analysis that has been specifically designed for repeated measures datasets. mPCA accounts for between-subject variance while highlighting within-subject changes (Liquet et al., 2012), allowing the detection of subtle changes within patients between different measurements. The data was mean-

centred and scaled before performing the mPCA. The sign of the response time measures was flipped so that an increase measured a positive change from the baseline, as in other tasks. The first component was then extracted for each task group, resulting in one score per domain, per patient, per session. I then used the linear mixed effects (LME) model to test whether patients improved on episodic memory scores from baseline to post-TI and whether this improvement was greater than changes observed in general cognition scores. The LME model was fit using the lme4 package in R (version 4.4.2) with the "Session" (baseline vs. post-TI), "Task Domain" (Episodic Memory vs. General Cognition), and their interaction as fixed effects, and a random intercept for the "Subject". Model parameters were estimated by maximum likelihood (ML). ANOVA with Satterthwaite approximations for degrees of freedom was used to test each fixed effect, followed by post hoc pairwise comparisons of Estimated Marginal Means (EMMs) with Tukey adjustment (using the *emmeans* package). Finally, I explored whether patients' MMSE scores and demographic variables predicted the degree of improvement in episodic memory performance using linear regression. To select a predictor that best explained the variance in performance change and avoid overfitting, I employed a stepwise selection process for the fixed effects based on the Akaike Information Criterion (AIC) using the MASS package in R. The analysis began with a null model (intercept only) and iteratively added or removed predictors based on their contribution to reducing AIC in both forward and backwards selection steps. Only the factors that significantly improved the model were retained and reported.

In the second step of the analysis, I looked at which specific tasks patients improved on using a one-tailed t-test or Wilcoxon signed-rank test based on the distribution of the data. The significance values were corrected using False Discovery Rate (FDR). For the analysis of episodic memory task performance administered during the TI stimulation, I employed the mPCA to extract composite measures for accuracy and response time, resulting in one score per patient per day for each outcome measure. Using the likelihood-ratio test (LRT) on the LME, I compared the null model (m0: Performance ~ (1 | Subject)), with a model with Day as fixed-effect (m1: Performance ~ Day + (1 | Subject)) and a model with a random slope for the Day (m3: Performance ~ Day + (1 + Day | Subject)). This allowed me to test whether there was a group effect of Day on performance as well as significant inter-individual variability in the trajectories of change across the 10 days. Finally, I extracted individual patients' slopes from LME and performed regression analysis testing the relationship between changes in performance during TI therapy and improvements observed in episodic memory.

3.2.3.3 Brain Imaging

3.2.3.3.1 Regional Grey Matter volumes

Regional volumes were extracted for the left and right hippocampus at baseline and post-TI for each patient. The effect of the "Session" on hippocampal volume was tested using LME with "Session" (baseline or post-TI) and Hemisphere as fixed effects with interaction terms, and "Subject" as a random intercept. LME was used to test differences in change in volume between left and right hippocampal subfields with "Region" (Ant., Mid., Post.) and "Hemisphere" as fixed effects with interaction term and "Subject" as a random intercept. Any significant results underwent pairwise comparison using EMM with Tukey's adjustment of significance.

3.2.3.3.2 Voxel-based Morphometry (VBM)

Whole brain voxel-based morphometry (VBM) analysis was carried out using the Computational Anatomy Toolbox (CAT12.9), running on the Statistical Parametric Mapping Toolbox (SPM12 v7219, Wellcome Department of Cognitive Neurology, London, UK). For each patient, T1-weighted anatomical images from both time points were processed using the CAT12 longitudinal segmentation pipeline. Images from both time points for each patient were realigned using inverse-consistent rigid-body registrations to ensure precise intra-subject alignment. This step accounts for any differences in position between scans and corrects for head motion across time points. An intra-subject bias-field correction was then applied to address intensity inhomogeneities within each patient's image over time. The resulting images were then segmented into grey matter (GM), white matter (WM) and cerebrospinal fluid (CSF) using the standard segmentation pipeline. For spatial normalisation, a mean transformation was computed across both time points for each subject. This mean transformation was then applied to the tissue segments of each time point. The normalised GM values were then scaled by the Jacobian determinants derived from the spatial normalisation step and smoothed with a 6 mm full width at half-maximum (FWHM) Gaussian kernel to align the images to standard MNI space.

The pre-processed images were then used for voxel-wise statistics to assess changes in GM volume from baseline to post-TI. The statistical modelling involved first checking the sample homogeneity by inspecting the correlation of normalised, unsmoothed GM data across subjects for each session. The correlation values showed one outlier with a large deviation from the sample mean correlation. This subject was removed from further analysis. Next, a statistical model was set up with a flexible factorial design to examine within-subject changes in GM volume from baseline to post-TI. Two factors were

defined for the model: Subject (independent) and Time (baseline vs. post-TI: dependent). The main effects of both factors were included in the design. Finally, design orthogonality was checked to ensure the validity of statistical assumptions and T-test contrasts were set for each direction of change for baseline to post-TI (i.e., post-TI > baseline; and post-TI < baseline).

No clusters survived the FDR correction for the whole brain. I then performed cluster-based correction to reduce the risk of type 1 errors using the AlphaSim method implemented in the REST software toolkit (Version 1.8). AlphaSim uses Monte Carlo simulations to estimate the probability of observing clusters of a given size by chance, accounting for the spatial properties of the data. The following parameters were set: the statistical threshold at $p < 0.05$ at the cluster level with a voxel-level threshold of $p < 0.001$; cluster connection radius 5 mm; and the number of simulations at 5000. The minimum cluster size (k) identified was 150. Three clusters survived the correction, showing an increase from baseline to post-TI. The masks for each cluster were saved, and mean GM intensity values for each cluster were extracted per subject for each session for future analysis.

3.2.3.3.3 PET

The primary ROIs selected for analysis were the left and right hippocampi. However, in an exploratory analysis, I also looked at the SUVR in other regions of the brain to determine global trends in the SUVR measurements across two sessions. I used LME with “Session” and “Hemisphere” as fixed effects with an interaction term and “Subject” as a random intercept to determine whether hippocampal SUVR changed from baseline to post-TI and whether these changes were different for the stimulated (left) vs. non-stimulated (right) hippocampus.

3.2.3.3.4 CBF

The primary ROIs selected for the CBF analysis were the left and right hippocampi. I used LME with “Session” and “Hemisphere” as fixed effects with an interaction term and “Subject” as a random intercept to determine whether hippocampal CBF changed from baseline to post-TI and whether these changes were different for the stimulated (left) vs. non-stimulated (right) hippocampus. Regression analysis was employed to explore the relationship between AD biomarkers (e.g., MMSE scores and baseline hippocampal volumes) and baseline CBF, as well as changes in episodic memory performance from baseline to post-TI and changes in hippocampal CBF.

3.3 Results

3.3.1 Demographic and clinical characteristics

Table 3.4 shows a demographics summary for the 21 patients who completed the study (11 females and 10 males; mean age: 72.9 years ±6.6 SD, range: 62-86; mean MMSE score: 25.2 ±3.0 SD, range: 20-30; ethnic background: 90.5% self-identified as White). Females on average had lower mean MMSE (24.5 ±2.7 SD) than males (26.10 ±3.3 SD). When compared to the normative scores, females were 1.5 below average, for their age and years of education, and males were 0.9 below the norm (normative scores were extracted from Grigoletto et al., 1999). At the time of enrolment, 18 patients had a diagnosis of AD or MCI due to probable AD, and four were diagnosed with early-onset AD. The majority, 71% of patients, were receiving either Donepezil or Rivastigmine, 9.6% were taking Memantine, and 19.1% of patients were not on any AD medication.

The blood plasma biomarker analysis was used to classify patients based on ATN(I) biomarker system (Imbimbo et al., 2023), where "A" refers to Aβ biomarkers calculated as Aβ42/Aβ40 ratio, "T" to a tau biomarker (pTau-217), "N" to biomarkers of neurodegeneration (neurofilament light (NfL)) and "I" to inflammation (measured by glial fibrillary acidic protein (GFAP)). 14 patients were positive for A+T+N+,

Table 3.4 Patient demographic and clinical characteristics summary.

Age (Mean ±SD; range)	
Group	72.9 (±6.6; 62 – 86)
Female	73.1 (±6.2; 62 – 79)
Male	72.7 (±7.3; 64 – 86)
Sex	
F	11 (52.4%)
M	10 (47.6%)
MMSE (Mean ±SD; range; normative[1])	
Group	25.2 (±3.0; 20 – 30; 26.5)
Female	24.5 (±2.7; 20 – 29; > 26)
Male	26.10 (±3.3; 20 – 30; > 27)
Years of education (Mean ±SD; range)	
Group	13.1 (±3.7; 7 – 20)
Female	13.7 (±3.6; 7 – 20)
Male	12.6 (±4.06; 8 – 18)
Medication	
Donepezil, Rivastigmine	15 (71.4%)
Memantine	2 (9.5%)
None	4 (19.1%)
Ethnicity	
Asian (Indian, Chinese)	2 (9.5%)
White	19 (90.5%)

of these 10 were also positive for inflammation (A+T+N+(I+)). 3 patients were found positive on all except pTau-217 (A+N+(I+), in this group the assay for pTau-217 failed. The remaining 3 patients were positive for pTau-217 (T+) while other assays failed. A blood sample was not collected for one patient (**Table 3.5**). In summary, of the 20 blood plasma samples tested, 17 were positive on at least three biomarkers of AD, and three were positive for pTau-217.

Table 3.5 Results of patients' blood biomarkers of AD.

Patient	1	2	3	4	5	6	7	8	9	10	11	12	13	14	15	16	17	18	19	20
A	+	+	+	+	+	+	+	+	+	+	+	+	+	+	NA	+	+	NA	+	NA
T	+	+	+	+	+	+	NA	NA	NA	+	+	+	+	+	+	+	+	+	+	+
N	+	+	+	+	+	+	+	+	+	+	+	+	+	+	NA	+	+	NA	+	NA
I	+	+	+	-	+	+	+	+	+	+	+	-	+	-	NA	+	-	NA	+	NA

The blood plasma samples were tested for: Aβ42/Aβ40, pTau-181, pTau-217, neurofilament light (NfL) and glial fibrillary acidic protein (GFAP) to classify patients +/- for the key biomarkers of AD: (A) Aβ, (T) tau, (N) neurodegeneration measured by NfL, and (I) inflammation measured by GFAP in the blood. NA indicates assays that did not return a result. n=20, blood sample was not available for one patient.

3.3.2 Repeated 10-day TI stimulation of the hippocampus in early-stage AD patients is safe and well-tolerated

Of the 24 patients recruited, 3 dropped out at baseline for reasons unrelated to TI (**Table 3.1**). Among the 21 patients who completed the study, we achieved a 98.6% compliance rate for completing 10 consecutive days of 50-minute TI stimulation (excluding the weekends), totalling approximately 8.3 hours of stimulation. Cases where patients missed TI stimulation days were due to ill health unrelated to TI or, in one case, due to frustration with the length of the study protocol. In the latter case, the patient missed the 10th day of the stimulation and post-neurocognitive assessment but came back to complete the neuroimaging. TI tolerability and sensation thresholds were tested before each stimulation session. Most patients experienced skin sensations, e.g., tingling, heat, or vibrations. **Table 3.6** shows the average sensation thresholds for each patient during TI. On average, the intensity at which sensation thresholds were experienced during TI stimulation was approximately 4.5 times higher than for conventional low frequency tACS stimulation, with average sensation thresholds at 2.16mA for TI and 0.48mA for tACS across both channels. All but 4 patients found maximum

stimulation amplitudes delivered comfortable. For these 4 patients, the current amplitude was adjusted to the maximum comfortable threshold while maintaining a 1:3 ratio between the channels (**Table 3.7**). In cases where the current had to be reduced, patients tended to be female.

No serious adverse events related to the TI stimulation were reported. There was one instance of equipment malfunction that led to strong sensations on the skin that disappeared shortly after the TI hardware was restarted. The effects were transient, and the patient opted to continue with the experiment as normal. The incident was recorded as an adverse event (AE) and reported to the Chief Investigator as per the guidelines of the study protocol. Side effects were reported in 8.5% of cases, totalling 194 observations across 16 side effect categories, 10 days and 21 patients. Most of these side effects were rated as mild in severity and were related to difficulty concentrating, drowsiness, and

Table 3.6 Average stimulation sensation thresholds per patient across 10 days.

TI stimulation thresholds were ~4.5 times larger compared to conventional low frequency tACS stimulation across both electrode pairs.

Participants	**Mean sensation threshold (mA ±SD)**			
	tACS (5 Hz)		TI (Δf = 5 Hz)	
	e1-e2	**e3-e4**	**e1-e2**	**e3-e4**
1	0.30 (0.00)	0.55 (0.23)	None	None
2	0.61 (0.15)	0.63 (0.17)	None	None
3	0.50 (0.21)	0.90 (0.38)	None	3.00 (0.00)
4	0.54 (0.17)	0.52 (0.16)	1.75 (0.50)	2.75 (0.29)
5	0.21 (0.11)	0.50 (0.34)	1.50 (0.25)	2.88 (0.25)
6	0.46 (0.08)	0.62 (0.34)	1.30 (0.40)	2.05 (0.31)
7	0.46 (0.13)	0.61 (0.20)	2.00 (0.00)	2.79 (0.39)
8	0.32 (0.15)	0.50 (0.46)	1.75 (0.46)	2.56 (0.58)
9	0.21 (0.11)	0.45 (0.13)	1.64 (0.38)	1.94 (0.18)
10	0.16 (0.13)	0.44 (0.23)	1.50 (0.41)	2.86 (0.38)
11	0.57 (0.25)	0.97 (0.42)	2.00 (0.00)	2.79 (0.27)
12	0.34 (0.10)	0.72 (0.44)	1.92 (0.20)	1.93 (0.44)
13	0.22 (0.10)	0.48 (0.26)	1.88 (0.25)	2.83 (0.29)
14	0.26 (0.13)	0.50 (0.21)	1.65 (0.21)	2.01 (0.48)
15	0.34 (0.13)	0.62 (0.41)	1.88 (0.25)	3.00 (0.00)
16	0.22 (0.14)	0.44 (0.25)	2.00 (0.00)	3.00 (0.00)
17	0.78 (0.27)	0.78 (0.53)	2.00 (0.00)	2.75 (0.29)
18	0.62 (0.14)	0.58 (0.21)	1.30 (0.26)	3.00 (0.00)
19	0.32 (0.18)	0.42 (0.27)	1.60 (0.00)	2.58 (0.38)
20	0.36 (0.25)	0.48 (0.32)	1.75 (0.38)	2.45 (0.55)
21	0.44 (0.19)	0.36 (0.13)	1.83 (0.26)	2.00 (0.00)
Average	**0.39 (0.15)**	**0.57 (0.29)**	**1.74 (0.23)**	**2.59 (0.27)**

e=electrode

sensations under the electrodes during stimulation (**Figure 3.7-A, B**). Of the 113 cases of tiredness and trouble with concentration, only 14% were reported by the patients to be related to TI stimulation. Yet, impaired attention is commonly observed in AD patients, usually reported as difficulties with focus or concentration when carrying out daily tasks (Malhotra, 2019). Thus, given the demanding memory tasks the patients performed during the stimulation procedure, the trouble with concentration is most likely a symptom of the disease rather than a direct effect of TI stimulation.

Next, I tested whether TI had a cumulative effect on the frequency and intensity of side effects reported daily by the patients. The statistical analyses are detailed in section **3.2.3.1** of the methods. The odds of reporting side effects did not significantly increase with increasing number of TI sessions ($\chi^2(1)=1.86$, $p=0.173$). Additionally, neither patient age, gender, nor head size predicted the side effect incidence ($\chi^2(4)=3.44$, $p=0.173$; **Figure 3.7C**; **Table 3.8**). No relationship was found between the

Table 3.7 TI stimulation intensities delivered to each patient throughout 10 sessions.

Participant		Mean amplitude (mA)		Gender	Head Circumference
		e1-e2	e3-e4		
1		1.00	3.00	M	57.5
2		1.00	3.00	M	56.0
3		1.00	3.00	M	59.0
4		1.00	3.00	F	55.0
5		1.00	3.00	M	56.5
6	*	0.68	2.04	F	56.4
7		1.00	3.00	F	55.5
8		1.00	3.00	F	54.0
9	*	0.78	2.33	F	54.0
10		1.00	3.00	M	58.0
11		1.00	3.00	F	54.0
12	*	0.66	1.98	F	54.5
13		1.00	3.00	M	61.0
14	*	0.68	2.04	F	53.5
15		1.00	3.00	M	60.0
16		1.00	3.00	M	55.5
17		1.00	3.00	M	58.0
18		1.00	3.00	F	54.0
19		1.00	3.00	F	55.0
20		1.00	3.00	F	55.5
21		1.00	3.00	M	55.5

*Cases with reduced TI current due to discomfort; e=electrode.

cumulative number of TI sessions and average side effect intensity ($\beta=8.186\times10^{-5}$, $SE=2.13\times10^{-5}$, $p=0.969$; GLME with Gamma distribution and log-link function). Additionally, the likelihood of experiencing side effects 24 hours post-stimulation was significantly lower compared to immediately after the TI session, with an approximately 44.5-fold reduction in odds ($\chi^2(1)=148.15$, $p<0.001$, generalised linear mixed model (GLMM) fitted with a binomial distribution and a logit link function with the patient as a random effect; **Figure 3.7D**). The effect remained significant after controlling for patients' age, gender and head size ($\chi^2(4)=148.54$, $p<0.001$). The demographic factors did not show a relationship with the likelihood of reporting side effects ($p>.05$). The above results suggest that the majority of side effects experienced immediately after the stimulation were transient and disappeared before the start of the following session **(Figure 3.7E**; **Table 3.8).**

In summary, AD patients tolerated the repeated TI stimulation well, with a 98.6% compliance rate in the study overall. Minimal side effects related to the TI stimulation were reported, the most common being skin sensations such as tingling, heat, and vibrations. Additionally, 10 consecutive 50-minute daily TI stimulation did not lead to an increase in side effect frequency or intensity, suggesting that increased TI dose was not associated with an increase in side effects.

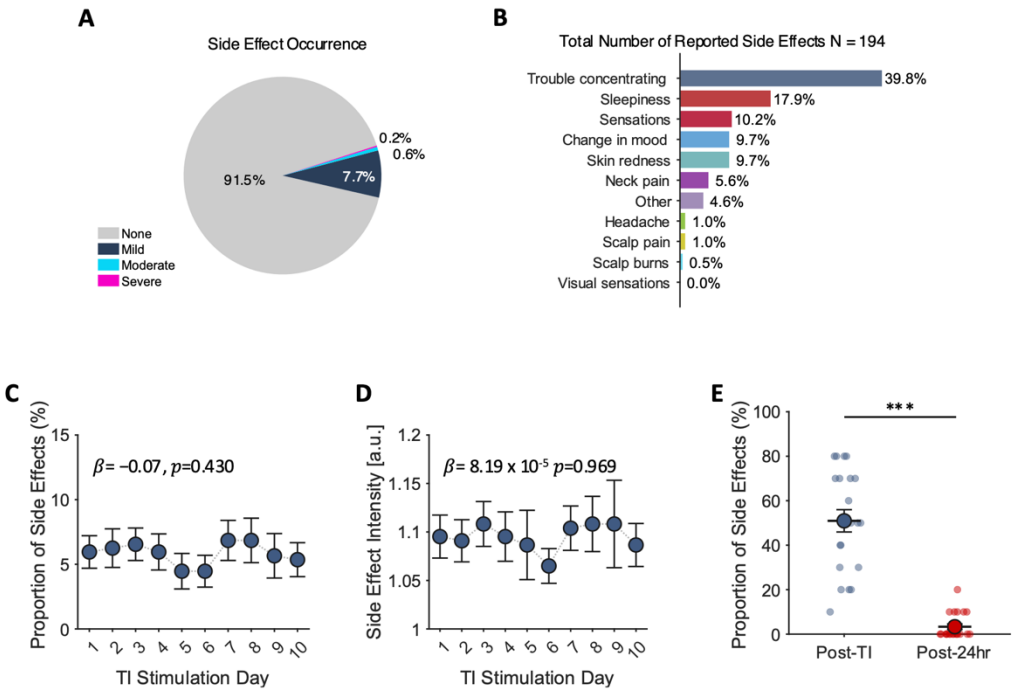


Figure 3.7 Safety and tolerability of repeated TI hippocampal stimulation in AD patients.

A. Distribution of side effects frequencies across patients assessed immediately after TI stimulation across all patients, sessions, and side effect categories. **B**. The distribution of each side effect occurrence relative to the total number of side effect reported. **C**. Proportion of side effects reported immediately after TI stimulation as a function of TI session day. Increasing number of TI stimulation sessions did not lead to increase in likelihood of reporting side effects ($\chi^2(1)=1.86$, p=0.173, GLME fitted with Gamma distribution and log-link function) **D.** No relationship was found between cumulative TI sessions and average side effect intensity ($\beta=8.19\times10^{-5}$, $SE=2.13\times10^{-5}$, p=0.969, GLME). **E**. The likelihood of reporting side effects significantly decreased 24 hrs. post-TI session, with ~44.5 fold decrease in odds ($\chi^2(1)=148.15$, p<0.001, GLMM fitted with a binomial distribution and a logit-link function with patient as random effect. Graphs show mean ±SEM *** Significant at p<0.001.

Table 3.8 Statistical results for Figure 3.7.

Test	Model	Predictor	Estimate	SE	CI Lower	CI Upper	*z*-value	*p*-value
The effect TI stimulation day on side effect frequency	Full	(Intercept)	0.72	0.42	-0.1	1.54	1.73	0.083
		Day	-0.07	0.05	-0.18	0.03	-1.37	0.430
	Full + covariates	(Intercept)	1.14	0.57	0.02	2.25	1.99	0.046 *
		Day	-0.07	0.05	-0.18	0.03	-1.37	0.430
		Age_centered	-0.01	0.04	-0.09	0.07	-0.28	0.783
		Gender(M)	-0.88	0.83	-2.51	0.74	-1.07	0.475
		Head_size_centerd	0.07	0.2	-0.32	0.47	0.37	0.783
Effect of TI stimulation day on side effect intensity		(Intercept)	0.09	0.02	0.05	0.12	4.89	0.000 ***
		Day	8.19E-05	2.13E-03	-4.10E-03	4.26E-03	0.04	0.969
Side effect frequency immediately vs. 24 hrs post-TI	Full	(Intercept)	-3.49	0.44	-4.36	-2.62	-7.85	0.000 ***
		Time(Immediate)	3.79	0.45	2.92	4.67	8.49	0.000 ***
	Full + covariates	(Intercept)	-3.32	0.54	-4.37	-2.27	-6.19	0.000 ***
		Time(Immediate)	3.79	0.45	2.92	4.66	8.51	0.000 ***
		Age_centered	0.00	0.03	-0.07	0.07	0.02	0.985
		Gender(M)	-0.35	0.66	-1.63	0.94	-0.53	0.598
		Head_size_centered	0.03	0.16	-0.29	0.34	0.17	0.866
LRT			**Log Lik.**	**AIC**	**BIC**	**Delta χ^2**	**Delta df**	***p*-value**
Effect of TI on side effect frequency	Reduced		-133.39	270.79	277.48	-	-	-
	Full		-132.47	270.93	280.97	1.86	1	0.173
	Full + covariates		-131.67	275.35	295.43	3.44	4	0.487
Side effect frequency immediately vs. 24 hrs post-TI stimulation	Reduced		-228.64	461.28	469.12	-	-	-
	Full		-154.56	315.13	326.89	148.15	1	0.000 ***
	Full + covariates		-154.37	320.74	344.27	148.54	4	0.000 ***

[1]Likelihood Ratio Test

3.3.3 AD patients showed selective improvement in episodic memory function following 10 days of TI stimulation

The statistical analysis methods are detailed in section **3.2.3.2.** To test whether patients improved on episodic memory scores from baseline to post-TI intervention and whether this improvement was greater than changes observed in other cognitive domains, I first performed factor analysis using multilevel PCA (mPCA) and extracted composite scores for episodic memory and general cognition separately, resulting in one value per domain per patient. This allowed me to reduce the dimensionality of the task space. Eight and 10 task outcome measures were included in mPCA for episodic memory and general cognition, respectively. The projection scores for the first principal component (PC1) that explained the most variance were then selected for further analysis. For episodic memory, the PC1 explained 36.9%, and in general cognition, 24.3% (**Figure 3.8A**). The linear contribution of each task to the corresponding PC1 loadings is displayed in **Figure 3.8B.**

Next, I tested whether patients improved in these composite measures of cognition following the 10 sessions of TI stimulation. The results are shown in **Figure 3.8** and **Table 3.9**. The statistical tests are detailed in section **3.2.3.2.2.** The analysis showed a significant main effect of Session ($F(1,80) = 17.99$, $p<0.001$; GLME), indicating an overall significant improvement in performance from baseline to post-TI. The main effect of the Task Domain (episodic vs. general cognition) was not significant ($F(1,80)=0.00$, $p=1.00$), suggesting that across both sessions, these two measures did not statistically differ from each other. Importantly, there was a significant interaction between Session (baseline vs. post-TI) and Task Domain ($F(1,80)=7.18$, $p=0.009$), indicating that the effect of Session was different between the two task groups. To investigate this interaction further, I performed a pairwise comparison on the estimated marginal means with Tukey adjustment for multiple comparisons. The episodic memory scores were significantly higher in post-TI compared to baseline ($t(80) = 4.89$, $p<0.001$). Change from baseline in general cognition score was not statistically significant ($t(80)=1.10$, $p=0.688$), confirming that positive change in episodic memory performance was significantly greater than in general cognition. Finally, I explored whether patients' MMSE scores and demographic variables (age, gender, and years of education) predicted the degree of improvement from baseline. A stepwise regression approach using AIC identified MMSE scores as the best predictor of change in performance, while the demographic factors did not significantly improve the model fit. The results showed that baseline MMSE was a significant predictor of the degree of improvement in episodic

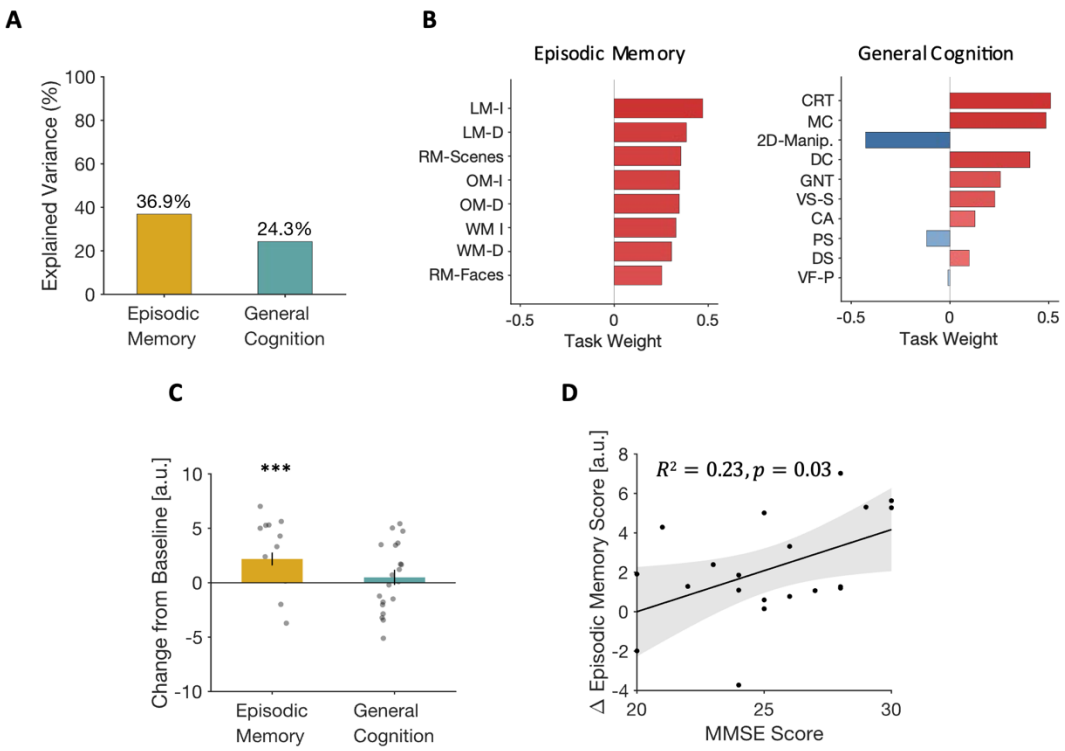


Figure 3.8 Neurocognitive task performance at baseline and post-TI stimulation.

A. Proportion of variance explained by the first component of the mPCA analysis in each task group. **B**. Task weights showing the contribution of each task variables to the first component. Higher weights indicate stronger contribution of that task to that weight. The negative weights reflect whether the task's variation aligned directly (positive) or inversely (negative) with top component. **C**. Change in composite scores from baseline post-TI. There was an overall improvement in performance across both task domains ($F(1,80) = 17.99$, $p < 0.001$; GLME). This effect was significantly different between the two task domain ($F(1,80) = 7.18$, $p = 0.009$), post-hoc comparisons on EMMs showing a significant increase in episodic memory composite score from baseline to post-TI ($t(80) = 4.89$, $p < 0.001$), while the change in general cognition, did not reach significance (significant ($t(80) = 1.10$, $p = 0.688$). Graphs show mean ±SEM. **D**. There was a significant positive relationship between change in episodic memory score and patients' MMSE, ($t(18) = 2.23$, $p = 0.032$, $R^2 = 0.23$), suggesting that patients with higher MMSE showed greater improvements in episodic memory. ***p<0.001; n=20.

memory scores ($t(18) = 2.23$, $p=0.032$, $R^2=0.23$), suggesting that patients with higher baseline MMSE scores showed greater improvement in episodic memory performance (**Figure 3.8D**).

I then explored which episodic memory tasks patients were improving on by comparing performance at baseline and post-TI on individual tasks. The results are presented in **Figure 3.9** and **Table 3.10** Following FDR correction, patients showed significant improvements on Logical Memory Immediate ($W=95$, $p=0.038$, $d=0.3$) and Delayed ($t(19)=2.94$, $p=0.018$, $d=0.3$), Object Memory Immediate ($t(19)=2.18$, $p=0.035$, $d=0.4$) and Delayed ($W=145$, $p=0.018$, $r=0.7$). Interestingly, a significant positive change was observed in Recognition Memory for Scenes ($t(19)=2.58$, $p=0.024$, $d=0.3$) but not in Faces ($t(19)=-0.23$, $p=0.590$). This is noteworthy since the task design for these two stimulus categories was

the same, only differing by whether the stimuli were a face or an object. No changes were observed in Word Memory Immediate (t(19)=1.69, p=0.071) or Delayed (t(19)=0.52, p=0.348).

To test whether the paired comparisons aligned with the results of the composite scores from factor analysis, I also investigated changes in the General Cognition task group. While some trends were observed, one of the tasks in this group showed improvement from baseline to post-TI following FDR correction (**Figure 3.10**; **Table 3.11**). Thus, paired comparisons on individual tasks support the results in the composite scores, suggesting that patients selectively improved episodic memory function following the TI stimulation.

Table 3.9 Statistical results for Figure 3.8.

Fixed-Effects

Predictor (Reference)	Estimate	SE	CL Lower	CL Upper	df	*t*-value	*p*-value
Intercept	-1.09	0.32	-1.71	-0.47	80	-3.46	0.001 ***
Session(2)	2.19	0.45	1.31	3.06	80	4.89	0.001 ***
Task_Domain (general-cog)	0.85	0.45	-0.03	1.72	80	1.89	0.062
Session:Task_Domain	-1.69	0.63	-2.93	-0.45	80	-2.68	0.009 **

ANOVA III

Effect	Sum Sq	Mean Sq	df1	df2	*F*-value	*p*-value
Session	35.91	35.91	1	80	17.99	5.9E-05
Task_Domain	0.00	0.00	1	80	0.00	1.0E+00
Session:Task_ Domain	14.34	14.34	1	80	7.18	8.9E-03

Contrast of EMMs	Estimate	SE	df	*t*-value	*p*-value Adjusted
Post_TI episodic - Baseline episodic	2.19	0.45	80	4.89	0.000 ***
Baseline control - Baseline episodic	0.85	0.45	80	1.90	0.239
Post_TI control - Baseline episodic	1.34	0.45	80	3.00	0.019 *
Post_TI control - Baseline control	0.49	0.45	80	1.10	0.688

p-value adjustment: Tukey method for comparing a family of 4 estimates

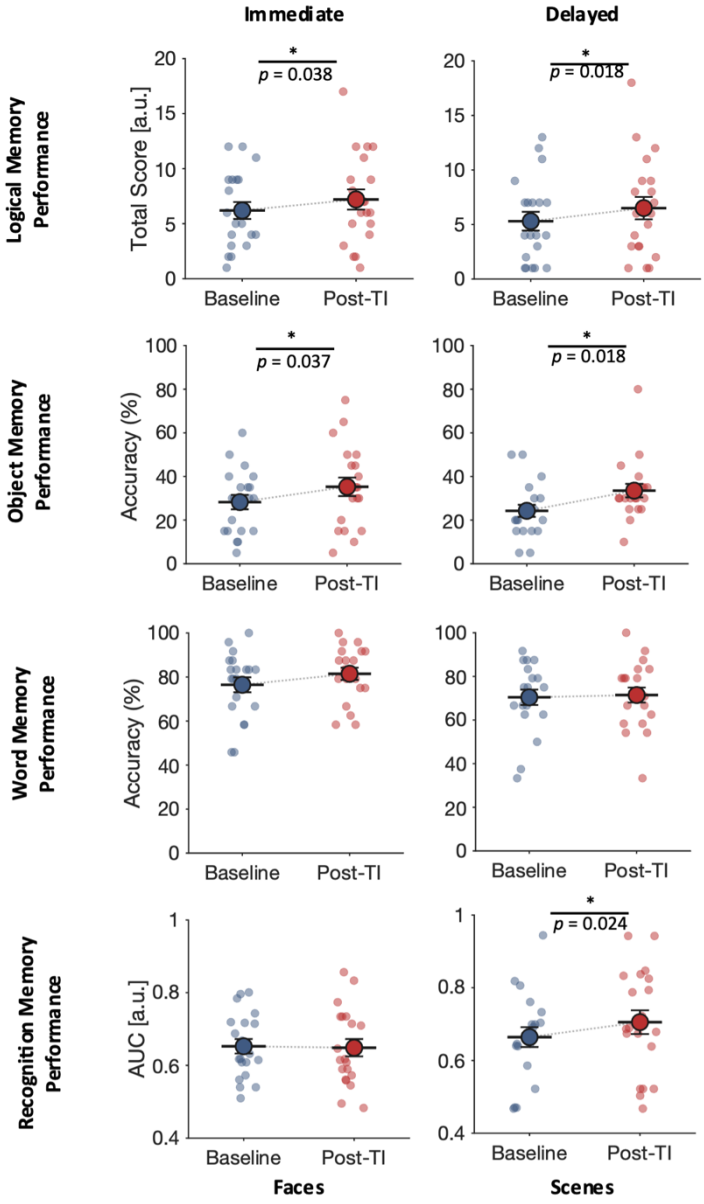


Figure 3.9 Performance on individual episodic memory tasks at baseline and post-TI. Paired hypothesis test (one tailed). $^{*}p < 0.05$ FDR corrected.

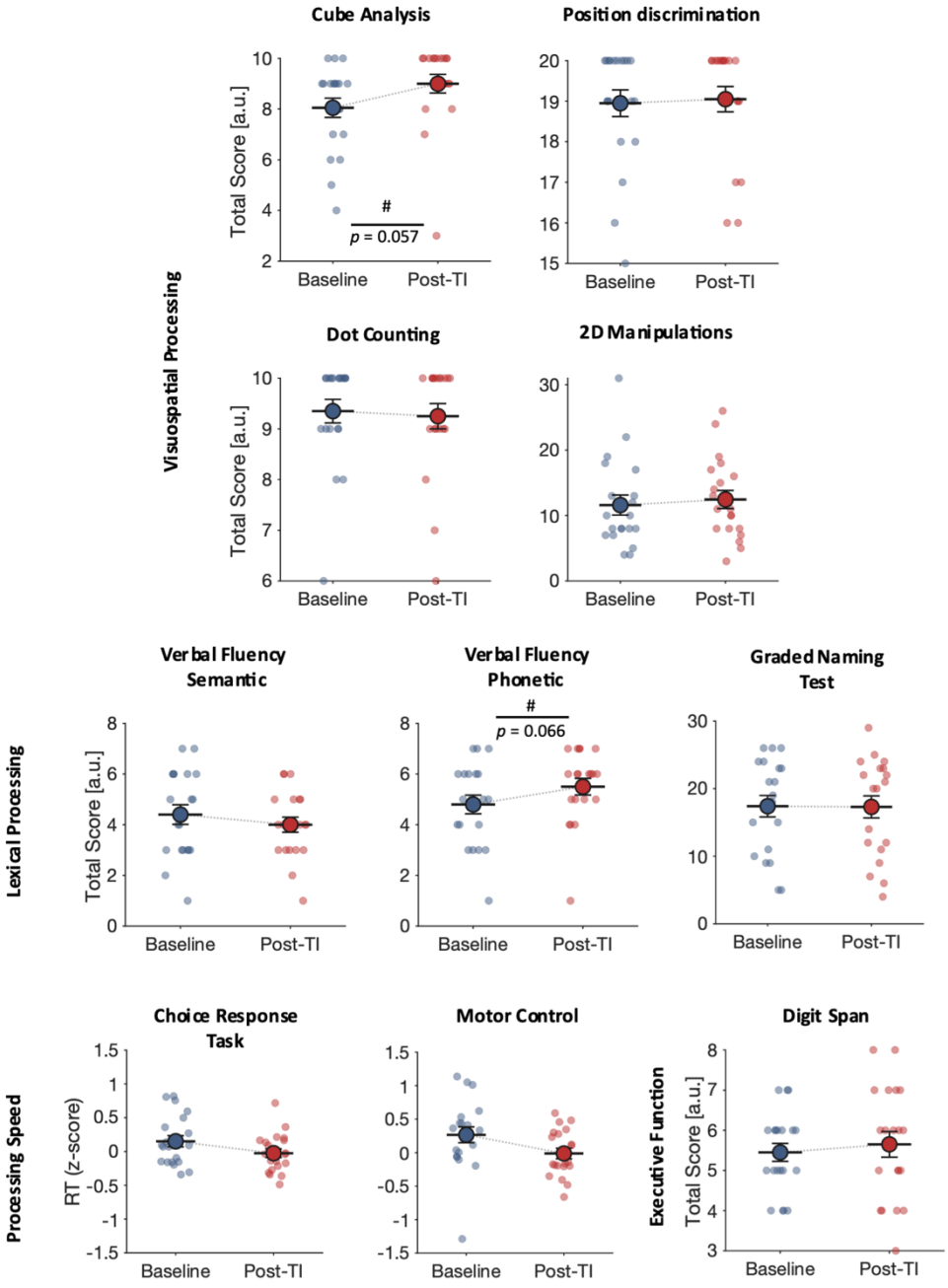


Figure 3.10 Performance on individual general cognition tasks at baseline and post-TI.

Paired hypothesis test (one tailed). $^{\#}p < 0.05$ prior to FDR correction.

Table 3.11 Statistical results for Figure 3.9.

Cognitive Domain	Task	Baseline Mean(SD)	Post TI Mean(SD)	Statistic[1]	Cohen's d_{av}	*p*-value Adjusted
Episodic Memory	Logical Memory Immediate	6.2(3.44)	7.2(4.11)	W=95	0.3	0.038 *
	Logical Memory Delayed	5.3(3.84)	6.5(4.58)	t(19)=2.94	0.3	0.018 *
	Word Memory Immediate	76.46(15.25)	81.46(12.42)	t(19)=1.69	0.4	0.071
	Word Memory Delayed	70.42(15.82)	71.46(15.43)	t(19)=0.52	0.1	0.348
	Object Memory Immediate	28.25(14.8)	35.25(18.95)	t(19)=2.18	0.4	0.035 *
	Object Memory Delayed	24.25(12.38)	33.5(13.87)	W=145	0.7	0.018 *
	Recognition Memory Faces AUC	0.65(0.09)	0.65(0.11)	t(19)=-0.23	-0.1	0.590
	Recognition Memory Scenes AUC	0.66(0.12)	0.71(0.15)	t(19)=2.58	0.3	0.024 *

p-value adjustment: FDR; [1]The test statistic was either a one-tailed Wilcoxon Signed-rank or a *t*-test based on the data distribution.

Table 3.10 Statistical results for Figure 3.10.

Cognitive Domain	Task	Baseline Mean(SD)	Post TI Mean(SD)	Statistic[1]	Cohen's d_{av}	*p*-value Adjusted
Executive Function	Digit Span	5.45(1)	5.65(1.42)	t(19)=0.85	0.2	0.398
Visuospatial Processing	Dot Counting	9.35(1.04)	9.25(1.12)	W=19	-0.1	0.785
	Position Discrimination	18.95(1.47)	19.05(1.39)	W=32	0.1	0.475
	Cube Analysis	8.05(1.7)	9.0(1.65)	W=104	0.6	0.057 #
	2D Manipulations	11.6(6.82)	12.45(6.18)	t(19)=0.72	0.1	0.398
Lexical Processing	Graded Naming Test	17.4(7.1)	17.3(7.29)	t(19)=-0.16	-0.01	0.703
	Verbal Fluency Phonetic	4.8(1.64)	5.5(1.47)	t(19)=2.4	0.5	0.066 #
	Verbal Fluency Semantic	4.4(1.73)	4.0(1.34)	t(19)=-1	-0.2	0.835
Processing Speed	Choice Response Time	0.15(0.37)	-0.03(0.29)	t(19)=-1.27	-0.5	0.276
	Motor Control	0.27(0.53)	-0.01(0.35)	t(19)=-1.5	-0.6	0.251

p-value adjustment: FDR; [1]The test statistic was either a one-tailed Wilcoxon Signed-rank or a *t*-test based on the data distribution. #p<0.05 (uncorrected).

3.3.4 Associative memory task performance during TI stimulation predicts the degree of improvement in episodic memory function

During TI simulation sessions across the 10 days, patients also performed associative memory tasks. The tasks are detailed in section **3.2.2.1.1**. In summary, five tasks were performed for 5 minutes each, repeated twice, totalling 50 minutes of daily memory training. The tasks included remembering word-word (WPA), words-scene (WSA), object-scene (OSA) and object-location (PAL) associations. To avoid boredom, they also performed card pairs; this was a self-paced trial-and-error task and is not analysed here. I first looked at whether patients showed overall improvement in accuracy and response time (RT) across sessions. To reduce the dimensionality of the task space, I adopted the mPCA approach to extract composite scores for accuracy and RT. The explained variance of the components is displayed in **Figure 3.11A**; the first principal component, which explained the most variance, was kept as a composite measure in each task group. Performance on individual tasks is shown (**Figure A2**). The likelihood ratio test revealed that on average, patients did not show an improvement in accuracy across the 10 days (m0 > m1: $\chi^2(1) = 3.23$, p=0.072; **Table 3.12)**. However, adding "Day" as a random slope significantly improved the model fit (m2 vs. m0: $\chi^2(3)=14.55$, $p < 0.001$) while the fixed effect remained non-significant ($\beta=-0.05$, $t(18) = -1.18$, p=0.253). This suggests that patients differed significantly in their trajectories of accuracy over time (**Figure 3.11B; Table 3.12).** In contrast, for RT for correct trials, there was a significant negative effect of "Day" ($\beta=-0.2$; $t(18) = -2.84$, p=0.046, LME, FDR corrected), implying an overall group-level reduction in RT. Additionally, adding a random slope for "Day" significantly improved the model fit ($\chi^2(2)= 64.91$, $p < 0.001$), indicating that patients varied in their rate of improvement in RT scores. Thus, while accuracy did not show a uniform group-level trend, patients got faster over time, with both measures displaying a significant inter-individual variability in the rate of change.

Next, I investigated whether individual learning trajectories during the intervention predicted the degree of improvement in episodic memory. To account for significant inter-individual variability in performance changes, I extracted individual patient slopes for accuracy and reaction time from the LME model, representing each patient's unique learning trajectory across the 10 days of training. These slopes were then regressed against changes in episodic memory composite scores. No relationship was observed between patients' rate of change in accuracy and episodic memory improvement ($R2= 0.06$; $t(16) = -1.01$, p=0.327). However, a significant negative relationship was found between RT and change in episodic memory composite score, with approximately 29% of variance explained ($R2= 0.29$; $t(16) = -2.53$, p=0.045; FDR corrected). These findings suggest that patients who showed greater

improvements in speed during associative memory tasks while they received TI stimulation also experienced greater episodic memory improvements following the intervention.

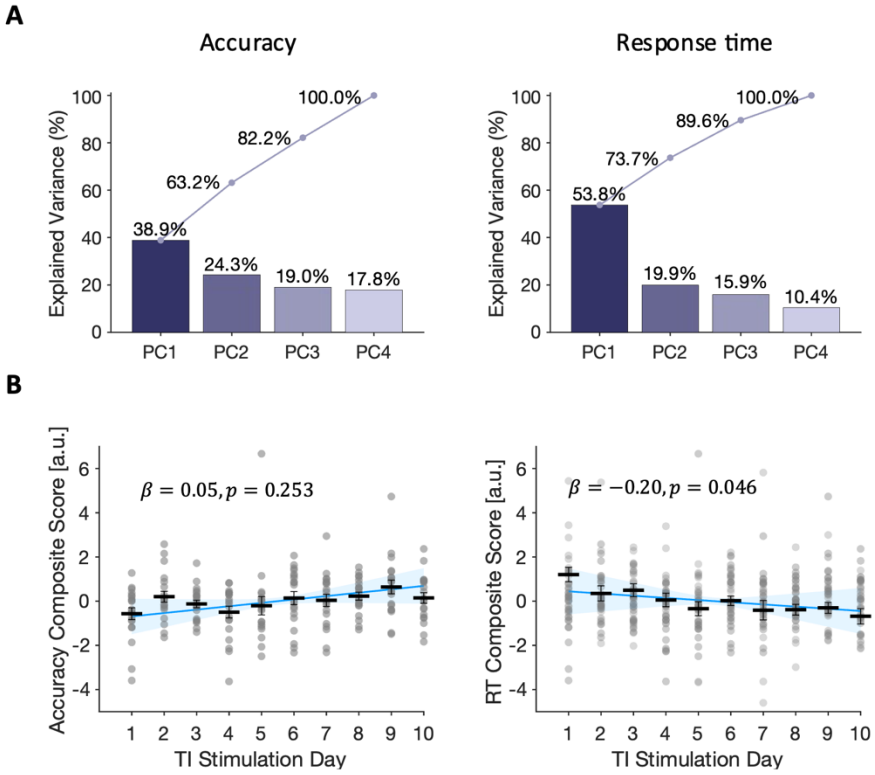


Figure 3.11 Performance on associative memory tasks performed during TI stimulation.

A. Variance explained by each principal component from mPCA analysis for accuracy and response time measures. The first principal component (PC1) which explained the most variance, was chosen as the composite measure of accuracy and response time**. B.** Patients' performance on associative memory tasks across 10 days of stimulation (mean ±SEM). On average, no significant improvements were observed in accuracy (β=−0.05, t(18) = -1.18 p=0.253) while patients showed a significant reduction in response time composite score (β=−0.2; t(18) = -2.84, p=0.046, LME, FDR corrected). n=18, two patients had missing data).

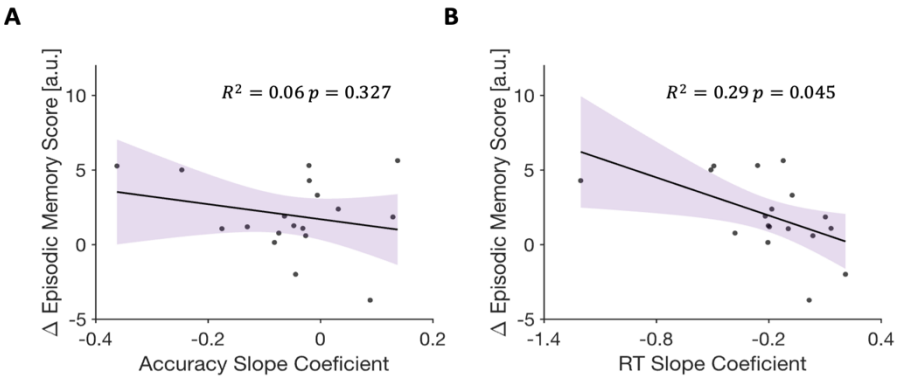


Figure 3.12 Relationship between memory training scores during TI stimulation and improvement in episodic memory score.

A. No relationship was observed between patients' rate of change in accuracy composite score from the associative memory tasks performed during TI stimulation across the 10 days and improvement in episodic memory (R^2= 0.06; t(16) = (-1.01), p=0.327. **B.** In contrast, a significant negative relationship was found between response time (RT) and change in episodic memory composite score, with approximately 29% of variance explained by RT slopes. (R^2= 0.29; t(16) = (-2.53), p=0.045; FDR corrected). Robust regression showed that the single observed outlier in RT slopes did not bias the observed slope (Error! Reference source not found.).

Table 3.12 Statistical results for Figure 3.11.

Model Formulas	Model Comparison	Log Lik.	AIC	BIC	Delta χ^2	Delta df	*p*-value
m0 = Accuracy ~ (1 | Subject);	m0 > m1	-261.52	531.04	543.65	3.23	1	0.072
m1 = Accuracy ~ Day + (1 | Subject);	m2 > m1	-255.86	523.72	542.64	11.32	2	0.003 **
m2 = Accuracy ~ Day + (1 + Day | Subject)	m2 > m1	-255.86	523.72	542.64	14.55	3	0.002 **
m0 = RT ~ (1 | Subject);	m1 > m0	-297.80	603.61	616.22	26.60	1	0.000 ***
m1 = RT ~ Day + (1 | Subject);	m2 > m1	-265.35	542.70	561.62	64.91	2	0.000 ***
m2 = RT ~ Day + (1 + Day | Subject)	m2 > m0	-265.35	542.70	561.62	91.52	3	0.000 ***

Dependent Variable	Predictor	Estimate	SE	CL Lower	CL Upper	df	*t*-value	*p*-value Adjusted
Accuracy	(Intercept)	0.28	0.26	-0.22	0.78	19.52	1.11	-
	Day	-0.05	0.04	-0.14	0.03	18.51	-1.18	0.253
RT	(Intercept)	1.08	0.44	0.22	1.94	18.08	2.46	-
	Day	-0.20	0.08	-0.36	-0.04	17.81	-2.48	0.046 *

p-value adjustment: FDR

3.3.5 Changes in Grey Matter volume following TI stimulation

The volumes of the hippocampus and its subfields were extracted following FreeSurfer's longitudinal segmentation pipeline (Reuter et al., 2012). No changes were observed in the hippocampal volumes from baseline to post-TI sessions (F(1,63)=0.02, p=0.897) and no differences were found between the left and right hippocampal volume at the group level (F(1,63)=0.04, p=0.847); **Figure 3.13A**; **Table**

3.14). Given that stimulation was targeted to the anterior segment of the left hippocampus, I also extracted the volumes of hippocampal subfields. No changes in volume were detected in the anterior, mid, or posterior segments of the hippocampus (F(1,105)=2.11, p=0.126) in either left or right hemisphere (F(1,105)=0.05, p=0.817; **Figure 3.13B**). As large volume changes were not expected to occur in such a short time window of 10 days, this analysis was primarily to further assess the safety of repeated TI stimulation in AD patients. To explore whether small volumetric changes could be detected, I performed whole-brain VBM. Three clusters survived correction for the contrast post-TI > Baseline (cluster level correction p<0.05; cluster size >150; voxel-level threshold p<0.001; **Figure 3.13C-i**). The volumes extracted from these clusters showed, on average ~4% increase in absolute volume from baseline to post-TI (**Figure 3.13C-ii, Table 3.14**). The cluster coordinates corresponded to parts of the right superior and middle frontal gyri. I next tested whether these changes correlated with either episodic or general cognition scores. No significant correlations were observed (**Figure 3.14**).

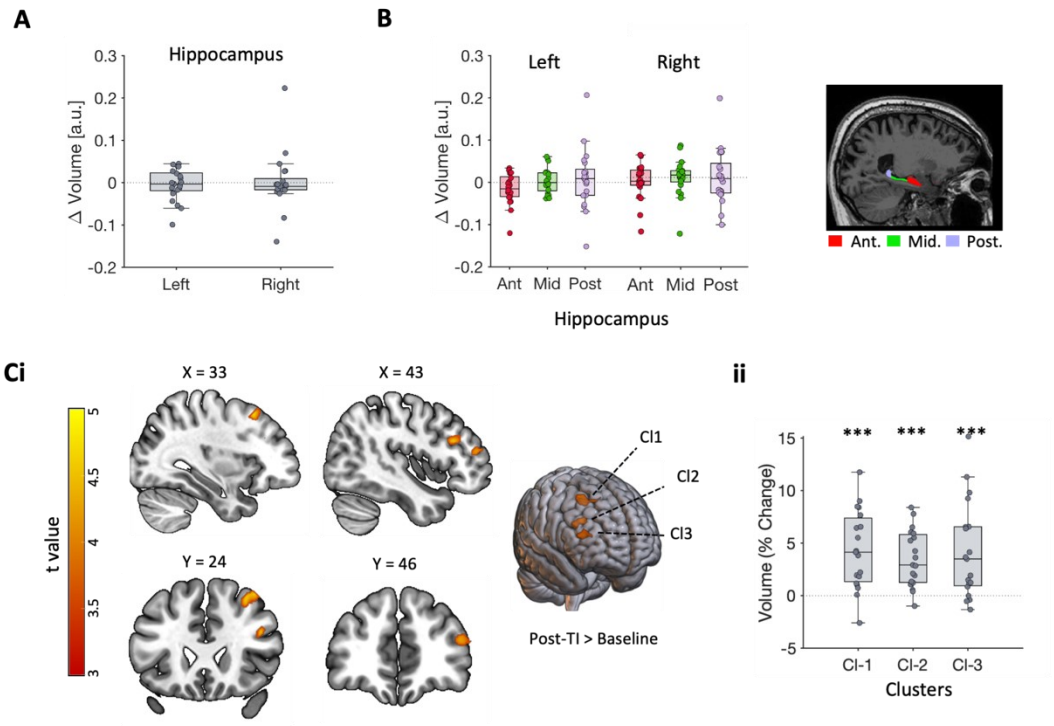


Figure 3.13 Changes in brain volume following TI stimulation.

A. No changes were observed in the hippocampal volumes (F(63,1)=0.02, p=897) and no differences were detected between left and right hemisphere (F(63,1)=0.04, p=847). **B**. The volumes of hippocampal subfields did not change from baseline. **C(i-ii).** The whole brain VBM revealed three clusters with statistically significant increase in volume from baseline to post-TI. (n=20, one patient detected as an outlier was not included in the analysis. Cluster level correction at p<0.05; cluster size >150; voxel-level threshold of p<0.001). ***p<0.001.

Table 3.13 Statistical results for Figure 3.13.

Effect on volume	Sum Sq	Mean Sq	df1	df2	*F*-value	*p*-value
Session	9.27E-05	9.27E-05	1	63	0.02	0.897
Hemisphere	2.04E-04	2.04E-04	1	63	0.04	0.847
Session:Hemisphere	1.54E-04	1.54E-04	1	63	0.03	0.867
Effect on change in volume						
Region (Ant. Mid. Post)	6.97E-03	3.48E-03	2	105	2.11	0.126
Hemisphere	8.88E-05	8.88E-05	1	105	0.05	0.817
Region:Hemisphere	1.09E-03	5.45E-04	2	105	0.33	0.720

VBM Cluster	Mean Change (%) (SD)	Test Statistic	*p*-value Adjusted
Cl-1	4.16 (3.71)	$t(19) = 5.01$	<0.001 ***
Cl-2	4.05 (3.58)	$t(19) = 5.07$	<0.001 ***
Cl-3	4.12 (4.50)	$t(19) = 4.10$	<0.001 ***

p-value adjustment: FDR

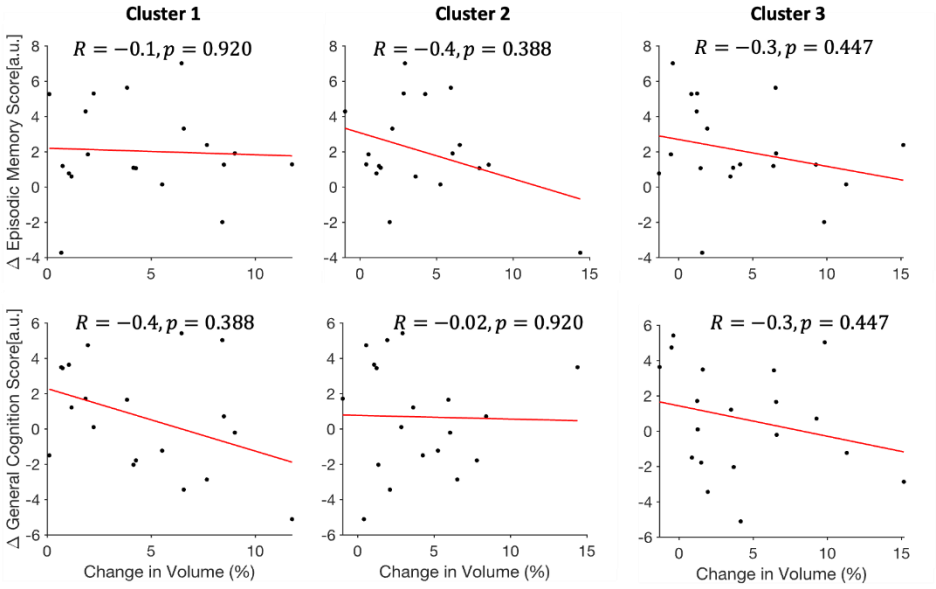


Figure 3.14 Correlation between changes in cluster volumes and performance from baseline to post-TI.

No relationship was observed between increase in cluster volume and changes in episodic memory or general cognition task scores (p>0.05; FDR corrected).

3.3.6 Baseline hippocampal volume predicts the degree of improvement in episodic memory

Considering that hippocampal volume is a key disease biomarker in Alzheimer's Disease (AD), I examined whether baseline hippocampal volumes predicted the extent of improvement in episodic memory performance. The regression analysis demonstrated a significant positive relationship with both the left (R^2=0.23, t(18)=2.28, p=0.035) and right (R^2=0.31, t(18)=2.85, p=0.035) hippocampi, indicating that patients with larger hippocampal volumes experienced greater improvements in memory. I then investigated whether this relationship was also evident in hippocampal subfields. The right middle hippocampus exhibited the strongest association with improvements in episodic memory, explaining approximately 43% of the variance through baseline right middle hippocampal volume (R^2=0.43, t(18)=2.85, p=0.035, **Figure 3.15B, Table 3.15).** A moderate positive relationship was observed between the anterior (R^2=0.23, t(18)=2.33, p=0.038) and posterior (R^2=0.28, t(18)=2.65, p=0.033) right hippocampus and changes in memory performance. Interestingly, in the left hemisphere, the anterior hippocampus, which was the simulation target, did not demonstrate a significant relationship with memory performance (R^2=0.10, t(18)=1.39, p=0.180), while both the middle (R^2=0.29, t(18)=2.69, p=0.033) and posterior (R^2=0.24, t(18)=2.40, p=0.038) regions showed a significant positive correlation. To test whether the observed relationship was specific to episodic memory function, I also replicated the analysis for the general cognition performance scores. No significant relationships were found (**Figure A3**). In summary, the results indicate that patients with larger baseline hippocampal volumes experienced greater improvements in episodic memory function following TI stimulation.

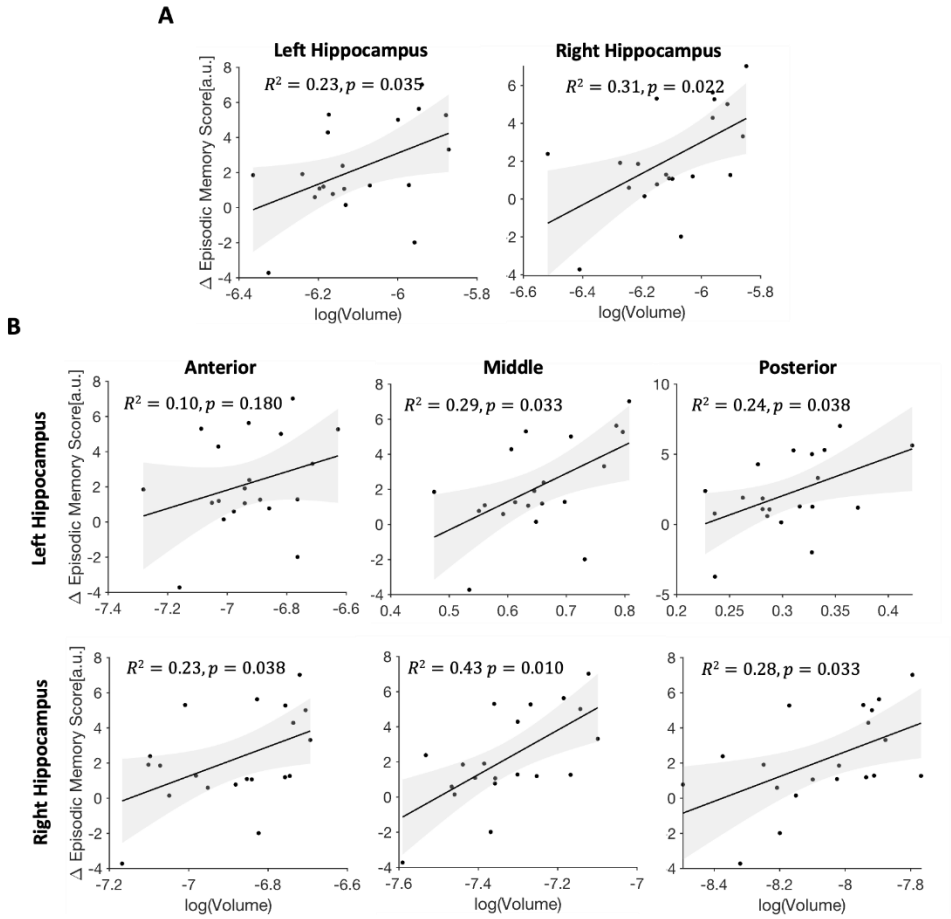


Figure 3.15 Relationship between baseline hippocampal volumes and improvement in episodic memory performance.

A. Regression analysis showed a significant positive relationship between baseline hippocampal volumes and improvements in episodic memory function. The right hippocampus displayed a had a stronger relationship with the changes in memory performance (R^2=0.31, t(18)=2.85, p=0.035) compared to the left (R^2=0.23, t(18)=2.28, p=0.035). **B.** When looking at the hippocampal subfields, middle right hippocampus was found to have the strongest relationship with improvement in performance (R^2=0.43, t(18)=2.85, p=0.035). Interestingly the left anterior hippocampus, which was the stimulation targe did not display a significant relationship with changes in episodic memory function (R^2=0.10, t(18)=1.39, p=0.180. All significance were adjusted using FDR.

Table 3.14 Statistical results for Figure 3.15.

Hemisphere	Predictor	Estimate	SE	CL Lower	CL Upper	*t*-value	df	R^2	*p*-value Adjusted
Left	Whole	8.84	3.87	0.70	16.97	2.28	18	0.23	0.035 *
	Ant.	5.23	3.75	-2.65	13.10	1.39	18	0.10	0.180
	Mid.	10.04	3.73	2.19	17.88	2.69	18	0.29	0.033 *
	Post.	8.29	3.46	1.02	15.55	2.40	18	0.24	0.038 *
Right	Whole	8.27	2.91	2.16	14.38	2.84	18	0.31	0.022 *
	Ant.	8.39	3.60	0.83	15.95	2.33	18	0.23	0.038 *
	Mid.	12.65	3.44	5.41	19.88	3.67	18	0.43	0.010 *
	Post.	7.04	2.66	1.45	12.62	2.65	18	0.28	0.033 *

p-value adjustment: FDR

3.3.7 No changes in ^{18}F-BCPP-EF SUVR in the hippocampus following 10 days of TI stimulation

Figure 3.16. **A** shows an example of a patient's individual MRI and average Standardised Uptake Value (SUV) images (10 –90 min) of ^{18}F-BCPP-EF at baseline and post-TI. The image shows the heterogeneity of overall tracer uptake in different regions of the brain, with higher uptake in grey matter areas (e.g., striatum and cortex) and lower uptake in the white matter (e.g., CS). The CS serves as a pseudo-reference region with the lowest tracer uptake. The SUV ratios (SUVR) were calculated by normalising summed SUVs in the target region determined over 70-90 min after ^{18}F-BCPP-EF administration to that of CS. The average SUVR values in the hippocampus for each hemisphere were compared at baseline and post-TI. The main effect of the Session was not significant ($F(1,57)=0.33$, $p=0.566$), indicating that MC-1 density, measured by ^{18}F-BCPP-EF SUVR, did not change from baseline following 10 days of hippocampal stimulation (**Figure 3.16C, Table 3.16**). No differences were observed between the left and right hippocampus. On average, the hippocampus showed one of the lowest SUVR values (M=1.93; SD$\pm$0.20) across all available brain regions, only preceded by amygdala (M=1.92; SD$\pm$0.17), showing a significant difference, the highest being observed in the putamen (M=3.99; SD$\pm$0.31). This aligns with previous findings indicating that ^{18}F-BCPP-EF tracer uptake was lowest in the hippocampus (Mansur et al., 2021).

3.3.8 Relationship between hippocampal and global changes in ^{18}F-BCPP-EF SUVR

When looking at the changes across other regions of the brain, I observed a general trend towards reduction from baseline in all brain regions apart from the caudate. There was approximately -0.54% ($\pm$3.2%) global reduction in SUVR values from baseline (**Figure 3.16D**). Additionally, in most patients, upward or downward changes were observed across most brain regions (**Figure 3.16B**). To investigate whether the hippocampal SUVR values tracked these brain-wide SUVR changes from baseline to post-TI, I computed a Global Mean SUVR per patient per session by averaging all available regions, excluding the hippocampus. I then mean-centred the values and fit an LME model in which ROI SUVR were predicted by Session (baseline vs. post), Global Mean SUVR, and their interaction, with a random intercept for Subject. The results revealed for the left hippocampus, there was no significant main effect of Session ($p=0.285$) while the main effect of Global Mean SUVR was highly significant ($F(1,24)=98.73$, $p<0.001$), with modest negative interaction with the Session ($F(1,19)=9.64$, $p=0.006$), indicating that hippocampal SUVR is strongly correlated with global SUVR and that this relationship changes slightly from baseline to post (**Table 3.17**). I then directly regressed each patient's hippocampal SUVR change from baseline to the global SUVR change. The model explained approximately 81% of the variance in the changes observed in the left hippocampus ($t(17)=8.1$, $p<0.001$, $R^2=0.81$) and 72% in the right ($t(17)=6.63$, $p<0.001$, $R^2=0.72$; **Figure 3.17; Table 3.17**). Taken

together, these results indicate that hippocampal SUVR changes closely mirrored overall variations in SUVR in the brain, and no unique session-specific effects were detected. A recent paper investigating the test-retest variance of ^{18}F-BCPP-EF found that SUVR had a global mean test-retest variance of 8% ±3% suggested that global downward/upward shifts at retest could in part be attributed to differences in tracer uptake, as well as variations observed in the CS reference region (Mansur et al., 2021).

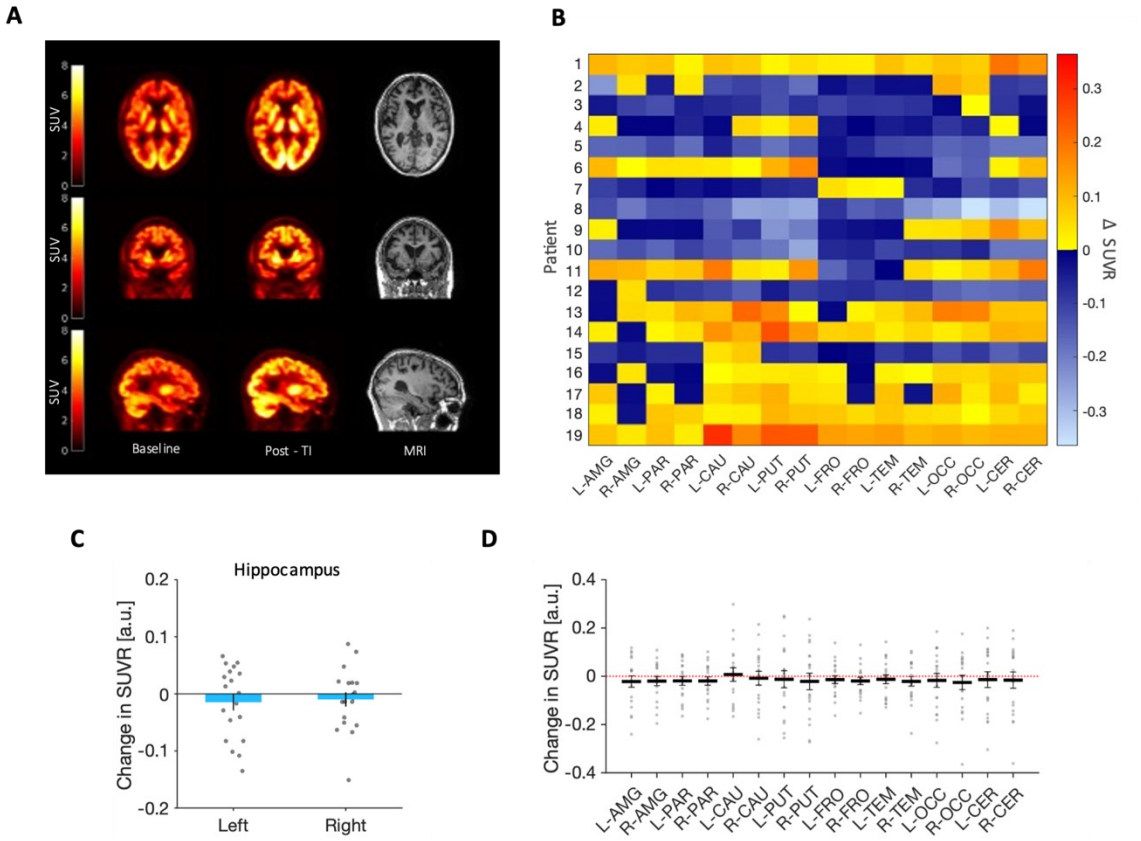


Figure 3.16 Changes in ^{18}F-BCPP-EF SUVR from baseline to post-TI.

A. Example patient's individual MRI and average SUV images (10 –90 min) of ^{18}F-BCPP-EF at baseline and post-TI. Image shows the heterogeneity of overall tracer uptake in different regions of the brain, with higher uptake in grey matter areas (e.g., striatum and cortex) and lower update in the white matter (e.g., centrum semiovale (CS)). CS serves as a pseudo-reference region with low racer uptake. The SUVR values were calculated buy normalizing summed SUVs in the target region determined over 70-90 min after ^{18}F-BCPP-EF administration to that of CS. **B.** The heatmap shows the mean change in SUVR from baseline to post-TI per patient. In most cases a general trend was observed where the direction of change was consistent across most brain regions. These global trends could indicate the effect of test-retest variance on the SUVR measurements. **C.** No significant changes were observed in SUVR values from baseline to post-TI ($F(1,57) = 0.33$, $p = 0.566$). Additionally no differences were found between left (stimulated) right hippocampus ($F(1,57) = 1.05$, $p = 0.310$). **D.** There was a global downward trend in SUVR values across all regions except the caudate (CAU) which also had the largest signal overall.

Table 3.15 Statistical results for Figure 3.16.

Effect	Sum Sq	Mean Sq	df1	df2	*F*-value	*p*-value
Session	2.88E-03	2.88E-03	1	57	0.33	0.566
Hemisphere	9.06E-03	9.06E-03	1	57	1.05	0.310
Session:Hemisphere	1.07E-04	1.07E-04	1	57	0.01	0.912

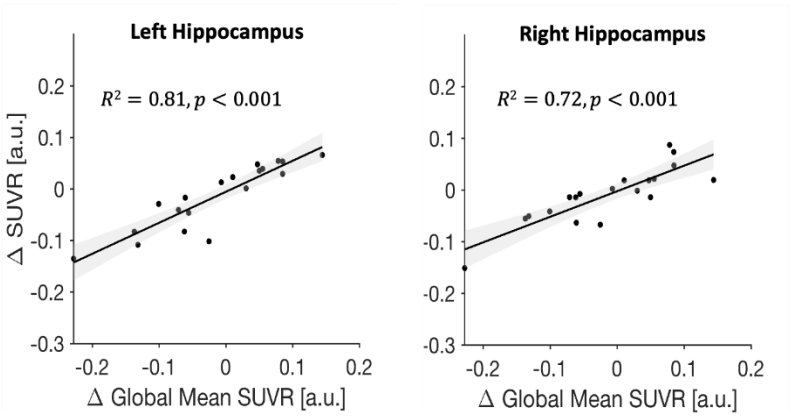


Figure 3.17 Relationship between hippocampal and brain wide SUVR changes.

The changes in the hippocampal SUVR from baseline to post-TI were largely predicted by brain wide changes in the Global Mean SUVR, with over 81% variance explained in the stimulated left hippocampus (R^2=0.81, t(17)=8.56, p< 0.001) and 72% in the right (R^2=0.72, t(17)=6.63, p< 0.001). These results indicate that session-to-session variance in the hippocampal ^{18}F-BCPP-EF SUVR were primarily governed by global changes.

Table 3.16 Statistical results for Figure 3.17.

Hemisphere	Effect	Sum Sq	Mean Sq	df1	df2	*F*-value	*p-value* Adjusted
Left	Session	3.44E-04	3.44E-04	1	19	1.49	0.238
	Global_mean	2.29E-02	2.29E-02	1	24	98.73	<0.001 ***
	Session:Global_mean	2.23E-03	2.23E-03	1	19	9.64	0.006 **
Right	Session	3.82E-05	3.82E-05	1	19	0.10	0.758
	Global_mean	2.01E-02	2.01E-02	1	25	51.51	<0.001 ***
	Session:Global_mean	1.35E-04	1.35E-04	1	19	0.35	0.563

Hemisphere	Term	Estimate	SE	CL Lower	CL Upper	*t*-value	df	R^2	*p*-value Adjusted
Left	Global_Mean_change	0.60	0.07	0.45	0.75	8.51	17	0.81	<0.001 ***
Right	Global_Mean_change	0.49	0.07	0.34	0.65	6.63	17	0.72	<0.001 ***

p-value adjustment: FDR

Considering this, the observed differences in the current study are within the range of test-retest variability.

3.3.9 No changes in hippocampal perfusion following 10 days of TI stimulation

Cerebral blood flow (CBF) images were produced for each patient to quantify absolute blood perfusion in the hippocampus. **Figure 3.18** shows anatomical and overlaid CBF images for an example patient with the sagittal plane at the left hippocampus (indicated by a white arrow). The mean hippocampal CBF at baseline across patients was 37.91 ml/100g/min (±6.61 SD; range: 26.95–48.26) for the left hippocampus and 36.81 ml/100g/min (±5.65 SD; range: 27.14–48.32) for the right hippocampus. This is in line with the values reported previously in AD patients with similar age groups (Li et al., 2020) and validates the image acquisition and analysis procedures. Additionally, it points to reduced hippocampal perfusion in the current patient group compared to healthy older adults reported in the literature (Li et al., 2020; Wang et al., 2022). There was a 2.1% increase from baseline in absolute CBF of the left hippocampus and 0.4% in the right hippocampus. However, these changes did not reach significance (F(1,63)=0.37, p=0.546; **Figure 3.19A; Table 3.18).** When comparing the CBF values normalised to the whole brain (nCBF), a reduction was observed, but this too was not statistically

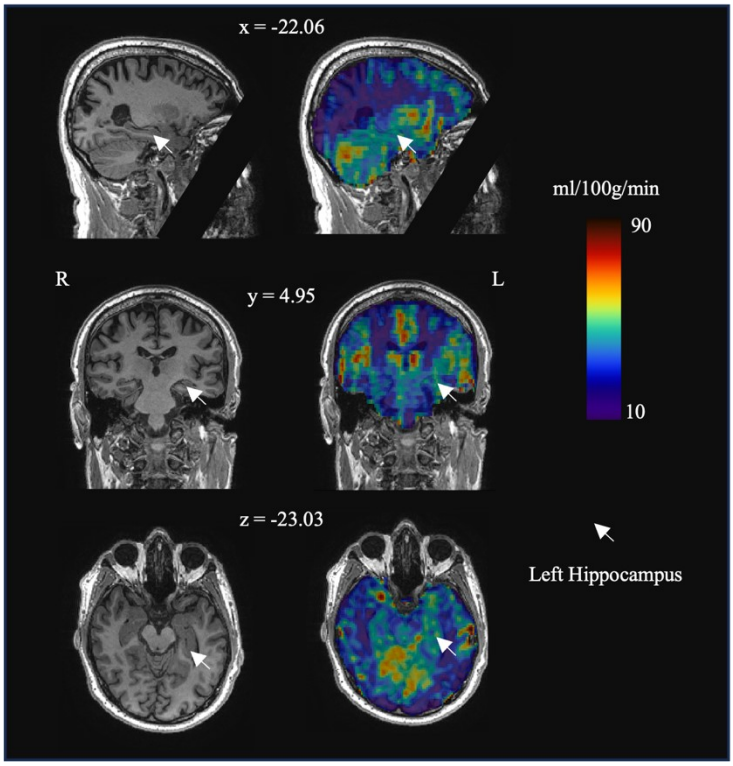


Figure 3.18 Perfusion image of an example patient.

CBF image is overlayed on patient's anatomical scan with coordinates showing the plane with left hippocampus.

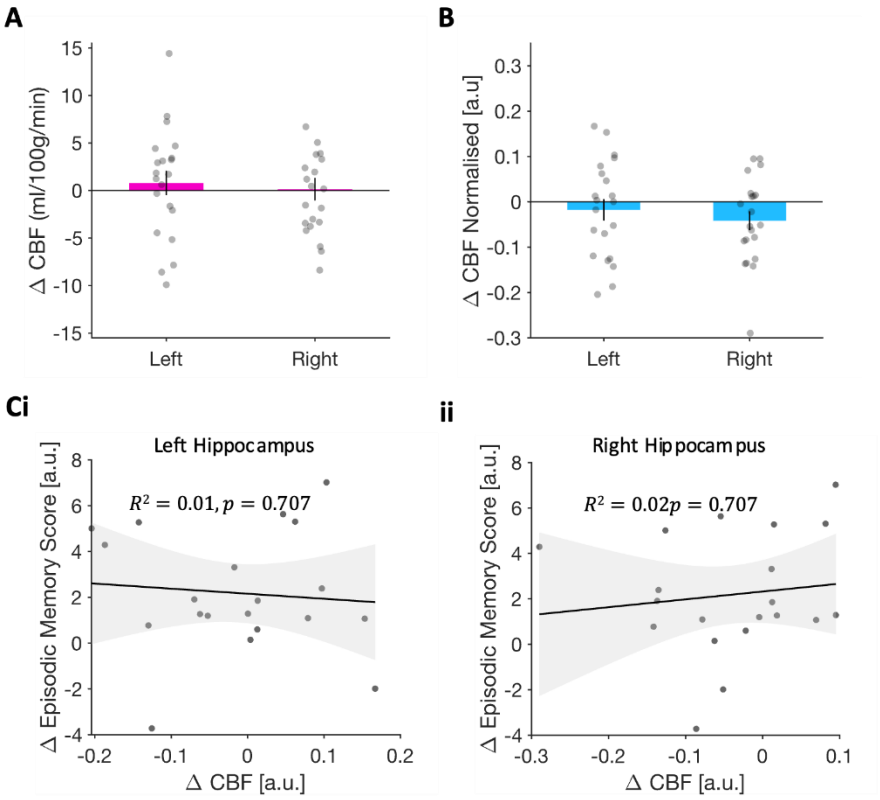


Figure 3.19 Changes in hippocampal perfusion from baseline to post-TI.

A. No changes were observed in the absolute CBF values in the left or right hippocampus from baseline to post-TI (F(1,63)=0.37, p=0.546). **B.** To account for potential test-retest variability in the perfusion images, the hippocampal CBF values were normalised by whole brain CBF. This showed a non-significant downward trend in both hemispheres (F(1,63)=3.88, p=0.053). **C(i-ii)**. No relationship was observed between changes in CBF and improvements in episodic memory scores (left hemisphere: R^2= 0.01; t(18) = -0.38, p=0.707; right hemisphere: R^2= 0.01; t(18)=0.54, p=0.707). p-value adjustment: FDR.

significant (F(1,63)=3.88, p=0.053; **Figure 3.19B**). There was a significant main effect of Hemisphere (F(1,63)=6.25, p=0.015), but post-hoc pairwise comparisons only showed a significantly greater CBF in the left hippocampus during baseline compared to right hippocampus post-TI (s2 < s1: t(66.2) = -3.08; p=0.015); No relationship was observed between changes in hippocampal CBF and improvements in episodic memory scores (left hemisphere: R2= 0.01; t(18) = -0.38, p=0.707; right hemisphere: R2= 0.01; t(18)=0.54, p=0.707).

Interestingly, no relationship was observed between baseline hippocampal volumes and baseline nCBF (**Figure 3.20 A**). Additionally, no relationship was observed between patients' MMSE and baseline hippocampal nCBF (**Figure 3.20 B**).

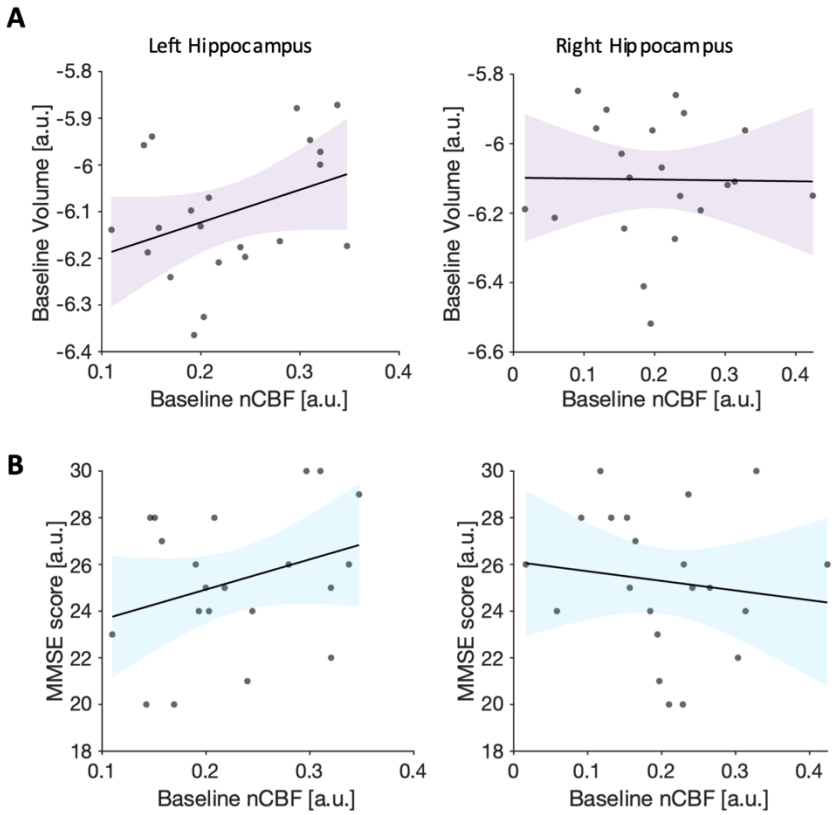


Figure 3.20 Relationship between hippocampal CBF and AD biomarkers.

A. No relationship was observed between baseline volume and baseline CBF in left (R^2= 0.13; t(19)=0.1.17, p=0.208) or right (R^2= -1.98E-04; t(19)=-0.06, p=0.952) hippocampus. **B**. No relationship was observed between patients' MMSE scores and baseline CBF in left (R^2= 0.10; t(19)=0.1.43, p=0.338) or right (R^2=0.02; t(19)=-0.58, p=0.572). p-value adjustment: FDR.

.

Table 3.17 Statistical results Figure 3.19.

LME on raw and normalized hippocampal CBF values. For normalization, the regional CBF values were divided by whole brain CBF, and log transformed.

Predictor	Dependent Variable	Sum Sq	Mean Sq	df1	df2	*F*-value	*p*-value	
Session	Raw_CBF	4.61	4.61	1	63	0.37	0.546	
Hemisphere	Raw_CBF	42.68	42.68	1	63	3.42	0.069	
Session:Hemisphere	Raw_CBF	2.21	2.21	1	63	0.18	0.675	
Session	nCBF	0.02	0.02	1	63	3.88	0.053	
Hemisphere	nCBF	0.03	0.03	1	63	6.25	0.015	*
Session:Hemisphere	nCBF	2.99E-03	2.99E-03	1	63	0.63	0.430	

Predictor	Dependent Variable	Estimate	SE	CL Lower	CL Upper	*t*-value	df	R^2	*p*-value Adjusted
L_HPC_delta_nCBF	Delta_EM	-2.21	5.78	-14.34	9.93	-0.38	18	0.01	0.707
R_HPC_delta_nCBF	Delta_EM	3.45	6.40	-9.99	16.89	0.54	18	0.02	0.707

p-value adjustment: FDR

Table 3.18 Statistical results for Figure 3.20.

Regression analysis testing the relationship between AD biomarkers (MMSE scores and hippocampal volumes at baseline) and baseline hippocampal CBF.

Predictor	Dependent Variable	Estimate	SE	CL Lower	CL Upper	*t*-value	df	R^2	*p*-value Adjusted
L_HPC_cbf	mmse	12.92	9.04	-6.00	31.85	1.43	19	0.10	0.338
R_HPC_cbf	mmse	-4.12	7.16	-19.12	10.87	-0.58	19	0.02	0.572
L_HPC_cbf	L_HPC_vol	0.70	0.41	-0.16	1.56	1.71	19	0.13	0.208
R_HPC_cbf	R_HPC_vol	-0.03	0.42	-0.91	0.86	-0.06	19	1.98E-04	0.952

p-value adjustment: FDR

3.4 Discussion

In this chapter, I presented the first application of repeated TI stimulation of the hippocampus in 21 AD patients. The primary goal of the study was to assess the safety and tolerability of repeated TI stimulation, measured via self-reported questionnaires and brain imaging.

Patients tolerated TI stimulation well, and no serious adverse effects were reported. Three participants withdrew from the study for reasons unrelated to TI, resulting in a compliance rate of 98.6%. We successfully delivered the maximum current intensities (1mA and 3mA per electrode pair) in 80% of patients without discomfort. The most reported side effect was “trouble concentrating”. While this is not typically associated with TES, it is a commonly reported symptom in AD patients (Malhotra, 2019). No additional side effects were observed beyond the mild skin sensations frequently reported with conventional TES (Antal et al., 2017; Matsumoto & Ugawa, 2017). Additionally, most side effects were transient and disappeared before the subsequent TI session. Finally, cumulative exposure to TI stimulation did not lead to an increase in side effect occurrence or severity, and no changes in hippocampal volume were observed at the end of the intervention compared to baseline. Based on these observations, I conclude that repeated TI hippocampal stimulation in AD patients is safe and well tolerated.

The second aim of the study was to establish a proof of concept that repeated TI stimulation can improve episodic memory function in AD. To test this, I compared performance on episodic memory tasks to that from other cognitive domains, including processing speed, executive function, visuospatial and lexical processing. Overall, patients improved significantly across both task groups. However, gains were significantly greater in episodic memory compared to general cognition, while changes in general cognition scores alone did not reach significance. A direct comparison of individual tasks in each category supported this finding, with 5 out of 8 episodic memory performance measures showing a significant improvement from baseline, whereas none of the tasks in the general cognition group showed statistical significance. Interestingly, participants demonstrated greater improvements in delayed episodic memory compared to immediate and did not improve on word and face recognition tasks, indicating a potential differential effect on different episodic memory processes.

Given that the present study does not have a control condition, it is challenging to isolate the effects of the stimulation from other factors that may have influenced the performance. Below, I will discuss these potential confounding factors and their possible independent contribution to the observed results.

What are the potential effects of practice on the observed selective improvements in episodic memory?

There are three key elements to consider here: 1) the effect on procedural learning and memory; 2) the effect of learning on memory due to repeated exposure to the test stimuli at baseline and post-TI; and 3) the effect of episodic memory training during the 10 days of concurrent TI stimulation. Procedural learning refers to improvements in skills or task performance through repetition; it does not involve explicit recollection and has minimal reliance on the hippocampus (De Wit et al., 2023; Machado et al., 2009). During implicit learning, improvements in performance at re-test are observed in the absence of intervention, even when task stimuli are not repeated (Almkvist & Graff, 2022; Basche et al., 2024). In AD, procedural learning is relatively preserved until the later stages of the disease (De Wit et al., 2021) and could therefore account for performance improvements independent of the TI effects. However, implicit learning is not domain-specific and has been observed across motor, verbal, auditory, visuospatial, and other cognitive tasks (De Wit et al., 2021). Thus, if procedural learning were the primary driver of cognitive performance improvements in AD patients, its effects would likely be evident across multiple cognitive domains, including motor and visuospatial tasks, rather than being selective to episodic memory. Given this, I argue that procedural learning alone does not account for the observed selective improvement in episodic memory performance.

The second element of practice that may have contributed to the observed cognitive changes is learning due to repeated exposure to the task stimuli at baseline and post-TI. However, the literature on learning in AD is inconsistent. Generally, it is accepted that AD and MCI patients exhibit a disease-related decline in learning with task repetition compared to healthy older adults, which is particularly pronounced in episodic memory (Duff et al., 2024; Jutten et al., 2020; Holm et al., 2022; Casaletto et al., 2017). However, some studies report a complete absence of learning in episodic memory in AD and propose that the lack of learning on standard neurocognitive measures should serve as a biomarker of the disease (De Simone et al., 2021; Hassenstab et al., 2015). In contrast, a recent systematic review suggests that both MCI and AD patients can exhibit learning effects on episodic memory tests even in the absence of an intervention (Holm et al., 2022). Interestingly, learning effects were rarely observed for both immediate and delayed recall of Logical Memory. Studies with similar re-test intervals of 1–2 weeks as in the current study have reported both improvement (Lee et al., 2023) and no learning (Duff et al., 2007; 2011; 2015) on Logical Memory in MCI and AD patients.

The inconsistencies in the literature on learning and memory in AD, particularly when assessed using standard neurocognitive batteries, likely stem from the high heterogeneity of clinical presentation of

the disease. However, an important observation across these studies is that learning effects, similar to procedural memory, are not domain-specific (Holm et al., 2022; Yan & Dick, 2006; Chan et al., 2024). In the present study, stimuli were repeated across all tasks, including general cognition tasks. Therefore, selective improvements in episodic memory cannot be solely attributed to re-test learning, as such effects would also be expected in other cognitive domains.

Finally, patients received cognitive testing only in associative memory throughout the 10 days of TI therapy. Additionally, a significant positive relationship was observed between improvements in the RT composite measure from associative memory tasks and gains in episodic memory composite scores. One could argue that the daily practice of associative memory tasks alone could account for the selective improvement observed in episodic memory function, even in the absence of intervention effects. However, evidence from past research on the efficacy of cognitive training in AD patients is highly inconsistent, particularly in studies with training durations similar to the present study. For example, a systematic review of randomised controlled trials (RCTs) found that only 5 out of 23 studies reported improvements in episodic memory following cognitive training in AD patients (Kallio et al., 2017). Moreover, cognitive improvements were often task-specific, with limited transfer to other domains or even to different tasks within the same domain (Kang et al., 2024; Finn & McDonald, 2015; Heugten et al., 2016).

In the present study, it is not possible to isolate the specific contributions of memory training from the effects of TI stimulation. The improvements observed in task performance, both during TI stimulation and following the intervention, are likely attributable to a combination of TI stimulation and memory training, and it is unlikely that training alone would have resulted in such selective improvements in episodic memory. Previous research looking at combined brain stimulation and cognitive training in AD supports this argument. For example, a recent review analysing data from 15 RCTs found that integrating non-invasive brain stimulation (NIBS) with cognitive training in MCI and AD patients was more effective than a control condition alone (Yang et al., 2024). Similarly, a meta-analysis reported that repetitive TMS (rTMS) combined with cognitive training led to greater treatment outcomes compared to a control condition alone (Liu et al., 2024).

What are the potential mechanisms underlying the selective improvement in episodic memory function observed in AD patients following repeated TI stimulation?

The mechanisms by which hippocampal-targeted TI stimulation improved episodic memory can be divided into 1) online effects (during stimulation) and 2) offline effects (memory improvements lasting 24 hours after stimulation has ended).

Online effects: One of the primary mechanisms through which TI stimulation may enhance episodic memory function during stimulation is by biasing state-dependent neuronal spike timing to better align with hippocampal theta oscillations. Support for this argument comes from two recent studies: Vieira et al. (2024) demonstrated that TI stimulation modulates neuronal spike-timing in non-human primates at rest, leading to phase perturbations of ongoing oscillatory activity. Additionally, Zheng et al. (2024) causally linked the phase precision of hippocampal neurons relative to endogenous theta rhythms to episodic memory function and demonstrated that the strength of phase precision predicted recognition success. Based on the above evidence, it is plausible that theta-TI applied to the hippocampus could improve memory by enhancing task-related spike-time precision. Support for this argument also comes from the study outlined in Chapter 2, showing that TI stimulation of the hippocampus improved episodic memory performance (Violante, Alania et al., 2023). In addition, TI may also stabilise the transient task-induced theta oscillations and/or enhance large-scale hippocampal-cortical synchronisation that supports episodic memory function (Zheng et al., 2024; Gattas et al., 2023). Given that hippocampal-cortical connectivity is weakened in AD (Canter et al., 2016; van Nifterick et al., 2023), TI stimulation may restore synchrony within these large-scale networks, thereby improving memory function.

Offline effects: The persistence of memory improvements following repeated TI stimulation suggests that the intervention could have induced lasting neuroplastic changes in hippocampal memory networks. One likely mechanism is spike-timing-dependent plasticity (STDP), which is tightly linked to theta-phase spike-timing in the hippocampus (Andrade-Talavera et al., 2023). Given that hippocampal neurons encode temporal sequences by firing at progressively earlier phases of theta cycles (Zheng et al., 2024), repeated TI stimulation may reinforce phase-locked firing patterns over time, strengthening synaptic connections in a manner consistent with STDP-induced long-term potentiation (LTP).

Other NIBS techniques have also demonstrated cognitive benefits in AD, further supporting that targeting network dysfunction and synaptic plasticity is a viable therapeutic approach. Gamma-frequency (40 Hz) tACS has been shown to enhance episodic memory function and modulate cholinergic neurotransmission, a key pathway involved in AD-related cognitive decline (Benussi et al., 2021). Transcranial direct current stimulation (tDCS) has also shown effectiveness in targeting

aberrant network activity and related memory function in AD patients (Majdi et al., 2022). Similarly, theta-burst rTMS applied to the dorsolateral prefrontal cortex (DLPFC) has been found to slow cognitive decline and reduce hippocampal atrophy, suggesting that theta-frequency neuromodulation may promote neuroprotection and functional recovery in memory networks (Wu et al., 2024). NIBS interventions have also been linked to synaptic plasticity mechanisms both for diagnostic purposes and treatments (Chou et al., 2022). The findings from these studies align with the mechanisms proposed for TI stimulation, reinforcing the role of network synchronisation and synaptic plasticity in cognitive recovery. Importantly, TI offers the ability to target the hippocampus directly, which is the main limitation of other modalities, and thus it could offer greater therapeutic potential by more precisely modulating key disease biomarkers associated with cognitive decline in AD

Can TI stimulation explain observed VBM changes?

The VBM results revealed cluster-specific increases from baseline to post-stimulation in areas of the middle and superior frontal gyri. Some studies have reported these coordinates to be associated with episodic memory performance (e.g., Henson et al., 1999; Becker et al., 2015) and semantic processing in Alzheimer's disease (Peelle et al., 2014). However, no relationship was found between change in cluster volumes and cognitive performance in the present study. Additionally, the cluster coordinates are unlikely to have been exposed to the TI envelope directly, thus reducing the potential TI contribution. Therefore, the observed changes are likely an epiphenomenon and could be attributed to a combination of factors beyond direct TI effects. Notably, patients participated in a three-week study involving daily visits, during which they engaged in frequent interactions with different members of the research team. This level of sustained social engagement, structured cognitive stimulation, and increased physical activity may have contributed to structural changes. Prior research has demonstrated that social and cognitive enrichment can enhance neuroplasticity and influence brain structure, particularly in prefrontal regions associated with cognitive control and social cognition (Elamin et al., 2012; Colavitta et al., 2023).

No volumetric changes were observed in the TI-targeted hippocampal regions, which was expected given the relatively short duration of the stimulation protocol. Additionally, repeated TI stimulation could likely offer neuroprotective effects over longer periods, delaying synaptic loss with disease progression. Neuroprotective effects of NIBS have been observed previously; for example, AD patients who underwent one year of rTMS therapy exhibited delayed grey matter volume loss compared to controls (Wu et al., 2024), suggesting that prolonged neuromodulation may help preserve structural integrity in neurodegenerative conditions.

How can the absence of CBF changes be explained?

The lack of changes in the regional CBF could be due to the poor sensitivity of ROI-based CBF analysis in a repeated measures design. A recent study investigating repeated tACS stimulation of the medial temporal cortex in AD patients found no changes in the regional CBF following 2 weeks of 1-hour daily stimulation (Sprugnoli et al., 2021). However, the voxel-wise analysis showed a significant increase in the CBF in the targeted regions. Therefore, future analysis will focus on voxel-wise statistics to test whether TI induced more subtle changes in the blood perfusion in the targeted hippocampal region.

How can the absence of ^{18}F-BCPP-EF SUVR changes be explained?

As demonstrated in the results section, the observed changes in regional SUVR were largely driven by global fluctuations in SUVR. This is likely attributable to the test-retest variability of ^{18}F-BCPP-EF, which has been reported to be 8% ± 3% (Mansur et al., 2021). Such variability may obscure true TI-related effects, particularly in a small sample size. Moreover, baseline SUVR values in the hippocampus did not correlate with MMSE scores or regional volumes, which was unexpected and inconsistent with previous findings (Terada et al., 2022). A potential explanation for this discrepancy is the choice of reference region. The centrum semiovale (CS) was used as the reference region in the present study due to its minimal specific binding of ^{18}F-BCPP-EF tracer. However, it should be noted that CS is not entirely free of MC-I and can introduce test-retest variability. Moreover, this variance could be larger in the AD population due to white matter degeneration and microstructural damage associated with the disease (Chen et al., 2023). In contrast, whole-brain normalisation accounts for global tracer uptake and may provide a more stable reference and should be explored in the future. Additionally, voxel-based analysis could offer greater sensitivity in detecting subtle regional changes that may be overlooked in an ROI-based approach and should also be explored.

Summary and future directions

In summary, the present study was successful in two of its aims and demonstrated that repeated TI hippocampal stimulation in AD patients is safe and well tolerated and provided feasibility for the therapeutic benefits of TI hippocampal stimulation on episodic memory function. However, to causally establish the therapeutic benefits of hippocampal TI stimulation on memory function and underpinning physiology, a randomised, double-blind, sham-controlled study is required, which is currently underway. In the present study, additional support for the TI stimulation effects on memory function and imaging could be provided from the analysis of remaining outcome measures. Patient-specific electrode locations on the T1-weighted structural scans were acquired using a

neuronavigation system for a subset of patients (n=13). The analysis of envelope magnitude in the hippocampus and its relationship with observed changes in performance could validate the direct contribution of TI to improvements in episodic memory.

Chapter 4: Combined TI stimulation and EEG monitoring in humans: hardware approaches for recording artefact-free EEG during TI stimulation.

4.1 Project Overview

Much like the topic of its investigation, this project followed a non-linear path. Originally, I set out to implement custom-made hardware solutions to record artefact-free EEG recordings during concurrent electrical stimulation and test the direct effects of TI on brain activity. However, the scope of detecting and fully eliminating small non-linear stimulation artefacts in the EEG during TI stimulation only became evident through an iterative process of hardware optimisation and implementation in experimental procedures. As a matter of course, this chapter is divided into two sections: (1) iterative development and validation tests of combined custom-made and commercial hardware to allow artefact-free EEG recording during TI stimulation and (2) implementing the hardware in a study testing the neuromodulatory effects of TI on steady-state visually evoked potentials (SSVEPs).

4.2 Introduction

Transcranial alternating current stimulation (tACS) offers a means to non-invasively modulate brain oscillations by applying weak sinusoidal currents to the scalp to entrain endogenous neuronal rhythms, influencing spike timing and thereby modulating cognitive and perceptual processes through frequency-specific and network-targeted neuromodulation (Herrmann et al., 2013; Herrmann et al., 2016; Antal et al., 2017; Vöröslakos et al., 2018; Helfrich et al., 2014). While effective entrainment depends on matching or closely approximating applied frequencies with endogenous brain rhythms, in vivo monitoring of neural activity during stimulation remains challenging. The sinusoidal currents used in tACS introduce large electrical artefacts in EEG recordings, which spectrally overlap with the target brain rhythms (Noury et al., 2016; Kasten et al., 2018; Kasten & Herrmann, 2019; Vosskuhl et al., 2020; Holzmann et al., 2021). As a result, many tACS studies have relied on pre- and post-stimulation electrophysiological measurements and behavioural endpoints to infer neuromodulatory effects, providing only indirect evidence for ongoing oscillatory changes during stimulation and their behavioural effects (e.g., Polanía et al., 2012; Vossen et al., 2015; Kasten et al., 2016; Aktürk et al., 2022).

Over the last decade, several approaches have been developed to address the challenge of recording brain activity concurrently with tACS. These have primarily centred on artefact removal strategies, such as notch filtering, template subtraction, adaptive filtering, and advanced spatial filtering techniques (e.g., Kasten et al., 2018; Kasten & Herrmann, 2019; Holzmann et al., 2021; Vosskuhl et al., 2020). Although these strategies can significantly attenuate the stimulation artefacts, they have several limitations. Simple filtering often removes or distorts genuine neural signals near the stimulation frequency (Kasten & Herrmann, 2019). Template-based approaches rely on stable artefact waveforms that may not account for non-linearities or physiological modulations (Kasten & Herrmann, 2019; Noury et al., 2016). Moreover, even sophisticated methods cannot guarantee the complete elimination of the tACS artefact and can lead to residual signals being mistaken for true neuronal entrainment (Noury et al., 2016; Kasten & Herrmann, 2019).

Recently, amplitude-modulated tACS (AM-tACS) and temporal interference (TI) have emerged as novel non-invasive brain stimulation strategies, providing a promising alternative to standard tACS by potentially enabling real-time EEG/MEG recording during stimulation. Although the two methods differ in how the applied waveform is generated, both rely on delivering a high-frequency carrier waveform (often in the kilohertz range) modulated in amplitude by a low frequency of interest. In AM-tACS, the waveform is pre-modulated and thus a single waveform is applied (Witkowski et al., 2016). By contrast, TI stimulation delivers two high-frequency currents with offset frequencies in the same range as frequencies of interest (e.g., 2000 Hz and 2010 Hz). At the point of overlap, the interference of the two waveforms produces an AM signal with an envelope frequency equal to the difference between the carriers (Grossman et al., 2017).

In both AM-tACS and TI, neurons are believed to respond predominantly to the low frequency envelope while effectively filtering out the high-frequency carriers (Grossman et al., 2017; Witkowski et al., 2016). This is due to the intrinsic low-pass characteristics of neuronal membranes, although the exact mechanism by which neurons demodulate the envelope signal is still under active investigation (Grossman et al., 2017).

Since the applied stimulation contains spectral power predominantly at carrier frequencies, this should, in principle, allow real-time EEG recording. This is because linear stimulation artefacts shift into higher frequencies, which are usually above the dynamic range of neural activity. Removing these artefacts during post-processing (or real-time) should, in theory, recover artefact-free brain signals at the frequencies of interest.

However, in practice, in addition to the linear artefacts at the carrier frequencies, artefacts also emerge at the target (i.e., modulation) frequencies. These artefacts are primarily driven by non-linearities in both the stimulation and recording hardware (Kasten et al., 2018; Von Conta et al., 2022). Although artefact removal strategies have also been applied in TI and AM-tACS (e.g., Haslacher et al., 2021; 2023), just like in tACS, completely removing these artefacts remains challenging and can bias the analysis of electrophysiological data (Kasten & Herrmann, 2019; Noury et al., 2016).

In this chapter, I aim to address this challenge by implementing hardware filters to allow artefact-free EEG recording in real time during TI stimulation. Specifically, I first implement a front-end low-pass filter (LPF) developed by our collaborators to attenuate large kilohertz electric fields before they enter the recording amplifier. I then demonstrate that while LPF effectively accounts for artefacts originating in the recording hardware, very small residual artefacts remain, which are in the range of natural brain activity and can bias the EEG analysis at the target frequency. While sources of such small artefacts are more difficult to establish, I tested the high-pass filtering (HPF) strategy to suppress any potential non-linear artefacts originating in the current source before applying the TI stimulation to the head.

Finally, I demonstrate frequency-specific and state-dependent effects of TI stimulation of the right visual cortex on steady-state visually-evoked potential (SSVEPs) during concurrent EEG monitoring.

4.3 Methods

4.3.1 Pilot study

4.3.1.1 Participants and experimental setup

Five healthy young adults were recruited in the study (mean age $\pm$ SEM: 26 $\pm$3.5 years old; three female, four male; one left-handed). The scalp was prepared using an ethanol solution followed by NUPREP gel, and 16 Ag-AgCl electrodes were attached to the skin using Ten20 conductive paste. Electrode locations are displayed in **Figure 4.2**. EEG data were recorded using a BrainAmp EEG amplifier and BrainVision Recorder (Brain Products GmbH, Gilching, Germany) with a sampling rate of 5000 Hz using sixteen 4 mm Ag-AgCl electrodes, including reference and ground set to FCz and AFz, respectively (**Figure 4.2 A**). A custom TI stimulation was delivered using a custom-made differential current source via 2 channels targeting the right visual cortex (V1) at the O2 channel. Four self-adhesive carbon fibre TENS electrodes were cut into shapes 1 cm x 1.5 cm for the posterior and 2 cm x 2 cm for the anterior sites and attached to the scalp using Ten20 paste (see **Figure 4.1 A** for electrode locations). The area between the TI and EEG electrodes was thoroughly cleaned using an ethanol

solution to avoid bridging. Electrodes were fixed in place using surgical tape to prevent displacement during the experiment. Participants were instructed to sit still and look at a black cross positioned in front, at eye level. The EEG was recorded for 50 s with a 10 s baseline, 30 s stimulation (TI-10 Hz or sham) and 10 s post-stimulation. Each condition was repeated 12 times and was delivered in a counterbalanced order. During 10 Hz TI, 2000 Hz and 2010 Hz current in each electrode pair was ramped up for 5 s from 0-2 mA, remained stable for 20 s and ramped down for 5 s to 0 mA. In the sham condition, the current was ramped down immediately following the ramp-up and stayed off for the duration of the block. All devices used during stimulation were battery-operated.

4.3.1.2 Data acquisition

Data was extracted and pre-processed in MATLAB using a custom analysis pipeline. EEG data was high-pass filtered using a fourth-order Butterworth filter with a cut-off frequency of 1 Hz and visually inspected for artefact. The data was then divided into baseline and stimulation segments, and a 15-second segment was taken from the middle of the block in the 10 Hz TI or after the ramp-down in the sham condition.

4.3.2 Technical validation tests

All technical validation tests reported here were done in vivo involving volunteers from our team. The experimental setup was replicated to match the pilot study, except a single channel recording from O2 was acquired for speed and simplicity. All hardware was the same as in the pilot study; however, in the validation tests, I also used Brain Product's actiCHamp recording hardware as it offered a higher sampling rate, which was necessary for monitoring f1 and f2 sum frequencies.

4.3.3 Data analysis

4.3.3.1 Frequency domain analysis and Signal-to-Noise (SNR) computation

Given that intermodulation (IMD) artefacts are expected at a known frequency, the data were analysed in the frequency domain. First, I computed the one-sided power spectral density (PSD) over the entire 15-second window for each block using the Fourier transformation. I then implemented signal-to-noise ratio (SNR) analysis, which is frequently applied to the steady state response (SSR) data to detect responses to sensory stimuli (Meigen & Bach, 2000). The SNR at each frequency was derived by normalising the PSD at that frequency by an estimate of the noise floor, computed from surrounding spectral bins.

The noise power $\mathrm{N}(f)$ at a given frequency f was estimated as:

$$\mathrm{N}(f) = \frac{1}{2n}\sum_{k=1}^{n}[P(f - k\Delta f) + P(f + k\Delta f)]$$

Where $\mathrm{N}(f)$ is the estimated noise power at frequency f, computed from surrounding spectral bins. $P(f)$ represents the PSD at frequency f, obtained from Fourier analysis. The parameter n specifies the number of bins included on each side of f for averaging while k indicates the number of bins skipped before averaging (**Figure 4.5**). Δf represents the frequency resolution determined by the length of the FFT window. This approach ensures a robust noise estimate by preventing contamination from immediate neighbouring bins, thereby reducing spectral leakage and smoothing the noise spectrum. Finally, the SNR at each frequency bin was computed by dividing the spectral power by the estimated mean noise at that frequency:

$$\mathrm{SNR}(f) = \frac{P(f)}{\mathrm{N}(f)}$$

4.3.3.2 Detecting low frequency spectral peaks using permutation testing

To determine whether the peak at the modulation difference frequency (f2–f1) was statistically larger than the background EEG activity, a Monte Carlo permutation-based significance test was conducted. First, a null distribution of SNR values was generated by randomly sampling SNR values from neighbouring frequency bins within a pre-defined spectral window ($\pm$ 1 Hz), excluding frequencies immediately adjacent to the target frequency. For each permutation (n = 1000), a single SNR value was randomly drawn from the noise distribution to construct a surrogate dataset representing expected variability in SNR under the null hypothesis. The empirical p-value was then computed as the proportion of permuted SNR values that exceeded or matched the observed SNR at the target frequency. Finally, the presence of a statistically significant peak was determined by comparing the p-value to a predefined significance threshold (α < 0.01). If the p-value fell below this threshold, the peak was classified as significant, indicating that the SNR at the target frequency exceeded what would be expected by chance (see **Figure 4.5** for a visual summary of the pipeline).

4.3.3.3 EEG data simulation

To simulate EEG data, I generated a time-series signal that incorporates physiologically relevant spectral characteristics. First, I transformed white Gaussian noise into pink ($1/f$) noise by applying a frequency-dependent scaling factor in the Fourier domain — scaling each frequency component by

$1/\sqrt{f}$ — to impose the power-law decay characteristic of EEG signals. I then scaled the resulting pink noise so that its average amplitude within the alpha band (8–12 Hz) matched a predefined target value. This was accomplished by computing the power spectrum using FFT, extracting the power within the alpha range, and calculating a scaling factor as the ratio of the desired alpha amplitude and the measured amplitude. Next, I generated a sinusoidal signal at the specified target frequency and added it to the scaled noise to represent an intermodulation artefact. In the sensitivity analysis, this step was omitted. To further simulate inter-individual variability in endogenous alpha rhythms, I imposed a Gaussian-shaped multiplicative bump on the spectrum in the 8–12 Hz range. This bump, centred around 10 Hz with adjustable gain and width, selectively enhanced the spectral power while preserving the underlying noise and allowing me to randomly vary the parameters in each integration. Finally, I transformed the modified spectrum back to the time domain using an inverse FFT.

4.3.4 Study 1

4.3.4.1 Participants

Twenty-six participants were recruited for the study, but two subjects were excluded due to technical problems during data acquisition. Thus, the final cohort included 24 participants (12 females; mean age $\pm$SEM: 29.6 $\pm$4.2 years old). All participants were healthy, with no history of neurological or psychiatric illnesses and met the inclusion criteria for non-invasive electrical brain stimulation and visual light stimulation. Participants received detailed study information and gave written consent before the start of the experiment.

4.3.4.2 Experimental procedure

The study design is summarised in **Figure 4.1**. Participants were seated in a dark room while receiving TI stimulation targeting the occipital cortex at the O2 channel, and visual flicker stimulation at 33 Hz. Each experimental run consisted of six blocks. Each block included an initial 20 s baseline period, approximately 400 s of concurrent LED flicker and TI stimulation, and a 20 s post-stimulation period. EEG was recorded using the same procedure and hardware as in the pilot study.

4.3.4.2.1 Electrical stimulation

TI stimulation was delivered using a custom-built, battery-operated stimulation device. Four self-adhesive carbon-fibre TENS electrodes were cut into 1 cm × 1.5 cm for the posterior electrodes, and 2 cm × 2 cm for the anterior electrodes. The skin was cleaned using ethanol solution, and TI electrodes were attached at O2–T7 (Ch1) and PO8–FC8 (Ch2) using Ten20 conductive paste. The areas between

TI and EEG electrodes were carefully cleaned using an ethanol solution to prevent bridging. Three stimulation conditions were applied in a counterbalanced order: TI-10 Hz (f1 = 2000 Hz, f2 = 2010 Hz), TI-27 Hz (f1 = 2000 Hz, f2 = 2027 Hz), and sham (stimulation current ramped down immediately after initial ramp-up). For each active TI condition, the current was ramped up from 0 to 2 mA over 5 s, maintained at 2 mA for approximately 400 s, and then ramped down over 5 s to 0 mA.

Participant sensation thresholds are displayed in **Table 4.1.** The final stimulation current amplitude per subject was decided based on participants' sensation thresholds. The maximum amplitude with minimum sensations were used. In some cases, the current was reduced slightly due to high-pass filter requirements. Across the group, 1.88 $\pm$0.15 mA was delivered per channel (**Table A9**).

Table 4.1 Sensation thresholds during TI stimulation at 10 Hz.

Sensation	Occurrence (out of 26)	Sensation Threshold mA Mean ($\pm$SD)
No Sensation	19	2.00 (max)
Pressure	1	1.50 (0.00)
Tingling/Prickling	2	1.30 (0.21)
Vibration	2	1.75 (0.30)
Pulsing	1	1.50 (0.00)
Scalp pain	1	1.40 (0.00)

4.3.4.2.2 Light stimulation

The visual stimulation was delivered concurrently with TI stimulation using an LED array with 6 LEDs positioned 60 cm in front of the participant at eye level. The LED was switched ON for 1 s, followed by an OFF interval of $\sim$1.7 s with slight jitter across trials. 115 LED trials were delivered in each block, with 230 trials in total across two repetitions in each stimulation condition.

4.3.4.3 Data Analysis

EEG data was pre-processed using custom scripts in MATLAB. The raw EEG signal was extracted and visually checked for quality control. The data was then downsampled to 1000 Hz, bandpass filtered between 1 and 45 Hz using a second-order Butterworth filter and re-referenced to the median average.

4.3.4.3.1 Low frequency peak detection tests

For peak detection analysis, the original reference channel was used instead of the median average. The data was analysed in the frequency domain using the SNR approach as described in section **4.3.3.1**. Automated peak detection was performed using permutation testing as described in section **4.3.3.2**. Lastly, SNR at the target frequency was extracted in each condition and compared with a linear mixed-effects model (LME).

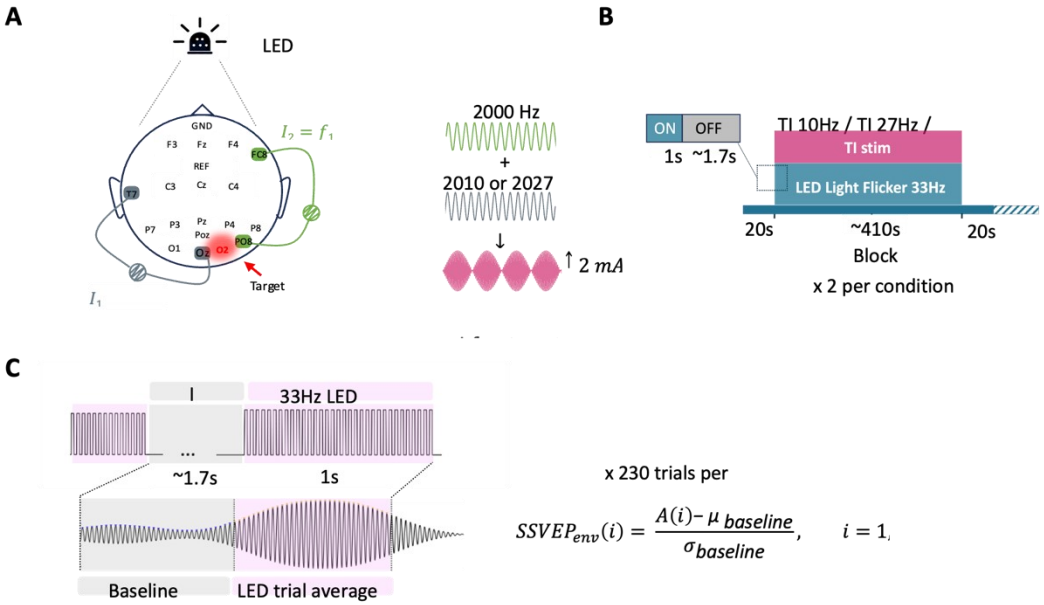


Figure 4.1 Study 1 experimental paradigm.

A. Participants in study 1 received TI stimulation of the occipital cortex targeting the O2 channel. At the same time, a visual light flicker was delivered using LED. EEG was recorded from 16 channels including the reference (REF) and ground (GND) electrodes positioned at FCz and AFz respectively. TI was delivered from 2 channels using 2000 Hz carrier frequency modulation frequencies ($\Delta\mathbf{f}$) at 10 Hz or 27 Hz at 2mA via four self-adhesive electrodes positioned at O2 -T7 on the left and PO8-FC8 on the right side of the head. The experiment was conducted in a dark room **B.** The Experimental timeline included ~440 s blocks of EEG recording, LED, and TI stimulation with 3 TI stimulation conditions repeated twice, thus summing to 6 blocks in total. Each block started with a 20 s baseline recording. followed by ~400 seconds of LED with concurrent TI stimulation and EEG recording. The block ended with 20 s post-stimulation EEG recording at rest. TI was delivered in three stimulation conditions: TI 10 Hz, TI 27 Hz or sham, during which the current was ramped down immediately after ramping up and remained off throughout the block. The condition order was counterbalanced across subjects using a Latin square. LED flicker was delivered at 33 Hz with 1 s ON and ~1.7 s OFF (jittered inter-trial interval) paradigm. **C.** Estimation of steady-state visually evoked potential (SSVEP) envelope. The narrow-band filtered EEG data was divided into LED onset trials, for each trial EEG data was extracted at each LED pulse and normalised by subtracting the mean and dividing by the standard deviation of the pre-LED baseline interval during which LED was off. This resulted in 33 values per LED trial which were then averaged across 230 trials in total per participant.

4.3.4.3.2 Analysis of steady-state visually evoked potentials (SSVEPs)

The steady-state visually evoked potentials (SSVEP) analysis was performed in the time domain and focused on the stimulated (O2) and the contralateral (O1) channels. The pre-processed EEG data were segmented into epochs aligned with the LED stimulation trials and then band-pass filtered again around the target frequency (32–34 Hz) using a second-order Butterworth filter to isolate the steady-state component. The filtered signal was then transformed using the Hilbert transform to obtain the analytic signal. The instantaneous amplitude of the 33 Hz response was extracted by taking the absolute value of the analytic signal. To compute the SSVEP envelope, the instantaneous EEG amplitude at each LED pulse was normalised to the pre-LED baseline period (1 s period before the onset of the LED) using the following formula:

$$SSVEP_{env}(i) = \frac{A(i) - \mu_{\text{baseline}}}{\sigma_{\text{baseline}}}, \; i = 1, \ldots, 33$$

Where $A(i)$ is the instantaneous amplitude at each LED pulse, μ and σ are the mean and standard deviation of the amplitude during the baseline period (see **Figure 4.1C**). To assess the effects of stimulation condition on SSVEP, I performed a cluster permutation test on the SSVEP envelope for each condition contrasted against the sham. Given that the pre-LED baseline period was also exposed to TI stimulation, I also performed a cluster permutation test on the baseline period. If any significant clusters were detected, median average values were extracted in each cluster for each subject and compared in subsequent parametric tests in a linear mixed-effects model. Any post-hoc pairwise comparisons were performed on EMMs with Tukey's correction for significance. Participants who did not display visually detectable Event-Related Potential (ERP) in the average of O1 and O2 channel data in the sham condition were excluded from the analysis. Six subjects were excluded from this analysis due to a lack of ERP in the sham condition; thus, the final n = 18.

4.3.4.3.3 Baseline alpha frequency

The baseline instantaneous alpha frequency for each experimental block was computed from the 20 s period recorded at rest before the start of each block while subjects had their eyes open in a dark room. The EEG data were band-pass filtered at 10 $\pm$2 Hz using a Butterworth filter with zero-phase filtering (using MATLAB's filtfilt function). The data was then divided into 5 s overlapping epochs with a 0.5 s sliding window. The analytic signal was computed per epoch by applying the Hilbert transform to the filtered time series. Instantaneous phase values were extracted, and any discontinuities were corrected by unwrapping the phase. Finally, the time derivative of the unwrapped phase was

calculated and scaled to convert the rate of phase change into instantaneous frequency in Hertz, and median average values across epochs were extracted.

4.3.4.3.4 TI Phase Extraction at LED Onset

The applied TI waveform was recorded for each channel using a data acquisition (DAQ) device at a 100 kHz sampling rate. The TI waveform was then aligned and downsampled to match the EEG data. Lastly, the waveform was narrowband filtered around the stimulation frequency, the analytic signal was obtained using the Hilbert transform, and the instantaneous phase was extracted at each LED onset trial.

4.4 Results

4.4.1 Mitigation of low frequency non-linear artefacts originating in the recording hardware with low-pass filtering

Given that a primary source of low frequency intermodulation distortion (IMD) in EEG during TI stimulation arises from non-linear interactions within the recording hardware, a straightforward strategy is to prevent the high-frequency stimulation currents from reaching the amplifier inputs. To achieve this, I added a low-pass filter (LPF) in the signal path between the EEG electrodes and the amplifier to attenuate the kilohertz-range carrier signals before the amplification step (**Figure 4.2**). Specifically, a custom-built, 16-channel, 8th-order active Butterworth LPF was developed in-house (I did not develop the filter) with a cut-off frequency of 100 Hz and a steep roll-off at higher frequencies, achieving ~50 dB attenuation at 2 kHz carrier signals when zero gain is used (**Figure 4.2C**). The filter was designed to handle input ranges up to 2 Vpp, which is ~5 times larger than many commercial EEG amplifiers (e.g., actiCHamp, $\pm$400 mV).

I tested the effectiveness of this LPF in a pilot study (details in **Section 4.3.1**). In brief, two carrier frequencies were applied (f1 = 2000 Hz, f2 = 2010 Hz) from two stimulation channels, with maximum modulation targeted at the right visual cortex (O2 channel; **Figure 4.2A**). The current was ramped up over 5 s and then maintained at 2 mA for 20 s before ramping down. This was compared to a sham condition in which the TI current was ramped down immediately after ramp-up and remained off. EEG was recorded throughout each 20-s block and an additional 10-s baseline and post-stimulation periods. Subjects underwent 12 blocks of TI stimulation and EEG recording in each condition (**Figure 4.2B**).

Figure 4.3A shows an exemplary O2-channel EEG recording from a single subject, comparing data with and without the LPF during concurrent TI stimulation. When no filter was used, a prominent 10 Hz IMD artefact emerged as the TI ramped up. These artefactual oscillations were orders of magnitude larger than endogenous brain activity. Frequency-domain analysis of the middle 15 s segment showed a strong 10 Hz peak (and its harmonics), and topographical mapping indicated the highest power at the stimulation target site where maximal modulation of the two currents was expected.

In contrast, with the LPF in the path, the raw EEG traces during stimulation were visually indistinguishable from the baseline, and no 10 Hz or harmonic peaks were detected in the frequency-domain analysis. The topographical plot similarly showed that 10 Hz power remained at typical physiological levels across the scalp.

To further analyse these data at the group level, I employed a common windowing approach for EEG power spectrum analysis. The EEG was band-pass filtered between 2 and 45 Hz, and the middle 15 s segment during stable TI delivery was extracted and divided into three 5 s non-overlapping epochs.

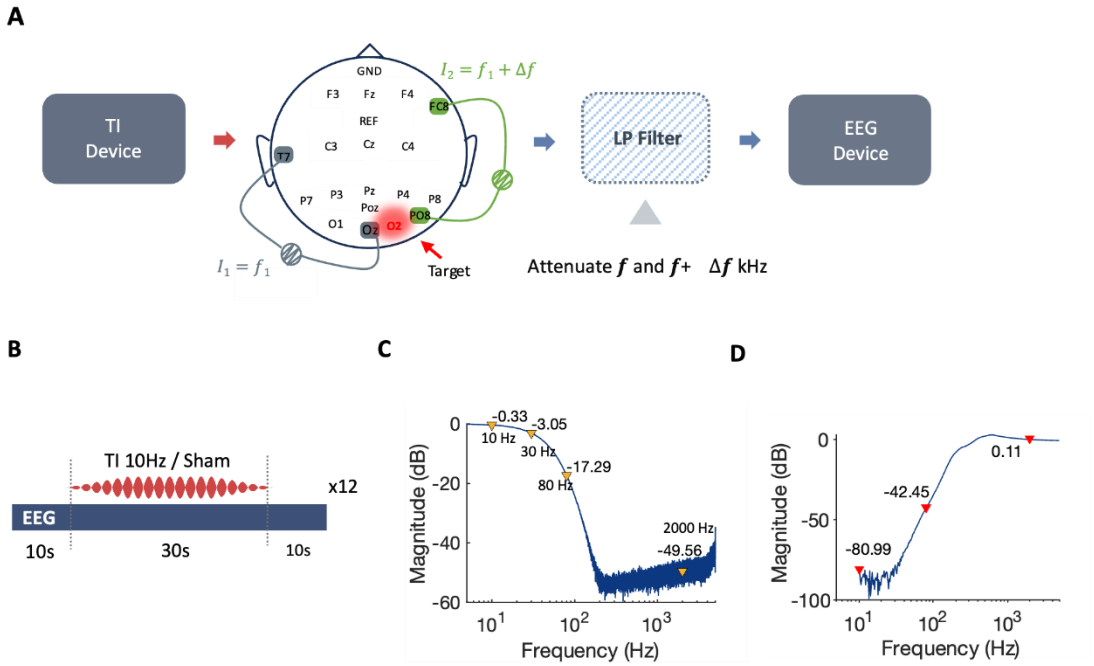


Figure 4.2 The low-pass filter (LPF) solution for low frequency non-linear artefact.

A. The experimental setup for the pilot study combines TI stimulation targeting O2 and front-end 14-channel low-pass (LP) filter to attenuate applied TI voltages before EEG amplification. **B**. Experimental timeline for the pilot study. Participants received 12 blocks of sham and 10 Hz TI stimulation for 30 s. Baseline EEG was recorded 10 pre- and post-stimulation period. **C**. Frequency response of the 8th order front-end LP filter showing ~ 50dB attenuation of TI carrier frequencies at 2000 Hz. **D**. Frequency response of the high-pass filter (HPF).

Each epoch's Power Spectral Density (PSD) was computed using the Fast Fourier Transform (FFT), averaged across epochs and then across blocks. I also computed the average alpha-band (8–12 Hz) power for each epoch for statistical comparison. **Figure 4.4Ai-iii** illustrates the PSD in the alpha range for both sham and TI-10 Hz conditions. No significant difference in alpha-band power emerged between conditions ($F(1,82) = 1.08$, $p = 0.302$).

However, when the entire 15-s segment was analysed without epoching (and then averaged across 12

blocks and participants), a more distinct 10 Hz peak emerged in the TI-10 Hz condition, which was significantly larger than the 10 Hz PSD in sham ($F(1,82) = 4.99$, $p = 0.028$). The topographical distribution of sham-subtracted 10 Hz power closely matched the epoched data, with the largest differences again at the areas receiving maximal TI (**Figure 4.4Bi–iii).**

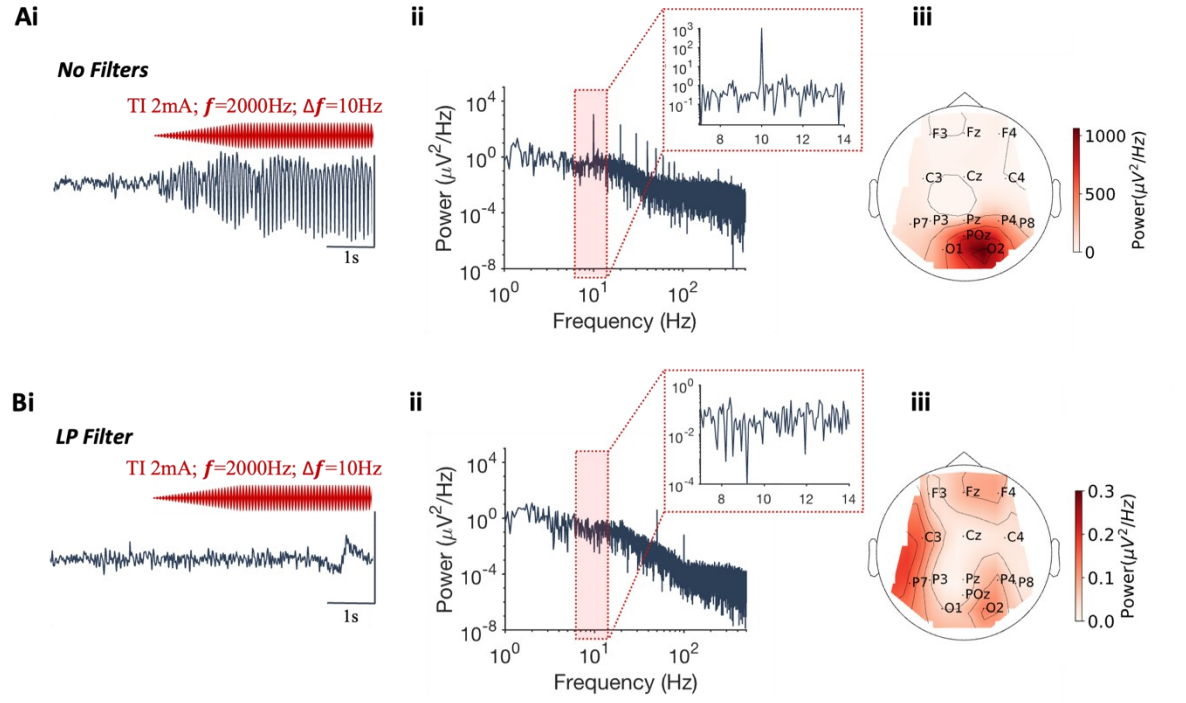


Figure 4.3 Demonstration of LPF solution for low frequency non-linear artefact.

A. An example EEG recording (15 seconds) during concurrent 10 Hz TI stimulation targeting O2. **(i)**. In the raw signal, large artefacts at the difference frequency of 10 Hz can be observed during TI at the O2 channel. **(ii)**. The power spectrum shows clear artefacts at 10 Hz and its harmonics that are orders of magnitude higher compared to nearby frequencies. iii. The topographical plot shows that Δf artefact is largest in the target area. **B**. The same recording but with LP filter added before the EEG amplifier. The TI signal is no longer detectable in the raw **(i)** EEG signal at O2 or in the power spectrum **(ii)**, and 10 Hz power is not dominant at O2, which has the largest exposure to the TI **(iii)**.

Because this 10 Hz peak lies within the alpha band, where the background physiological signal is largest, I computed a signal-to-noise ratio (SNR) of the PSD to better isolate narrow-band peaks from the broader EEG background. This approach is routinely used in steady-state response analyses to highlight stimulus-locked signals. If IMD artefacts persist, they should appear as narrow-band peaks at the TI difference frequency. **Ci** shows the averaged SNR spectrum across blocks and subjects at electrode O2. A clear 10 Hz peak emerged during TI stimulation, with significantly elevated SNR at 10 Hz compared to sham ($F(1,82) = 4.43$, $p = 0.038$). Topographical maps of the SNR difference from the sham at 10 Hz showed the largest SNR at the stimulation target.

In summary, this pilot study demonstrates that front-end LPF integration effectively suppressed the large IMD artefact originating in the recording hardware. However, the analysis of longer, un-epoched data showed a small but statistically significant 10 Hz peak during stimulation, highlighted by the SNR analysis. While effects of such magnitude could reflect genuine entrainment of alpha oscillations, it is also likely that it represents a residual artefact from the stimulation hardware. The pilot analysis indicated that once the large IMD artefacts are accounted for by low-pass filtering, detecting or ruling out subtle IMD artefacts in the EEG becomes challenging and may greatly depend on experimental conditions and signal-processing methods. Consequently, my subsequent tests focused on identifying the optimal experimental and analysis protocols for in vivo experiments to reliably detect subtle IMD artefacts that might remain after LPF implementation.

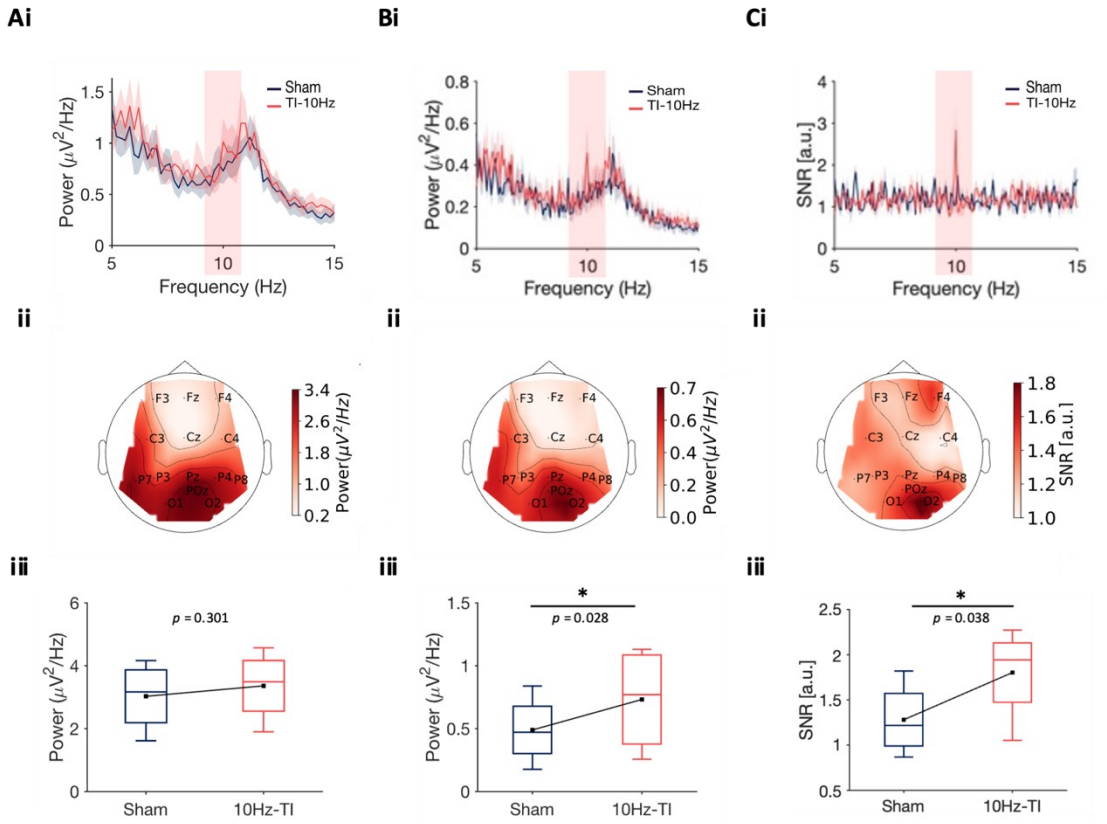


Figure 4.4 Pilot study testing the effectiveness of LPF in suppressing IMD artefacts.

A(i-ii) The experimental setup included a TI device delivering 10Hz TI (Δf=10Hz; f=2000Hz; I=2mA) targeting O2, signal from the recording electrodes passed through LPF filter before entering the EEG amplifier. TI was delivered for 30 seconds (including 5s ramp up/ramp down). In the sham condition TI was ramped up before it was immediately ramped down. 12 blocks of each condition were delivered in a counterbalanced order. **B(i-iii)** Group level results of PSD analysis on the 15s EEG segment showing that no obvious artefact can be detected in the PSD at 10Hz compared to sham, indicating the effectiveness of LPF in suppressing IMD artefacts emerging due to recording hardware. **C(i)** the SNR analysis, which is traditionally used for detecting induced steady state responses (SSR) in the EEG during sensory stimulation, showed a significant peak at 10Hz compared to the sham condition at a group level (β=-1.20; t=-2.35, p=0.021). This indicated a small TI artefact in the EEG, possibly originating in the TI hardware and showed how it can bias the EEG analysis. The line plots show mean and standard error. The box chart shows median and interquartile range (IQR), error lines extend to the values within 1.5×IQR. Connected line depicts differences in mean SNR at 10Hz. n=5.

4.4.2 Experimental protocol and signal processing methods influence the detection of subtle IMD artefact

The pilot study analysis suggested two main factors that may significantly affect the detection of subtle IMD peaks in the EEG: (1) recording duration and (2) background EEG activity. To examine these systematically, I ran a follow-up in vivo study and simulation. I replicated the setup used in the pilot study but recorded EEG only from the O2 channel, where the largest artefacts were previously observed. I extended the recording duration to 3 minutes and delivered TI stimulation at 10, 30, and

80 Hz difference frequencies to explore how both stimulus frequency and background EEG power influence artefact detection.

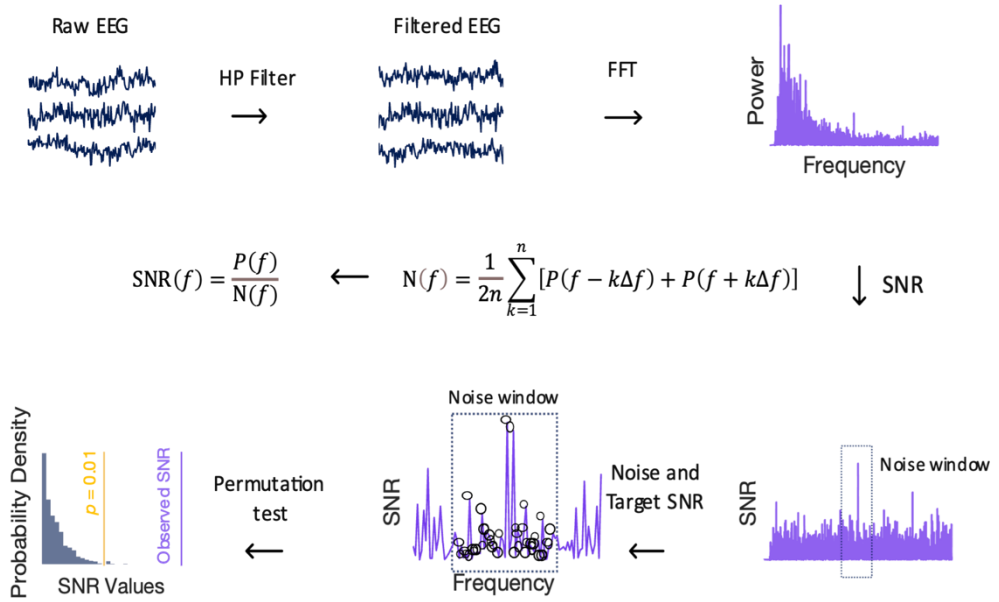


Figure 4.5 Signal processing pipeline for detecting IMD in the EEG recording.

The raw EEG data is high-pass filtered and visually inspected. The data is then converted to the frequency domain using Fourier analysis, and spectral power is computed. The SNR at each frequency bin is then calculated by dividing the spectral power by the estimated mean noise at that frequency. Finally, the probability distribution is created by randomly sampling a noise SNR from the 2 Hz window 1000 times in a permutation test, and the empirical significance value is determined by dividing the number of noise SNR values that are greater than the target SNR by the total number of permutations. If $p > 0.01$, the peak at the target frequency is considered significant.

4.4.2.1 The effect of recording duration on detecting small non-linear low frequency artefacts

Figure 4.6 illustrates how recording duration influences the SNR and detection rate of a potential 10 Hz IMD artefact. Panel A shows a representative subject's data during 10 Hz TI stimulation. A small (~0.1 $\mu V^2/Hz$) IMD peak emerged at 10 Hz when the FFT was computed on the full 180 s recording. In the PSD, it can be seen how such a small artefact can be easily masked by the large background physiological signal. To account for this, I employed an SNR-based spectral analysis to attenuate broadband background activity while preserving narrow-band signals at the target frequency. Comparing the PSD and SNR of the spectrum of a 180-s recording in panel A highlights this effect. It also shows how the SNR peak at 10 Hz becomes indistinguishable from background noise when shorter segments (e.g., <120 s) are used. This demonstrates that increasing the total recording length

increases the likelihood of detecting subtle artefacts, particularly in lower-frequency bands like alpha (8–12 Hz), where endogenous EEG power is high.

To validate this effect, I applied the SNR analysis to synthetic data. A detailed description of EEG data simulation and IMD peak detection analysis using permutation testing is outlined in sections **4.3.3.1** and **4.3.3.2. Figure 4.6Bi-ii** shows that both the SNR at 10 Hz and the probability of accurately detecting IMD increased linearly with recording duration. At 180 s, 94% of simulated IMD cases were correctly identified, with a 0.9% false-positive rate (consistent with α=0.01 set in the permutation test). Thus, analysing longer recordings offers the highest sensitivity and specificity for detecting

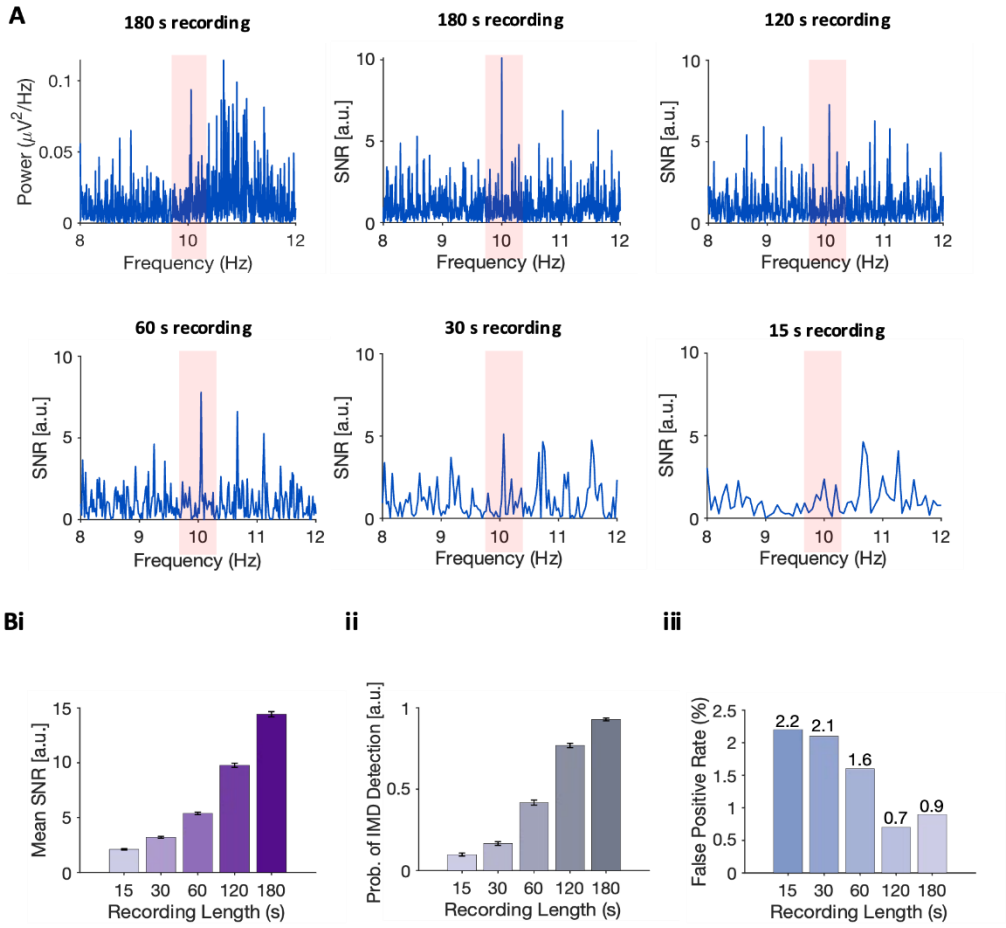


Figure 4.6 Effect of recording duration on IMD detection.

A. Example EEG recording during 10-Hz TI stimulation. When the IMD artefact is small relative to the background EEG, longer recording durations substantially improve its detectability. **B**. IMD detection using a permutation test applied to simulated EEG data with SNR levels comparable to those observed in the real recording. (**i-ii)**. As recording duration increases, the SNR at the target frequency improves, resulting in a markedly higher probability of artefact detection. IMD detection was performed over 1000 simulations using a permutation test on each recording for IMD detection with a significance threshold of $p < 0.01$. (**iii).** A corresponding sensitivity test was performed on simulated EEG data without the target IMD peak, showing that the false positive rate for 120 and 180-second windows, which had the highest IMD detection rates, remained within 1% acceptance rate.

subtle IMD artefacts. However, real EEG can include additional transients and noise. Additionally, if the IMD amplitude is smaller than the background fluctuations, detection rates will drop, and false positives may rise. Visual inspection of the data remains the best practice in addition to data-driven detection of the peaks.

4.4.2.2 The effect of background EEG on detecting small IMD artefact

Even with longer recordings, if the IMD falls within a frequency band dominated by strong endogenous activity, it can remain undetectable. **Figure 4.7 A** shows the SNR spectrum of a 180-s O2-channel recording in a subject with high alpha power. At 10 Hz, the IMD peak (~0.1 $\mu V^2/Hz$) is within the high alpha activity, which masks the artefact. By contrast, at 30 and 80 Hz, where physiological power is much lower, the IMD peaks have a significantly higher SNR and are easily detected. It should be noted that the power of the IMD peak also decreases with increasing stimulation frequency, which is due to the signal attenuation by the LPF (**Figure 4.7B**). Importantly, the decrease in power of the IMD peak follows the LPF's frequency response (see **Figure 4.7Bi** and **Figure 4.2C**), which suggests that the residual low frequency IMD artefacts are produced upstream, at the stimulator/electrode level, before the signal enters the low-pass filter and the EEG amplifier. The analysis of synthetic data showed that at higher difference frequencies, e.g., in this case 80 Hz, a shorter 60–120 s recording could still achieve 91–99% artefact detection accuracy (**Figure 4.2Di–ii**).

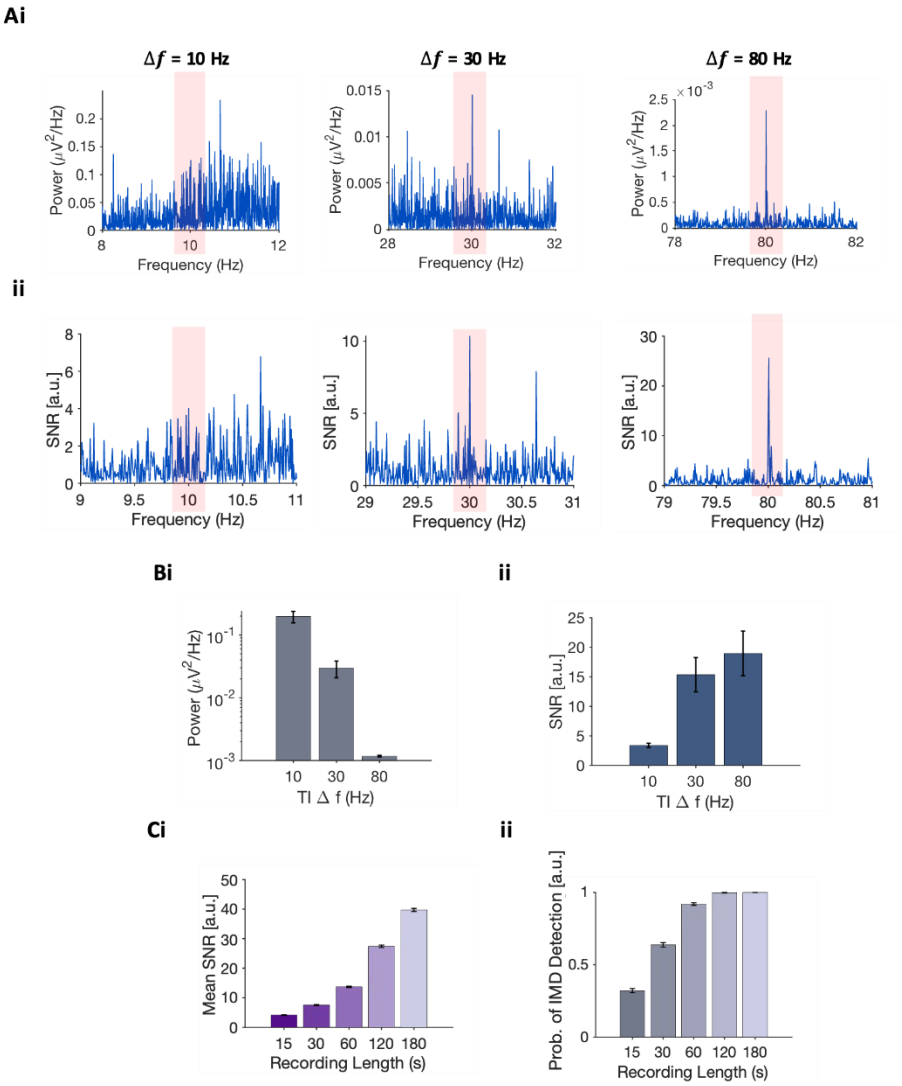


Figure 4.7 Effect of background biological signal power on low frequency IMD peak detection.

A. Exemplary subject's recording during TI stimulation from O2 channel with modulation frequencies at 10, 30 and 80 Hz. The power spectrum **(i)** and corresponding SNR **(ii)** demonstrate that with small non-linear low frequency artefacts, when the background biological noise is high, the artefact peak is not detectable. However, when the modulation frequency is shifted into high frequencies where the physiological signal is much smaller, the SNR at the target frequency increases considerably, and the peaks are easily detected. **B**. Average PSD **(i)** and SNR **(ii)** at each TI frequency showing that despite a decrease in power due to LPF frequency response, the SNR increases with increasing TI frequencies. **C**. Results of peak detection analysis on a synthetic data at TI frequency at 80 Hz showing that when the background biological signal is small and SNR is high **(i)**, the IMD peak can be more reliably detected even with shorter recordings **(ii)**.

4.4.2.3 Recommended in vivo testing parameters for detecting small IMD artefacts in a combined TI-EEG setup

In summary, after implementing a hardware low-pass filter, I still observed small IMD artefacts (0.1–0.2 $\mu V^2/Hz$) that likely originate upstream, before the signal enters the low-pass filter and the EEG amplifier. At such low amplitudes, they can easily be masked by endogenous EEG (especially in high-power bands like alpha). The experimental and signal processing parameters can aid the detection of these subtle IMD artefacts. I, therefore, recommend the following protocol for future TI-EEG experiments employing hardware LPFs or other solutions that reduce IMD artefact to the physiological level:

- Include a control, artefact detection block at the beginning and end of each session to check for residual IMD.
- In these control blocks, use higher, e.g., 30–80 Hz difference frequencies (avoiding line noise) to reduce overlap with strong endogenous rhythms.
- Collect continuous EEG for at least 3 minutes to enable greater sensitivity and noise flow reduction in frequency-domain analyses.
- Compute the spectrum of the entire unsegmented recording to maximise frequency resolution.
- Use SNR Analysis to detect narrow-band signals at the difference frequency against the endogenous signal and noise.

4.4.3 Mitigation strategies for non-linear low frequency artefacts originating in the stimulation hardware

In the previous section, I found that since the power of the residual low frequency IMD artefact follows the frequency response of the LPF, suggesting they are present at the sensor level - i.e., they are produced before the signal enters the EEG amplifier. These in vivo recordings also show that while IMD components are present at the difference frequency (f2-f1), no peaks are detected at the sum (f2 + f1). The second intermodulation distortion (IMD2) products create frequency components at the sum and the difference of the two signals. The absence of the IMD peak at the sum suggests that this component is attenuated by the LPF before the signal is amplified, while the components at the difference frequency, which are within the passband of the LPF, get amplified.

Taken together, these observations suggest that the residual small, low frequency artefacts are generated at the skin-electrode or stimulator-electrode interface and propagate through the scalp along with the stimulating current. There could be two primary sources of non-linear artefacts at the

skin-electrode interface: (1) hardware non-linearities in the current source itself, and (2) non-linearities in the electrode-electrolyte interface. Given the low current densities used in human studies, the stimulator hardware is the more likely candidate here. To address this, I added a custom high-pass filter (HPF) directly after the TI current outputs, removing low frequency components before the kHz signals reach the head (see **Figure 4.2D** for the frequency response of the HPF).

Figure 4.8 compares EEG recordings with and without this HPF for TI stimulation at the difference frequencies of 10 Hz and 80 Hz. When only the LPF is used, IMD peaks of ~0.1 $\mu V^2/Hz$ are apparent, matching previous results. Adding the HPF eliminated these peaks without affecting background EEG power. Thus, adding HPF in the stimulator path helped to attenuate the residual low frequency artefacts originating in the stimulation hardware. The next section describes the application of this HPF+LPF configuration in an experiment testing the effect of TI stimulation over the occipital cortex on SSVEPs.

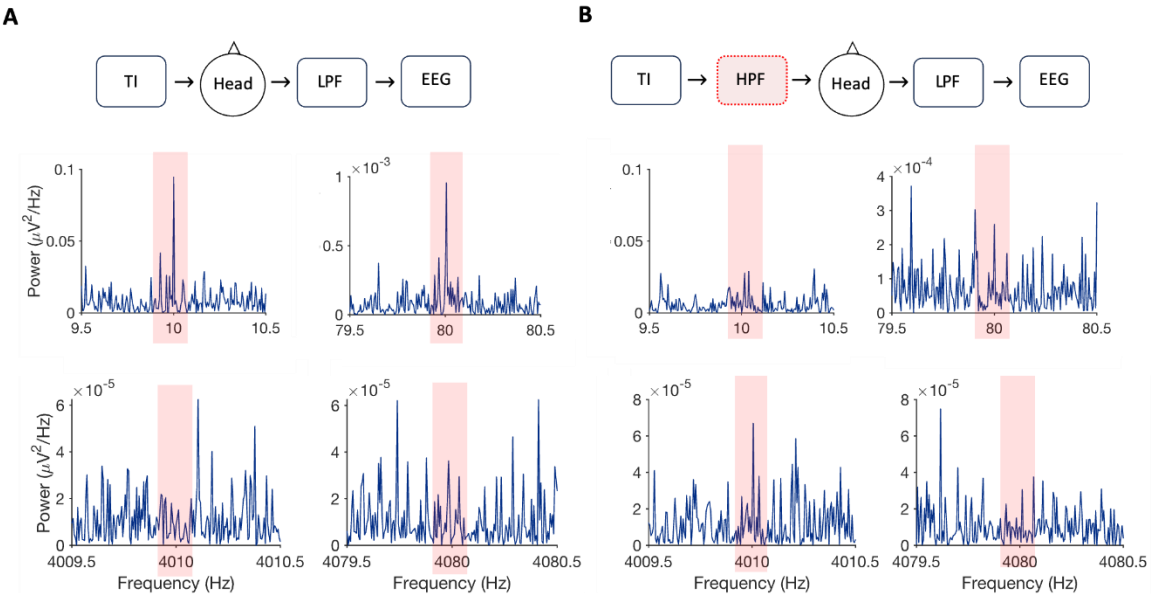


Figure 4.8 High-pass filter solution for the low frequency IMD artefacts originating in the stimulation hardware.

A. An exemplary recording during TI stimulation at 10 Hz and 80 Hz after implementing a low-pass filter (LPF) showing a small (under $0.1uV^2$) IMD artefact. None of the recordings when implementing the LPF filter showed IMD artefact the at the sum frequencies (4010 and 4080 Hz) further supporting that that LPF successfully removed the artefact originating in the recording hardware. Thus, the small IMD artefacts are likely originating either in the stimulation hardware. **B.** After implementing a high-pass filter (HPF) before the current was applied to the scalp, the observed peaks were suppressed while the noise-floor was maintained, suggesting that implementing both LPF and HPF solutions allows artefact free recording during concurrent TI stimulation and EEG recording.

4.4.4 Non-linear artefacts persist after the implementation of both low-pass (LP) and high-pass filters (HP)

Figure 4.9 summarises the artefact detection analysis for 24 healthy volunteers who received TI stimulation of the occipital cortex, targeting the O2 channel. TI was delivered at 10 Hz (f1 = 2000 Hz; f2 = 2010 Hz; I1 = 2 mA), 27 Hz (f1 = 2000 Hz; f2 = 2027 Hz; I2 = 2 mA), or sham (the current ramped down immediately after ramp-up). Each block lasted ~410 s, including a 5-s ramp-up and 5-s ramp-down period (see **Figure 4.1** for the study design), and each condition was repeated twice in a counterbalanced order.

The power spectral density (PSD) analysis of the full 400 s EEG recording, averaged across repetitions and subjects, revealed a subtle peak at 10.05 Hz and a more prominent peak at 27.01 Hz in the O2 channel (**Figure 4.9Ai–ii).** The peak at 10.05 Hz was more pronounced in the SNR of the spectrum (panel **Bi-ii).** In both active stimulation conditions, the SNR at the modulation frequency was higher in the target area compared to sham, though this effect was more pronounced at 27 Hz. Overall, ~27% of the recordings (out of 50 in total) were classified as containing an IMD artefact at 10 Hz, while ~60% of the recordings showed a detectable artefact at 27 Hz (panels **Ci** and **Di**). The SNR peak in both TI conditions was significantly greater than sham alpha vs. sham: $F(1,94) = 12.06$, $p < 0.001$; beta vs. sham: $F(1,94) = 31.98$, $p < 0.001$; panel **Cii** & **Dii**). In the 10 Hz condition, once I excluded blocks identified as artefact-contaminated, the SNR was no longer statistically different from sham ($F(1,45) = 1.48$, $p = 0.230$; **Figure 4.9Ciii**). Given that the average artefact power at 27 Hz was ~0.035 $\mu V^2/Hz$ following ~3.05 dB of LPF attenuation, we can infer the estimated amplitude of the artefact at 10 Hz to be on average ~0.071 $\mu V^2/Hz$. This amplitude is in the same range as the observed physiological EEG signals in the alpha band and explains why the 10 Hz artefacts were identified less frequently.

In summary, the artefact detection analysis showed that even after implementing both the HPF and LPF, small residual low frequency artefacts were still present in at least 60% of the recordings. The potential sources of these residual artefacts are explored in the Discussion section of the chapter.

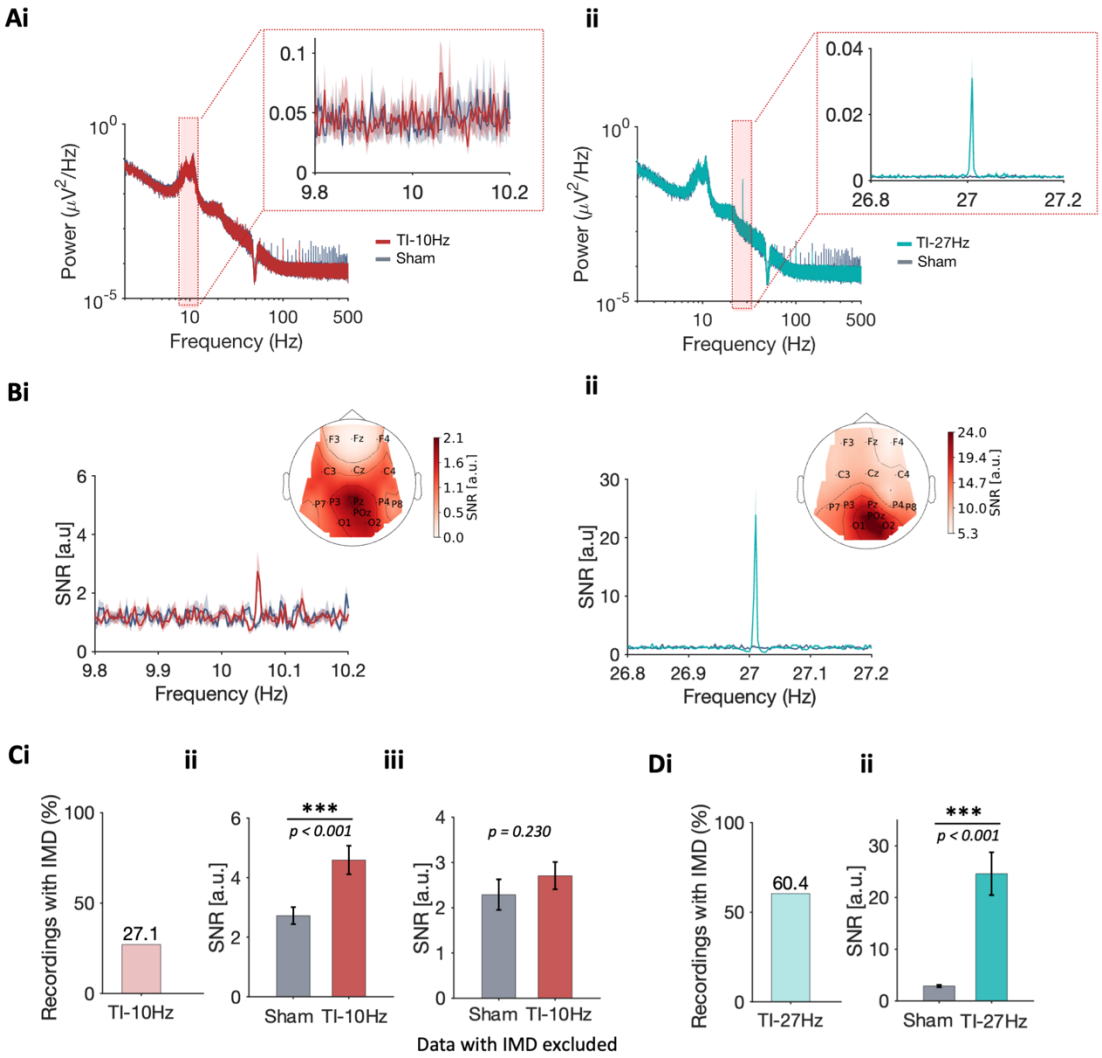


Figure 4.9 Low frequency non-linear artefacts following implementation of high-pass and low-pass hardware filters.

A. Average power spectrum across the group during **(i)** Alpha (Δf=10 Hz) and **(ii)** Beta (Δf=27 Hz) stimulation compared to sham at the O2 channel. A subtle peak can be detected at around 10 Hz in the Alpha stimulation condition, while the artefact at 27 Hz is visible. **B.** The SNR of the PSD. **(i)** The peak is now easily detectable at 10.05 Hz. The topographical plot shows the distribution of sham-subtracted SNR at 10 Hz. The largest differences are observed around the stimulation target (O2). **(ii)** The low-frequency artefacts are considerably more prominent in the 27 Hz condition due to the low background noise and nigh SNR at 27 Hz. The magnitude of the artefact is also largest in the target area. **Ci.** Approximately 27% of the recordings were detected to contain artefact at 10 Hz in the Alpha stimulation condition. **(ii)** The SNR at 10 Hz was significantly larger during stimulation compared to sham ($F(1,94) = 12.06$, $p < 0.001$). **(iii)** Once identified, artefactual recordings were removed from the analysis, SNR at 10 Hz was no longer statistically significant during TI stimulation compared to sham ($F(1,45) = 1.48$, $p = 0.230$). **Di.** In the beta stimulation condition, around 60 % of the recordings were classified to contain artefact at the stimulation frequency. **(ii)** SNR at 27 Hz was significantly larger during stimulation compared to sham ($F(1,94) = 31.98$, $p < 0.001$). ***$p < 0.001$; n=24.

4.4.5 Alpha and Beta TI stimulation of the occipital cortex differentially modulate SSVEP

The results of the SSVEP analysis at the target O2 channel are summarised in **Figure 4.10**. A group-level cluster-based permutation test identified a significant cluster in the TI-27 Hz condition during the early SSVEP period (**Figure 4.10Ai-iii**). No significant differences were observed between the TI-10 Hz condition and sham within this time window. In a follow-up parametric analysis focusing on the average SSVEP amplitude within the significant cluster, TI-27 Hz led to a significantly larger SSVEP envelope compared to sham (β = 3.1, $t(34)$ = 2.05, p = 0.048).

It should be noted that the SSVEP amplitude was computed as the instantaneous EEG amplitude time-locked to each LED pulse and normalised (z-scored) to the pre-LED baseline (a ~1.7 s jittered intertrial interval when the LED was off). Because TI stimulation is delivered continuously (i.e., during both LED-on and LED-off periods), I also examined the effect of stimulation on the EEG amplitude during the baseline (LED-off) period. I first applied the same cluster permutation to this period, which identified a large cluster in the TI-10 Hz condition compared to sham, while no differences were observed between TI-27Hz and sham (**Figure 4.10Bi-ii**). The follow-up parametric test showed that pre-LED baseline amplitude was significantly reduced during Alpha-TI stimulation compared to sham (panel **C**). Analysis of the entire baseline window revealed a significant main effect of condition on amplitude ($F(2,36)$ = 7.8, p = 0.002); post-hoc pairwise comparisons indicated that baseline amplitude was significantly lower during TI-10 Hz compared to sham (p = 0.001), while no significant differences were found between TI-27 Hz and sham (p = 0.249) or between the two TI conditions (p = 0.083). In summary, these findings suggest state and frequency-dependent effects of TI stimulation, where TI stimulation at 10 Hz reduced baseline EEG amplitude without significantly altering the overall SSVEP, while TI stimulation at 27 Hz enhanced the SSVEP amplitude.

Given the observed frequency and state-specific effects of alpha and beta TI stimulation on SSVEP, I tested whether baseline alpha frequency predicted the observed modulation. The baseline alpha frequency was computed from the 20-s rest period before the start of the stimulation block. A regression analysis revealed a significant negative relationship between baseline alpha frequency and the change in SSVEP amplitude extracted from the significant cluster (β = –15.18; $F(1,16)$ = 7.94; p = 0.012), explaining approximately 33% of the variance (R^2 = 0.33). These results indicate that individuals with lower baseline alpha frequencies experienced a greater enhancement of the SSVEP under TI-27 Hz stimulation, whereas those with higher baseline alpha frequencies show a diminished effect, with effects even reversing in a subset of participants with higher baseline alpha frequency (**Figure 4.10D**). In contrast, no significant relationship was observed between baseline alpha frequency and

the effects of TI-10 Hz on amplitude during LED-off ($p > 0.05$). Additionally, no relationship was found between effects on LED-off amplitude and the magnitude offset between baseline alpha frequency

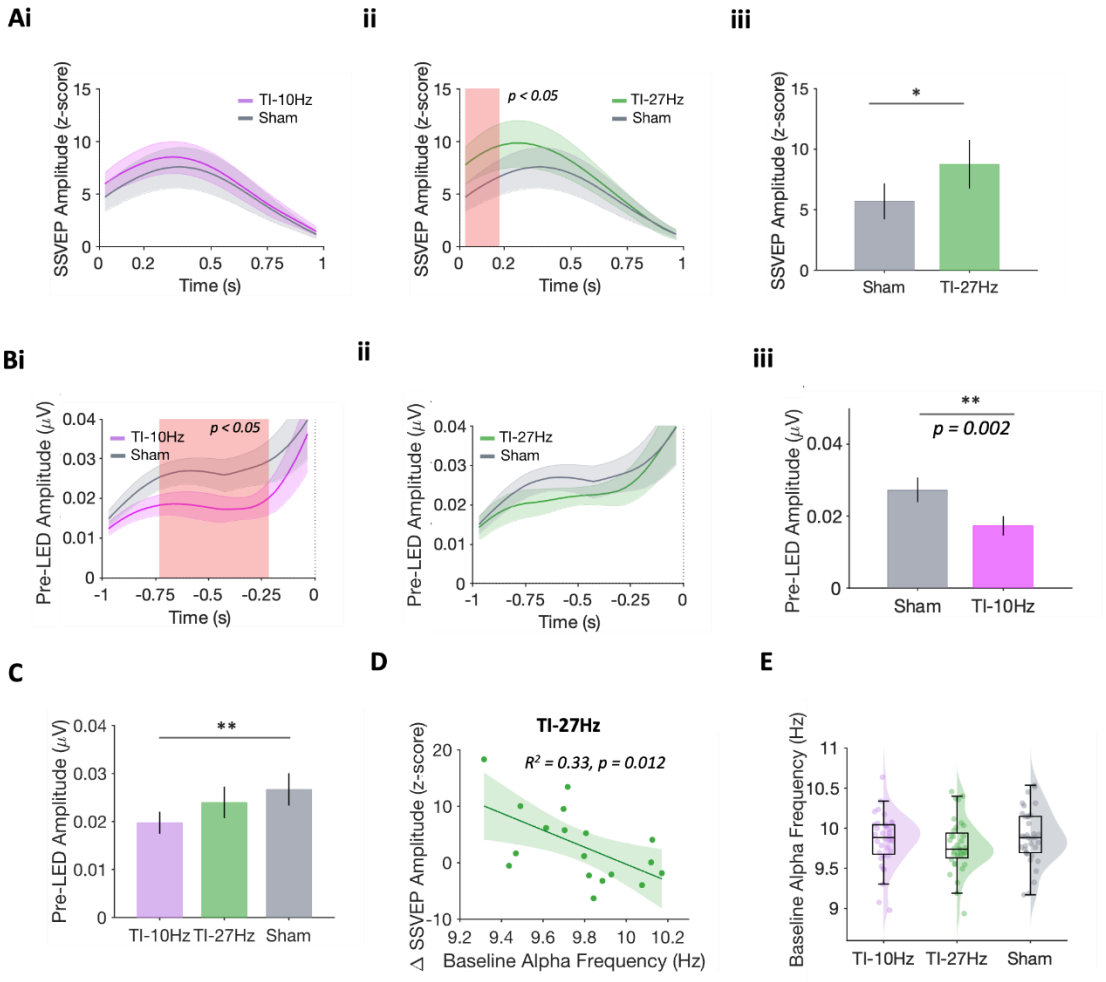


Figure 4.10 The effects of TI stimulation of the right visual cortex on SSVEP at the O2 channel.

A. Cluster permutation test on the SSVEP envelope for TI-10 Hz (**i**) and TI-27 Hz (**ii**) against sham. One significant cluster ($p < 0.05$) was found in the TI-27 Hz condition compared to sham at the start of the LED trial. No differences were observed in the TI-10 Hz condition. (**iii)**. A follow-up parametric test on the average amplitude within the cluster showed SSVEP amplitude during the TI-27 Hz condition in this cluster was significantly greater than the sham (**β**= 3.1, t(34) = 2.05, p = 0.048). **B.** A cluster permutation test on the pre-LED baseline period (i.e., inter-trial interval during which LED was off ~1.7 s). **(i).** A large, significant cluster was identified in the TI-10 Hz condition ($p < 0.05$). **ii.** No differences were observed in the TI-27Hz condition. (**Iii).** A follow-up parametric test on the average amplitude within the cluster showed SSVEP amplitude during the TI-10 Hz condition in this cluster was significantly lower than sham (**β**= -0.01, t(34) = -3.23, p = 0.002. **C.** There was a significant main effect of stimulation on average pre-LED baseline ($F(2,36) = 7.8$, p = 0.002). Median pre-LED amplitude was significantly lower under 10 Hz stimulation compared to sham (p = 0.001). Amplitude was also lower in the 27 Hz condition but did not reach significance (p = 0.249). **D.** The effects of 27 Hz stimulation showed a significant relationship with participants' baseline (before the start of the block) Alpha frequency, such that individuals with lower baseline alpha frequencies showed a greater enhancement (i.e., larger difference from sham) in the SSVEP under stimulation, this effect was reduced with increasing Alpha frequency, with effects reversing for a subset of participants (as indicated by negative values) ($R^2 = 0.33$, $F(1,16) = 7.94$; p = 0.012). **E.** No significant differences were observed in baseline Alpha frequency between conditions ($p > 0.05$). *$p < 0.05$, **$p < 0.01$; n=18.

and applied 10 Hz stimulation. Baseline alpha frequencies did not differ significantly across the three conditions.

4.4.6 The effects of alpha and beta TI stimulation on SSVEP are spatially distinct

Next, I examined the contralateral unstimulated site at the O1 channel (**Figure 4.11**). No significant differences were found in the SSVEP amplitude z-scores between stimulation and sham conditions (panel **Ai–ii)**. However, a cluster-based permutation test on the pre-LED baseline period identified a significant cluster indicating reduced amplitude in the TI-10 Hz condition compared to sham ($p < 0.05$), whereas no significant clusters emerged for the TI-27 Hz vs. sham comparison (panel **Bi–ii**). A subsequent parametric analysis of the median amplitude within this significant cluster confirmed that the pre-LED baseline amplitude was significantly reduced during TI-10 Hz stimulation relative to sham (β = -0.01, $t(34)$ = -2.6, p = 0.014). However, an analysis using the entire baseline window revealed no significant differences between the three conditions ($p > 0.05$; **Figure 4.11D**).

These findings suggest that the effects of TI-10 Hz stimulation on pre-LED baseline EEG amplitude were bilateral, reducing amplitude at both the stimulated (O2) and unstimulated (O1) occipital sites. In contrast, the effects of TI-27 Hz appeared localised to the stimulated area, enhancing SSVEP amplitude in the early SSVEP response period.

4.4.6.1 Controlling for TI stimulation artefact in time-domain SSVEP analysis

The primary motivation for the time-domain analysis was to ensure that stimulation effects on SSVEP amplitude were not confounded by non-linear artefacts at the target stimulation frequencies. Because TI stimulation is delivered continuously and is not time-locked to the LED pulses, which are presented with a jittered intertrial interval, the phase of the TI signal is effectively randomised relative to the LED onset. Consequently, when computing the SSVEP, which is computed by time-locking the EEG signal to each LED pulse, any small TI artefact should cancel out when data is averaged across trials.

To verify this, I analysed the instantaneous TI phase at the onset of each LED trial**. Figure 4.12A** shows the group-average phase resultant computed across 230 LED trials per subject, demonstrating low phase consistency of the TI signal across trials in each condition. The phase histogram of the instantaneous TI phase at LED onset showed a uniform distribution, and a corresponding Rayleigh test confirmed that the TI phase was randomly distributed (**Figure 4.12Bi–ii**). Additionally, to rule out any residual influence of the TI waveform on the observed effects of 27 Hz stimulation, I performed a circular–linear correlation between the TI phase (at the LED onset) and the average change in SSVEP

z-score within the significant cluster. This correlation was not significant (R = 0.10, p = 0.906). Finally, I found no relationship between the magnitude of the TI artefact at 27 Hz and the effects of beta stimulation on the SSVEP amplitude (**Figure 4.12D**).

In summary, these analyses provide robust evidence that the observed changes in SSVEP amplitude during 27 Hz TI stimulation are not driven by residual electrical artefact. The random distribution of TI phase, the absence of a significant phase–SSVEP relationship, and the minimal artefact magnitude all

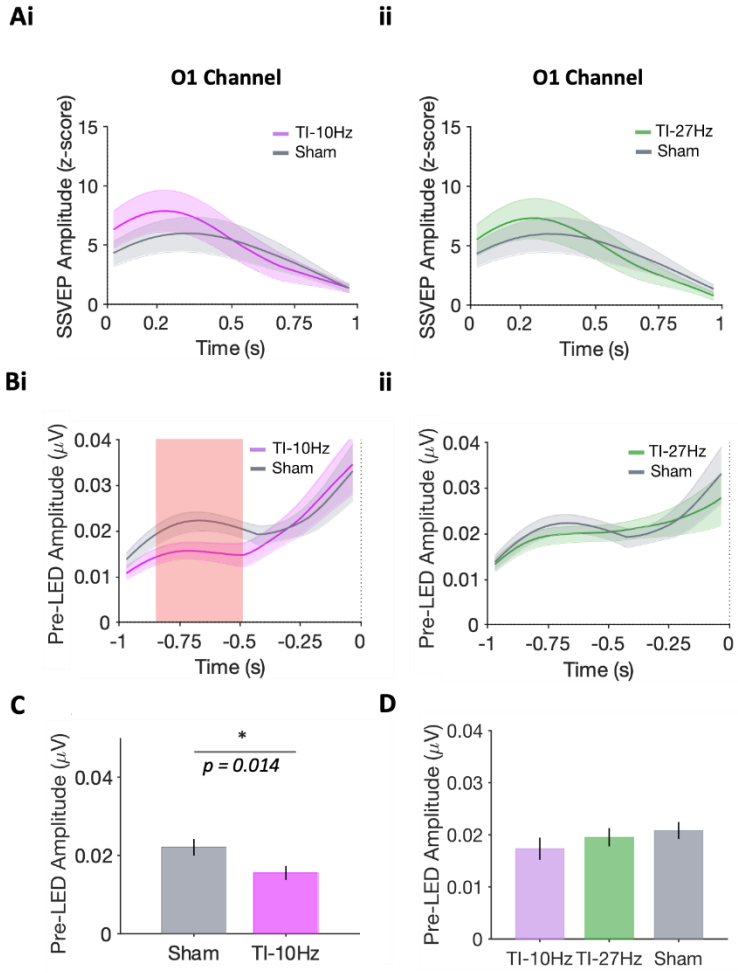


Figure 4.11 Effect of f TI on SSVEP and pre-LED baseline amplitude at the unstimulated O1 channel.

A. Cluster permutation test on SSVEP envelope. **i**. No differences were observed in SSVEP amplitude between stimulation and sham conditions. **B**. A cluster permutation test on the pre-LED baseline period (i.e., inter-trial interval during which LED was off ~1.7 s). **i**. A significant luster ($p < 0.05$) was found in the TI-10 Hz condition compared to sham. ii. No differences were observed in the TI-27 Hz condition. **C**. A follow-up parametric test on the average amplitude within the cluster showed pre-LED amplitude during TI-10 Hz condition in this cluster was significantly lower than sham (β= -0.01, t(34) = -2.6, p = 0.014). **D**. Average amplitude across whole pre-LED baseline window was not statistically different between conditions ($p > 0.05$). *$p < 0.05$; n=18.

support the conclusion that the observed enhancement in SSVEP reflects genuine neural modulation rather than contamination from stimulation artefact.

4.4.7 TI stimulation of the occipital cortex modulates event-related potentials (ERPs)

In addition to SSVEPs, TI stimulation also showed significant but small effects on event-related potentials (ERPs). Permutation test revealed significant clusters that aligned with P1 and N1 ERP components. Specifically, both TI conditions reduced the N1 component compared to sham, while the P1 component was reduced only during TI-10 Hz stimulation (cluster threshold set at $p < 0.05$). Follow-up parametric tests on average ERP amplitudes extracted from these clusters showed significant differences from sham at the trial level, however, these differences were not evident when the values were averaged across trials. Given the small effect sizes for the ERPs, no further analyses were performed on these measures. Summary results are provided in **Figure A7** in the Appendix.

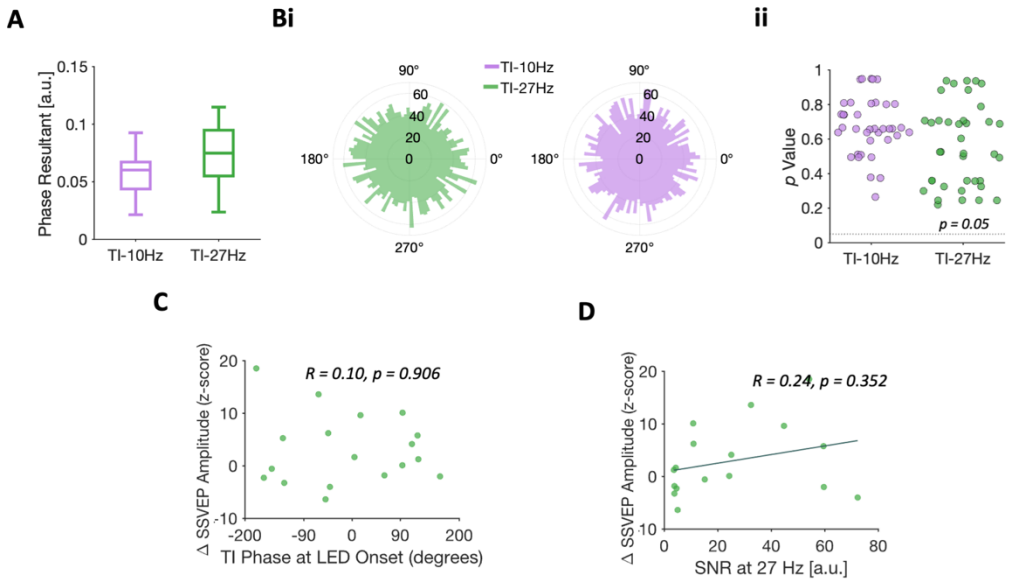


Figure 4.12 Tests for the confounding effects of low frequency artefacts on the observed effects of TI-27Hz on SSVEP.

A. The phase resultant for the instantaneous TI phase across 230 LED trials, averaged across the group showing low phase consistency across the group. **B**. Instantaneous phase of TI at each LED trial showing uniform phase distribution relative to LED onset **(i)** with corresponding Reyleigh test showing no significant clustering across subjects **(ii)**. **C**. Results of circular-linear correlation between TI phase at LED onset and delta SSVEP z-score in the significant cluster under 27 Hz TI stimulation showing no significant relationship (R = 0.10, p = 0.906). **D.** Correlation between SNR of the PSD at 27 Hz during TI stimulation and delta SSVEP z-scores in the significant cluster demonstrating that the amplitude of the non-linear artefact did not confound the observed changes in the SSVEP amplitude during TI stimulation (R = 0.24, p = 0.352).

4.5 Discussion

In this chapter, I demonstrated a novel approach to account for non-linear low frequency artefacts in the recording hardware during concurrent TI stimulation and EEG recording. I also showed that small residual artefacts, below 0.1 $\mu V^2/Hz$, may remain unaccounted for, which can easily be mistaken for genuine physiological responses and thereby bias EEG analysis. Finally, I provided the first proof-of-concept evidence that TI can modulate endogenous brain activity in a state- and frequency-dependent manner in 18 healthy young adults.

4.5.1 Mitigation of low frequency non-linear artefact in a combined TI-EEG setup

Eliminating low frequency electrical artefact in the EEG, introduced by non-linear mixing of carrier waveforms in both downstream (stimulator → electrode → skin) and upstream (skin → EEG sensor → amplifier) signal pathways, has been a major technological challenge in the field. The key scientific contribution of this project is the demonstration that: (1) low-pass filtering is an effective mitigation strategy for removing the large non-linear artefact originating in the recording hardware; (2) after accounting for hardware-related non-linearities, small residual artefacts remain that are in the same range as endogenous brain activity; (3) these residual artefact can be easily masked by large physiological signals at the subject level while simultaneously biasing the analysis at the group level, which underscores the importance of implementing appropriate experimental and signal processing methods to detect them; and (4) in the present setup, the residual non-linear artefacts do not originate in the stimulation hardware, suggesting that they likely arise at the electrode–gel–skin interface.

What is the evidence that the LPF filter successfully accounted for non-linear artefacts, and what are the potential sources of residual low frequency artefacts?

The key evidence that the residual artefacts originate before EEG signal is amplified comes from the observation that: (1) attenuation at different modulation frequencies (e.g., 10, 27/30, and 80 Hz) closely follows the LPF frequency response, and (2) no components are observed at the sum frequencies (i.e., at 4000 + Δf). Although adding a high-pass filter (HPF) in the signal path showed removing residual artefact in the in vivo validation tests, approximately 60% of the recordings still showed an artefact, which was in the same range as those observed when only the LPF was used. This observation strongly indicates that the TI hardware is not the source of these artefacts.

Given the complex interface between stimulation electrodes, conductive gel, and skin, small deviations from linearity can arise due to multiple factors, including electrode material, gel

composition, skin preparation, temperature, and individual variations in skin impedance (McAdams et al., 1996; Yamamoto and Yamamoto, 1981). In addition, non-linearities may also emerge from physiological modulation of stimulation artefact, e.g., those induced by heartbeat and respiration (Noury et al., 2016). Consequently, several factors likely contribute to the manifestation of low frequency non-linear artefact in the EEG, which also explains the variability observed in the present study. Because it is impossible to completely eliminate non-linearity from the setup, the key strategy is to identify the most significant contributors and develop targeted mitigation strategies. For example, electrochemical processes at the electrode–tissue interface have been shown to induce non-linearities that depend on electrode material properties (Merrill et al., 2005). Although these effects have been reported for implanted electrodes where the current densities are much larger than those typically used in non-invasive brain stimulation, evidence indicates that the electrode–skin interface can exhibit non-linear behaviour even at low currents in humans (Yamamoto and Yamamoto, 1981). Therefore, testing stimulation electrodes made of non-polarizable Ag/AgCl, which have been shown to exhibit a more linear response (Kurniawan et al., 2021), would be an important next step.

What is the evidence that the observed peaks are not genuine physiological responses to TI stimulation?

It is well established that the brain can respond to external stimuli with sub-hertz precision, as demonstrated by frequency-domain analyses of SSVEPs (e.g., Herrmann, 2001; Norcia et al., 2015). Given that the observed peaks during TI stimulation closely mimic the entrainment effects seen with visual flicker, one might argue that they reflect true TI entrainment of brain rhythms. However, a key piece of evidence against this interpretation comes from the observed frequency response to different Δf stimulation frequencies. In both the validation tests and study 1, the attenuation in the observed peaks at Δf closely tracks the low-pass filter response, indicating that the original signal was approximately the same magnitude at 10, 27/30, and 80 Hz. In contrast, genuine physiological responses typically vary with stimulus frequency; for example, visual responses often exhibit resonance effects, peaking around 10 Hz, and diminishing with increasing stimulus frequency (Herrmann, 2001; Vialatte et al., 2010). This lack of the expected frequency-dependent variation suggests that the observed peaks are not a result of neural entrainment but are instead electrical artefacts introduced during TI stimulation.

4.5.2 State and frequency-dependent effects of TI stimulation on SSVEPs

The present findings demonstrate that TI stimulation at 27 Hz selectively enhanced the SSVEP amplitude at the stimulated occipital site (O2) during the early phase of the flicker-evoked response,

whereas TI at 10 Hz reduced the EEG amplitude during the LED-off baseline period, which was observed at both occipital channels (O1 and O2). Additionally, inter-individual differences in baseline alpha frequency (measured before the onset of TI stimulation and LED flicker) predicted the degree of SSVEP increase in the TI-27 Hz condition; specifically, individuals with lower baseline alpha frequencies showed larger gains in SSVEP amplitude, whereas participants with higher baseline alpha frequencies experienced a diminished effect. Below, I discuss potential mechanisms of action that could explain the observed effects of TI on SSVEPs based on existing literature on tACS. Although previous literature has mostly relied on before-and-after effects of tACS, due to experimental limitations in recording brain activity during stimulation, the assumed mechanisms of action for TI and tACS are the same, and theories developed regarding tACS effects on brain oscillations align well with the current observations.

What is the possible mechanism of action of localised effects of beta-TI on 33 Hz SSVEP?

One of the primary proposed mechanisms underlying tACS effects on the brain is the direct entrainment of neural oscillations (Lakatos et al., 2019; Vöröslakos et al., 2018; Vogeti et al., 2022). Moreover, the efficacy of tACS to entrain brain oscillations is heavily dependent on frequency matching, with effects diminishing as the applied waveform deviates from the target endogenous oscillation (Riddle & Frohlich, 2021; Luo et al., 2025; Vöröslakos et al., 2018). For example, several studies have shown maximum effects when alpha tACS is close to or matches the individual alpha frequency (Neuling et al., 2013; Stecher et al., 2017; Kasten et al., 2019; Vossen et al., 2015). This phenomenon has also been observed with externally evoked oscillations: Dowsett et al. (2020) found that 10 Hz tACS significantly boosted a 10 Hz SSVEP, whereas the same 10 Hz tACS had no significant effect on a slightly different (8.6 Hz) SSVEP. More recently, Haslacher et al. (2023) demonstrated that by precisely aligning the phase of amplitude-modulated tACS with a 6 Hz SSVEP, they could induce symmetrical enhancement and suppression of evoked oscillatory activity, underscoring the critical importance of phase alignment for effective neuromodulation. Based on this, given that 27 Hz is distinct from 33 Hz and not harmonically related, it is unlikely that the observed increase in the 33 Hz SSVEP is via direct entrainment. One possible mechanism is that 27 Hz TI modulates cortical excitability without directly entraining the network. A recent study demonstrated that TI stimulation modulates neuronal spike timing in non-human primates at rest, leading to phase perturbations of ongoing oscillatory activity (Vieira et al., 2024). Thus, via spike-time biasing the applied 27 Hz TI could create periodic high-excitability phases in the cortex that intermittently align with the visual input cycle, facilitating the amplification of neural responses to the 33 Hz visual stimulus. This mechanism is consistent with studies showing that non-invasive brain stimulation can modulate network excitability

in a state-dependent manner, thereby affecting downstream neural responses (Bradley et al., 2022; He et al., 2023; Luo et al., 2025) and explains the localised effects of the stimulation.

Additionally, the effects on local cortical excitability may also explain the observed relationship with baseline alpha frequency. Research indicates that individual alpha frequency (IAF) is tightly linked to the temporal window over which visual information is integrated (Cecere et al., 2015). Individuals with lower baseline alpha frequencies have longer alpha cycles, which translate into broader windows of heightened cortical excitability. When 27 Hz TI is applied, these extended windows provide a larger temporal margin during which TI-induced excitability peaks can align with the 33 Hz visual flicker, thereby facilitating larger effects on SSVEP. Conversely, participants with higher baseline alpha frequencies experience shorter alpha cycles and, therefore, briefer excitability windows, resulting in diminished effects of beta-TI on SSVEP amplitude.

What is the potential mechanism of action of 10 Hz TI effects on the pre-LED baseline period?

TI stimulation at 10 Hz significantly reduced the pre-LED baseline amplitude but did not alter the overall SSVEP. Moreover, this effect emerged bilaterally while the stimulation was targeted to the right visual cortex. Such state-dependent and more global effects of alpha stimulation are consistent with previous research. During LED stimulation, the network is in a highly excited state, being entrained to the 33 Hz visual flicker; because the visually evoked oscillations are far from the applied 10 Hz waveform, TI at 10 Hz does not modulate these evoked oscillations. Previous studies have shown that the effects of alpha tACS on SSVEPs diminish even with a frequency mismatch as small as 1.4 Hz (Dowsett et al., 2020). In contrast, during the pre-LED baseline period, when sensory input is minimal, TI-10 Hz can entrain alpha oscillations and suppress gamma amplitude. This pattern reflects the interplay between top-down inhibitory processes mediated by alpha and stimulus-driven excitatory activity in the gamma range. The inhibitory function of alpha oscillations has been well documented (Klimesch et al., 2007; Jensen & Mazaheri, 2010), and the "gating by inhibition" hypothesis proposes that alpha activity regulates information flow by selectively inhibiting stimulus-irrelevant networks while allowing relevant processes to proceed (Foxe & Snyder, 2011). Additionally, because alpha-band activity operates at a large-scale network level (Foxe & Snyder, 2011; Jensen & Mazaheri, 2010; Klimesch, 2012), it can account for the bilateral effects of TI-10 Hz observed during the pre-LED baseline.

Overall, these findings suggest that the frequency-specific effects of TI stimulation on SSVEPs are mediated by distinct mechanisms: beta TI at 27 Hz modulates cortical excitability in a localised, state-

dependent manner, while alpha TI at 10 Hz also exerts state-dependent but broader, inhibitory effects on baseline neural activity.

4.5.3 Limitations and future directions

While the present study provides novel contributions to the field, several limitations must be acknowledged. First, only a single stimulation electrode configuration was explored in the validation studies. Although this limitation is less critical for demonstrating the effectiveness of the LPF in eliminating recording hardware contributions, it is important for investigating the sources of the small residual IMD artefact. Future experiments should systematically evaluate different electrode placements, sizes, and continuously monitor electrode impedance to address the effects of maximum field overlap, current density, and fluctuations in impedance over time. Additionally, combining phantom tests with in vivo experiments would help assess hardware linearity in a linear system (e.g., using resistors). Incrementally adding various non-linear components present in the setup to the phantom tests will allow a robust controlled characterisation of non-biological elements to the non-linearity, which can then be contrasted with in vivo tests, incorporating the contribution of the skin and complex impedance.

In study 1, the experimental paradigm was designed to maximise the number of trials for time-domain SSVEP analysis, ensuring that any observed effects were not confounded by stimulation artefact. However, unlike time-domain analysis, distinguishing genuine neural responses from stimulation artefacts would be challenging in the frequency domain and can bias the analysis. While this approach effectively minimised artefact-related confounds, the inability to directly analyse stimulation effects at the applied frequencies means that the interpretation of the observed effects relies largely on theoretical assumptions. Therefore, identifying and mitigating residual artefacts is crucial to reliably assess the direct effects of TI on brain oscillations.

Finally, the analysis was limited to two channels. Although the total number of channels was reduced to 14 due to the LPF, exploring the stimulation effects on additional channels would provide further insight into the spatial distribution of the observed effects.

Chapter 5: General Discussion

5.1 Overview of experimental chapters

The roadmap to developing effective NIBS interventions for cognitive decline in AD is complex and requires both technological innovation and deeper mechanistic insight into disease pathology, how it disrupts neural systems and, consequently, brain function. In this PhD, I focused on two long-standing technological limitations of established NIBS approaches that have hindered their clinical translation: (i) the limited ability to selectively target deep brain structures, and (ii) the absence of reliable approaches for real-time monitoring of electrophysiological activity during stimulation.

In Chapter 1, I introduced TI stimulation – a novel NIBS method that uses two transcranially applied high-frequency electric fields to deliver low frequency focal stimulation to deep brain areas without engaging the overlying cortical structures (Grossman et al., 2017). I also summarised our first-in-human application of TI, in which we non-invasively modulated task-evoked hippocampal activity measured with BOLD-fMRI in healthy young adults (Violante et al., 2023). In the first experimental chapter, I extended this work by showing that longer (~34 min) hippocampal theta-band TI stimulation significantly improved hippocampal-dependent episodic-memory performance compared to sham control, confirming the behavioural efficacy of the method (Chapter 2).

Building on this work, in Chapter 3, I evaluated the safety, tolerability, and feasibility of repeated hippocampal TI stimulation (1-hour daily sessions over 10 days) in 21 patients with early-stage AD. Despite the demanding and complex nature of the experimental protocol, the study achieved a 98% compliance rate, supporting the overall feasibility and acceptability of the intervention. No serious stimulation-related adverse events were reported, and patients tolerated the applied current intensities without discomfort. Neurocognitive assessments revealed selective improvements in hippocampal-dependent episodic memory following the TI intervention; however, no changes were observed in hippocampal CBF or MC1 density measured with pCASL and PET imaging, respectively. As I previously discussed, the interpretation of these results is limited by the absence of a control condition, which prevents the separation of stimulation effects from practice, learning, or placebo. Moreover, the study was likely underpowered to detect subtle metabolic or perfusion changes as the power calculations to select sample size were based on test-retest variance of ^{18}F-BCPP-EF binding in healthy older adults (Mansur et al., 2021) and TI effect size of 5%, which was set arbitrarily due to first-in-patient application of the method.

In Chapter 4, I addressed the second major technological limitation of NIBS methods: the inability to monitor brain activity during stimulation due to large stimulation artefacts contaminating electrophysiological recordings. In combined TI-EEG experiments, these artefacts arise from non-linearities in the experimental hardware, which mix the high-frequency carrier signals and generate electrical artefacts at the difference (Δf) and sum frequencies. I first demonstrated that the recording hardware was the primary source of non-linear artefacts in the EEG, corroborating findings from previous research (Kasten et al., 2019). I then showed that inserting a custom LPF between the EEG electrodes and amplifier to suppress the carrier frequencies before they reached non-linear front-end circuits effectively removed artefacts originating in the recording device. Furthermore, I demonstrated that when additional non-linearities were present in the stimulation hardware, implementing an HPF between the current source and scalp electrodes successfully mitigated these artefacts. Together, the LPF-HPF strategy enabled artefact-free EEG recordings during TI.

Even after implementing the dual-filter approach, I observed subtle residual Δf components in a subset of recordings. These artefacts were undetectable when Δf lay within spectral ranges dominated by strong endogenous brain activity (e.g., the alpha band) but became apparent when the SNR was enhanced by increasing EEG recording duration to three minutes and shifting Δf to 27 Hz, where the background power was considerably lower. I hypothesise that these residual signals may originate at the electrode-electrolyte interface. Controlled phantom experiments will be required to validate this hypothesis and develop additional mitigation strategies.

Finally, I demonstrated frequency- and state-dependent effects of TI stimulation on SSVEPs. Specifically, beta TI stimulation at 27 Hz targeting the right primary visual cortex significantly increased the early gamma (33 Hz) SSVEP envelope compared to sham, while alpha TI at 10 Hz reduced the amplitude of the pre-LED baseline period. These findings indicate that TI can modulate cortical activity in a state- and frequency-dependent manner: alpha TI reduced baseline gamma amplitude without significantly altering the SSVEP itself, whereas beta TI enhanced SSVEP amplitude. Moreover, these effects were spatially distinct – beta TI effects were localised to the stimulation site, while baseline reductions during alpha TI were bilateral.

5.2 Key advances and contributions

The work presented in this thesis offers key new insights into the application of TI stimulation in human research and its potential to develop therapeutic interventions for cognitive decline in AD.

First-in-human evidence of hippocampal TI stimulation on memory performance

At the start of my PhD, TI was an emerging neuromodulation technique that showed promise for non-invasive and selective stimulation of deep brain structures. At that time, however, it had only been validated in animal models (Grossman et al., 2017). In our initial application of TI in healthy young adults, we demonstrated that TI could selectively modulate task-evoked hippocampal activity, providing the first evidence of its physiological effects on brain function. Building on this work, my research showed that longer stimulation (~35 min) of the hippocampus led to measurable improvements in memory performance. This provided the first experimental evidence for the efficacy of TI as a non-invasive deep brain stimulation method in humans, advancing the field from a concept validated in rodents to a human-ready research and intervention method. It established a foundation for mechanistic studies in humans and set the groundwork for the clinical translation of TI as a novel neuromodulation strategy for cognitive enhancement and therapeutic applications.

Advancing understanding of hippocampal theta rhythms in episodic memory

This work also contributes to advancing knowledge on the role of hippocampal theta rhythms in episodic memory. While previous research has linked hippocampal theta oscillations to memory encoding and retrieval (Zheng et al., 2025; Wang et al., 2023), evidence for a causal relationship has remained limited. By enabling non-invasive targeting of the hippocampus during memory tasks, TI provides a unique tool to establish causal brain-behaviour relationships. The findings from this study support the hypothesis that hippocampal theta rhythms govern episodic memory performance and suggest that modulating hippocampal theta rhythms can facilitate hippocampal-dependent memory processes. However, it is important to note that this study cannot fully establish a causal link between hippocampal theta modulation and memory improvements. Definitive evidence would require invasive intracranial recordings or, at a minimum, the inclusion of frequency-specific control conditions to dissociate theta-specific effects from non-specific neuromodulation.

Established the safety, tolerance and feasibility of repeated hippocampal stimulation in AD patients

The experimental work presented in Chapter 3 provides the first systematic evaluation of the safety, tolerability, and feasibility of repeated hippocampal TI stimulation in patients with AD. I demonstrated that multi-session TI is safe and well-tolerated in this population, with 98% of participants completing the full intervention protocol. This represents a critical step in translating TI from proof-of-concept studies in healthy adults to clinical research in patient populations. Feasibility and pilot studies are increasingly recognised as essential phases in the development of complex interventions as they can strengthen the methodological rigour and success of subsequent full-scale clinical trials (Skivington et

al., 2021). This is particularly relevant for innovative approaches such as TI, which involve multiple interacting components, including technical, logistical, and patient-related factors that affect the implementation and evaluation of the method. This study provided important insights into whether patients could adhere to a demanding three-week intervention protocol and successfully engage in cognitive tasks, which is an important consideration for TI delivery, given the expected state-dependent effects of the intervention (Violante et al., 2023). It also identified uncertainties and challenges in protocol administration, and the knowledge gained has directly informed the design, implementation strategies, and power calculations of our ongoing double-blind, sham-controlled, crossover clinical trial in AD patients, thereby accelerating the development of TI towards a therapeutic intervention.

Moreover, while this study was not designed to establish definitive efficacy in the absence of a control condition, preliminary findings suggest that repeated hippocampal TI stimulation may enhance episodic memory performance in AD patients. These results support the potential of TI as a non-invasive neuromodulation strategy for targeting hippocampal-dependent cognitive functions and provide a strong rationale for conducting a full-scale efficacy study.

Development of methodological frameworks to record artefact-free EEG activity during TI stimulation

In Chapter 4, I developed and validated methodological frameworks for recording artefact-free EEG during TI stimulation, addressing a critical barrier in the field. The inability to monitor brain activity in real time has limited mechanistic insights into how non-invasive brain stimulation influences neural dynamics. While I did not develop the hardware filters myself, I integrated the custom-designed filters into experimental protocols and conducted systematic tests that provided iterative feedback to the collaborating engineering teams. This feedback was critical in optimising the devices, identifying failure points, and informing design improvements. As a result, the hardware is now fully developed and available to other labs, enabling broader adoption of EEG monitoring during TI.

Beyond the technical contributions, this chapter also provides the first evidence for frequency- and state-dependent effects of TI on brain activity in humans. These findings offer novel insights into how TI modulates neural dynamics and lay the groundwork for mechanistic investigations of TI's effects on brain activity.

5.3 Future directions

TI has rapidly gained popularity as a novel non-invasive deep brain stimulation technique, with growing interest in its applications in both basic research and clinical translation. To sustain this momentum and ensure the successful and widespread adoption of TI in the field of NIBS, it will be critical to build robust evidence of its efficacy across diverse contexts and applications.

Future research must also focus on understanding the mechanisms of action of TI, specifically, how it modulates brain network activity, and identify neurophysiological factors that influence its effects. The experimental framework for concurrent TI-EEG monitoring developed in this thesis will play a critical role in allowing us to address these mechanistic questions. Real-time monitoring of brain activity during stimulation will also support efforts to develop personalised TI interventions by enabling researchers to tailor stimulation to individual patient profiles.

To progress TI towards real-world clinical implementation, it will be equally important to move beyond efficacy trials and undertake effectiveness and implementation research. While efficacy studies evaluate interventions in highly controlled environments, effectiveness studies examine how TI performs under routine clinical or real-life conditions where patients are most likely to receive the intervention. Implementation research will play a key role in identifying contextual factors that influence the adoption, delivery, and impact of TI across diverse therapeutic settings. Conducting these investigations in parallel will allow insights from each research application to iteratively refine and innovate both the intervention and its delivery. This dynamic research approach will increase the likelihood of developing a TI intervention that is effective, acceptable, and capable of achieving a meaningful public health impact.

Finally, for TI to achieve success in both basic research and clinical translation, the field must prioritise the development of methodological and reporting standards at this early stage of adoption. Establishing shared frameworks and standardised terminology for describing interventions and stimulation protocols will enhance reproducibility and enable researchers to build effectively on existing evidence. These efforts will be critical for ensuring the scientific rigour and translational progress of TI.

Bibliography

Acerbo, E., Jegou, A., Luff, C., Dzialecka, P., Botzanowski, B., Missey, F., Ngom, I., Lagarde, S., Bartolomei, F., Cassara, A., Neufeld, E., Jirsa, V., Carron, R., Grossman, N., & Williamson, A. (2022). Focal non-invasive deep-brain stimulation with temporal interference for the suppression of epileptic biomarkers. *Frontiers in Neuroscience*, *16*. https://doi.org/10.3389/fnins.2022.945221

Aktürk, T., de Graaf, T. A., Güntekin, B., Hanoğlu, L., & Sack, A. T. (2022). Enhancing memory capacity by experimentally slowing theta frequency oscillations using combined EEG-tACS. *Scientific Reports*, *12*(1), 14199. https://doi.org/10.1038/s41598-022-18665-z

Aldehri, M., Temel, Y., Alnaami, I., Jahanshahi, A., & Hescham, S. (2018). Deep brain stimulation for Alzheimer's Disease: An update. *Surgical Neurology International*, *9*(1), 58. https://doi.org/10.4103/sni.sni_342_17

Almkvist, O., & Graff, C. (2022). Practice effects in cognitive assessments three years later in non-carriers but not in symptom-free mutation carriers of autosomal-dominant Alzheimer's disease: Exemplifying procedural learning and memory? *Frontiers in Aging Neuroscience*, *14*. https://doi.org/10.3389/fnagi.2022.905329

Alsop, D. C., Casement, M., de Bazelaire, C., Fong, T., & Press, D. Z. (2008). Hippocampal hyperperfusion in Alzheimer's disease. *NeuroImage*, *42*(4), 1267–1274. https://doi.org/10.1016/j.neuroimage.2008.06.006

Alzheimer's Association. (2024). 2024 Alzheimer's disease facts and figures. *Alzheimer's & Dementia: The Journal of the Alzheimer's Association*, *20*(5), 3708–3821. https://doi.org/10.1002/alz.13809

Andrade-Talavera, Y., Fisahn, A., & Rodríguez-Moreno, A. (2023). Timing to be precise? An overview of spike timing-dependent plasticity, brain rhythmicity, and glial cells interplay within neuronal circuits. *Molecular Psychiatry*, *28*(6), 2177–2188. https://doi.org/10.1038/s41380-023-02027-w

Antal, A., Alekseichuk, I., Bikson, M., Brockmöller, J., Brunoni, A. R., Chen, R., Cohen, L. G., Dowthwaite, G., Ellrich, J., Flöel, A., Fregni, F., George, M. S., Hamilton, R., Haueisen, J., Herrmann, C. S., Hummel, F. C., Lefaucheur, J. P., Liebetanz, D., Loo, C. K., … Paulus, W. (2017). Low intensity transcranial electric stimulation: Safety, ethical, legal regulatory and application guidelines. *Clinical Neurophysiology*, *128*(9), 1774–1809. https://doi.org/10.1016/j.clinph.2017.06.001

Antal, A., Luber, B., Brem, A.-K., Bikson, M., Brunoni, A. R., Kadosh, R. C., Dubljević, V., Fecteau, S., Ferreri, F., & Flöel, A. (2022). Non-invasive brain stimulation and neuroenhancement. *Clinical Neurophysiology Practice*, *7*, 146–165.

Argyropoulos, G. P. D., Dell'Acqua, C., Butler, E., Loane, C., Roca-Fernandez, A., Almozel, A., Drummond, N., Lage-Martinez, C., Cooper, E., Henson, R. N., & Butler, C. R. (2022). Functional Specialization of the Medial Temporal Lobes in Human Recognition Memory: Dissociating Effects of Hippocampal

versus Parahippocampal Damage. *Cerebral Cortex*, *32*(8), 1637–1652. https://doi.org/10.1093/cercor/bhab290

Avgerinos, K. I., Manolopoulos, A., Ferrucci, L., & Kapogiannis, D. (2024). Critical assessment of anti-amyloid-β monoclonal antibodies effects in Alzheimer's disease: A systematic review and meta-analysis highlighting target engagement and clinical meaningfulness. *Scientific Reports*, *14*(1), 25741. https://doi.org/10.1038/s41598-024-75204-8

Bahadori, A. R., Javadnia, P., Davari, A., Sheikhvatan, M., Ranji, S., Shafiee, S., & Tafakhori, A. (2024). Efficacy and safety of deep brain stimulation in drug resistance epilepsy: A systematic review and meta-analysis. *Neurosurgical Review*, *47*(1), 855. https://doi.org/10.1007/s10143-024-03090-9

Barnett, J. H., Blackwell, A. D., Sahakian, B. J., & Robbins, T. W. (2016). The Paired Associates Learning (PAL) Test: 30 Years of CANTAB Translational Neuroscience from Laboratory to Bedside in Dementia Research. In T. W. Robbins & B. J. Sahakian (Eds.), *Translational Neuropsychopharmacology* (pp. 449–474). Springer International Publishing. https://doi.org/10.1007/7854_2015_5001

Basche, K. E., Berron, D., Peterson, A., Rosario, H., Johnson, S. C., Düzel, E., & Clark, L. R. (2024). Procedural practice effects in remote digital memory assessment. *Alzheimer's & Dementia*, *20*(S3), e091794. https://doi.org/10.1002/alz.091794

Becker, N., Laukka, E. J., Kalpouzos, G., Naveh-Benjamin, M., Bäckman, L., & Brehmer, Y. (2015). Structural brain correlates of associative memory in older adults. *NeuroImage*, *118*, 146–153. https://doi.org/10.1016/j.neuroimage.2015.06.002

Begemann, M. J., Brand, B. A., Ćurčić-Blake, B., Aleman, A., & Sommer, I. E. (2020). Efficacy of non-invasive brain stimulation on cognitive functioning in brain disorders: A meta-analysis. *Psychological Medicine*, *50*(15), 2465–2486. https://doi.org/10.1017/S0033291720003670

Benussi, A., Cantoni, V., Cotelli, M. S., Cotelli, M., Brattini, C., Datta, A., Thomas, C., Santarnecchi, E., Pascual-Leone, A., & Borroni, B. (2021). Exposure to gamma tACS in Alzheimer's disease: A randomized, double-blind, sham-controlled, crossover, pilot study. *Brain Stimulation: Basic, Translational, and Clinical Research in Neuromodulation*, *14*(3), 531–540. https://doi.org/10.1016/j.brs.2021.03.007

Benussi, A., Cantoni, V., Grassi, M., Brechet, L., Michel, C. M., Datta, A., Thomas, C., Gazzina, S., Cotelli, M. S., Bianchi, M., Premi, E., Gadola, Y., Cotelli, M., Pengo, M., Perrone, F., Scolaro, M., Archetti, S., Solje, E., Padovani, A., … Borroni, B. (2022). Increasing Brain Gamma Activity Improves Episodic Memory and Restores Cholinergic Dysfunction in Alzheimer's Disease. *Annals of Neurology*, *92*(2), 322–334. https://doi.org/10.1002/ana.26411

Bikson, M., Grossman, P., Thomas, C., Zannou, A. L., Jiang, J., Adnan, T., Mourdoukoutas, A. P., Kronberg, G., Truong, D., Boggio, P., Brunoni, A. R., Charvet, L., Fregni, F., Fritsch, B., Gillick, B., Hamilton, R. H.,

Hampstead, B. M., Jankord, R., Kirton, A., … Woods, A. J. (2016). Safety of Transcranial Direct Current Stimulation: Evidence Based Update 2016. *Brain Stimulation*, *9*(5), 641–661. https://doi.org/10.1016/j.brs.2016.06.004

Booth, S. J., Taylor, J. R., Brown, L. J. E., & Pobric, G. (2022). The effects of transcranial alternating current stimulation on memory performance in healthy adults: A systematic review. *Cortex; a Journal Devoted to the Study of the Nervous System and Behavior*, *147*, 112–139. https://doi.org/10.1016/j.cortex.2021.12.001

Bradley, C., Nydam, A. S., Dux, P. E., & Mattingley, J. B. (2022). State-dependent effects of neural stimulation on brain function and cognition. *Nature Reviews Neuroscience*, *23*(8), 459–475. https://doi.org/10.1038/s41583-022-00598-1

Bradshaw, A. C., & Georges, J. (2024). Anti-Amyloid Therapies for Alzheimer's Disease: An Alzheimer Europe Position Paper and Call to Action. *The Journal of Prevention of Alzheimer's Disease*, *11*(2), 265–273. https://doi.org/10.14283/jpad.2024.37

Bright, P., Hale, E., Gooch, V. J., Myhill, T., & Van Der Linde, I. (2018). The National Adult Reading Test: Restandardisation against the Wechsler Adult Intelligence Scale—Fourth edition. *Neuropsychological Rehabilitation*, *28*(6), 1019–1027. https://doi.org/10.1080/09602011.2016.1231121

Brodeur, M. B., Guérard, K., & Bouras, M. (2014). Bank of Standardized Stimuli (BOSS) phase II: 930 new normative photos. *PloS One*, *9*(9), e106953. https://doi.org/10.1371/journal.pone.0106953

Brunoni, A. R., Amadera, J., Berbel, B., Volz, M. S., Rizzerio, B. G., & Fregni, F. (2011). A systematic review on reporting and assessment of adverse effects associated with transcranial direct current stimulation. *International Journal of Neuropsychopharmacology*, *14*(8), 1133–1145. https://doi.org/10.1017/S1461145710001690

Busche, M. A., & Hyman, B. T. (2020). Synergy between amyloid-β and tau in Alzheimer's disease. *Nature Neuroscience*, *23*(10), 1183–1193.

Buzsáki, G. (2006). *Rhythms of the Brain*. Oxford university press. https://books.google.com/books?hl=en&lr=&id=Q_xQEAAAQBAJ&oi=fnd&pg=PR15&dq=info:BR7tNMFpVZcJ:scholar.google.com&ots=2NOZUN8JUw&sig=49UClqVpzfdyrtFXEgS_5vIDZIc

Buzsáki, G., & and Watson, B. O. (2012). Brain rhythms and neural syntax: Implications for efficient coding of cognitive content and neuropsychiatric disease. *Dialogues in Clinical Neuroscience*, *14*(4), 345–367. https://doi.org/10.31887/DCNS.2012.14.4/gbuzsaki

Camacho-Conde, J. A., Gonzalez-Bermudez, M. D. R., Carretero-Rey, M., & Khan, Z. U. (2022). Brain stimulation: A therapeutic approach for the treatment of neurological disorders. *CNS Neuroscience & Therapeutics*, *28*(1), 5–18. https://doi.org/10.1111/cns.13769

Canter, R. G., Penney, J., & Tsai, L.-H. (2016). The road to restoring neural circuits for the treatment of Alzheimer's disease. *Nature*, *539*(7628), 187–196. https://doi.org/10.1038/nature20412

Caplan, J. B., & Madan, C. R. (2016). Word Imageability Enhances Association-memory by Increasing Hippocampal Engagement. *Journal of Cognitive Neuroscience*, *28*(10), 1522–1538. https://doi.org/10.1162/jocn_a_00992

Casaletto, K. B., Marx, G., Dutt, S., Neuhaus, J., Saloner, R., Kritikos, L., Miller, B., & Kramer, J. H. (2017). Is "Learning" episodic memory? Distinct cognitive and neuroanatomic correlates of immediate recall during learning trials in neurologically normal aging and neurodegenerative cohorts. *Neuropsychologia*, *102*, 19–28. https://doi.org/10.1016/j.neuropsychologia.2017.05.021

Cecere, R., Rees, G., & Romei, V. (2015). Individual Differences in Alpha Frequency Drive Crossmodal Illusory Perception. *Current Biology*, *25*(2), 231–235. https://doi.org/10.1016/j.cub.2014.11.034

Cernera, S., Alcantara, J. D., Opri, E., Cagle, J. N., Eisinger, R. S., Boogaart, Z., Pramanik, L., Kelberman, M., Patel, B., Foote, K. D., Okun, M. S., & Gunduz, A. (2021). Wearable sensor-driven responsive deep brain stimulation for essential tremor. *Brain Stimulation*, *14*(6), 1434–1443. https://doi.org/10.1016/j.brs.2021.09.002

Chan, A. T. C., Ip, R. T. F., Tran, J. Y. S., Chan, J. Y. C., & Tsoi, K. K. F. (2024). Computerized cognitive training for memory functions in mild cognitive impairment or dementia: A systematic review and meta-analysis. *Npj Digital Medicine*, *7*(1), 1. https://doi.org/10.1038/s41746-023-00987-5

Chan, J. Y. C., Liu, J., Chan, A. T. C., & Tsoi, K. K. F. (2024). Exergaming and cognitive functions in people with mild cognitive impairment and dementia: A meta-analysis. *Npj Digital Medicine*, *7*(1), 154. https://doi.org/10.1038/s41746-024-01142-4

Chen, S., Cao, Z., Nandi, A., Counts, N., Jiao, L., Prettner, K., Kuhn, M., Seligman, B., Tortorice, D., Vigo, D., Wang, C., & Bloom, D. E. (2024). The global macroeconomic burden of Alzheimer's disease and other dementias: Estimates and projections for 152 countries or territories. *The Lancet Global Health*, *12*(9), e1534–e1543. https://doi.org/10.1016/S2214-109X(24)00264-X

Chen, Y., Wang, Y., Song, Z., Fan, Y., Gao, T., & Tang, X. (2023). Abnormal white matter changes in Alzheimer's disease based on diffusion tensor imaging: A systematic review. *Ageing Research Reviews*, *87*, 101911. https://doi.org/10.1016/j.arr.2023.101911

Chou, Y., Sundman, M., Ton That, V., Green, J., & Trapani, C. (2022). Cortical excitability and plasticity in Alzheimer's disease and mild cognitive impairment: A systematic review and meta-analysis of transcranial magnetic stimulation studies. *Ageing Research Reviews*, *79*, 101660. https://doi.org/10.1016/j.arr.2022.101660

Chua, E. F., Schacter, D. L., Rand-Giovannetti, E., & Sperling, R. A. (2007). Evidence for a specific role of the anterior hippocampal region in successful associative encoding. *Hippocampus*, *17*(11), 1071–1080. https://doi.org/10.1002/hipo.20340

Clark, I. A., Kim, M., & Maguire, E. A. (2018). Verbal Paired Associates and the Hippocampus: The Role of Scenes. *Journal of Cognitive Neuroscience*, *30*(12), 1821–1845. https://doi.org/10.1162/jocn_a_01315

Colavitta, M. F., Grasso, L., & Barrantes, F. J. (2023). Environmental Enrichment in Murine Models and Its Translation to Human Factors Improving Conditions in Alzheimer Disease. *The Journal of Prevention of Alzheimer's Disease*, *10*(2), 287–300. https://doi.org/10.14283/jpad.2023.5

Corriveau-Lecavalier, N., Adams, J. N., Fischer, L., Molloy, E. N., & Maass, A. (2024). Cerebral hyperactivation across the Alzheimer's disease pathological cascade. *Brain Communications*, *6*(6), fcae376. https://doi.org/10.1093/braincomms/fcae376

Cotovio, G., Ventura, F., Rodrigues da Silva, D., Pereira, P., & Oliveira-Maia, A. J. (2023). Regulatory Clearance and Approval of Therapeutic Protocols of Transcranial Magnetic Stimulation for Psychiatric Disorders. *Brain Sciences*, *13*(7), 1029. https://doi.org/10.3390/brainsci13071029

Cunnane, S. C., Trushina, E., Morland, C., Prigione, A., Casadesus, G., Andrews, Z. B., Beal, M. F., Bergersen, L. H., Brinton, R. D., de la Monte, S., Eckert, A., Harvey, J., Jeggo, R., Jhamandas, J. H., Kann, O., la Cour, C. M., Martin, W. F., Mithieux, G., Moreira, P. I., … Millan, M. J. (2020). Brain energy rescue: An emerging therapeutic concept for neurodegenerative disorders of ageing. *Nature Reviews Drug Discovery*, *19*(9), 609–633. https://doi.org/10.1038/s41573-020-0072-x

Dale, A. M., Fischl, B., & Sereno, M. I. (1999). Cortical surface-based analysis: I. Segmentation and surface reconstruction. *Neuroimage*, *9*(2), 179–194.

Dale, A. M., & Sereno, M. I. (1993). Improved localizadon of cortical activity by combining EEG and MEG with MRI cortical surface reconstruction: A linear approach. *Journal of Cognitive Neuroscience*, *5*(2), 162–176.

Daly. (2024). A philosophy of science approach to the amyloid hypothesis of Alzheimer's disease. *European Journal of Neuroscience*, *60*(5), 4707–4722. https://doi.org/10.1111/ejn.16500

Dantas, J. M., Mutarelli, A., Navalha, D. D. P., Dagostin, C. S., Romeiro, P. H. C. L., Felix, N., Nogueira, A., Batista, S., Teixeira, L., & Caramelli, P. (2024). Efficacy of anti-amyloid-ß monoclonal antibody therapy in early Alzheimer's disease: A systematic review and meta-analysis. *Neurological Sciences*, *45*(6), 2461–2469. https://doi.org/10.1007/s10072-023-07194-w

Davidson, B., Bhattacharya, A., Sarica, C., Darmani, G., Raies, N., Chen, R., & Lozano, A. M. (2024). Neuromodulation techniques – From non-invasive brain stimulation to deep brain stimulation. *Neurotherapeutics*, *21*(3), e00330. https://doi.org/10.1016/j.neurot.2024.e00330

Davidson, B., Vetkas, A., Germann, J., Tang-Wai, D., & Lozano, A. M. (2024). Deep brain stimulation for Alzheimer's disease – current status and next steps. *Expert Review of Medical Devices*, *21*(4), 285–292. https://doi.org/10.1080/17434440.2024.2337298

de Graaff, M. L. A., van der Heide, I., Rademakers, J. J. D. J. M., van Valkengoed, I. G. M., Francke, A. L., Woonink, A., & Bijnsdorp, F. M. (2025). Is caregiver burden associated with sex and gender-related characteristics? A large-scale survey study among family caregivers of people with dementia. *BMC Geriatrics*, *25*(1), 171. https://doi.org/10.1186/s12877-025-05795-y

de Rover, M., Pironti, V. A., McCabe, J. A., Acosta-Cabronero, J., Arana, F. S., Morein-Zamir, S., Hodges, J. R., Robbins, T. W., Fletcher, P. C., Nestor, P. J., & Sahakian, B. J. (2011). Hippocampal dysfunction in patients with mild cognitive impairment: A functional neuroimaging study of a visuospatial paired associates learning task. *Neuropsychologia*, *49*(7), 2060–2070. https://doi.org/10.1016/j.neuropsychologia.2011.03.037

De Simone, M. S., Perri, R., Rodini, M., Fadda, L., De Tollis, M., Caltagirone, C., & Carlesimo, G. A. (2021). A Lack of Practice Effects on Memory Tasks Predicts Conversion to Alzheimer Disease in Patients With Amnestic Mild Cognitive Impairment. *Journal of Geriatric Psychiatry and Neurology*, *34*(6), 582–593. https://doi.org/10.1177/0891988720944244

De Vries, L. E., Huitinga, I., Kessels, H. W., Swaab, D. F., & Verhaagen, J. (2024). The concept of resilience to Alzheimer's Disease: Current definitions and cellular and molecular mechanisms. *Molecular Neurodegeneration*, *19*(1), 33. https://doi.org/10.1186/s13024-024-00719-7

De Wit, L., Kessels, R. P. C., Kurasz, A. M., Amofa, P., O'Shea, D., Marsiske, M., Chandler, M. J., Piai, V., Lambertus, T., & Smith, G. E. (2023). Declarative Learning, Priming, and Procedural Learning Performances comparing Individuals with Amnestic Mild Cognitive Impairment, and Cognitively Unimpaired Older Adults. *Journal of the International Neuropsychological Society*, *29*(2), 113–125. https://doi.org/10.1017/S1355617722000029

De Wit, L., Marsiske, M., O'Shea, D., Kessels, R. P. C., Kurasz, A. M., DeFeis, B., Schaefer, N., & Smith, G. E. (2021). Procedural Learning in Individuals with Amnestic Mild Cognitive Impairment and Alzheimer's Dementia: A Systematic Review and Meta-analysis. *Neuropsychology Review*, *31*(1), 103–114. https://doi.org/10.1007/s11065-020-09449-1

Delbeuck, X., Van der Linden, M., & Collette, F. (2003). Alzheimer's disease as a disconnection syndrome? *Neuropsychology Review*, *13*(2), 79–92. https://doi.org/10.1023/a:1023832305702

Desikan, R. S., Ségonne, F., Fischl, B., Quinn, B. T., Dickerson, B. C., Blacker, D., Buckner, R. L., Dale, A. M., Maguire, R. P., & Hyman, B. T. (2006). An automated labeling system for subdividing the human cerebral cortex on MRI scans into gyral based regions of interest. *Neuroimage*, *31*(3), 968–980.

Dhaynaut, M., Cappon, D., Paciorek, R., Macone, J., Connor, A., Guehl, N., Pascual-Leone, A., Fakhri, G. E., & Santarnecchi, E. (2020). Effects of modulating gamma oscillations via 40Hz transcranial alternating current stimulation (tACS) on Tau PET imaging in mild to moderate Alzheimer's Disease. *Journal of Nuclear Medicine*, *61*(supplement 1), 340–340.

Dhaynaut, M., Sprugnoli, G., Cappon, D., Macone, J., Sanchez, J. S., Normandin, M. D., Guehl, N. J., Koch, G., Paciorek, R., Connor, A., Press, D., Johnson, K., Pascual-Leone, A., El Fakhri, G., & Santarnecchi, E. (2022). Impact of 40 Hz Transcranial Alternating Current Stimulation on Cerebral Tau Burden in Patients with Alzheimer's Disease: A Case Series. *Journal of Alzheimer's Disease*, *85*(4), 1667–1676. https://doi.org/10.3233/JAD-215072

Diedrich, L., Kolhoff, H. I., Chakalov, I., Vékony, T., Németh, D., & Antal, A. (2024). Prefrontal theta—Gamma transcranial alternating current stimulation improves non-declarative visuomotor learning in older adults. *Scientific Reports*, *14*(1), 4955. https://doi.org/10.1038/s41598-024-55125-2

Ding, M., Schmidt-Mende, K., & Modig, K. (2025). Social Factors, Age, and Health at Time of Dementia Diagnosis. *JAMA Network Open*, *8*(2), e2461117. https://doi.org/10.1001/jamanetworkopen.2024.61117

Dowsett, J., Herrmann, C. S., Dieterich, M., & Taylor, P. C. J. (2020). Shift in lateralization during illusory self-motion: EEG responses to visual flicker at 10 Hz and frequency-specific modulation by tACS. *European Journal of Neuroscience*, *51*(7), 1657–1675. https://doi.org/10.1111/ejn.14543

Drozdick, L. W., Holdnack, J. A., Weiss, L. G., & Zhou, X. (2013). Chapter 1—Overview of the WAIS–IV/WMS–IV/ACS. In J. A. Holdnack, L. W. Drozdick, L. G. Weiss, & G. L. Iverson (Eds.), *WAIS-IV, WMS-IV, and ACS* (pp. 1–73). Academic Press. https://doi.org/10.1016/B978-0-12-386934-0.00001-8

Dubois, B., Von Arnim, C. A. F., Burnie, N., Bozeat, S., & Cummings, J. (2023). Biomarkers in Alzheimer's disease: Role in early and differential diagnosis and recognition of atypical variants. *Alzheimer's Research & Therapy*, *15*(1), 175. https://doi.org/10.1186/s13195-023-01314-6

Duff, K., Beglinger, L. J., Schultz, S. K., Moser, D. J., McCaffrey, R. J., Haase, R. F., Westervelt, H. J., Langbehn, D. R., Paulsen, J. S., & Group, H. S. (2007). Practice effects in the prediction of long-term cognitive outcome in three patient samples: A novel prognostic index. *Archives of Clinical Neuropsychology*, *22*(1), 15–24.

Duff, K., Hammers, D. B., Koppelmans, V., King, J. B., & Hoffman, J. M. (2024). Short-Term Practice Effects on Cognitive Tests Across the Late Life Cognitive Spectrum and How They Compare to Biomarkers of Alzheimer's Disease. *Journal of Alzheimer's Disease*, *99*(1), 321–332. https://doi.org/10.3233/JAD-231392

Duff, K., Horn, K. P., Foster, N. L., & Hoffman, J. M. (2015). Short-term practice effects and brain hypometabolism: Preliminary data from an FDG PET study. *Archives of Clinical Neuropsychology*, *30*(3), 264–270.

Duff, K., Lyketsos, C. G., Beglinger, L. J., Chelune, G., Moser, D. J., Arndt, S., Schultz, S. K., Paulsen, J. S., Petersen, R. C., & McCaffrey, R. J. (2011). Practice effects predict cognitive outcome in amnestic mild cognitive impairment. *The American Journal of Geriatric Psychiatry*, *19*(11), 932–939.

Duyckaerts, C., Delatour, B., & Potier, M.-C. (2009). Classification and basic pathology of Alzheimer disease. *Acta Neuropathologica*, *118*(1), 5–36. https://doi.org/10.1007/s00401-009-0532-1

Égerházi, A., Berecz, R., Bartók, E., & Degrell, I. (2007). Automated Neuropsychological Test Battery (CANTAB) in mild cognitive impairment and in Alzheimer's disease. *Progress in Neuro-Psychopharmacology and Biological Psychiatry*, *31*(3), 746–751. https://doi.org/10.1016/j.pnpbp.2007.01.011

Elamin, M., Pender, N., Hardiman, O., & Abrahams, S. (2012). Social cognition in neurodegenerative disorders: A systematic review. *Journal of Neurology, Neurosurgery & Psychiatry*, *83*(11), 1071–1079. https://doi.org/10.1136/jnnp-2012-302817

Feigin, V. L., Vos, T., Nichols, E., Owolabi, M. O., Carroll, W. M., Dichgans, M., Deuschl, G., Parmar, P., Brainin, M., & Murray, C. (2020). The global burden of neurological disorders: Translating evidence into policy. *The Lancet. Neurology*, *19*(3), 255–265. https://doi.org/10.1016/S1474-4422(19)30411-9

Finn, M., & McDonald, S. (2015). Repetition-lag training to improve recollection memory in older people with amnestic mild cognitive impairment. A randomized controlled trial. *Aging, Neuropsychology, and Cognition*, *22*(2), 244–258. https://doi.org/10.1080/13825585.2014.915918

Fischl, B., & Dale, A. M. (2000). Measuring the thickness of the human cerebral cortex from magnetic resonance images. *Proceedings of the National Academy of Sciences*, *97*(20), 11050–11055. https://doi.org/10.1073/pnas.200033797

Fischl, B., Liu, A., & Dale, A. M. (2001). Automated manifold surgery: Constructing geometrically accurate and topologically correct models of the human cerebral cortex. *IEEE Transactions on Medical Imaging*, *20*(1), 70–80.

Fischl, B., Salat, D. H., Busa, E., Albert, M., Dieterich, M., Haselgrove, C., Van Der Kouwe, A., Killiany, R., Kennedy, D., & Klaveness, S. (2002). Whole brain segmentation: Automated labeling of neuroanatomical structures in the human brain. *Neuron*, *33*(3), 341–355.

Fischl, B., Salat, D. H., Van Der Kouwe, A. J., Makris, N., Ségonne, F., Quinn, B. T., & Dale, A. M. (2004). Sequence-independent segmentation of magnetic resonance images. *Neuroimage*, *23*, S69–S84.

Fischl, B., Sereno, M. I., & Dale, A. M. (1999). Cortical surface-based analysis: II: inflation, flattening, and a surface-based coordinate system. *Neuroimage*, *9*(2), 195–207.

Fischl, B., Sereno, M. I., Tootell, R. B. H., & Dale, A. M. (1999). High-resolution intersubject averaging and a coordinate system for the cortical surface. *Human Brain Mapping*, *8*(4), 272–284. https://doi.org/10.1002/(SICI)1097-0193(1999)8:4<272::AID-HBM10>3.0.CO;2-4

Fischl, B., Van Der Kouwe, A., Destrieux, C., Halgren, E., Ségonne, F., Salat, D. H., Busa, E., Seidman, L. J., Goldstein, J., & Kennedy, D. (2004). Automatically parcellating the human cerebral cortex. *Cerebral Cortex*, *14*(1), 11–22.

Foxe, J. J., & Snyder, A. C. (2011). The role of alpha-band brain oscillations as a sensory suppression mechanism during selective attention. *Frontiers in Psychology*, *2*, 154.

Frere, S., & Slutsky, I. (2018). Alzheimer's Disease: From Firing Instability to Homeostasis Network Collapse. *Neuron*, *97*(1), 32–58. https://doi.org/10.1016/j.neuron.2017.11.028

Gattas, S., Larson, M. S., Mnatsakanyan, L., Sen-Gupta, I., Vadera, S., Swindlehurst, A. L., Rapp, P. E., Lin, J. J., & Yassa, M. A. (2023). Theta mediated dynamics of human hippocampal-neocortical learning systems in memory formation and retrieval. *Nature Communications*, *14*(1), 8505.

Grabner, H., Grabner, M., & Bischof, H. (2006). Real-time tracking via on-line boosting. *Bmvc*, *1*(5), 6. https://citeseerx.ist.psu.edu/document?repid=rep1&type=pdf&doi=03ae968c3ecb5ba30a6df7b00518db6ec785d8c3

Grossman, N., Bono, D., Dedic, N., Kodandaramaiah, S. B., Rudenko, A., Suk, H.-J., Cassara, A. M., Neufeld, E., Kuster, N., & Tsai, L.-H. (2017). Noninvasive deep brain stimulation via temporally interfering electric fields. *Cell*, *169*(6), 1029–1041.

Grover, S. (2024). *Causal Investigations of Rhythmic Electrophysiological Mechanisms Underlying Healthy Cognition and Disease Using Transcranial Alternating Current Stimulation* [Ph.D.]. https://www.proquest.com/docview/3165209291/abstract/FB2C279D449C4A9FPQ/1

Grover, S., Fayzullina, R., Bullard, B. M., Levina, V., & Reinhart, R. M. G. (2023). A meta-analysis suggests that tACS improves cognition in healthy, aging, and psychiatric populations. *Science Translational Medicine*, *15*(697), eabo2044. https://doi.org/10.1126/scitranslmed.abo2044

Guo, J., Wang, Z., Liu, R., Huang, Y., Zhang, N., & Zhang, R. (2020). Memantine, Donepezil, or Combination Therapy—What is the best therapy for Alzheimer's Disease? A Network Meta-Analysis. *Brain and Behavior*, *10*(11), e01831. https://doi.org/10.1002/brb3.1831

Hampel, H., Hardy, J., Blennow, K., Chen, C., Perry, G., Kim, S. H., Villemagne, V. L., Aisen, P., Vendruscolo, M., Iwatsubo, T., Masters, C. L., Cho, M., Lannfelt, L., Cummings, J. L., & Vergallo, A. (2021). The Amyloid-β Pathway in Alzheimer's Disease. *Molecular Psychiatry*, *26*(10), 5481–5503. https://doi.org/10.1038/s41380-021-01249-0

Hampshire, A., Ballard, C., & Williams, G. (2020). Computerized neuropsychological tests undertaken on digital platforms are cost effective, achieve high engagement, distinguish and are highly sensitive to

longitudinal change: Data from the PROTECT and GBIT studies: Advancing clinical trial design and methods in a digital age. *Alzheimer's & Dementia*, *16*(S10), e041122. https://doi.org/10.1002/alz.041122

Hampshire, A., Lerede, A., Middleton, R., Rodgers, J., Tuite-Dalton, K., Trender, W., Hellyer, P., & Nicholas, R. (2022). *Online assessment and monitoring of cognitive decline in neurological conditions*. BMJ Publishing Group Ltd. https://jnnp.bmj.com/content/93/9/e2.3.abstract

Han, S., Sui, J., & Zhu, Y. (2006). Self-face recognition in attended and unattended conditions: An event-related brain potential study. *Neuroreport*, *17*(4), 423–427.

Hanslmayr, S., Axmacher, N., & Inman, C. S. (2019). Modulating human memory via entrainment of brain oscillations. *Trends in Neurosciences*, *42*(7), 485–499.

Hansen, N. (2012). Action Mechanisms of Transcranial Direct Current Stimulation in Alzheimer's Disease and Memory Loss. Frontiers in Psychiatry, 3. https://doi.org/10.3389/fpsyt.2012.00048

Hansson, O., Blennow, K., Zetterberg, H., & Dage, J. (2023). Blood biomarkers for Alzheimer's disease in clinical practice and trials. *Nature Aging*, *3*(5), 506–519. https://doi.org/10.1038/s43587-023-00403-3

Harada, N., Nishiyama, S., Kanazawa, M., & Tsukada, H. (2013). Development of novel PET probes, [18F]BCPP-EF, [18F]BCPP-BF, and [11C]BCPP-EM for mitochondrial complex 1 imaging in the living brain. *Journal of Labelled Compounds & Radiopharmaceuticals*, *56*(11), 553–561. https://doi.org/10.1002/jlcr.3056

Hariz, M., & Blomstedt, P. (2022). Deep brain stimulation for Parkinson's disease. *Journal of Internal Medicine*, *292*(5), 764–778. https://doi.org/10.1111/joim.13541

Harpaz, D., Eltzov, E., Seet, R. C. S., Marks, R. S., & Tok, A. I. Y. (2017). Point-of-Care-Testing in Acute Stroke Management: An Unmet Need Ripe for Technological Harvest. *Biosensors*, *7*(3), 30. https://doi.org/10.3390/bios7030030

Haslacher, D., Narang, A., Sokoliuk, R., Cavallo, A., Reber, P., Nasr, K., Santarnecchi, E., & Soekadar, S. R. (2023a). In vivo phase-dependent enhancement and suppression of human brain oscillations by transcranial alternating current stimulation (tACS). *NeuroImage*, *275*, 120187. https://doi.org/10.1016/j.neuroimage.2023.120187

Haslacher, D., Narang, A., Sokoliuk, R., Cavallo, A., Reber, P., Nasr, K., Santarnecchi, E., & Soekadar, S. R. (2023b). In vivo phase-dependent enhancement and suppression of human brain oscillations by transcranial alternating current stimulation (tACS). *NeuroImage*, *275*, 120187. https://doi.org/10.1016/j.neuroimage.2023.120187

Haslacher, D., Nasr, K., Robinson, S. E., Braun, C., & Soekadar, S. R. (2021). Stimulation artifact source separation (SASS) for assessing electric brain oscillations during transcranial alternating current stimulation (tACS). *NeuroImage*, *228*, 117571. https://doi.org/10.1016/j.neuroimage.2020.117571

Hassenstab, J., Ruvolo, D., Jasielec, M., Xiong, C., Grant, E., & Morris, J. C. (2015). Absence of practice effects in preclinical Alzheimer's disease. *Neuropsychology*, *29*(6), 940–948. https://doi.org/10.1037/neu0000208

Helfrich, R. F., Schneider, T. R., Rach, S., Trautmann-Lengsfeld, S. A., Engel, A. K., & Herrmann, C. S. (2014). Entrainment of Brain Oscillations by Transcranial Alternating Current Stimulation. *Current Biology*, *24*(3), 333–339. https://doi.org/10.1016/j.cub.2013.12.041

Henson, R. N. A., Shallice, T., & Dolan, R. J. (1999). Right prefrontal cortex and episodic memory retrieval: A functional MRI test of the monitoring hypothesis. *Brain*, *122*(7), 1367–1381. https://doi.org/10.1093/brain/122.7.1367

Herrmann, C. S. (2001). Human EEG responses to 1–100 Hz flicker: Resonance phenomena in visual cortex and their potential correlation to cognitive phenomena. *Experimental Brain Research*, *137*(3), 346–353. https://doi.org/10.1007/s002210100682

Herrmann, C. S., Rach, S., Neuling, T., & Strüber, D. (2013). Transcranial alternating current stimulation: A review of the underlying mechanisms and modulation of cognitive processes. *Frontiers in Human Neuroscience*, *7*. https://doi.org/10.3389/fnhum.2013.00279

Herrmann, C. S., Strüber, D., Helfrich, R. F., & Engel, A. K. (2016). EEG oscillations: From correlation to causality. *International Journal of Psychophysiology: Official Journal of the International Organization of Psychophysiology*, *103*, 12–21. https://doi.org/10.1016/j.ijpsycho.2015.02.003

Herweg, N. A., Solomon, E. A., & Kahana, M. J. (2020). Theta Oscillations in Human Memory. *Trends in Cognitive Sciences*, *24*(3), 208–227. https://doi.org/10.1016/j.tics.2019.12.006

Hill, A. T., Fitzgerald, P. B., & Hoy, K. E. (2016). Effects of anodal transcranial direct current stimulation on working memory: A systematic review and meta-analysis of findings from healthy and neuropsychiatric populations. *Brain Stimulation*, *9*(2), 197–208.

Holm, S. P., Wolfer, A. M., Pointeau, G. H. S., Lipsmeier, F., & Lindemann, M. (2022). Practice effects in performance outcome measures in patients living with neurologic disorders – A systematic review. *Heliyon*, *8*(8), e10259. https://doi.org/10.1016/j.heliyon.2022.e10259

Holzmann, R., Koppehele-Gossel, J., Voss, U., & Klimke, A. (2021). Investigating Nuisance Effects Induced in EEG During tACS Application. *Frontiers in Human Neuroscience*, *15*. https://doi.org/10.3389/fnhum.2021.637080

Hong, S., Beja-Glasser, V. F., Nfonoyim, B. M., Frouin, A., Li, S., Ramakrishnan, S., Merry, K. M., Shi, Q., Rosenthal, A., Barres, B. A., Lemere, C. A., Selkoe, D. J., & Stevens, B. (2016). Complement and

microglia mediate early synapse loss in Alzheimer mouse models. *Science*, *352*(6286), 712–716. https://doi.org/10.1126/science.aad8373

Hsieh, S., Schubert, S., Hoon, C., Mioshi, E., & Hodges, J. R. (2013). Validation of the Addenbrooke's Cognitive Examination III in frontotemporal dementia and Alzheimer's disease. *Dementia and Geriatric Cognitive Disorders*, *36*(3–4), 242–250.

Hu, K., Wan, R., Liu, Y., Niu, M., Guo, J., & Guo, F. (2022). Effects of transcranial alternating current stimulation on motor performance and motor learning for healthy individuals: A systematic review and meta-analysis. Frontiers in Physiology, 13. https://doi.org/10.3389/fphys.2022.1064584

Huang, P., Lin, L., Zhang, J., Cheng, Y., & Pan, X. (2024). Efficacy analysis of three brain stimulation techniques for Alzheimer's disease: A meta-analysis of repeated transcranial magnetic stimulation, transcranial direct current stimulation, and deep brain stimulation. *Expert Review of Neurotherapeutics*, *24*(1), 117–127. https://doi.org/10.1080/14737175.2023.2293225

Ichise, M., Toyama, H., Innis, R. B., & Carson, R. E. (2002). Strategies to Improve Neuroreceptor Parameter Estimation by Linear Regression Analysis. *Journal of Cerebral Blood Flow & Metabolism*, *22*(10), 1271–1281. https://doi.org/10.1097/01.WCB.0000038000.34930.4E

Iglesias, J. E., Augustinack, J. C., Nguyen, K., Player, C. M., Player, A., Wright, M., Roy, N., Frosch, M. P., McKee, A. C., Wald, L. L., Fischl, B., & Van Leemput, K. (2015). A computational atlas of the hippocampal formation using ex vivo, ultra-high resolution MRI: Application to adaptive segmentation of in vivo MRI. *NeuroImage*, *115*, 117–137. https://doi.org/10.1016/j.neuroimage.2015.04.042

Iglesias, J. E., Saygin, Z. M., Kliemann, D., Van Der Kouwe, A. J. W., Boyd, E., Reuter, M., Stevens, A., Van Leemput, K., McKee, A., Frosch, M. P., Fischl, B., & Augustinack, J. C. (2017). High-resolution magnetic resonance imaging reveals nuclei of the human amygdala: Manual segmentation to automatic atlas. *NeuroImage*, *155*, 370–382. https://doi.org/10.1016/j.neuroimage.2017.04.046

Iglesias, J. E., Van Leemput, K., Augustinack, J., Insausti, R., Fischl, B., & Reuter, M. (2016). Bayesian longitudinal segmentation of hippocampal substructures in brain MRI using subject-specific atlases. *NeuroImage*, *141*, 542–555. https://doi.org/10.1016/j.neuroimage.2016.07.020

Imbimbo, B. P., Watling, M., Imbimbo, C., & Nisticò, R. (2023). *Plasma ATN(I) classification and precision pharmacology in Alzheimer's disease*.

Indahlastari, A., Hardcastle, C., Albizu, A., Alvarez-Alvarado, S., Boutzoukas, E. M., Evangelista, N. D., Hausman, H. K., Kraft, J., Langer, K., & Woods, A. J. (2021). A Systematic Review and Meta-Analysis of Transcranial Direct Current Stimulation to Remediate Age-Related Cognitive Decline in Healthy Older Adults. Neuropsychiatric Disease and Treatment, Volume 17, 971–990. https://doi.org/10.2147/ndt.s259499

Jafari, Z., Kolb, B. E., & Mohajerani, M. H. (2020). Neural oscillations and brain stimulation in Alzheimer's disease. *Progress in Neurobiology*, *194*, 101878. https://doi.org/10.1016/j.pneurobio.2020.101878

Jamadar, S. D., Behler, A., Deery, H., & Breakspear, M. (2025). The metabolic costs of cognition. *Trends in Cognitive Sciences*, S136466132400319X. https://doi.org/10.1016/j.tics.2024.11.010

Jehi, L. (2025). Advances in Therapy for Refractory Epilepsy. *Annual Review of Medicine*, *76*(Volume 76, 2025), 389–402. https://doi.org/10.1146/annurev-med-050522-034458

Jensen, O., & Mazaheri, A. (2010). Shaping Functional Architecture by Oscillatory Alpha Activity: Gating by Inhibition. *Frontiers in Human Neuroscience*, *4*. https://doi.org/10.3389/fnhum.2010.00186

Jeong, J. (2004). EEG dynamics in patients with Alzheimer's disease. *Clinical Neurophysiology*, *115*(7), 1490–1505.

Jia, B., Xu, Y., & Zhu, X. (2025). Cognitive resilience in Alzheimer's disease: Mechanism and potential clinical intervention. *Ageing Research Reviews*, *106*, 102711. https://doi.org/10.1016/j.arr.2025.102711

Jog, M. A., Anderson, C., Kubicki, A., Boucher, M., Leaver, A., Hellemann, G., Iacoboni, M., Woods, R., & Narr, K. (2023). Transcranial direct current stimulation (tDCS) in depression induces structural plasticity. Scientific Reports, 13(1). https://doi.org/10.1038/s41598-023-29792-6

Johansson, J. D., & Zsigmond, P. (2021). Comparison between patient-specific deep brain stimulation simulations and commercial system SureTune3. *Biomedical Physics & Engineering Express*, *7*(5), 055001. https://doi.org/10.1088/2057-1976/ac0dcd

Jovicich, J., Czanner, S., Greve, D., Haley, E., van Der Kouwe, A., Gollub, R., Kennedy, D., Schmitt, F., Brown, G., & MacFall, J. (2006). Reliability in multi-site structural MRI studies: Effects of gradient non-linearity correction on phantom and human data. *Neuroimage*, *30*(2), 436–443.

Jutten, R. J., Grandoit, E., Foldi, N. S., Sikkes, S. A. M., Jones, R. N., Choi, S., Lamar, M. L., Louden, D. K. N., Rich, J., Tommet, D., Crane, P. K., & Rabin, L. A. (2020). Lower practice effects as a marker of cognitive performance and dementia risk: A literature review. *Alzheimer's & Dementia: Diagnosis, Assessment & Disease Monitoring*, *12*(1). https://doi.org/10.1002/dad2.12055

Kallio, E.-L., Öhman, H., Kautiainen, H., Hietanen, M., & Pitkälä, K. (2017). Cognitive Training Interventions for Patients with Alzheimer's Disease: A Systematic Review. *Journal of Alzheimer's Disease*, *56*(4), 1349–1372. https://doi.org/10.3233/JAD-160810

Kang, J. M., Kim, N., Yun, S. K., Seo, H.-E., Bae, J. N., Kim, W.-H., Na, K.-S., Cho, S.-E., Ryu, S.-H., Noh, Y., Youn, J.-H., Kang, S.-G., Lee, J.-Y., & Cho, S.-J. (2024). Exploring transfer effects on memory and its neural mechanisms through a computerized cognitive training in mild cognitive impairment: Randomized controlled trial. *Psychogeriatrics*, *24*(5), 1075–1086. https://doi.org/10.1111/psyg.13161

Kasten, F. H., Dowsett, J., & Herrmann, C. S. (2016). Sustained Aftereffect of α-tACS Lasts Up to 70 min after Stimulation. *Frontiers in Human Neuroscience*, *10*. https://doi.org/10.3389/fnhum.2016.00245

Kasten, F. H., Duecker, K., Maack, M. C., Meiser, A., & Herrmann, C. S. (2019). Integrating electric field modeling and neuroimaging to explain inter-individual variability of tACS effects. *Nature Communications*, *10*(1), 5427. https://doi.org/10.1038/s41467-019-13417-6

Kasten, F. H., & Herrmann, C. S. (2019a). Recovering Brain Dynamics During Concurrent tACS-M/EEG: An Overview of Analysis Approaches and Their Methodological and Interpretational Pitfalls. *Brain Topography*, *32*(6), 1013–1019. https://doi.org/10.1007/s10548-019-00727-7

Kasten, F. H., & Herrmann, C. S. (2019b). Recovering Brain Dynamics During Concurrent tACS-M/EEG: An Overview of Analysis Approaches and Their Methodological and Interpretational Pitfalls. *Brain Topography*, *32*(6), 1013–1019. https://doi.org/10.1007/s10548-019-00727-7

Kasten, F. H., Negahbani, E., Fröhlich, F., & Herrmann, C. S. (2018). Non-linear transfer characteristics of stimulation and recording hardware account for spurious low frequency artifacts during amplitude modulated transcranial alternating current stimulation (AM-tACS). *NeuroImage*, *179*, 134–143. https://doi.org/10.1016/j.neuroimage.2018.05.068

Kehler, L., Francisco, C. O., Uehara, M. A., & Moussavi, Z. (2020). The effect of transcranial alternating current stimulation (tACS) on cognitive function in older adults with dementia. *2020 42nd Annual International Conference of the IEEE Engineering in Medicine & Biology Society (EMBC)*, 3649–3653. https://doi.org/10.1109/EMBC44109.2020.9175903

Kim, B.-H., Kim, S., Nam, Y., Park, Y. H., Shin, S. M., & Moon, M. (2025). Second-generation anti-amyloid monoclonal antibodies for Alzheimer's disease: Current landscape and future perspectives. *Translational Neurodegeneration*, *14*(1), 6. https://doi.org/10.1186/s40035-025-00465-w

Kinon, B. J., Leucht, S., Tamminga, C., Breier, A., Marcus, R., & Paul, S. M. (2024). *Rationale for Adjunctive Treatment Targeting Multiple Mechanisms in Schizophrenia*.

Klimesch, W. (2012). Alpha-band oscillations, attention, and controlled access to stored information. *Trends in Cognitive Sciences*, *16*(12), 606–617.

Klimesch, W., Sauseng, P., & Hanslmayr, S. (2007). EEG alpha oscillations: The inhibition–timing hypothesis. *Brain Research Reviews*, *53*(1), 63–88. https://doi.org/10.1016/j.brainresrev.2006.06.003

Knopman, D. S., Amieva, H., Petersen, R. C., Chételat, G., Holtzman, D. M., Hyman, B. T., Nixon, R. A., & Jones, D. T. (2021). Alzheimer disease. *Nature Reviews Disease Primers*, *7*(1), 33. https://doi.org/10.1038/s41572-021-00269-y

Koen, J. D., Barrett, F. S., Harlow, I. M., & Yonelinas, A. P. (2017). The ROC Toolbox: A toolbox for analyzing receiver-operating characteristics derived from confidence ratings. *Behavior Research Methods*, *49*(4), 1399–1406. https://doi.org/10.3758/s13428-016-0796-z

Korczyn, A. D., & Grinberg, L. T. (2024a). Is Alzheimer disease a disease? *Nature Reviews Neurology*, *20*(4), 245–251. https://doi.org/10.1038/s41582-024-00940-4

Korczyn, A. D., & Grinberg, L. T. (2024b). Is Alzheimer disease a disease? *Nature Reviews Neurology*, *20*(4), 245–251. https://doi.org/10.1038/s41582-024-00940-4

Krause, M. R., Vieira, P. G., Csorba, B. A., Pilly, P. K., & Pack, C. C. (2019). Transcranial alternating current stimulation entrains single-neuron activity in the primate brain. Proceedings of the National Academy of Sciences, 116(12), 5747–5755. https://doi.org/10.1073/pnas.1815958116

Kurniawan, J. F., Tjhia, B., Wu, V. M., Shin, A., Sit, N. L. J., Pham, T., Nguyen, A., Li, C., Kumar, R., Aguilar-Rivera, M., Lerman, I., Kunkel, D. C., & Coleman, T. P. (2021). An Adhesive-Integrated Stretchable Silver-Silver Chloride Electrode Array for Unobtrusive Monitoring of Gastric Neuromuscular Activity. *Advanced Materials Technologies*, *6*(5). https://doi.org/10.1002/admt.202001229

Lakatos, P., Gross, J., & Thut, G. (2019). A New Unifying Account of the Roles of Neuronal Entrainment. *Current Biology*, *29*(18), R890–R905. https://doi.org/10.1016/j.cub.2019.07.075

Lanctôt, K. L., Hahn-Pedersen, J. H., Eichinger, C. S., Freeman, C., Clark, A., Tarazona, L. R. S., & Cummings, J. (2024). Burden of Illness in People with Alzheimer's Disease: A Systematic Review of Epidemiology, Comorbidities and Mortality. *The Journal of Prevention of Alzheimer's Disease*, *11*(1), 97–107. https://doi.org/10.14283/jpad.2023.61

Lang, S., Gan, L. S., Alrazi, T., & Monchi, O. (2019). Theta band high definition transcranial alternating current stimulation, but not transcranial direct current stimulation, improves associative memory performance. Scientific Reports, 9(1). https://doi.org/10.1038/s41598-019-44680-8

Lee, S.-C., Chien, T.-H., Chu, C.-P., Lee, Y., & Chiu, E.-C. (2023). Practice effect and test–retest reliability of the Wechsler Memory Scale-Fourth Edition in people with dementia. *BMC Geriatrics*, *23*(1), 209. https://doi.org/10.1186/s12877-023-03913-2

Lee, T. L., Lee, H., & Kang, N. (2023). A meta-analysis showing improved cognitive performance in healthy young adults with transcranial alternating current stimulation. *Npj Science of Learning*, *8*(1), 1. https://doi.org/10.1038/s41539-022-00152-9

Lejko, N., Larabi, D. I., Herrmann, C. S., Aleman, A., & Ćurčić-Blake, B. (2020). Power and functional connectivity of alpha oscillations in mild cognitive impairment: A systematic review and meta-analysis: Neuroimaging / Optimal neuroimaging measures for early detection. *Alzheimer's & Dementia*, *16*(S5), e040792. https://doi.org/10.1002/alz.040792

Leng, F., Hinz, R., Gentleman, S., Hampshire, A., Dani, M., Brooks, D. J., & Edison, P. (2023). Neuroinflammation is independently associated with brain network dysfunction in Alzheimer's disease. *Molecular Psychiatry*, *28*(3), 1303–1311. https://doi.org/10.1038/s41380-022-01878-z

Li, D., Liu, Y., Zeng, X., Xiong, Z., Yao, Y., Liang, D., Qu, H., Xiang, H., Yang, Z., Nie, L., Wu, P.-Y., & Wang, R. (2020). Quantitative Study of the Changes in Cerebral Blood Flow and Iron Deposition During Progression of Alzheimer's Disease. *Journal of Alzheimer's Disease*, *78*(1), 439–452. https://doi.org/10.3233/JAD-200843

Lisman, J., Grace, A. A., & Duzel, E. (2011). A neoHebbian framework for episodic memory; role of dopamine-dependent late LTP. *Trends in Neurosciences*, *34*(10), 536–547.

Liu, A., Vöröslakos, M., Kronberg, G., Henin, S., Krause, M. R., Huang, Y., Opitz, A., Mehta, A., Pack, C. C., Krekelberg, B., Berényi, A., Parra, L. C., Melloni, L., Devinsky, O., & Buzsáki, G. (2018a). Immediate neurophysiological effects of transcranial electrical stimulation. *Nature Communications*, *9*(1), 5092. https://doi.org/10.1038/s41467-018-07233-7

Liu, A., Vöröslakos, M., Kronberg, G., Henin, S., Krause, M. R., Huang, Y., Opitz, A., Mehta, A., Pack, C. C., Krekelberg, B., Berényi, A., Parra, L. C., Melloni, L., Devinsky, O., & Buzsáki, G. (2018b). Immediate neurophysiological effects of transcranial electrical stimulation. *Nature Communications*, *9*(1), 5092. https://doi.org/10.1038/s41467-018-07233-7

Liu, G., Xue, B., Guan, Y., & Luo, X. (2024). Effects of repetitive transcranial magnetic stimulation combined with cognitive training on cognitive function in patients with Alzheimer's disease: A systematic review and meta-analysis. *Frontiers in Aging Neuroscience*, *15*, 1254523. https://doi.org/10.3389/fnagi.2023.1254523

Long, J. M., & Holtzman, D. M. (2019). Alzheimer Disease: An Update on Pathobiology and Treatment Strategies. *Cell*, *179*(2), 312–339. https://doi.org/10.1016/j.cell.2019.09.001

Lopez-Lee, C., Torres, E. R. S., Carling, G., & Gan, L. (2024). Mechanisms of sex differences in Alzheimer's disease. *Neuron*, *112*(8), 1208–1221. https://doi.org/10.1016/j.neuron.2024.01.024

Lozano, A. M., Lipsman, N., Bergman, H., Brown, P., Chabardes, S., Chang, J. W., Matthews, K., McIntyre, C. C., Schlaepfer, T. E., Schulder, M., Temel, Y., Volkmann, J., & Krauss, J. K. (2019). Deep brain stimulation: Current challenges and future directions. *Nature Reviews Neurology*, *15*(3), 148–160. https://doi.org/10.1038/s41582-018-0128-2

Luo, H., Ye, X., Cai, H.-T., Wang, M., Wang, Y., Liu, Q., Xu, Y., Mao, Z., Cai, Y., Hong, J., Zhang, C., Wei, P., Lu, Y., Liu, Q., Xu, J., & Yuan, T.-F. (2025). Frequency-specific and state-dependent neural responses to brain stimulation. *Molecular Psychiatry*. https://doi.org/10.1038/s41380-025-02892-7

Ma, D. S., Correll, J., & Wittenbrink, B. (2015). The Chicago face database: A free stimulus set of faces and norming data. *Behavior Research Methods*, *47*(4), 1122–1135. https://doi.org/10.3758/s13428-014-0532-5

Ma, D. S., Kantner, J., & Wittenbrink, B. (2021). Chicago Face Database: Multiracial expansion. *Behavior Research Methods*, *53*(3), 1289–1300. https://doi.org/10.3758/s13428-020-01482-5

Machado, S., Cunha, M., Minc, D., Portella, C. E., Velasques, B., Basile, L. F., Cagy, M., Piedade, R., & Ribeiro, P. (2009). Alzheimer's disease and implicit memory. *Arquivos de Neuro-Psiquiatria*, *67*(2a), 334–342. https://doi.org/10.1590/S0004-282X2009000200034

Majdi, A., Deng, Z., Sadigh-Eteghad, S., De Vloo, P., Nuttin, B., & Mc Laughlin, M. (2023). Deep brain stimulation for the treatment of Alzheimer's disease: A systematic review and meta-analysis. *Frontiers in Neuroscience*, *17*, 1154180. https://doi.org/10.3389/fnins.2023.1154180

Majdi, A., van Boekholdt, L., Sadigh-Eteghad, S., & Mc Laughlin, M. (2022). A systematic review and meta-analysis of transcranial direct-current stimulation effects on cognitive function in patients with Alzheimer's disease. *Molecular Psychiatry*, *27*(4), 2000–2009. https://doi.org/10.1038/s41380-022-01444-7

Malhotra, P. A. (2019). Impairments of attention in Alzheimer's disease. *Current Opinion in Psychology*, *29*, 41–48.

Mallach, A., Weinert, M., Arthur, J., Gveric, D., Tierney, T. S., & Alavian, K. N. (2019). *Post mortem* examination of Parkinson's disease brains suggests decline in mitochondrial biomass, reversed by deep brain stimulation of subthalamic nucleus. *The FASEB Journal*, *33*(6), 6957–6961. https://doi.org/10.1096/fj.201802628R

Mankin, E. A., & Fried, I. (2020). Modulation of Human Memory by Deep Brain Stimulation of the Entorhinal-Hippocampal Circuitry. *Neuron*, *106*(2), 218–235. https://doi.org/10.1016/j.neuron.2020.02.024

Mansur, A., Rabiner, E. A., Tsukada, H., Comley, R. A., Lewis, Y., Huiban, M., Passchier, J., & Gunn, R. N. (2021). Test–retest variability and reference region-based quantification of^{18} F-BCPP-EF for imaging mitochondrial complex I in the human brain. *Journal of Cerebral Blood Flow & Metabolism*, *41*(4), 771–779. https://doi.org/10.1177/0271678X20928149

Mar-Barrutia, L., Real, E., Segalás, C., Bertolín, S., Menchón, J. M., & Alonso, P. (2021). Deep brain stimulation for obsessive-compulsive disorder: A systematic review of worldwide experience after 20 years. *World Journal of Psychiatry*, *11*(9), 659–680. https://doi.org/10.5498/wjp.v11.i9.659

Marucci, G., Buccioni, M., Ben, D. D., Lambertucci, C., Volpini, R., & Amenta, F. (2021). Efficacy of acetylcholinesterase inhibitors in Alzheimer's disease. *Neuropharmacology*, *190*, 108352. https://doi.org/10.1016/j.neuropharm.2020.108352

Matsumoto, H., & Ugawa, Y. (2017). Adverse events of tDCS and tACS: A review. *Clinical Neurophysiology Practice*, *2*, 19–25. https://doi.org/10.1016/j.cnp.2016.12.003

Mayberg, H. S., Lozano, A. M., Voon, V., McNeely, H. E., Seminowicz, D., Hamani, C., Schwalb, J. M., & Kennedy, S. H. (2005). Deep Brain Stimulation for Treatment-Resistant Depression. *Neuron*, *45*(5), 651–660. https://doi.org/10.1016/j.neuron.2005.02.014

McAdams, E. T., Jossinet, J., Lackermeier, A., & Risacher, F. (1996). Factors affecting electrode-gel-skin interface impedance in electrical impedance tomography. *Medical and Biological Engineering and Computing*, *34*(6), 397–408. https://doi.org/10.1007/BF02523842

McKhann, G. M., Knopman, D. S., Chertkow, H., Hyman, B. T., Jack, C. R., Kawas, C. H., Klunk, W. E., Koroshetz, W. J., Manly, J. J., Mayeux, R., Mohs, R. C., Morris, J. C., Rossor, M. N., Scheltens, P., Carrillo, M. C., Thies, B., Weintraub, S., & Phelps, C. H. (2011). The diagnosis of dementia due to Alzheimer's disease: Recommendations from the National Institute on Aging-Alzheimer's Association workgroups on diagnostic guidelines for Alzheimer's disease. *Alzheimer's & Dementia: The Journal of the Alzheimer's Association*, *7*(3), 263–269. https://doi.org/10.1016/j.jalz.2011.03.005

Medaglia, J. D., Lynall, M.-E., & Bassett, D. S. (2015). Cognitive Network Neuroscience. *Journal of Cognitive Neuroscience*, *27*(8), 1471–1491. https://doi.org/10.1162/jocn_a_00810

Meigen, T., & Bach, M. (2000). *On the statistical significance of electrophysiological steady-state responses*.

Menardi, A., Rossi, S., Koch, G., Hampel, H., Vergallo, A., Nitsche, M. A., Stern, Y., Borroni, B., Cappa, S. F., Cotelli, M., Ruffini, G., El-Fakhri, G., Rossini, P. M., Dickerson, B., Antal, A., Babiloni, C., Lefaucheur, J.-P., Dubois, B., Deco, G., … Santarnecchi, E. (2022). Toward noninvasive brain stimulation 2.0 in Alzheimer's disease. *Ageing Research Reviews*, *75*, 101555. https://doi.org/10.1016/j.arr.2021.101555

Merrill, D. R., Bikson, M., & Jefferys, J. G. (2005). Electrical stimulation of excitable tissue: Design of efficacious and safe protocols. *Journal of Neuroscience Methods*, *141*(2), 171–198.

Mondadori, C. R., Buchmann, A., Mustovic, H., Schmidt, C. F., Boesiger, P., Nitsch, R. M., Hock, C., Streffer, J., & Henke, K. (2006). Enhanced brain activity may precede the diagnosis of Alzheimer's disease by 30 years. *Brain*, *129*(11), 2908–2922.

Murray, N. W. G., Graham, P. L., Sowman, P. F., & Savage, G. (2023). Theta tACS impairs episodic memory more than tDCS. Scientific Reports, 13(1). https://doi.org/10.1038/s41598-022-27190-y

Nabulsi, N. B., Finnema, S. J., Eid, T., Detyniecki, K., Lin, S., Chen, M.-K., Dhaher, R., Matuskey, D., Baum, E., Holden, D., Spencer, D. D., Mercier, J., Hannestad, J., Huang, Y., & Carson, R. E. (2016). Imaging synaptic density in the living human brain. *Science Translational Medicine*, *8*(348). https://doi.org/10.1126/scitranslmed.aaf6667

Nair, D. R., Laxer, K. D., Weber, P. B., Murro, A. M., Park, Y. D., Barkley, G. L., Smith, B. J., Gwinn, R. P., Doherty, M. J., Noe, K. H., Zimmerman, R. S., Bergey, G. K., Anderson, W. S., Heck, C., Liu, C. Y., Lee, R. W., Sadler, T., Duckrow, R. B., Hirsch, L. J., … on behalf of the RNS System LTT Study. (2020). Nine-year prospective efficacy and safety of brain-responsive neurostimulation for focal epilepsy. *Neurology*, *95*(9). https://doi.org/10.1212/WNL.0000000000010154

Neuling, T., Rach, S., & Herrmann, C. S. (2013). Orchestrating neuronal networks: Sustained after-effects of transcranial alternating current stimulation depend upon brain states. *Frontiers in Human Neuroscience*, *7*, 161. https://doi.org/10.3389/fnhum.2013.00161

Nierenberg, A. A., Agustini, B., Köhler-Forsberg, O., Cusin, C., Katz, D., Sylvia, L. G., Peters, A., & Berk, M. (2023). Diagnosis and Treatment of Bipolar Disorder: A Review. *JAMA*, *330*(14), 1370. https://doi.org/10.1001/jama.2023.18588

Nissim, N. R., McAfee, D. C., Edwards, S., Prato, A., Lin, J. X., Lu, Z., Coslett, H. B., & Hamilton, R. H. (2023). Efficacy of Transcranial Alternating Current Stimulation in the Enhancement of Working Memory Performance in Healthy Adults: A Systematic Meta-Analysis. Neuromodulation: Technology at the Neural Interface, 26(4), 728–737. https://doi.org/10.1016/j.neurom.2022.12.014

Nitsche, M. A., & Paulus, W. (2000). Excitability changes induced in the human motor cortex by weak transcranial direct current stimulation. *The Journal of Physiology*, *527*(3), 633–639. https://doi.org/10.1111/j.1469-7793.2000.t01-1-00633.x

Norcia, A. M., Appelbaum, L. G., Ales, J. M., Cottereau, B. R., & Rossion, B. (2015). The steady-state visual evoked potential in vision research: A review. *Journal of Vision*, *15*(6), 4. https://doi.org/10.1167/15.6.4

Noury, N., Hipp, J. F., & Siegel, M. (2016). Physiological processes non-linearly affect electrophysiological recordings during transcranial electric stimulation. *NeuroImage*, *140*, 99–109. https://doi.org/10.1016/j.neuroimage.2016.03.065

Palop, J. J., & Mucke, L. (2016). Network abnormalities and interneuron dysfunction in Alzheimer disease. *Nature Reviews Neuroscience*, *17*(12), 777–792. https://doi.org/10.1038/nrn.2016.141

Peelle, J. E., Powers, J., Cook, P. A., Smith, E. E., & Grossman, M. (2014). Frontotemporal neural systems supporting semantic processing in Alzheimer's disease. *Cognitive, Affective, & Behavioral Neuroscience*, *14*(1), 37–48. https://doi.org/10.3758/s13415-013-0239-6

Perlmutter, J. S., & Mink, J. W. (2006). DEEP BRAIN STIMULATION. *Annual Review of Neuroscience*, *29*(1), 229–257. https://doi.org/10.1146/annurev.neuro.29.051605.112824

Picton, B., Wong, J., Lopez, A. M., Solomon, S. S., Andalib, S., Brown, N. J., Dutta, R. R., Paff, M. R., Hsu, F. P., & Oh, M. Y. (2023). Deep Brain Stimulation as an Emerging Therapy for Cognitive Decline in

Alzheimer Disease: Systematic Review of Evidence and Current Targets. *World Neurosurgery*. https://doi.org/10.1016/j.wneu.2023.12.083

Podda, M. V., Cocco, S., Mastrodonato, A., Fusco, S., Leone, L., Barbati, S. A., Colussi, C., Ripoli, C., & Grassi, C. (2016). Anodal transcranial direct current stimulation boosts synaptic plasticity and memory in mice via epigenetic regulation of Bdnf expression. Scientific Reports, 6(1). https://doi.org/10.1038/srep22180

Polanía, R., Nitsche, M. A., Korman, C., Batsikadze, G., & Paulus, W. (2012). The Importance of Timing in Segregated Theta Phase-Coupling for Cognitive Performance. *Current Biology*, *22*(14), 1314–1318. https://doi.org/10.1016/j.cub.2012.05.021

Rajendran, K., & Krishnan, U. M. (2024). Mechanistic insights and emerging therapeutic stratagems for Alzheimer's disease. *Ageing Research Reviews*, *97*, 102309. https://doi.org/10.1016/j.arr.2024.102309

Reddy, S., Kabotyanski, K. E., Hirani, S., Liu, T., Naqvi, Z., Giridharan, N., Hasen, M., Provenza, N. R., Banks, G. P., Mathew, S. J., Goodman, W. K., & Sheth, S. A. (2024). Efficacy of Deep Brain Stimulation for Treatment-Resistant Depression: Systematic Review and Meta-Analysis. *Biological Psychiatry: Cognitive Neuroscience and Neuroimaging*, *9*(12), 1239–1248. https://doi.org/10.1016/j.bpsc.2024.08.013

Reuter, M., Rosas, H. D., & Fischl, B. (2010). Highly accurate inverse consistent registration: A robust approach. *Neuroimage*, *53*(4), 1181–1196.

Reuter, M., Schmansky, N. J., Rosas, H. D., & Fischl, B. (2012). Within-subject template estimation for unbiased longitudinal image analysis. *Neuroimage*, *61*(4), 1402–1418.

Riddle, J., & Frohlich, F. (2021). Targeting neural oscillations with transcranial alternating current stimulation. *Brain Research*, *1765*, 147491. https://doi.org/10.1016/j.brainres.2021.147491

Roemer-Cassiano, S. N., Wagner, F., Evangelista, L., Rauchmann, B.-S., Dehsarvi, A., Steward, A., Dewenter, A., Biel, D., Zhu, Z., Pescoller, J., Gross, M., Perneczky, R., Malpetti, M., Ewers, M., Schöll, M., Dichgans, M., Höglinger, G. U., Brendel, M., Jäkel, S., & Franzmeier, N. (2025). Amyloid-associated hyperconnectivity drives tau spread across connected brain regions in Alzheimer's disease. *Science Translational Medicine*, *17*(782), eadp2564. https://doi.org/10.1126/scitranslmed.adp2564

Rostami, R., Kazemi, R., Mozaffarinejad, F., Nasiri, Z., Rostami, M., L.Hadipour, A., & Sadeghihassanabadi, F. (2021). 6 Hz transcranial alternating current stimulation of mPFC improves sustained attention and modulates alpha phase synchronization and power in dorsal attention network. Cognitive Neuroscience, 12(1), 1–13. https://doi.org/10.1080/17588928.2020.1817881

Saelens, J., Gramser, A., Watzal, V., Zarate, C. A., Lanzenberger, R., & Kraus, C. (2024). Relative effectiveness of antidepressant treatments in treatment-resistant depression: A systematic review and network meta-analysis of randomized controlled trials. *Neuropsychopharmacology*. https://doi.org/10.1038/s41386-024-02044-5

Sarazin, M., Chauviré, V., Gerardin, E., Colliot, O., Kinkingnéhun, S., de Souza, L. C., Hugonot-Diener, L., Garnero, L., Lehéricy, S., Chupin, M., & Dubois, B. (2010). The amnestic syndrome of hippocampal type in Alzheimer's disease: An MRI study. *Journal of Alzheimer's Disease: JAD*, *22*(1), 285–294. https://doi.org/10.3233/JAD-2010-091150

Scheltens, P., De Strooper, B., Kivipelto, M., Holstege, H., Chételat, G., Teunissen, C. E., Cummings, J., & Van Der Flier, W. M. (2021). Alzheimer's disease. *The Lancet*, *397*(10284), 1577–1590. https://doi.org/10.1016/S0140-6736(20)32205-4

Segal, A., Parkes, L., Aquino, K., Kia, S. M., Wolfers, T., Franke, B., Hoogman, M., Beckmann, C. F., Westlye, L. T., Andreassen, O. A., Zalesky, A., Harrison, B. J., Davey, C. G., Soriano-Mas, C., Cardoner, N., Tiego, J., Yücel, M., Braganza, L., Suo, C., … Fornito, A. (2023). Regional, circuit and network heterogeneity of brain abnormalities in psychiatric disorders. *Nature Neuroscience*, *26*(9), 1613–1629. https://doi.org/10.1038/s41593-023-01404-6

Ségonne, F., Dale, A. M., Busa, E., Glessner, M., Salat, D., Hahn, H. K., & Fischl, B. (2004). A hybrid approach to the skull stripping problem in MRI. *Neuroimage*, *22*(3), 1060–1075.

Self, W. K., & Holtzman, D. M. (2023). Emerging diagnostics and therapeutics for Alzheimer disease. *Nature Medicine*, *29*(9), 2187–2199. https://doi.org/10.1038/s41591-023-02505-2

Sha, Z., Wager, T. D., Mechelli, A., & He, Y. (2019). Common Dysfunction of Large-Scale Neurocognitive Networks Across Psychiatric Disorders. *Biological Psychiatry*, *85*(5), 379–388. https://doi.org/10.1016/j.biopsych.2018.11.011

Shtoots, L., Nadler, A., Partouche, R., Sharir, D., Rothstein, A., Shati, L., & Levy, D. A. (2024). Frontal midline theta transcranial alternating current stimulation enhances early consolidation of episodic memory. *Npj Science of Learning*, *9*(1), 8. https://doi.org/10.1038/s41539-024-00222-0

Siskind, D., Orr, S., Sinha, S., Yu, O., Brijball, B., Warren, N., MacCabe, J. H., Smart, S. E., & Kisely, S. (2022). Rates of treatment-resistant schizophrenia from first-episode cohorts: Systematic review and meta-analysis. *The British Journal of Psychiatry*, *220*(3), 115–120. https://doi.org/10.1192/bjp.2021.61

Skivington, K., Matthews, L., Simpson, S. A., Craig, P., Baird, J., Blazeby, J. M., Boyd, K. A., Craig, N., French, D. P., McIntosh, E., Petticrew, M., Rycroft-Malone, J., White, M., & Moore, L. (2021). Framework for the development and evaluation of complex interventions: Gap analysis, workshop and consultation-informed update. Health Technology Assessment, 25(57), 1–132. https://doi.org/10.3310/hta25570

Sperling, R., Chua, E., Cocchiarella, A., Rand-Giovannetti, E., Poldrack, R., Schacter, D. L., & Albert, M. (2003). Putting names to faces: Successful encoding of associative memories activates the anterior hippocampal formation. *NeuroImage*, *20*(2), 1400–1410. https://doi.org/10.1016/S1053-8119(03)00391-4

Sprugnoli, G., Munsch, F., Cappon, D., Paciorek, R., Macone, J., Connor, A., El Fakhri, G., Salvador, R., Ruffini, G., Donohoe, K., Shafi, M. M., Press, D., Alsop, D. C., Pascual Leone, A., & Santarnecchi, E. (2021). Impact of multisession 40Hz tACS on hippocampal perfusion in patients with Alzheimer's disease. *Alzheimer's Research & Therapy*, *13*(1), 203. https://doi.org/10.1186/s13195-021-00922-4

Stagg, C. J., & Nitsche, M. A. (2011). Physiological Basis of Transcranial Direct Current Stimulation. The Neuroscientist, 17(1), 37–53. https://doi.org/10.1177/1073858410386614

Stam, C. J., Van Nifterick, A. M., De Haan, W., & Gouw, A. A. (2023). Network Hyperexcitability in Early Alzheimer's Disease: Is Functional Connectivity a Potential Biomarker? *Brain Topography*, *36*(4), 595–612. https://doi.org/10.1007/s10548-023-00968-7

Steinmetz, J. D., Seeher, K. M., Schiess, N., Nichols, E., Cao, B., Servili, C., Cavallera, V., Cousin, E., Hagins, H., Moberg, M. E., Mehlman, M. L., Abate, Y. H., Abbas, J., Abbasi, M. A., Abbasian, M., Abbastabar, H., Abdelmasseh, M., Abdollahi, M., Abdollahi, M., … Dua, T. (2024). Global, regional, and national burden of disorders affecting the nervous system, 1990–2021: A systematic analysis for the Global Burden of Disease Study 2021. *The Lancet Neurology*, *23*(4), 344–381. https://doi.org/10.1016/S1474-4422(24)00038-3

Taddei, R. N., & E. Duff, K. (2025). Synapse vulnerability and resilience underlying Alzheimer's disease. *eBioMedicine*, *112*, 105557. https://doi.org/10.1016/j.ebiom.2025.105557

Tang, Y., Xing, Y., Sun, L., Wang, Z., Wang, C., Yang, K., Zhu, W., Shi, X., Xie, B., Yin, Y., Mi, Y., Wei, T., Tong, R., Qiao, Y., Yan, S., Wei, P., Yang, Y., Shan, Y., Zhang, X., … Zhao, G. (2024). TRanscranial AlterNating current stimulation FOR patients with mild Alzheimer's Disease (TRANSFORM-AD): A randomized controlled clinical trial. *Alzheimer's Research & Therapy*, *16*(1), 203. https://doi.org/10.1186/s13195-024-01570-0

Targa Dias Anastacio, H., Matosin, N., & Ooi, L. (2022). Neuronal hyperexcitability in Alzheimer's disease: What are the drivers behind this aberrant phenotype? *Translational Psychiatry*, *12*(1), 257. https://doi.org/10.1038/s41398-022-02024-7

Terada, T., Therriault, J., Kang, M. S., Savard, M., Pascoal, T. A., Lussier, F., Tissot, C., Wang, Y.-T., Benedet, A., Poltronetti, N. M., Ottoy, J., Arias, J. F., Bezgin, G., Matsudaira, T., Bunai, T., Obi, T., Tsukada, H., Ouchi, Y., & Rosa-Neto, P. (2022). Mitochondrial complex I abnormalities underlie neurodegeneration and cognitive decline in Alzheimer's disease. *European Journal of Neurology*, *29*(5), 1324–1334. https://doi.org/10.1111/ene.15246

Therriault, J., Schindler, S. E., Salvadó, G., Pascoal, T. A., Benedet, A. L., Ashton, N. J., Karikari, T. K., Apostolova, L., Murray, M. E., Verberk, I., Vogel, J. W., La Joie, R., Gauthier, S., Teunissen, C., Rabinovici, G. D., Zetterberg, H., Bateman, R. J., Scheltens, P., Blennow, K., … Rosa-Neto, P. (2024). Biomarker-based staging of Alzheimer disease: Rationale and clinical applications. *Nature Reviews Neurology*, *20*(4), 232–244. https://doi.org/10.1038/s41582-024-00942-2

Tzioras, M., McGeachan, R. I., Durrant, C. S., & Spires-Jones, T. L. (2023). Synaptic degeneration in Alzheimer disease. *Nature Reviews Neurology*, *19*(1), 19–38. https://doi.org/10.1038/s41582-022-00749-z

Tziortzi, A., Searle, G., Tsoumpas, C., Long, C., Shotbolt, P., Rabiner, E., Jenkinson, M., & Gunn, R. N. (2011). MR-DTI and PET multimodal imaging of dopamine release within subdivisions of basal ganglia. *Journal of Physics: Conference Series*, *317*(1), 012005. https://iopscience.iop.org/article/10.1088/1742-6596/317/1/012005/meta

Van Dyck, C. H., Swanson, C. J., Aisen, P., Bateman, R. J., Chen, C., Gee, M., Kanekiyo, M., Li, D., Reyderman, L., Cohen, S., Froelich, L., Katayama, S., Sabbagh, M., Vellas, B., Watson, D., Dhadda, S., Irizarry, M., Kramer, L. D., & Iwatsubo, T. (2023). Lecanemab in Early Alzheimer's Disease. *New England Journal of Medicine*, *388*(1), 9–21. https://doi.org/10.1056/NEJMoa2212948

van Heugten, C. M., Ponds, R. W. H. M., & Kessels, R. P. C. (2016). Brain training: Hype or hope? *Neuropsychological Rehabilitation*, *26*(5–6), 639–644. https://doi.org/10.1080/09602011.2016.1186101

van Heuven, W. J. B., Mandera, P., Keuleers, E., & Brysbaert, M. (2014). Subtlex-UK: A New and Improved Word Frequency Database for British English. *Quarterly Journal of Experimental Psychology*, *67*(6), 1176–1190. https://doi.org/10.1080/17470218.2013.850521

van Nifterick, A. M., Mulder, D., Duineveld, D. J., Diachenko, M., Scheltens, P., Stam, C. J., van Kesteren, R. E., Linkenkaer-Hansen, K., Hillebrand, A., & Gouw, A. A. (2023). Resting-state oscillations reveal disturbed excitation–inhibition ratio in Alzheimer's disease patients. *Scientific Reports*, *13*(1), Article 1. https://doi.org/10.1038/s41598-023-33973-8

Vanes, L. D., & Dolan, R. J. (2021). Transdiagnostic neuroimaging markers of psychiatric risk: A narrative review. *NeuroImage. Clinical*, *30*, 102634. https://doi.org/10.1016/j.nicl.2021.102634

Vanneste, S., Mohan, A., Yoo, H. B., Huang, Y., Luckey, A. M., McLeod, S. L., Tabet, M. N., Souza, R. R., McIntyre, C. K., Chapman, S., Robertson, I. H., & To, W. T. (2020). The peripheral effect of direct current stimulation on brain circuits involving memory. Science Advances, 6(45). https://doi.org/10.1126/sciadv.aax9538

Vialatte, F.-B., Maurice, M., Dauwels, J., & Cichocki, A. (2010). Steady-state visually evoked potentials: Focus on essential paradigms and future perspectives. *Progress in Neurobiology*, *90*(4), 418–438. https://doi.org/10.1016/j.pneurobio.2009.11.005

Vieira, P. G., Krause, M. R., & Pack, C. C. (2024). Temporal interference stimulation disrupts spike timing in the primate brain. *Nature Communications*, *15*(1), 4558. https://doi.org/10.1038/s41467-024-48962-2

Violante, I. R., Acerbo, E., Alania, K., Cassarà, A. M., Neufeld, E., Carron, R., Williamson, A., Kurtin, D. L., Rhodes, E., Hampshire, A., Kuster, N., Boyden, E. S., Pascual-Leone, A., & Grossman, N. (2023). Non-invasive temporal interference electrical stimulation of the human hippocampus. *Nature Neuroscience*, *26*(11), 1994–2004. https://doi.org/10.1038/s41593-023-01456-8

Vogel, J. W., Corriveau-Lecavalier, N., Franzmeier, N., Pereira, J. B., Brown, J. A., Maass, A., Botha, H., Seeley, W. W., Bassett, D. S., Jones, D. T., & Ewers, M. (2023). Connectome-based modelling of neurodegenerative diseases: Towards precision medicine and mechanistic insight. *Nature Reviews Neuroscience*, *24*(10), 620–639. https://doi.org/10.1038/s41583-023-00731-8

Vogeti, S., Boetzel, C., & Herrmann, C. S. (2022). Entrainment and Spike-Timing Dependent Plasticity – A Review of Proposed Mechanisms of Transcranial Alternating Current Stimulation. *Frontiers in Systems Neuroscience*, *16*, 827353. https://doi.org/10.3389/fnsys.2022.827353

von Conta, J., Kasten, F. H., Ćurčić-Blake, B., Schellhorn, K., & Herrmann, C. S. (2022). Characterizing low frequency artifacts during transcranial temporal interference stimulation (tTIS). *Neuroimage: Reports*, *2*(3), 100113. https://doi.org/10.1016/j.ynirp.2022.100113

Von Conta, J., Kasten, F. H., Schellhorn, K., Ćurčić-Blake, B., Aleman, A., & Herrmann, C. S. (2022). Benchmarking the effects of transcranial temporal interference stimulation (tTIS) in humans. *Cortex, 154*, 299–310. https://doi.org/10.1016/j.cortex.2022.05.017

Vöröslakos, M., Takeuchi, Y., Brinyiczki, K., Zombori, T., Oliva, A., Fernández-Ruiz, A., Kozák, G., Kincses, Z. T., Iványi, B., Buzsáki, G., & Berényi, A. (2018). Direct effects of transcranial electric stimulation on brain circuits in rats and humans. *Nature Communications*, *9*(1), 483. https://doi.org/10.1038/s41467-018-02928-3

Vossel, K. A., Beagle, A. J., Rabinovici, G. D., Shu, H., Lee, S. E., Naasan, G., Hegde, M., Cornes, S. B., Henry, M. L., Nelson, A. B., Seeley, W. W., Geschwind, M. D., Gorno-Tempini, M. L., Shih, T., Kirsch, H. E., Garcia, P. A., Miller, B. L., & Mucke, L. (2013). Seizures and Epileptiform Activity in the Early Stages of Alzheimer Disease. *JAMA Neurology*, *70*(9), 1158–1166. https://doi.org/10.1001/jamaneurol.2013.136

Vossel, K. A., Ranasinghe, K. G., Beagle, A. J., Mizuiri, D., Honma, S. M., Dowling, A. F., Darwish, S. M., Van Berlo, V., Barnes, D. E., Mantle, M., Karydas, A. M., Coppola, G., Roberson, E. D., Miller, B. L., Garcia,

P. A., Kirsch, H. E., Mucke, L., & Nagarajan, S. S. (2016). Incidence and impact of subclinical epileptiform activity in Alzheimer's disease. *Annals of Neurology*, *80*(6), 858–870. https://doi.org/10.1002/ana.24794

Vossen, A., Gross, J., & Thut, G. (2015). Alpha Power Increase After Transcranial Alternating Current Stimulation at Alpha Frequency (α-tACS) Reflects Plastic Changes Rather Than Entrainment. *Brain Stimulation*, *8*(3), 499–508. https://doi.org/10.1016/j.brs.2014.12.004

Vosskuhl, J., Mutanen, T. P., Neuling, T., Ilmoniemi, R. J., & Herrmann, C. S. (2020). Signal-Space Projection Suppresses the tACS Artifact in EEG Recordings. *Frontiers in Human Neuroscience*, *14*, 536070. https://doi.org/10.3389/fnhum.2020.536070

Wang, D., Marcantoni, E., Clouter, A., Shapiro, K. L., & Hanslmayr, S. (2024). Rhythmic sensory stimulation as a noninvasive tool to study plasticity mechanisms in human episodic memory. *Current Opinion in Behavioral Sciences*, *58*, 101412. https://doi.org/10.1016/j.cobeha.2024.101412

Wang, D., Parish, G., Shapiro, K. L., & Hanslmayr, S. (2023). Interaction between Theta Phase and Spike Timing-Dependent Plasticity Simulates Theta-Induced Memory Effects. *Eneuro*, *10*(3), ENEURO.0333-22.2023. https://doi.org/10.1523/ENEURO.0333-22.2023

Wang, X., Wang, D., Li, X., Wang, W., Gao, P., Lou, B., Pfeuffer, J., Zhang, X., Zhu, J., Li, C., & Chen, M. (2022). A diagnostic index based on pseudo-continuous arterial spin labeling and T1-mapping improves efficacy in discriminating Alzheimer's disease from normal cognition. *Frontiers in Neuroscience*, *16*, 974651. https://doi.org/10.3389/fnins.2022.974651

Wang, S., Xu, H., Liu, G., & Chen, L. (2025). Non-pharmacological treatment of Alzheimer's disease: An update. Frontiers in Aging Neuroscience, 17, 1527242. https://doi.org/10.3389/fnagi.2025.1527242

Warrington, E. K. (1997). The Graded Naming Test: A Restandardisation. *Neuropsychological Rehabilitation*, *7*(2), 143–146. https://doi.org/10.1080/713755528

Warrington, E. K., & James, M. (1991). A new test of object decision: 2D silhouettes featuring a minimal view. *Cortex*, *27*(3), 377–383.

Wischnewski, M., Alekseichuk, I., & Opitz, A. (2023). Neurocognitive, physiological, and biophysical effects of transcranial alternating current stimulation. *Trends in Cognitive Sciences*, *27*(2), 189–205. https://doi.org/10.1016/j.tics.2022.11.013

Witkowski, M., Garcia-Cossio, E., Chander, B. S., Braun, C., Birbaumer, N., Robinson, S. E., & Soekadar, S. R. (2016). Mapping entrained brain oscillations during transcranial alternating current stimulation (tACS). *NeuroImage*, *140*, 89–98. https://doi.org/10.1016/j.neuroimage.2015.10.024

Wu, X., Yan, Y., Hu, P., Wang, L., Wu, Y., Wu, P., Geng, Z., Xiao, G., Zhou, S., Ji, G., Qiu, B., Wei, L., Tian, Y., Liu, H., & Wang, K. (2024). Effects of a periodic intermittent theta burst stimulation in Alzheimer's disease. *General Psychiatry*, *37*(1), e101106. https://doi.org/10.1136/gpsych-2023-101106

Xie, C., Xiang, S., Shen, C., Peng, X., Kang, J., Li, Y., Cheng, W., He, S., Bobou, M., Broulidakis, M. J., Van Noort, B. M., Zhang, Z., Robinson, L., Vaidya, N., Winterer, J., Zhang, Y., King, S., Banaschewski, T., Barker, G. J., … ZIB Consortium. (2023). A shared neural basis underlying psychiatric comorbidity. *Nature Medicine*, *29*(5), 1232–1242. https://doi.org/10.1038/s41591-023-02317-4

Yamada, Y., & Sumiyoshi, T. (2021). Neurobiological Mechanisms of Transcranial Direct Current Stimulation for Psychiatric Disorders; Neurophysiological, Chemical, and Anatomical Considerations. *Frontiers in Human Neuroscience*, *15*. https://doi.org/10.3389/fnhum.2021.631838

Yamamoto, T., & Yamamoto, Y. (1981). Non-linear electrical properties of skin in the low frequency range. *Medical & Biological Engineering & Computing*, *19*(3), 302–310. https://doi.org/10.1007/bf02442549

Yan, J. H., & Dick, M. B. (2006). Practice Effects on Motor Control in Healthy Seniors and Patients with Mild Cognitive Impairment and Alzheimer's Disease. *Aging, Neuropsychology, and Cognition*, *13*(3–4), 385–410. https://doi.org/10.1080/138255890969609

Yang, T., Liu, W., He, J., Gui, C., Meng, L., Xu, L., & Jia, C. (2024). The cognitive effect of non-invasive brain stimulation combined with cognitive training in Alzheimer's disease and mild cognitive impairment: A systematic review and meta-analysis. *Alzheimer's Research & Therapy*, *16*(1), 140. https://doi.org/10.1186/s13195-024-01505-9

Yildiz, A., Siafis, S., Mavridis, D., Vieta, E., & Leucht, S. (2023). Comparative efficacy and tolerability of pharmacological interventions for acute bipolar depression in adults: A systematic review and network meta-analysis. *The Lancet Psychiatry*, *10*(9), 693–705. https://doi.org/10.1016/S2215-0366(23)00199-2

Yonelinas, A. P., & Parks, C. M. (2007). Receiver operating characteristics (ROCs) in recognition memory: A review. *Psychological Bulletin*, *133*(5), 800–832. https://doi.org/10.1037/0033-2909.133.5.800

Yu, J., Feng, Q., Yu, J., Zeng, Y., & Feng, L. (2020). Late-Life Cognitive Trajectories and their Associated Lifestyle Factors. *Journal of Alzheimer's Disease*, *73*(4), 1555–1563. https://doi.org/10.3233/JAD-191058

Zeineh, M. M., Engel, S. A., Thompson, P. M., & Bookheimer, S. Y. (2003). Dynamics of the hippocampus during encoding and retrieval of face-name pairs. *Science (New York, N.Y.)*, *299*(5606), 577–580. https://doi.org/10.1126/science.1077775

Zeng, Y., Liu ,Bingshuo, Zhou ,Lisi, Zeng ,Wenling, Tian ,Xiaona, Jiang ,Jiazhen, & and Dai, D. (2023). Safety issues of Donepezil combined with Memantine in Alzheimer's disease population: Real-world pharmacovigilance. *Expert Opinion on Drug Safety*, *0*(0), 1–11. https://doi.org/10.1080/14740338.2025.2467180

Zhang, S., Cui, X., Yu, S., & Li, X. (2025). Is transcranial alternating current stimulation effective for improving working memory? A three-level meta-analysis. Psychonomic Bulletin & Review, 32(2), 636–651. https://doi.org/10.3758/s13423-024-02595-0

Zhang, J., Zhang, Y., Wang, J., Xia, Y., Zhang, J., & Chen, L. (2024). Recent advances in Alzheimer's disease: Mechanisms, clinical trials and new drug development strategies. *Signal Transduction and Targeted Therapy*, *9*(1), 211. https://doi.org/10.1038/s41392-024-01911-3

Zhang, X.-Y., Zhang, H., Bao, Q.-N., Yin, Z.-H., Li, Y.-Q., Xia, M.-Z., Chen, Z.-H., Zhong, W.-Q., Wu, K.-X., Yao, J., & Liang, F.-R. (2024). Diagnostic value of arterial spin labeling for Alzheimer's disease: A systematic review and meta-analysis. *PLOS ONE*, *19*(11), e0311016. https://doi.org/10.1371/journal.pone.0311016

Zheng, J., Yebra, M., Schjetnan, A. G. P., Patel, K., Katz, C. N., Kyzar, M., Mosher, C. P., Kalia, S. K., Chung, J. M., Reed, C. M., Valiante, T. A., Mamelak, A. N., Kreiman, G., & Rutishauser, U. (2024). Theta phase precession supports memory formation and retrieval of naturalistic experience in humans. *Nature Human Behaviour*, *8*(12), 2423–2436. https://doi.org/10.1038/s41562-024-01983-9

Zheng, Q., & Wang, X. (2025). Alzheimer's disease: Insights into pathology, molecular mechanisms, and therapy. *Protein & Cell*, *16*(2), 83–120. https://doi.org/10.1093/procel/pwae026

Zott, B., Simon, M. M., Hong, W., Unger, F., Chen-Engerer, H.-J., Frosch, M. P., Sakmann, B., Walsh, D. M., & Konnerth, A. (2019). A vicious cycle of amyloid β-dependent neuronal hyperactivation. *Science (New York, N.Y.)*, *365*(6453), 559–565. https://doi.org/10.1126/science.aay0198

Appendix

Table A1 Perceptual sensations and threshold across participants (ID) for conventional transcranial alternating current stimulation (tACS) and TI stimulation – Session 1 behavioural experiment

Perceptual sensations reported by participants and thresholds (i.e. current intensity for which a perceptual sensation was first reported). Participants were exposed to short conventional tACS and TI stimulation during setup, immediately before entering the MRI scanner. TACS stimulation was always administered first, so participants would be aware of the possible sensations elicited by electrical stimulation. Current intensity was ramped in steps of 0.1 mA until a sensation was reported, starting from electrode pair e1-e2 and then moving to e3-e4. Table reproduced with permission from Violante, Alania et al. (2023)

	tACS (5 Hz)				TI (CF = 2 and 2.005 kHz, Δf = 5 Hz)			
	e1 – e2		e3 - e4		e1 – e2		e3 – e4	
ID	Threshold (mA)	Sensation	Threshold (mA)	Sensation	Threshold (mA)	Sensation	Threshold (mA)	Sensation
1	0.3	pinprick	0.3	pinprick	2	pinprick	2	pinprick
2	0.1	stinging	0.1	stinging	1.5	stinging	2	stinging
3	0.3	pinprick	0.3	pinprick	2	tingling	3	tingling
4	0.3	tingling	0.3	tingling	1.5	vibrations	1.5	vibrations
5	0.3	tingling	0.3	tingling	none	none	none	none
6	0.3	pinprick	0.7	tingling	1	numbing	2	tingling
7	0.5	tingling	0.3	tingling	none	none	2.5	pressure
8	0.5	pinprick	0.5	pinprick	none	none	none	none
9	0.3	stinging	0.5	stinging	2	vibrations	2	vibrations
10	0.1	pinprick	0.3	pinprick	none	none	none	none
11	0.1	tingling	0.3	tingling	none	none	none	none
12	0.5	tingling	0.5	tingling	none	none	none	none
13	0.7	phosphenes	0.5	pulling	1	push/pull	1	push/pull
14	0.3	pinprick	0.1	pinprick	1	white noise	1	white noise
15	0.3	pinprick	0.1	heat	2	pinprick	2	pinprick
16	0.1	tingling	0.3	tingling	2	tingling	2.5	tingling
17	0.3	pinching	0.3	pinprick	none	none	2	hair prickle
18	0.3	pinprick	0.3	pinprick	none	none	none	none
19	0.3	pinprick	0.5	pinprick	2	tingling	none	none
20	0.1	pinprick	0.1	pinprick	1.5	pain	1.5	pain
21	0.1	pinprick	0.5	pinprick	1	laughter	1	laughter

tACS – transcranial alternating current stimulation; TI – temporal interference stimulation; CF – carrier frequency; Δf – delta frequency or modulated frequency; e – electrode.

Table A2 Perceptual sensations and threshold across participants (ID) for conventional transcranial alternating current stimulation (tACS) and TI stimulation – Session 2 behavioural experiment

Perceptual sensations reported by participants and thresholds (i.e. current intensity for which a perceptual sensation was first reported). Participants were exposed to short conventional tACS and TI stimulation during setup, immediately before entering the MRI scanner. TACS stimulation was always administered first, so participants would be aware of the possible sensations elicited by electrical stimulation. Current intensity was ramped in steps of 0.1 mA until a sensation was reported, starting from electrode pair e1-e2 and then moving to e3-e4. Table reproduced with permission from Violante, Alania et al. (2023)

	tACS (5 Hz)				TI (CF = 2 and 2.005 kHz, Δf = 5 Hz)			
	e1 – e2		e3 - e4		e1 – e2		e3 – e4	
ID	Threshold (mA)	Sensation	Threshold (mA)	Sensation	Threshold (mA)	Sensation	Threshold (mA)	Sensation
1	0.3	tingling	0.3	tingling	1.5	vibrations	2	pinprick
2	0.1	tingling	0.1	tingling	1.5	stinging	2	stinging
3	0.1	pinprick	0.3	tingling	2	tickling	3	tingling
4	0.3	tingling	0.3	tingling	1.5	tingling	1.5	vibrations
5	0.3	tingling	RM	RM	2	twitching	none	none
6	0.3	tingling	0.3	tingling	2	tingling	2	tingling
7	0.5	tingling	0.3	tingling	none	none	2.5	pressure
8	0.3	pinprick	0.3	pinprick	none	none	none	none
9	0.3	tingling	0.3	tingling	none	none	2	vibrations
10	0.1	pinprick	0.5	pinprick	2	none	none	none
11	0.1	tingling	0.3	tingling	none	none	none	none
12	0.3	tingling	0.3	mild tingling	2	none	none	none
13	0.7	piercing	0.9	none	2	slight pulling in occipital region	1	push/pull
14	0.1	pinprick	0.5	faster pinpricks	1	white noise	1	white noise
15	0.1	pinprick	0.3	pinprick	1.5	pinprick	2	pinprick
16	0.3	touch	0.7	sting	2	tingling	2.5	tingling
17	0.5	pinprick/small needle	0.5	pinprick/ small needle	1	light tapping	2	hair prickle
18	0.1	tingling	0.1	tingling	none	none	none	none
19	0.3	tingling	0.5	slight tingling	1	hair moving	none	none
20	0.1	tingling	0.1	tingling	1.5	itchy	1.5	pain
21	0.1	pinprick	0.5	pinprick	1.5	headache	1.5	headache

tACS – transcranial alternating current stimulation; TI – temporal interference stimulation; CF – carrier frequency; Δf – delta frequency or modulated frequency; e – electrode.

Table A3 Blinding effectiveness

During the behavioural sessions participants were asked at 4 time points whether they thought they had stimulation and how confident they were. The two questions were combined into a weighted score (WS), whereby a “yes” answer was assigned a +1 value and “no” answer a value of -1, which were then multiplied by the confidence rating. Shown is the statistical model applied to investigate whether there was an effect of stimulation (ST: sham, TI 1:3) or time point (Q) in the weighted score for perceiving stimulation, the Analysis of Deviance Table (Type II Wald chisquare tests), generated by the Anova() function applied to the model fitted in R. a: Specification of the model fitted in the R language, Df, Degrees of freedom; χ2, Chi-square; P, P-value; N=21 (ID). Signif. codes: ‘***’ 0.001, ‘**’ 0.01, ‘*’ 0.05, ‘.’ 0.1. Table reproduced with permission from Violante, Alania et al. (2023)

Repeated measures analysis with mixed model lmer(WS ~ ST*Q + (1|S_ID) + (1|Session)+ (1 | ID) [a]	Df	x^2	P
Stimulation Type (ST)	1	0.0710	0.7899
Time point probed (Q)	3	4.7361	0.1922
Stimulation Type:Time point probed	3	3.0186	0.3888

Table A4 Summary of post-stimulation side effects questionnaire for TI and Sham sessions.

Summary statistics for adverse effects questionnaire (adapted from Brunoni et al., 2011). Subjects rated each item between 1 (absent) and 4 (severe). Average Intensity and Range calculated over the whole cohort of participants. Statistical analyses were performed Wilcoxon signed-rank tests, two-sided. Table reproduced with permission from Violante, Alania et al. (2023).

	TI session			**Sham session**			**Wilcoxon signed-rank tests**	
	Average Intensity (SD)	Number of incidences > 1 (out of 21)	Range	Average Intensity (SD)	Number of incidences > 1 (out of 21)	Range	Z	p
Headache	1.2(0.5)	3	1-3	1(0.2)	1	1-2	-1.063	0.288
Scalp pain	1.1(0.3)	2	1-2	1.1(0.2)	3	1-2	0.471	0.638
Burning	1.1(0.2)	1	1-2	1(0)	0	1	-1	0.317
Warmth/Heat	1.1(0.3)	2	1-2	1(0.2)	1	1-2	-0.592	0.554
Tingling	1.5(0.6)	8	1-3	1.4(0.6)	9	1-3	0	1
Itching	1.2(0.4)	5	1-2	1(0)	0	1	-2.354	0.019*
Metallic taste	1(0)	0	1	1(0)	0	1	-	-
Fatigue	1.6(0.7)	10	1-3	1.6(0.8)	9	1-3	-0.112	0.911
Sleepiness	1.7(0.9)	9	1-3	1.6(0.8)	8	1-3	-0.473	0.637
Acute mood change	1(0)	0	1	1(0)	0	1	-	-
Visual Sensation	1(0)	0	1	1(0)	0	1	-	-
Dizziness/ Nausea	1(0.2)	1	1-2	1(0)	0	1-2	-1	0.317
Nervousness/ Anxiety	1(0.2)	1	1-2	1(0)	0	1-2	-1	0.317
Discomfort/ Unpleasant	1.1(0.3)	2	1-2	1(0)	0	1-3	-1.432	0.152
Other	1(0)	0	1	1(0)	0	1	-	-

Table A5 The patient inclusion and exclusion criteria

Inclusion criteria
• Age 50-100 years old at screening (inclusive). • Diagnosis of mild cognitive impairment or probable Alzheimer's disease dementia. • Mini Mental State Examination (MMSE) score >=20. • Adequate visual and auditory acuity, in the investigator's judgment, sufficient to perform cognitive testing (eyeglasses and hearing aids are permitted). • Has the capacity to give informed consent. • Fluency in English. • For PET scanning, participants must agree to use contraception methods for four weeks after the scan.
Exclusion criteria
• Candidate is deemed by the investigator to be unable to provide informed consent. • Medical or psychiatric illness that would interfere in completing assessments or impair the safety of the subject for brain stimulation. Such illness includes but is not limited to epilepsy, brain tumour, intracranial infection and psychotic illness. • A known genetic mutation associated with familial Alzheimer's disease or any other autosomal dominant form of dementia. • Any contraindication to MRI as determined by screening and safety questionnaire including but not limited to cardiac pacemakers, aneurysm clips, cochlear implants and other ferromagnetic foreign bodies. History of claustrophobia or the inability to tolerate MRI scanning. • Ongoing treatment with medication that, in the opinion of the investigator, will compromise subject safety or the scientific integrity of the study. • For PET, the candidate has a history of prior radiation exposure for research purposes such that participation in this study would result in ionizing radiation exposure of >10mSv in the past year, in addition to the normal background exposure. • History of drug or allergy that, in the opinion of the investigators, may put the subject at risk through participation. • Where participation in the study would result in a donation of blood or blood products in excess of 500 ml within a period of 56 days. • History or presence of comorbid neurological diagnoses, not limited to but including, for example, space-occupying lesions, multiple sclerosis, that may influence the outcome or analysis of the scan results. • History of clinically significant head injury (e.g., craniotomy, requiring medical or surgical intervention). • A screening ECG outside the normal range. • Pulse rate <40 or >110 BPM or systolic blood pressure >150 and <100 or a diastolic blood pressure >100 and <60. • Abnormal Allen's test and/or prolonged Prothrombin Time. • Needle phobia. • Symptoms of coronavirus (COVID-19) infection, including fever, dry cough, sore throat, diarrhoea, and loss of taste or smell.

Table A6 Post-stimulation side effects questionnaire.

Brain Stimulation Side Effects Questionnaire

Subject ID: _____ Experiment date: _____

Do you have any of the following symptoms or side effects?	Enter a value (1-4) in the space below. 1-Absent 2-Mild 3-Moderate 4-Severe	If present: Is this related to stimulation? 1-None 2-Remote 3-Possible 4-Probable 5-Definite	Notes
Headache			
Neck Pain			
Scalp Pain			
Scalp Burns			
Sensations under the electrode (Tingling, itching, burning, pain)			
Skin Redness			
Visual sensation			
Sleepiness			
Trouble Concentrating			
Change in Mood			
Other (specify):			

Subject Number:
Date:
Researcher:

[redacted]

Hours of sleep last night: _____

Do you think you slept well last night? _____

Caffeine intake today: _____

Have you experienced any change in health since yesterday's visit?

Yes (please give details below) ☐ No ☐

_____
_____
_____

Alcohol intake (yesterday and today):

Yes (please give details below) ☐ No ☐

_____
_____
_____

Did you experience any adverse effects from yesterday's intervention?

Yes (please give details below) ☐ No ☐

_____
_____
_____

Are you happy to go ahead with today's intervention?

Yes ☐ No ☐

Figure A1 Custom-made post-stimulation questionnaire.

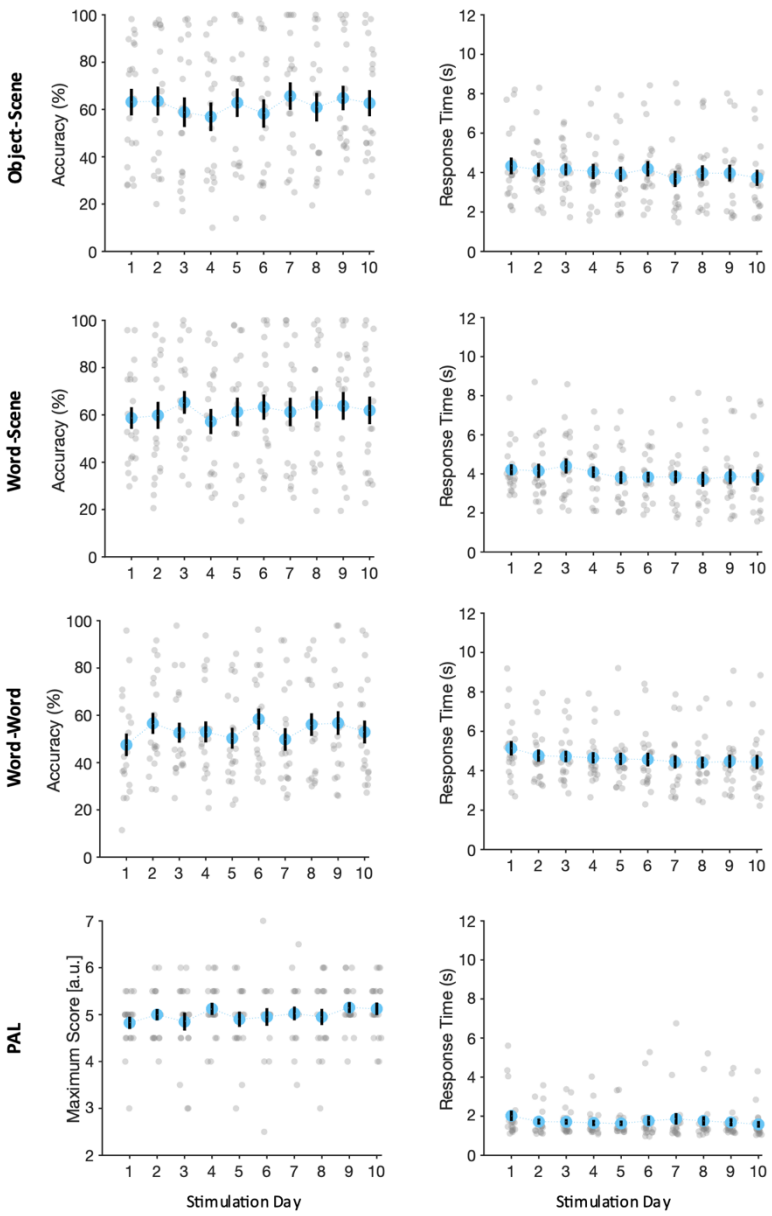


Figure A2 Performance on associative memory tasks performed during TI stimulation.

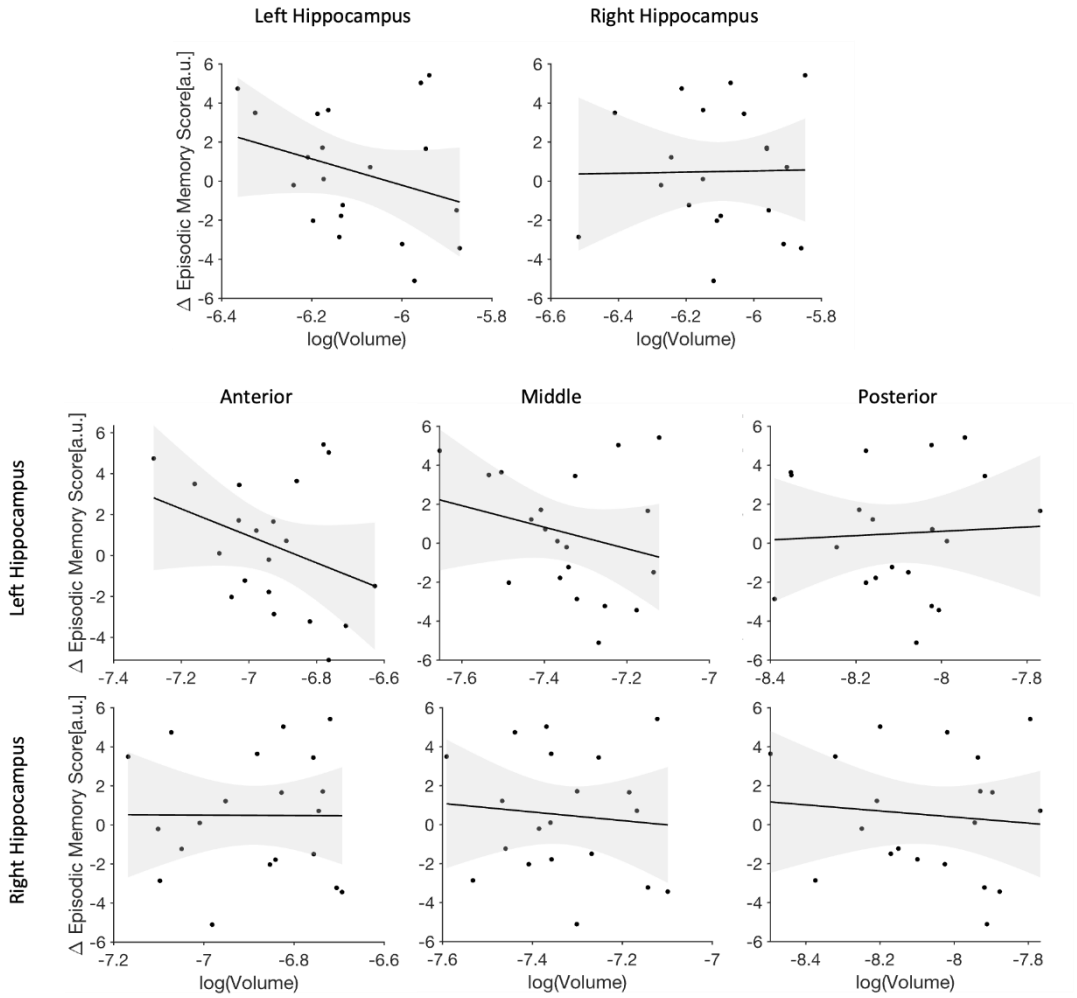


Figure A3 Relationship between change in general cognition tasks and baseline hippocampal volumes.

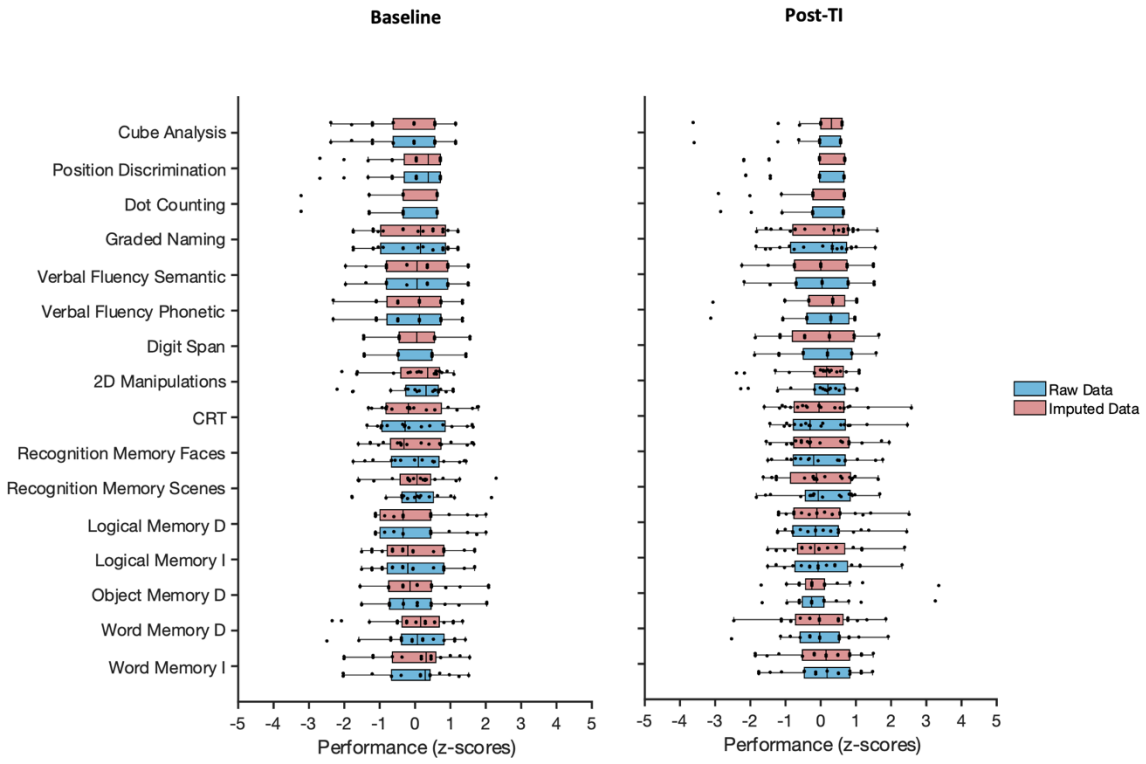


Figure A4 Raw and imputed data at basleine and post-TI.

Table A7 Percentage of imputed data across neurocognitive tasks.

Task	Proportion of Data Imputed (%)
Word Memory Immediate	10.0
Word Memory Delayed	10.0
Object Memory Immediate	0
Object Memory Delayed	5.0
Logical Memory Immediate	2.5
Logical Memory Delayed	2.5
Recognition Memory Scenes	20.0
Recognition Memory Faces	20.0
Choice Response Task	15.0
2D Manipulations	10.0
Digit Span	10.0
Motor Control	0
Verbal Fluency Phonetic	2.5
Verbal Fluency Semantic	2.5
Graded Naming Task	2.5
Dot Counting	2.5
Position Discrimination	2.5
Cube Analysis	2.5

Table A8 Raw and imputed data at baseline and post-TI.

Task	Baseline		Post TI	
	Raw Data Mean (SD)	**Imputed Data** Mean(SD)	**Raw Data** Mean (SD)	**Imputed Data** Mean(SD)
Word Memory Immediate (WM-I)	76.85 (15.27)	76.46(15.25)	81.02(12.88)	81.46(12.42)
Word Memory Delayed (WM-D)	71.99 (13.84)	70.42(15.82)	71.3(14.98)	71.46(15.43)
Object Memory Delayed (OM-I)	24.21 (12.72)	24.25(12.38)	33.68(14.22)	33.5(13.87)
Logical Memory Immediate (LM-I)	6.2 (3.44)	6.2(3.44)	7.32(4.19)	7.2(4.11)
Logical Memory Delayed (LM-D)	5.3 (3.84)	5.3(3.84)	6.68(4.63)	6.5(4.58)
Recognition Memory Scenes (RM-Scenes)	0.68(0.12)	0.66(0.12)	0.72(0.14)	0.71(0.15)
Recognition Memory Faces (RM-Faces)	0.67(0.09)	0.65(0.09)	0.65(0.11)	0.65(0.11)
Choice Response Task (CRT)	0.2(0.38)	0.15(0.37)	-0.04(0.31)	-0.03(0.29)
2D Manipulations (2D-Manip)	76.55(21.77)	75.24(22.54)	77.24(22.16)	77.12(20.98)
Digit Span (DS)	5.5(1.04)	5.45(1)	5.72(1.45)	5.65(1.42)
Verbal Fluency Phonetic (VF-Phonetic)	4.8(1.64)	4.8(1.64)	5.58(1.46)	5.5(1.47)
Verbal Fluency Semantic (VF-Semantic)	4.4(1.73)	4.4(1.73)	3.95(1.35)	4(1.34)
Graded Naming Task (GNT)	17.4(7.1)	17.4(7.1)	17.58(7.38)	17.3(7.29)
Dot Counting (VOSP-DC)	9.35(1.04)	9.35(1.04)	9.26(1.15)	9.25(1.12)
Position Discrimination (VOSP-PD)	18.95(1.47)	18.95(1.47)	19.05(1.43)	19.05(1.39)
Cube Analysis (VOSP-CA)	8.05(1.7)	8.05(1.7)	9.05(1.68)	9(1.65)

Table A9 Stimulation current amplitudes delivered in study 1.

Subject	TI amplitude (mA)
s1	2
s2	2
s3	2
s4	1.9
s5	1.9
s6	1.9
s7	2
s8	2
s9	2
s10	1.9
s11	2
s12	1.9
s13	1.8
s14	1.8
s15	1.9
s16	1.8
s17	1.9
s18	1.9
s19	1.9
s20	1.9
s21	1.4
s22	1.9
s23	1.9
s24	1.9
s25	1.7
s26	1.5
Mean	1.87
SD	0.14

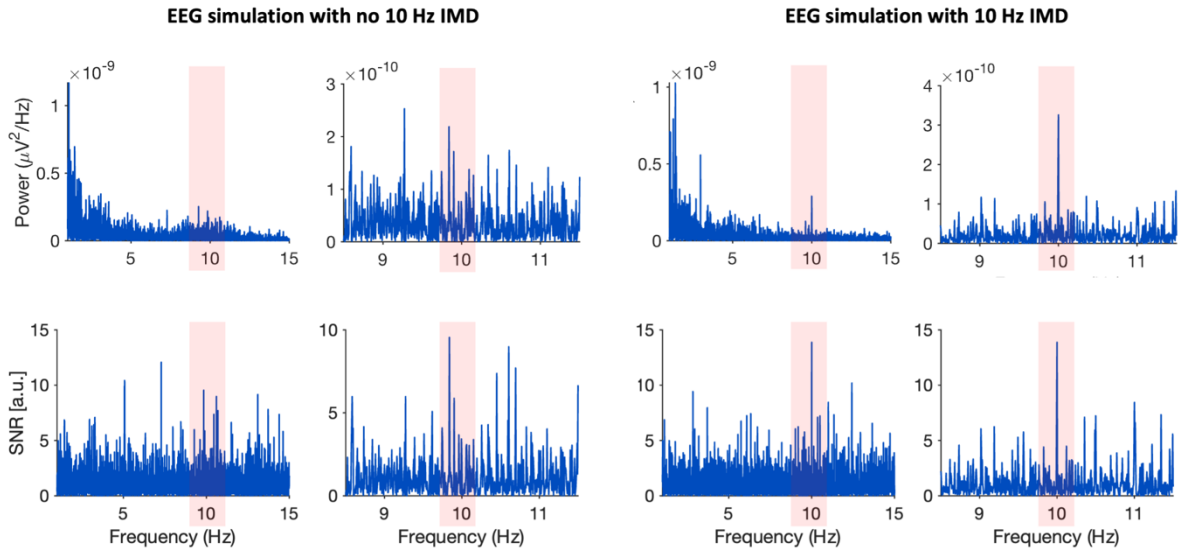


Figure A5 Synthetic EEG data simulation with and without low frequency IMD component.

Table A10 Statistical results for Figure 4.10.

(B)

Predictor	Estimate	SE	CL-Lower	CL-Upper	*t* Value	DF	*p* Value
(Intercept)	5.74	1.73	2.21	9.26	3.31	34	0.002
Condition_TI_27Hz	3.11	1.52	0.02	6.21	2.05	34	0.048 *

Formula: 'z_score ~ Condition (sham/TI_27Hz) + (1|Subject)'

(E)

Predictor	Sum Sq	Mean Sq	DF1	DF2	*F* Value	p Value
Condition	7.61E-04	3.81E-04	2	36	7.81	0.002 **

Contrast	Estimate	SE	CI-Lower	CI-Upper	t Value	DF	p Value
Sham - TI_10Hz	9.16E-03	2.39E-03	4.47E-03	0.014	3.83	38.12	0.001 **
Sham - TI_27Hz	3.88E-03	2.39E-03	-8.13E-04	0.009	1.62	38.12	0.249
TI_10Hz - TI_27Hz	-5.28E-03	2.39E-03	-9.97E-03	-0.001	-2.21	38.12	0.083

(Formula: median_Baseline_amp ~ Condition (sham/TI_10Hz/TI_27Hz) + (1 | Subject)

(C)

Predictor	Estimate	SE	*t* Value	DF1	DF2	*F* Value	R^2	Adj. R^2	*p* Value
(Intercept)	151.55	52.93	2.86	1	16	-	-	-	0.011
Baseline_alpha	-15.18	5.41	-2.81	1	16	7.87	0.33	0.29	0.013 *

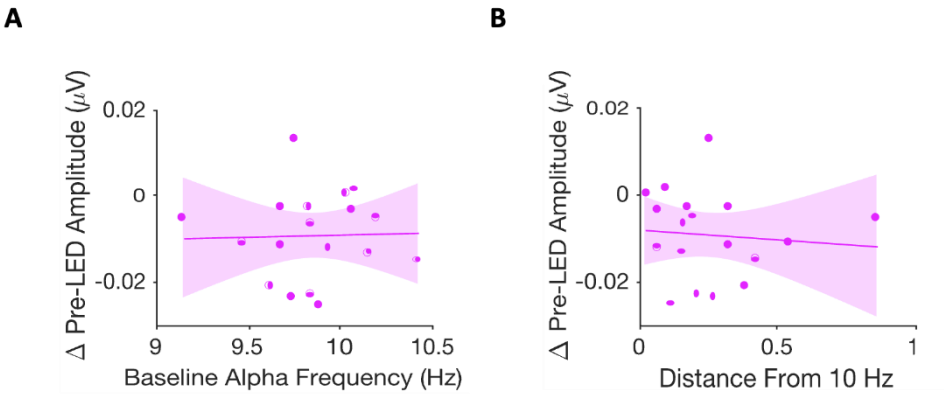


Figure A6 Relationship between baseline alpha frequency and the effect of TI-10 Hz on pre-LED baseline.

Table A11 Statistics for Figure A 6 Relationship between baseline alpha frequency and the effect of TI-10 Hz on pre-LED baseline.

Hemisphere	Predictor	Estimate	SE	CL Lower	CL Upper	*t*-value	df	R^2	*p*-value Adjusted
Left	Whole	-6.73	4.91	-17.04	3.58	-1.37	0.09	18	0.374
	Ant.	-6.60	4.36	-15.76	2.56	-1.51	0.11	18	0.856
	Mid.	-5.52	5.02	-16.06	5.02	-1.10	0.06	18	0.856
	Post.	1.10	4.65	-8.67	10.88	0.24	0.00	18	0.978
Right	Whole	0.31	4.11	-8.32	8.93	0.07	0.00	18	0.941
	Ant.	-0.12	4.81	-10.24	9.99	-0.03	0.00	18	0.980
	Mid.	-2.20	5.32	-13.37	8.97	-0.41	0.01	18	0.978
	Post.	-1.56	3.66	-9.25	6.12	-0.43	0.01	18	0.978

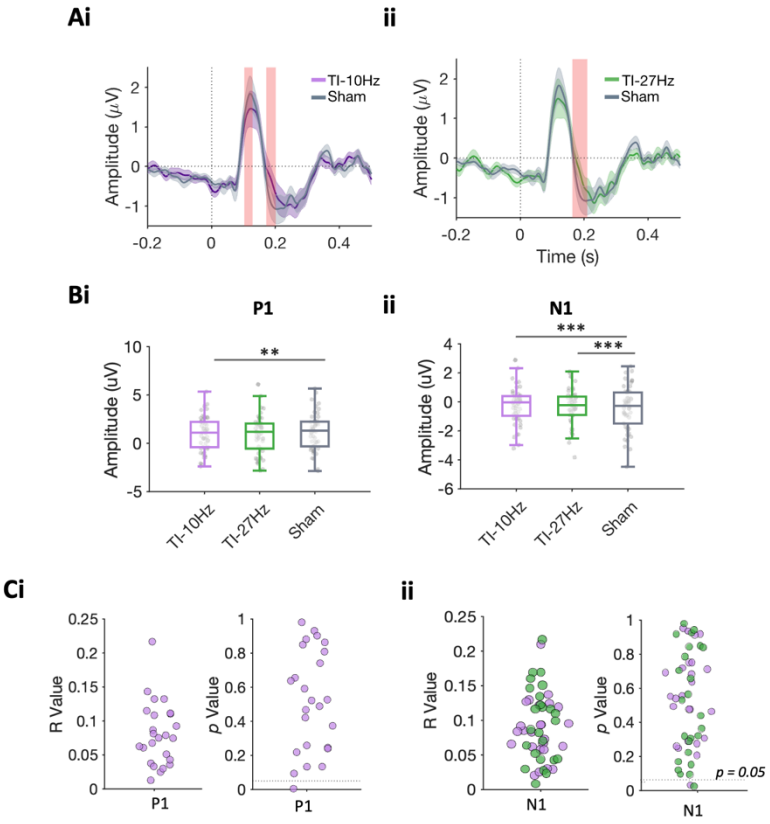


Figure A7 The effect of TI on ERP.

A. The cluster permutation test compares the effect of TI stimulation on visually evoked potentials (VEPs) against sham for each condition at the stimulation at O2 channel. **i.** TI-10 Hz reduced VEPs at the 102 - 128 ms and 171 – 201 ms compared to sham, aligning with P1 and N1 ERP components respectively. **ii.** TI-27Hz stimulation also reduced the N1 component amplitude compared to sham at the stimulation site (164 – 210 ms post LED onset) **B.** The follow-up parametric tests confirmed the effects of TI on P1 and N1 components at a trial level. **C.** Circular-linear correlation results of instantaneous TI phase at LED onset and change in amplitude of significant clusters for the significant clusters corresponding to **(i)** P1 and N1 **(ii)** ERP components demonstrating no significant relationship. **p < 0.01, ***p < 0.001; n=18.